ENERGY CHANGES IN RELATION TO THE ELECTRONIC CHARGE DISTRIBUTION: I. HYDROGEN BOND FORMATION. II. ROTATION AND INVERSION BARRIERS. III. HYDROLYSIS REACTIONS OF "HIGH-ENERGY" PHOSPHORUS COMPOUNDS.

By

JAMES RICHARD CHEESEMAN, B.SC.

A Thesis

Submitted to the School of Graduate Studies

in Partial Fulfilment of the Requirements

for the Degree

Doctor of Philosophy

McMaster University

ENERGY CHANGES IN RELATION TO THE ELECTRONIC CHARGE DISTRIBUTION

DOCTOR OF PHILOSOPHY (1992) McMASTER UNIVERSITY
(Chemistry) Hamilton, Ontario

TITLE: Energy Changes in Relation to the Electronic ChargeDistribution: I. Hydrogen Bond Formation. II. Rotation and Inversion Barriers. III. Hydrolysis Reactions of "High-Energy" Phosphorus Compounds.

AUTHOR: James Richard Cheeseman, B.Sc.
(University of Wisconsin, Madison)

SUPERVISOR: Professor R. F. W. Bader

NUMBER OF PAGES: xii, 152, 49

Abstract

This thesis is an investigation into the relationship between changes in the distribution of electronic charge, brought about through some form of structural change or reaction, and the corresponding energy changes. This relationship is examined in four different applications, the first two of which involve the formation of weak to intermediate strength hydrogen bonds. The third application addresses barriers to rotation and inversion and the fourth is an investigation into the hydrolytic cleavage of the P-O-P and P-O-C linkages in "high energy" phosphate molecules. In each case, the energy changes are given in terms of the mechanical properties of the atoms using the theory of atoms in molecules and topological theory of molecular structure.

The first application is an investigation into the formation of hydrogen bonds which result from the dimerization of formamide to its open or cyclic form. It is shown that an important factor governing the changes in the relative stabilities of the atoms on forming the dimers are the opposing flows of σ and π density through the conjugated N-C-O fragments.

The weak hydrogen bonded complexes studied in the second application include the Van der Waals complexes NeHCl, NeHF, ArHCl, ArHF and the progressively stronger interactions found in NNHCN, NNHCl, NNHF, HCNHCN, HCNHCl and HCNHF. These weak interactions, which result from the mutual penetration of the non-bonded Van der Waals radii of the H atom of the acid and the terminal base atom, involve little charge transfer between the base and the acid but do result in charge reorganization within the reactants. The principal source of the molecular dipole moment enhancement is shown to originate from internal polarization of the base atom in the Van der Waals complexes and from the intramolecular charge transfer which occurs between the acid and base fragments for the remaining complexes.

The third application addresses barriers to internal rotation and inversion through the relative changes in the attractive and repulsive potential energies using the virial theorem. The rotation barriers in ethane, methanol and methylamine are found to result

from an increase in the attractive potential energies in spite of a decrease in the repulsive potential energy, while just the opposite is found for the inversion barriers in NH_3, PH_3, and H_3O^+ and for the barrier to bending in H_2O.

The atomic and group contributions to the overall hydrolysis reaction energies of the neutral and charged forms of diphosphoric acid, methyldiphosphate and phosphoenolpyruvate are determined in the final application. The stabilizing effects of solvation are shown to be important in the reactions which involve charge separation.

Acknowledgements

I wish to thank all of the members of the Theoretical Chemistry Laboratory for their assistance, cooperation and friendship during my stay at McMaster. In chronological order they are: Marshall Carroll, Preston MacDougall, Carlo Gatti, Cheng Chang, Weiliang Cao, Kathleen Gough, Keith Laidig, Danny Legare, Peng Fei Zou, Paul Krug, Todd Keith, Paul Popelier and Ian Bytheway. Of these, I would like to give special thanks to Todd Keith, my friend and co-worker.

Finally, I would like to thank my supervisior, Richard Bader, for providing me with such an excellent and unique opportunity to do what I love most.

TABLE OF CONTENTS

LIST OF TABLES

LIST OF FIGURES

This thesis is dedicated to my parents, James T. Cheeseman and Mary Ellen Cheeseman.

This thesis includes two previously published journal articles entitled "The Mechanics of Hydrogen Bond Formation in Conjugated Systems"[1] and "Origin of Rotation and Inversion Barriers"[2]. In addition to contributing towards the preparation of the former manuscript, all of the calculations and required programming were completed by the author. The later article was a natural development from previous collaborations and discussions with Professor K. Wiberg and co-workers who were interested in barriers to rotation and inversion. Although this work benefited from discussions with the Wiberg group, all of the calculations were completed by the author and the manuscript was prepared in this laboratory.

1 Cheeseman, J. R.; Carroll, M. T. and Bader, R. F. W. (1988) *Chem. Phys. Lett.* 143, 450.

2 Bader, R. F. W.; Cheeseman, J. R.; Laidig, K. E.; Wiberg, K. B. and Breneman, C. (1990) *J. Amer. Chem. Soc.* 112, 6530

Table 0.1. Definition of Atomic Units used in this Thesis.

Length	1 au = a_0 = 0.529177 Å
	= 5.29177×10^{-11} m
Elementary charge	1 au = e = 1.60219×10^{-19} C
	= 4.8029×10^{-10} esu
Charge density	1 au = e/a_0^3 = 6.7483 eÅ^{-3}
	= 1.0812×10^{12} C m^{-3}
Laplacian density	1 au = e/a_0^5 = 24.099 eÅ^{-5}
	= 3.8611×10^{32} C m^{-5}
Dipole moment	1 au = ea_0 = 2.542 Debyes
	= 8.479×10^{-30} C m
Energy	1 au = e^2/a_0 = 627.51 kcal/mol
	= 2.6255×10^3 kJ/mol
	= 27.212 eV
	= 2.1947×10^5 cm^{-1}

INTRODUCTION

In molecular quantum mechanics we now have the ability to calculate good, approximate wave functions for a great number molecules, but the problem still lies in the extraction of the chemistry. This thesis is concerned with the relationship between changes in the distribution of electronic charge, brought about through some form of structural change or reaction, and the corresponding energy changes.

Chapter 1 is a brief review of the theory of atoms in molecules and the topological theory of molecular structure (Bader, 1990). Also included is an account of several recent applications of the theory to a variety of chemical problems.

A hydrogen bond, YB-HX results from the mutual penetration of the van der Waals envelopes of the H atom of the acid and the B atom of the base, the strength of the interaction increasing with the degree of mutual penetration. Chapter 2 is an investigation into the formation of hydrogen bonds resulting from the dimerization of formamide to its cyclic or open form. An important factor governing the changes in the relative stabilities of the atoms on forming the dimers are the opposing flows of σ and π density through the conjugated N-C-O fragments.

The hydrogen-bonded complexes studied in Chapter 3 include the van der Waals complexes NeHCl, NeHF, ArHCl and ArHF and also the progressively stronger interactions found in NNHCN, NNHCl, NNHF, HCNHCN, HCNHCL and HCNHF. These weak interactions involve little charge transfer between the base and the acid but do result in charge reorganization within the reactants. This redistribution of charge can be measured by an examination of the dipole and quadrupole polarizations of the charge

distribution. The origin of the dipole moment enhancement, which occurs upon complex formation, is determined through the separation of the total molecular dipole into acid and base polarization and charge transfer contributions. The calculated dissociation energies and dipole moment enhancements compare well with the experimentally determined values. In addition, calculated changes in the electric field gradient at the nitrogen nucleus are compared with experimentally determined nuclear quadrupole coupling constants.

Chapter 4 investigates the origin of the barriers to rotation in ethane, methanol, methylamine and the barriers to inversion in NH_3, PH_3 H_3O^+ and the barrier to bending in H_2O. The origins of the barriers are shown to be related to the changes in the attractive and repulsive potential energies through the use of the virial theorem.

Chapter 5 is a study of the hydrolytic cleavage of the P-O-P or P-O-C linkages in diphosphoric acid, methyldiphosphoric acid and phosphoenolpyruvate. The stabilizing effects of solvation are shown to be important in the reactions which involve charge separation. As in Chapter 4, the changes in both the total and atomic energies are related to the changes in the attractive and repulsive potential energies.

CHAPTER 1

The Theory of Atoms in Molecules

This chapter introduces the concepts of the theory of atoms in molecules (Bader, 1990 and references within) that are used in this thesis. The electronic charge distribution contains the information necessary to discuss molecular systems in chemical terms: atoms, bonds and molecular structure.

1.1 The Definiton of an Atom in a Molecule and the Topological Classification of the Electronic Charge Distribution

An atom Ω in a molecule is defined to be a region of real space with a surface $S(\mathbf{r},\Omega)$ satisfying the condition

$$\nabla\rho(\mathbf{r})\cdot\hat{\mathbf{n}}(\mathbf{r}) = 0, \forall \mathbf{r} \in S(\mathbf{r},\Omega) \tag{1}$$

where $\nabla\rho(\mathbf{r})$ is the gradient of the electronic charge density $\rho(\mathbf{r})$ at a point $\mathbf{r}$ on the surface and $\hat{\mathbf{n}}(\mathbf{r})$ is the unit vector normal to the surface at $\mathbf{r}$. An entirely equivalent definition of an atom in a molecule is the volume of real space traversed by the complete set of trajectories or paths of steepest ascent of $\nabla\rho$ which terminate at the nucleus of the atom (Fig. 1.1). Every trajectory of $\nabla\rho$ originates and terminates at a critical point in this field, a point where $\nabla\rho = 0$. A critical point, with coordinate $\mathbf{r}_c$ is characterized by the number of nonzero eigenvalues of the associated matrix of second derivatives of $\rho(\mathbf{r}_c)$ which determine its rank σ and the algebraic sum of their signs which determine its signature λ. There are just four possible signature values for critical points of rank three and these are listed below as (σ,λ) (taken from Bader, 1990):

(3,-3) All curvatures are negative and ρ is a local maximum at $\mathbf{r}_c$.

(3,-1) Two curvatures are negative and ρ is a maximum at $\mathbf{r}_c$ in the plane defined by their corresponding axes. ρ is a minimum at $\mathbf{r}_c$ along the third axis which is perpendicular to this plane.

(3,+1) Two curvatures are positive and ρ is a minimum at $\mathbf{r}_c$ in the plane defined by their corresponding axes. ρ is a maximum at $\mathbf{r}_c$ along the third axis which is perpendicular to this plane.

(3,+3) All curvatures are positive and ρ is a local minimum at $\mathbf{r}_c$.

The local maxima, as found at the positions of the nuclei, behave topologically as do $(\sigma,\lambda) = (3,-3)$ critical points. A (3,-1) or bond critical point is found between every pair of nuclei which are considered to be linked by a chemical bond. A (3,+1) or ring critical point is found in the interior region enclosed by a ring of atoms linked by (3,-1) critical points. In tetrahedrane (C_4H_4), for example, there is a ring critical point on each of the four three-carbon faces and a (3,+3) or cage critical point in the center of the tetrahedron.

The (3,-3) critical points define the atoms and their basins while the (3,-1) critical points define the interatomic surfaces and the atomic interaction lines. The nuclei of two atoms which share a common interatomic surface are linked by a line along which the charge density is a maximum with respect to any neighboring line. The existence of a (3,-1) critical point and its associated atomic interaction line indicates that charge density is accumulated between the nuclei that are so linked. The presence of an atomic interaction line in an equilibrium nuclear configuration satisfies both the necessary and sufficient conditions that the atoms be bonded to each other, and in this case the atomic interaction line is called a "bond path" and the (3,-1) critical point referred to as a "bond critical point". The union of the closures of the bond paths or atomic interaction lines defines the molecular graph (Fig. 1.2). A molecular structure is then defined as an equivalence class of molecular graphs. The recovery of a chemical structure in terms of the system's distribution of electronic charge is a most remarkable and important result.

1.2 The Laplacian of the Charge Density

The topology of the charge density ρ provides a faithful mapping of the models of atoms, bonds, and molecular structure but does not offer any indication of the presence of shell structure in an atom or of maxima in a molecular charge distribution corresponding to bonded or nonbonded pairs of electrons. The latter characteristics, anticipated on the basis of the Lewis model or the model of localized electron pairs, are, however, recovered in the properties of the Laplacian of the charge density ($\nabla^2\rho$). The Laplacian of ρ at a point $\mathbf{r}$ provides a measure of the difference between the average value of ρ at points neighboring $\mathbf{r}$ and its value at $\mathbf{r}$. When $\nabla^2\rho < 0$, $\rho(\mathbf{r})$ is greater than its average value at neighboring points; when $\nabla^2\rho > 0$, the opposite is true. The locations of maxima, minima, or saddle points in the Laplacian are determined by the positions of the critical points where $\nabla(\nabla^2\rho) = 0$. (refer to the (σ,λ) listing above, replacing ρ with $\nabla^2\rho$).

The form of the Laplacian for an isolated atom reflects the shell structure by exhibiting a corresponding number of pairs of spherical shells of local charge concentration and charge depletion (Figs. 1.1c,1.2). Upon chemical combination, local centers of charge concentration and charge depletion are created within the valence shell. The number, locations and magnitudes of the charge concentrations are found to be in agreement with the properties that are ascribed to the bonded and nonbonded electron pairs in models of electronic structure. It has been shown that sites of electrophilic and nucleophilic attack in a molecule correlate respectively with the sites of maximum charge concentration and charge depletion (Bader and MacDougal, 1985; Carrol et al, 1989)

The Laplacian of ρ has been shown to be directly related to the local contributions to the electronic energy of a system through

$$(\hbar^2/(4m))\nabla^2\rho(\mathbf{r}) = V(\mathbf{r}) + 2G(\mathbf{r})$$

where $V(\mathbf{r})$ is the potential energy density (its integral over all space yields the total electronic potential energy V) and $G(\mathbf{r})$ is the kinetic energy density (its integral over all space yields the total kinetic energy of the electrons, T). Since $V(\mathbf{r}) < 0$ for all $\mathbf{r}$, the above equation states that the lowering of the potential energy dominates the total energy in regions where the electronic charge density is concentrated (where $\nabla^2\rho < 0$).

1.3 Definition of Atomic Properties

The atomic average of a property A in atom Ω is obtained by the integration of a corresponding property density, $A(\mathbf{r})$, over the basin of the atom[1] .

$$A(\mathbf{r}) = \int d\mathbf{r}' (N/2) \{\psi^* \hat{A}\psi + (\hat{A}\psi)^*\psi\}$$

$$A(\Omega) = \int_{\Omega} d\mathbf{r} A(\mathbf{r})$$

where $d\mathbf{r}'$ denotes the integration over the spin coordinates of all electrons and the space coordinates of all electrons but one. All atomic properties can be expressed using either the one-density matrix $\Gamma^{(1)}(\mathbf{r},\mathbf{r}')$ or the diagonal elements $\Gamma^{(2)}(\mathbf{r}_1,\mathbf{r}_2)$ of the two density matrix. The sum of $A(\Omega)$ over all the atoms Ω in the molecule yields the molecular property. The difference between this sum of the atomic values and the molecular values is an indication of the quality of the integration procedure.

The electron density itself, $\rho(\mathbf{r})$, is the simplest example of a property density, and its integration over the basin of the atom yields the net atomic population $N(\Omega)$.

$$N(\Omega) = \int_{\Omega} d\mathbf{r} \rho(\mathbf{r})$$

---

[1] All equations are given in atomic units

The net charge on an atom $q(\Omega)$, is given by the sum of its nuclear charge Z_Ω and its average electronic charge $-N(\Omega)$,

$$q(\Omega) = (Z_\Omega - N(\Omega))$$

The kinetic energy densities $G(\mathbf{r})$ and $K(\mathbf{r})$ are defined as follows in terms of the first-order reduced density matrix $\Gamma^{(1)}(\mathbf{r},\mathbf{r}')$:

$$G(\mathbf{r}) = (1/2)\,[\nabla\cdot\nabla'\,\Gamma^{(1)}(\mathbf{r},\mathbf{r}')]_{\mathbf{r}=\mathbf{r}'}$$

$$K(\mathbf{r}) = (-1/2)\,[\nabla^2\Gamma^{(1)}(\mathbf{r},\mathbf{r}')]_{\mathbf{r}=\mathbf{r}'}$$

The difference between $G(\mathbf{r})$ and $K(\mathbf{r})$ is equal to the density $L(\mathbf{r})$, whose integral over an atom in a molecule vanishes:

$$L(\Omega) = \int_\Omega d\mathbf{r}L(\mathbf{r}) = (-1/4)\int_\Omega d\mathbf{r}\nabla^2\rho(\mathbf{r}) = \int_\Omega dS(\Omega)\nabla\rho(\mathbf{r})\cdot\hat{\mathbf{n}} = 0$$

Therefore, the integration over an atom in a molecule of either $G(\mathbf{r})$ or $K(\mathbf{r})$ yields the same value for the atomic kinetic energy $T(\Omega)$.

$$T(\Omega) = \int_\Omega d\mathbf{r}G(\mathbf{r}) = \int_\Omega d\mathbf{r}K(\mathbf{r})$$

$V_a(\Omega)$ is the attractive potential energy of interaction between the electronic charge density in the basin of atom Ω and all of the nuclei in the system.

$$V_a(\Omega) = -\sum_\alpha Z_\alpha e^2 \int_\Omega d\mathbf{r}\, r_{1\alpha}^{-1}\rho(\mathbf{r})$$

where Z_α is the nuclear charge for nucleus α.

$V_a^{\circ}(\Omega)$ is the attractive potential energy of interaction of the charge density in the basin of atom Ω with its own nucleus.

$$V_a^{\circ}(\Omega) = - Z_\Omega e^2 \int_\Omega dr\, r_\Omega^{-1} \rho(r)$$

$V_{ee}(\Omega)$, the contribution of the electron-electron repulsive potential energy of atom Ω, is defined in terms of the two-density matrix, $\Gamma^{(2)}(\mathbf{r}_1,\mathbf{r}_2)$, as follows.

$$V_{ee}(\Omega) = \int_\Omega dr_1 \int dr_2\, (e^2/r_{12})\, \Gamma^{(2)}(\mathbf{r}_1,\mathbf{r}_2)$$

The first moment of an atom's charge distribution $\mathbf{m}(\Omega)$ is obtained by averaging the vector $\mathbf{r}_\Omega$, with the origin at the nucleus, over the charge density contained in the atomic basin,

$$\mathbf{m}(\Omega) = - \int_\Omega dr\, \mathbf{r}_\Omega \rho(r)$$

The first moment provides a measure of the extent and direction of the dipolar polarization of the atom's charge density by determining the displacement of the atom's centroid of negative charge from the position of its nucleus.

In addition to the dipole polarization, another important atomic polarization is measured by the axial component of the quadrupole moment. This traceless tensor can be diagonalized to obtain three principal axes and their corresponding moments. The quadrupole polarization of an atomic density measured with respect to the z-axis for atom Ω is given by

$$Q_{zz}(\Omega) = - \int_\Omega dr(3z_\Omega^2 - r_\Omega^2)\rho(r)$$

and the remaining terms of the quadrupole tensor are defined in an analogous manner. For a spherically symmetric distribution of charge, each moment equals zero. $Q_{zz}(\Omega)$ is greater than zero for a perturbed spherical distribution which is flattened at the poles of

the z-axis. For an atom with electronic charge depleted in a plane and concentrated along the perpendicular (z) axis, $Q_{zz}(\Omega) < 0$. These three situations are illustrated by the corresponding distortions of a sphere in Fig. 1.3. $Q_{zz} > 0$ implies a transfer of electronic charge from along the z-axis to a torus-like distribution about this axis, while $Q_{zz} < 0$ implies an accumulation of electronic charge along this axis. The quadrupole moment is the charge density analogue of the π population of the orbital model.

1.4 Applications of the Theory of Atoms and Molecules

A recent review article by Bader (1991) includes an up to date summary of applications of the theory to a variety of chemical systems. Applications of the theory have demonstrated that the properties of the charge density at the bond critical points, together with the related concept of structural stability, enable one to determine the presence or absence of the predicted electronic effects of orbital theory and to translate these predictions into observable consequences in the charge distribution. The following applications demonstrate how structures and properties throughout a series of compounds can be systematically characterized in terms of parameters which summarize the important physical properties of the charge density.

For bonds between a given pair of atoms, one may define a bond order whose value is determined by ρ_b, the value of the charge density at the bond critical point. The variation of ρ_b with the equilibrium nuclear separation, R_e, has also been investigated (Bader et al, 1982) and particularly useful relationships between ρ_b and R_e have been presented by Boyd and co-workers (Boyd, 1987; Boyd and Choi, 1986; Boyd and Choi, 1985; Boyd et al, 1988). Ritchie et al (1986) have used the parameters of ρ_b to assign structures and properties to the bonds for three states of the C_4 system. Bachrach (1989) finds that the values of ρ_b for bonds to phosphorus provide excellent measures of bond order and bond length in the phosphines, phosphoalkanes and phosphoalkynes.

The bonded radius, the distance from the nucleus to the associated bond critical point, has been shown to parallel the relative electronegativity of two bonded atoms (Bader et al, 1971; Bader and Beddall, 1973; Bader and Messer, 1974). Boyd and co-workers have used these bonded radii to classify the bonds in diatomic hydrides and mixed halides of Al, Si and P (Boyd and Edgecombe, 1987; Choi et al, 1987).

A detailed analysis of the properties of the structures at a number of stationary points along the pathways of the Diels-Alder cycloaddition of ethylene to butadiene have been presented by Gatti et al (1988). Ritchie (1986) has used the topological parameters of the charge density to analyze the effects of vinyl and allylic fluorine substitution in isobutylene. Relations of the thermal stability of diazonium cations to the properties of the C-N linkage have been investigated by Glaser (1990).

The theory has also been used to assign structure and characterize the interactions in systems with unusual bonding. Ritchie and Bachrach (1987) have assigned structures and determined bond and atomic properties for a series of 23 organolithium compounds. Lammertsma and Leszczynsk (1990) found the topological properties of ρ to provide a concise description of the structure present in digallane, Ga_2H_4. Cioslowski (1990) has investigated the behavior of the nonnuclear attractors found in Li_2 as a function of the internuclear separation using Thom's catastrophe theory (Thom, 1975). Cioslowski (1990) has also studied the lowest energy bicyclic structure of $Li_2C_2O_2$ and found each Li to be bonded to an oxygen and a carbon.

Information obtained from calculated atomic populations and moments has been useful in determining the importance of classical models. The following examples point out, in particular, the inadequacy of the resonance model. Wiberg et al (1989) have determined the σ- and π-populations of the atoms in benzene and the azines in a study of π-electron delocalization and also investigated the importance of resonance stabilization in the allyl anion and cation (Wiberg et al, 1992). Glaser (1990) has shown how the Lewis resonance structures can be reinterpreted to bring their anticipated consequences

into line with the observed properties of the charge density. The polarization of the π density is of particular importance when an unsaturated system is bonded to a π-electron donor or abstractor group. Examples of opposing polarizations of the σ- and π-density distributions are provided by the substituted benzenes (Bader and Chang, 1989). Wiberg and Laidig (1987) also determined the charges and energies of the atoms in their study of the rotational barriers in esters and amides. Wiberg and Breneman (Wiberg and Breneman, 1990; Wiberg, 1991) have presented an extensive investigation of the effects of substituents on the atomic properties of methyl and *n*- and *tert*-butyl derivatives.

Streitwieser and co-workers independently developed a method of defining an atomic charge which is also based upon a spatial partitioning of the electronic charge density, by integrating the density in a direction perpendicular to a given plane. This method of integrated electron populations has been applied to a wide range of chemical problems (Streitwieser et al, 1979; Rajca and Streitwieser, 1988; Gronert et al, 1989).

The electron pairs of Lewis and the associated models of geometry and reactivity find physical expression in the topology of the Laplacian. The reactivities of a series of molecules in a Michael addition reaction have been analyzed on the basis of the properties of the Laplacian (Carroll et al, 1989). The properties of the Laplacian correctly predict that the attack occurs at the terminal carbon of the methylene group and that the approach of the nucleophile will be from above or below the plane of the nuclei along a line forming an angle of 115° with the C=C bond axis, the latter prediction being in agreement with calculations of the potential energy surface for this reaction. The Laplacian distribution has been used to predict the structures of a large number of hydrogen-bonded complexes by aligning the (3,+3) critical point on the nonbonded side of the proton in HF with the (3,-3) critical point of the base (Carroll et al 1988). Frenking et al (1989) have used the properties of the charge density at its critical points and the Laplacian distribution in a study of the binding of helium in singly and doubly charged first-row diatomic cations. Alcami et al (1990) have used the Laplacian of the charge

density to classify the interactions found in the complexes formed between the lithium ion and a number of azines. Aray and Murgich (1989) have demonstrated a direct relationship between the maxima in the valence shell of charge concentration (VSCC) of a nitrogen atom and the components of the electric field gradient at the same nucleus in a series of nitriles.

In summary, the theory of atoms in molecules has been useful in application to a wide variety of chemical problems by yielding descriptions of atoms, bonds, structure and structural stability, in addition to providing predictive models of molecular geometry and chemical reactivity.

Figure 1.1

a) Contour map of the electronic charge density ρ for a symmetry plane of $C_2B_3H_5$ containing the nuclei H-C-B(-H)-C-H. The contour plot is overlaid with bond paths and the atomic boundaries. Bond or (3,-1) critical points are denoted by dots.
The outermost charge density contour equals 0.001 au. The contours increase in order 2×10^n, 4×10^n, 8×10^n, with n increasing in steps of unity from n = -3.

b) A display of the gradient vector field of ρ for the same plane as (a). All of the trajectories of $\nabla\rho$ in the vicinity of a given nucleus terminate at that nucleus, in all three dimensions, thereby defining the basin of the atom. The (3,-1) critical points whose trajectories link the nuclei in this plane appear as (2,0) critical points. The two trajectories defining the bond path originate at each such point and the two trajectories indicating the intersection of the interatomic surface with the plane terminate there. A (3,+1) or ring critical point appears as a (2,0) denoted as a triangle, and a central cage or (3,+3) critical point, which appears as a (2,+2), is denoted by a star.

c) Contour map of the Laplacian of the charge density for the same plane as a) with bond paths and the atomic boundaries overlaid. The contours of the Laplacian of the electronic charge density (solid contours $\nabla^2\rho < 0$, dashed contours $\nabla^2\rho > 0$) increase and decrease froma zero contour in steps $\pm 2 \times 10^n$, $\pm 4 \times 10^n$, $\pm 8 \times 10^n$, begining with n = -3 and increasing in steps of unity. The innermost solid contour encompassing a nucleus with $Z > 1$ encloses the innermost region of charge concentration.

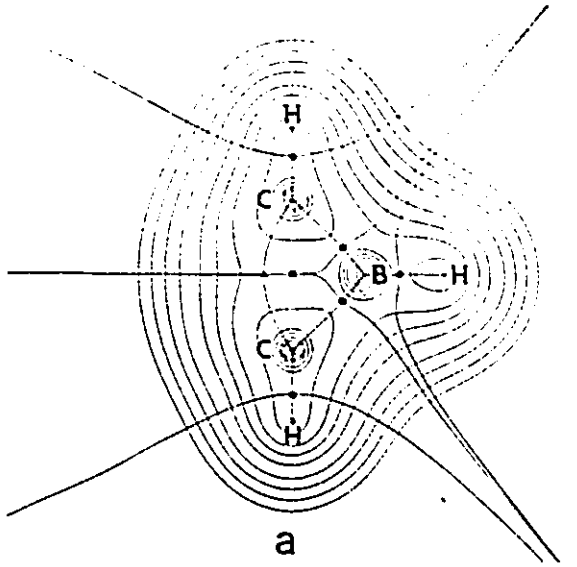

a

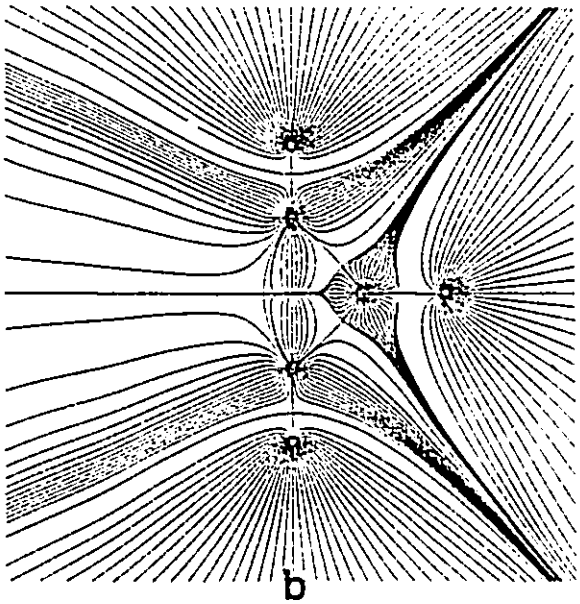

b

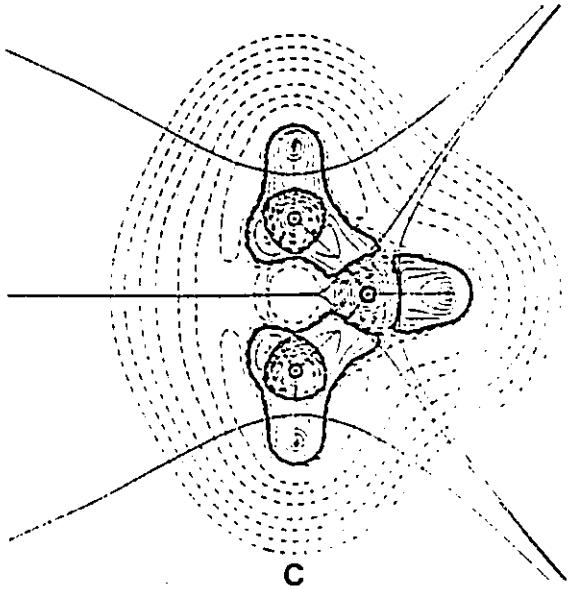

c

Figure 1.2

Molecular graphs for boranes and carboranes with bond critical points denoted by dots.

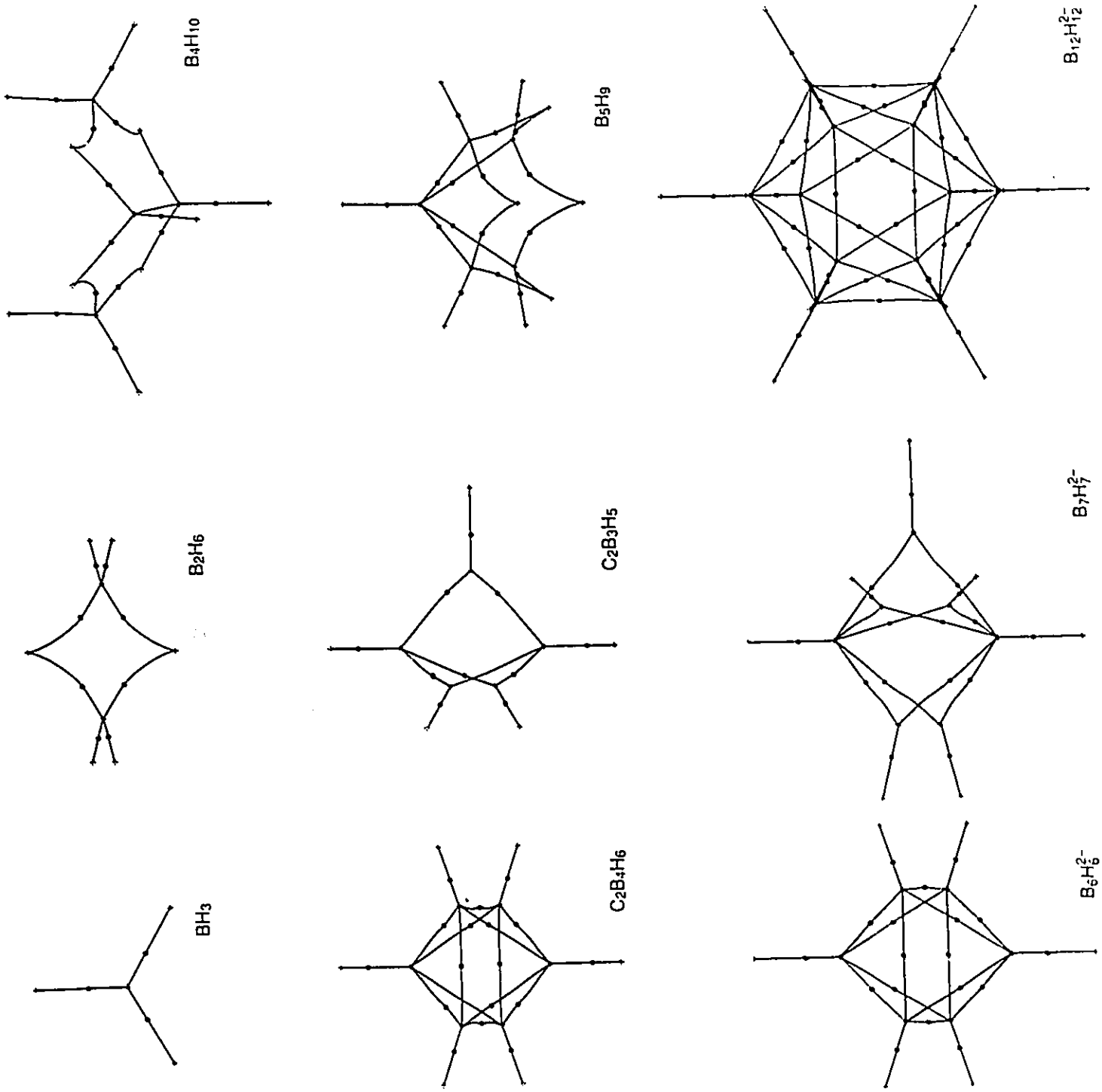
B_4H_{10}
B_5H_9
$B_{12}H_{12}^{2-}$
B_2H_6
$C_2B_3H_5$
$B_7H_7^{2-}$
BH_3
$C_2B_4H_6$
$B_6H_6^{2-}$

Figure 1.3

a) Relief maps of the Laplacian ($-\nabla^2\rho$) for the acrolein molecule in the plane containing the nuclei (top) and in the perpendicular plane along the C_1C_2 molecular axis (bottom). The largest valence-shell concentrations are found in the nonbonded region of the oxygen atom. While C_1 exhibits a shell of concentration (both planes show a "lip" around the inner-shell region of charge depletion), $\nabla^2\rho$ is actually positive over much of this shell in the perpendicular plane. The core, or first quantum shell, of each atom exhibits a spikelike charge concentration at the nucleus surrounded by a deep region of charge depletion. The arrow in the bottom diagram denotes the site of nucleophilic attack at C_1.

b) Contour maps of the Laplacian for the same two planes as in a). Contour values are givin Figure 1.1c.

a

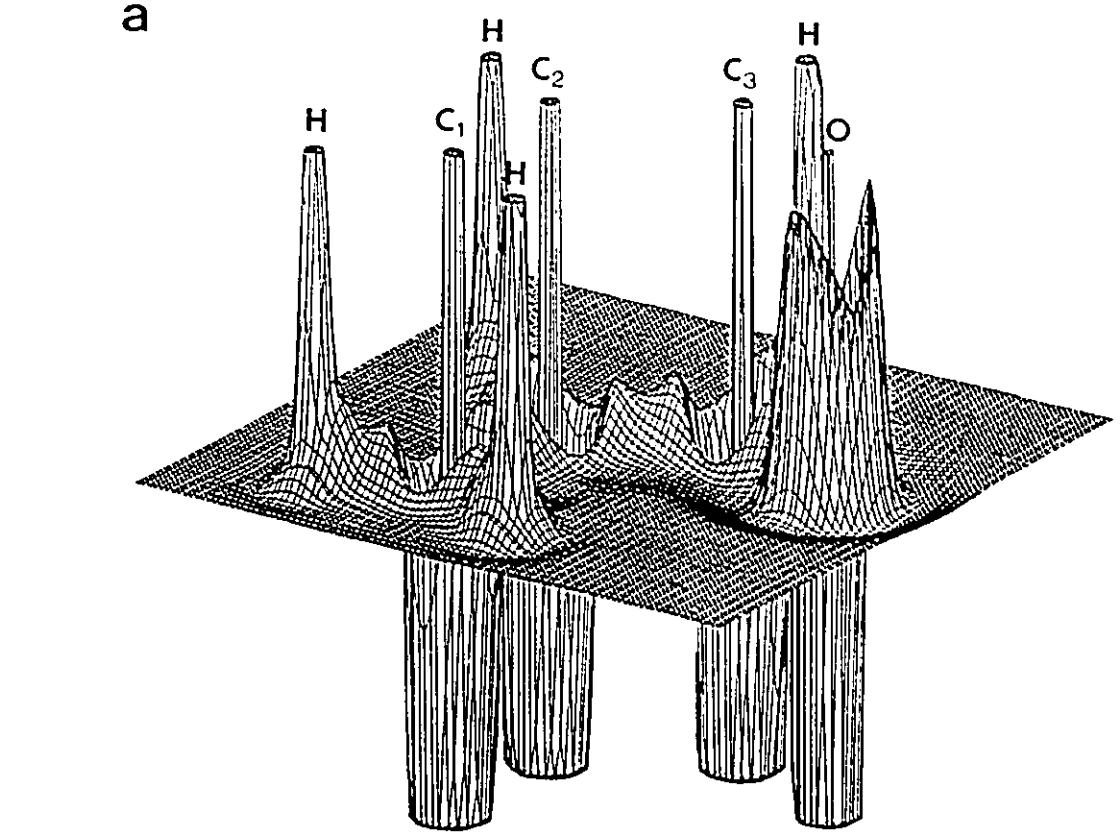

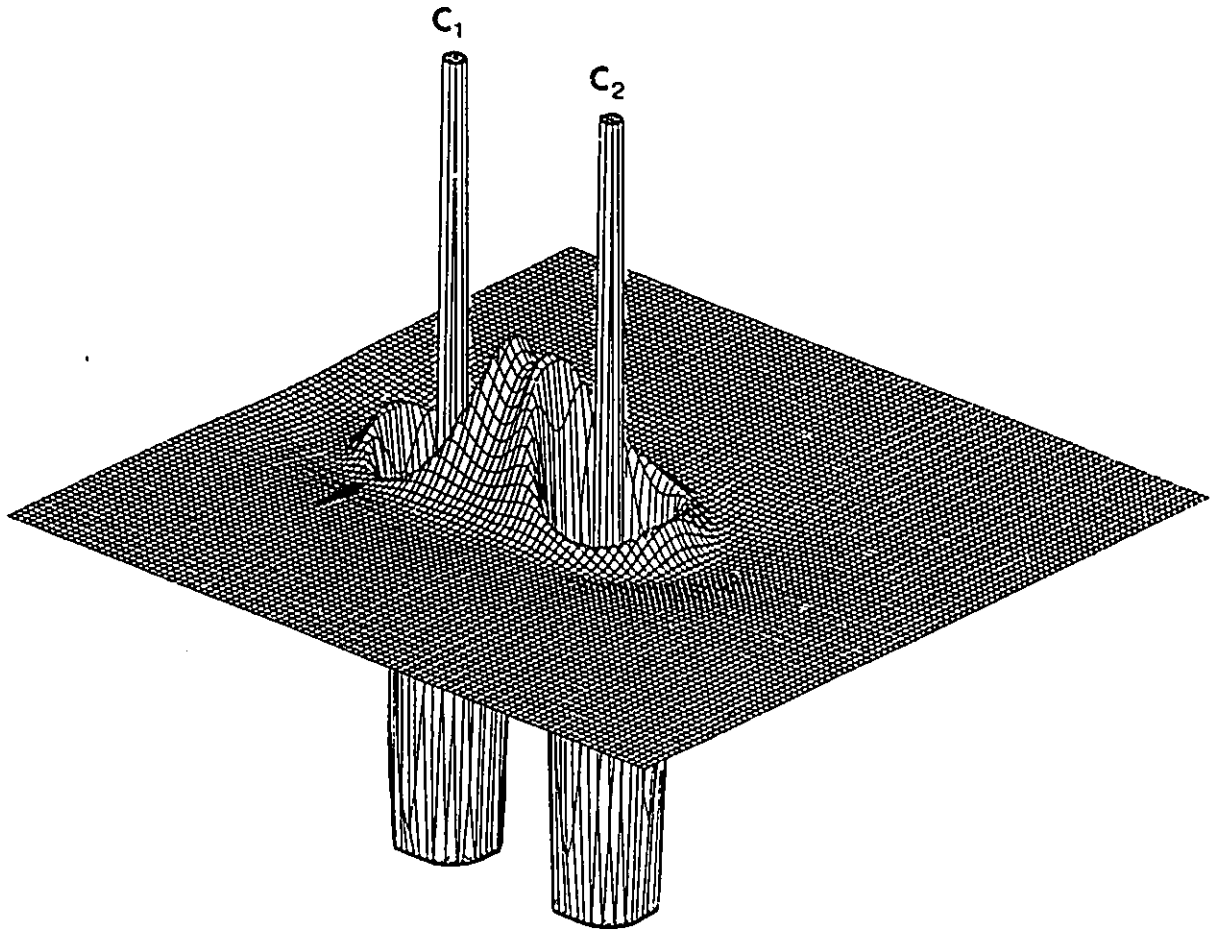

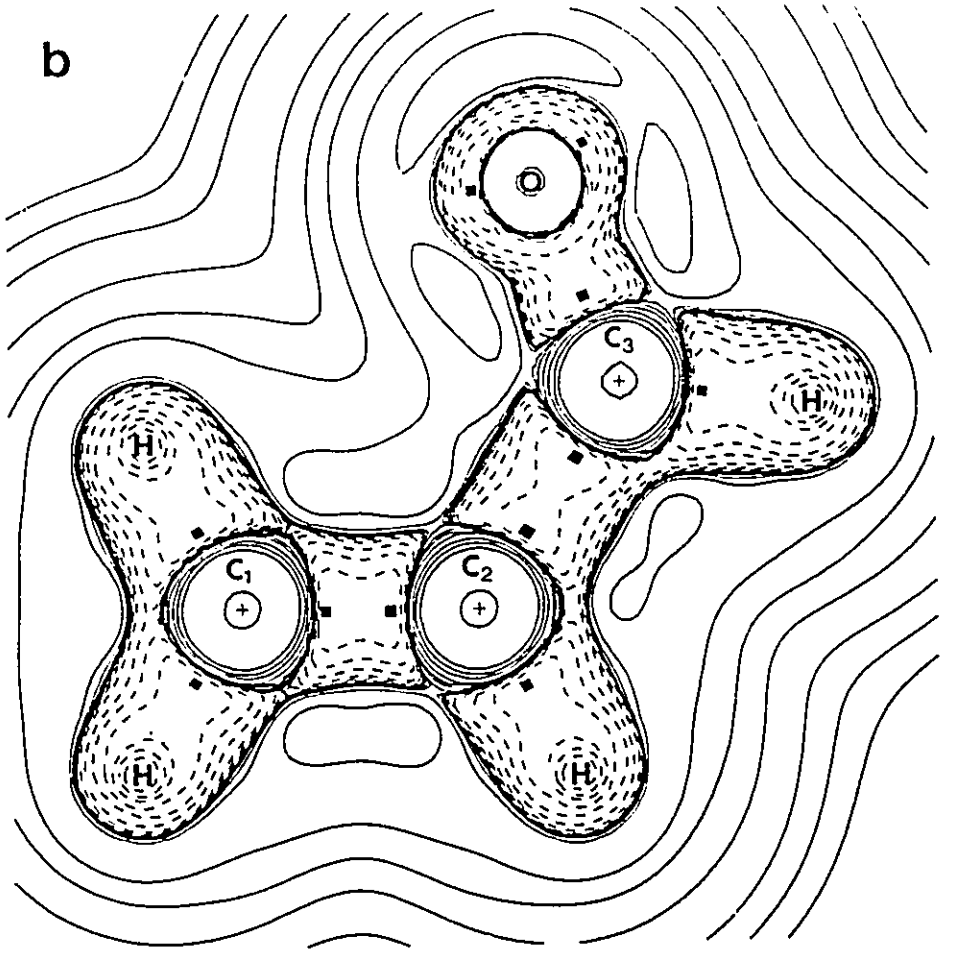
b
C3
H
H
C1
C2
H
H

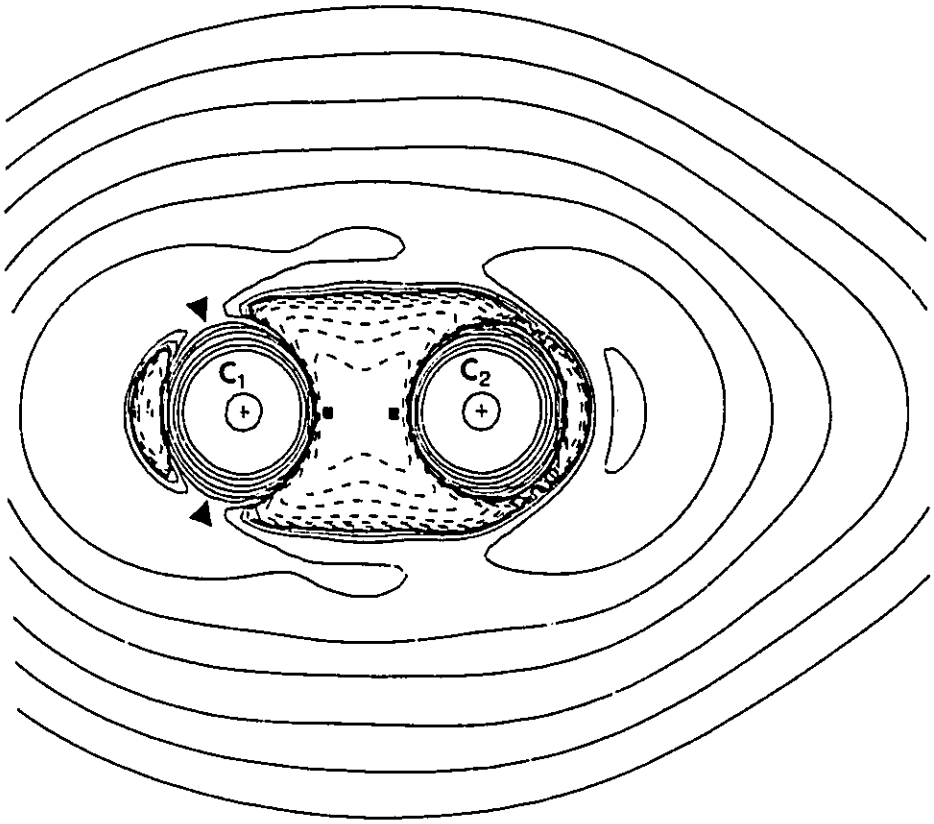
C1
C2

Figure 1.4

Pictorial demonstration of quadrupolar polarizations of an electronic charge distribution.

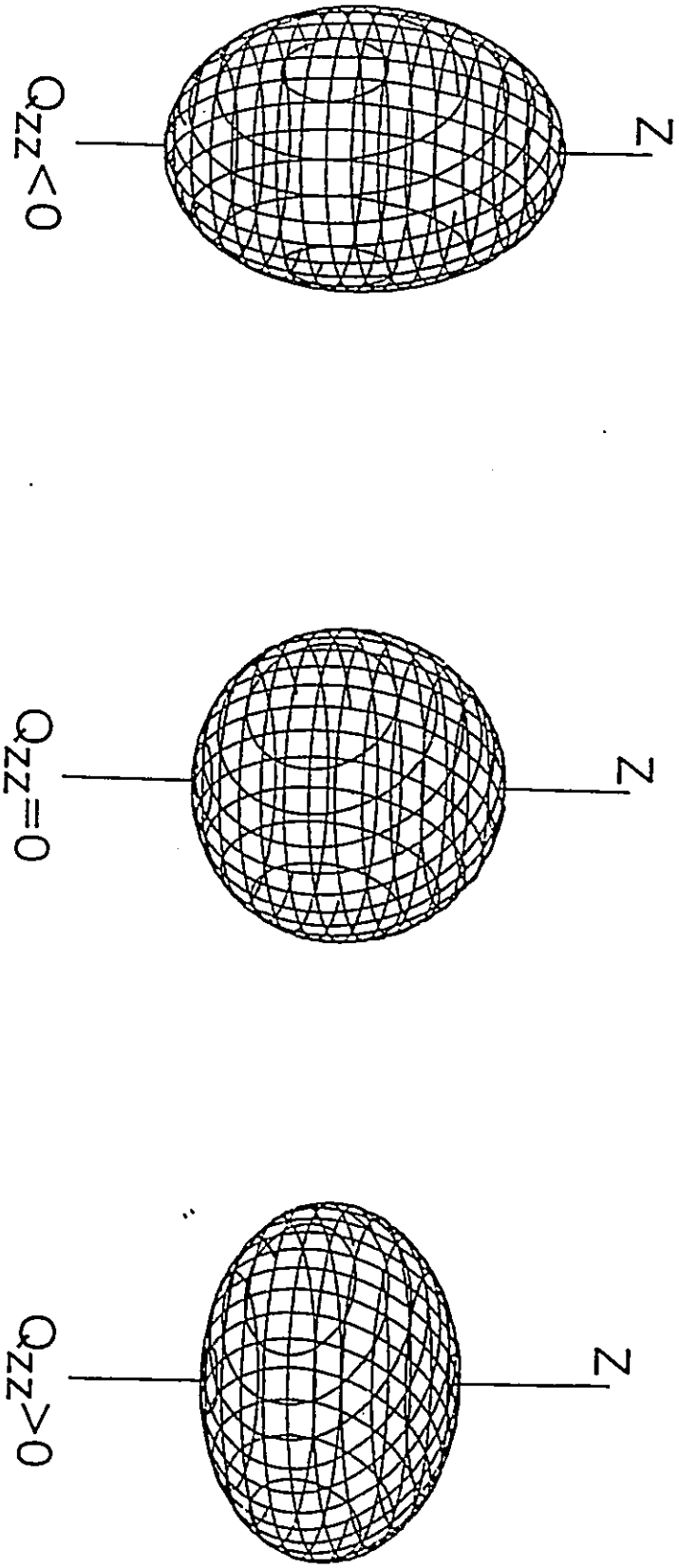
$Q_{zz}>0$
Z
$Q_{zz}=0$
Z
$Q_{zz}<0$
Z

CHAPTER 2

The Mechanics of Hydrogen Bond Formation in Conjugated Systems.

This thesis is concerned with the relationship between changes in the distribution of electronic charge, brought about through some form of structural change or reaction, and the resultant energy changes. In this chapter the formation of hydrogen bonds resulting from the dimerization of formamide to its cyclic or open form is investigated. The hydrogen bonds in the cyclic dimer are interesting because they serve as a simple model for one of the two kinds of hydrogen bonds found in DNA base pairs. The cyclic dimer is slightly more than twice as stable as its open form, the energy changes on dimer formation being -6.6 and -6.1 kcal/mol per hydrogen bond respectively. This chapter demonstrates that an important factor governing the changes in the relative stabilities of the atoms on forming the dimers are the opposing flows of σ and π density through the conjugated N-C-O fragments.

THE MECHANICS OF HYDROGEN BOND FORMATION IN CONJUGATED SYSTEMS

J.R. CHEESEMAN, M.T. CARROLL and R.F.W. BADER
Department of Chemistry, McMaster University, Hamilton, Ontario, Canada L8S 4M1

Received 28 October 1987

The theory of atoms in molecules provides an atomic view of the mechanics governing the interactions between molecules and as such it facilitates both an understanding of the interactions and the manner in which they can be modified. This theory is applied to a study of the changes in the energies, electron populations, volumes and moments of the atoms of formamide upon dimerization to form both the cyclic and open hydrogen-bonded structures. An important factor governing the changes in the relative stabilities of the atoms on forming the dimers are the opposing flows of σ and π density through conjugated N–C–O fragments, as measured by the shift in the electron populations into or out of the plane of the nuclei over each of the atomic basins and by the changes in the ellipticities of the atomic distributions.

1. Introduction

One of the two kinds of hydrogen bonds found in DNA base pairs, the –CO–HN– bond, occurs in the cyclic formamide dimer. This dimer can serve as a simple model of the hydrogen bond structure found in DNA [1]. In view of recent theoretical studies of hydrogen bonding in DNA base pairs [2], we wish to show how the theory of atoms in molecules [3–5] can be applied to determine the mechanics of hydrogen-bond formation at the atomic level. The extra stability associated with the formation of the cyclic dimer is determined by comparing its atomic properties with those of the open dimer which has but a single hydrogen bond.

An atom in a molecule is defined as a region of space bounded by a surface that satisfies the quantum boundary condition of zero flux in the gradient vector field of the charge density as expressed in

$$\nabla\rho(\boldsymbol{r})\cdot\boldsymbol{n}(\boldsymbol{r})=0 \quad \text{for every point } \boldsymbol{r} \text{ on the surface.} \tag{1}$$

The theory of atoms in molecules defines the average value of each observable for an atom in a molecule. These atomic averages obey the same quantum-mechanical relationships such as the Ehrenfest and virial theorems as do the average values for the entire system and the molecular average of an observable is given by the sum of its atomic contributions. The energy of atom Ω, $E(\Omega)$, is defined in terms of the virial theorem, which gives the potential energy as the virial of the Ehrenfest forces acting on the electrons over the basin of the atom. For a molecule at an energy minimum, the sum of the atomic energies equals the total energy of the system, including the nuclear repulsion. The average electron population of an atom $N(\Omega)$ is obtained by the integration of $\rho(\boldsymbol{r})$ over the basin of the atom and its net charge $q(\Omega)$ is given by the difference between the nuclear charge Z_Ω and $N(\Omega)$. The volume of an atom $v(\Omega)$, is defined to be a measure of the space enclosed by the intersection of the atomic surface with the 0.001 au charge density envelope. The changes in the energy, charge and volume of the atoms incurred on hydrogen-bond formation are the properties considered here. Calculation of the atomic properties and the analysis of the charge density are accomplished using the program PROAIM [6]. The theory has previously been applied to a study of the hydrogen bonds formed in the homo and hetero dimers of water and ammonia and in the corresponding protonated species [7].

The DNA base pairs and the model dimers possess a plane of symmetry. Because of this, one may distinguish between σ and π contributions to an atomic

0 009-2614/88/$ 03.50

population, the former contribution arising from the orbitals symmetric with respect to the symmetry plane, the latter coming from the orbitals which possess a nodal surface in this plane [8]. We shall demonstrate that an important factor governing the energy changes caused by the formation of hydrogen bonds in these molecules is the accompanying change in the relative contributions of the σ and π densities to the total atomic populations as caused by inter- and intra-atomic transfers of charge to these two partial populations. This transfer of density affects the conjugated system of charge which exists in the monomer and the resulting energy changes accompanying hydrogen bond formation in such a conjugated system differ markedly from those found for non-conjugated systems [7].

The most important characteristic of an atom is that the constancy in its properties, including its contribution to the total energy of a system, is observed to be directly determined by the constancy in its distribution of charge. When this distribution is the same in two different molecules, then the atom makes the same contributions to the total energy and all other properties in both systems. It is at this limit of near-perfect transferability that one can determine the properties of atoms in molecules experimentally, as corresponding additive contributions, and it has been demonstrated that the methyl and methylene groups as defined by theory recover their measured contributions to the heats of formation of normal hydrocarbons [9,10]. When the methylene group is placed in a cyclic or bicyclic system with geometric strain, there is a small change in its charge distribution corresponding to a shift in charge from the hydrogens to the carbon. The associated change in the total energy of the group is found to match the experimentally measured strain energy [9]. These examples demonstrate that quantum mechanics can be used to predict the properties of atoms in molecules, just as it predicts the properties of a total system and they show that whether the form of an atom changes by a little or by a lot, its energy and other properties change by corresponding amounts. The changes in the atomic energies encountered on the formation of a hydrogen bond are in direct response to the changes incurred in the distribution of charge over each atom in the system.

2. Molecular structure, geometry and energy

The topology of the charge density and its associated gradient vector field determines molecular structure. The interaction of two atoms leads to the formation of a (3, −1) critical point in the charge density [4,5]. A critical point in the charge density ρ, a point where $\nabla\rho = 0$, is classified in terms of the properties of the eigenvalues λ_i of its matrix of second derivatives as (rank, signature): rank is the number of non-zero eigenvalues and signature the algebraic sum of their signs. The eigenvectors associated with the two negative eigenvalues of a (3, −1) critical point define a set of trajectories of $\nabla\rho$ all of which terminate at this critical point thereby yielding the interatomic surface. This is the surface of zero flux, eq. (1), which separates the basins of the neighbouring atoms. The single positive eigenvalue defines a unique pair of trajectories that originate at this same critical point and define the atomic interaction line [4,11] – a line linking the nuclei of the two atoms along which the charge density is a maximum with respect to any neighbouring line. For a molecule in an equilibrium geometry this line is called a bond path and the existence of a bond path between a pair of nuclei is a necessary and sufficient condition for the existence of a bond between the atoms [11]. The network of bond paths defines the molecular graph and the structure of the molecule as illustrated in fig. 1.

All results are obtained from single-determinant SCF calculations using the 6-31G** basis set for geometries optimized at the 4-31G level. The energies and geometrical parameters are given in table 1. The open dimer was constrained to have the "trans" geometry illustrated in fig. 1 to prevent its closure to the cyclic form. Otherwise its geometry is fully optimized. The cyclic dimer is slightly more than twice as stable as its open form, the energy changes on dimer formation being −6.6 and −6.1 kcal mol^{-1} per hydrogen bond respectively. Geometry changes for the molecules participating in the hydrogen bonds are small, the NH_b bond length (where H_b is the H-bonded hydrogen) increasing by only 0.014 Å on formation of the cyclic dimer, for example.

The values of ρ and $\nabla^2\rho$ at a bond critical point r_c of the dimers are given in table 2 together with the changes from the monomer values. The relatively low

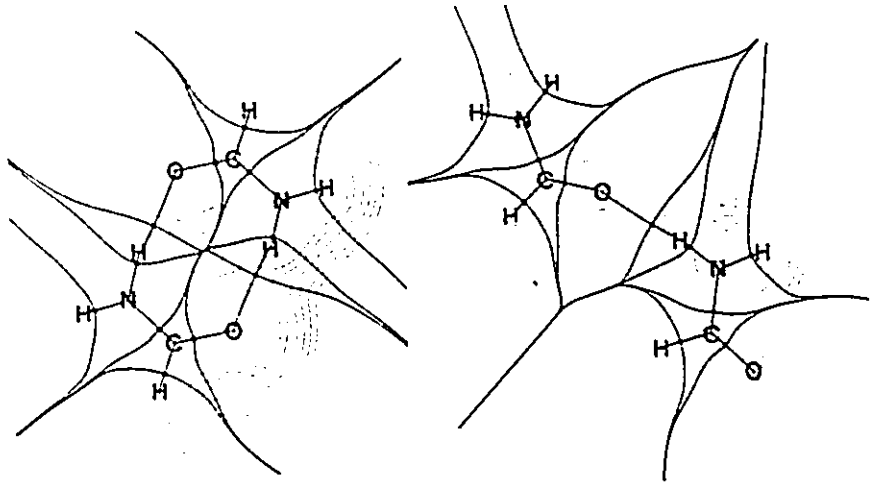

Fig. 1. Contour maps of the electronic charge density in the cyclic and open formamide dimers. The positions of (3, −1) or bond critical points in ρ are indicated by a dot. The pairs of trajectories which originate at each such critical point and define a bond path are shown, as are the pairs of trajectories which, in this plane, terminate at each such critical point and mark the intersection of the interatomic surface with the plane. The central point in the cyclic dimer is a (3, +1) or ring critical point for which $\rho = 0.0036$ au. The near planarity of an interatomic surface between H_b and O is characteristic of a hydrogen bond. The bond paths of the hydrogen bonds are noticeably inwardly curved in the cyclic dimer. The value of the outermost contour is 0.001 au. The remaining contours increase in value in steps 2×10^n, 4×10^n and 8×10^n with n starting at −3 and increasing in steps of unity.

Table 1
Calculated equilibrium geometries for formamide and its dimers [a]

Parameter	Monomer	Cyclic dimer	Open dimer	
			acid subunit	base subunit
CO	1.216	1.230	1.221	1.221
CN	1.347	1.328	1.338	1.338
CH_c	1.081	1.080	1.082	1.079
NH_s	0.992	1.006 [b]	0.992	0.993
NH_a	0.989	0.990	0.997 [b]	0.990
OH_b	–	1.903	1.959	
NO	–	2.898	2.951	
COH_b	–	125.4	161.1	
NH_bO	–	169.2	173.3	
NCO	124.7	125.1	125.6	124.4
NCH_c	113.8	115.0	113.3	114.3
H_cCO	121.5	119.9	121.0	121.3
CNH_s	119.5	120.3	119.1	119.7
CNH_a	121.9	120.9	121.5	121.9
H_aNH_s	118.6	118.8	119.4	118.5
SCF energy	−168.93953	−337.89992	−337.88881	

[a] Geometrical distances and angles are in Å and deg. Energies are in au. The subscripts s and a denote the hydrogens which are syn and anti to the keto oxygen, respectively. The subscripts b and c denote the hydrogen-bonded hydrogen and the hydrogen bonded to carbon, respectively.

[b] Geometrical distance to the hydrogen-bonded hydrogen.

Table 2
Values of the charge density and Laplacian at bond critical points [a]

	Bond	$\rho(r_c)$	$\nabla^2\rho(r_c)$
cyclic dimer	CO	0.4025 (−0.0122)	0.0204 (−0.1260)
	CN	0.3495 (0.0161)	−0.8271 (−0.0562)
	NH_b	0.3445 (−0.0160)	−1.9800 (0.0387)
	OH_b	0.0265	0.0882
	NH	0.3648 (0.0007)	−2.0328 (−0.0042)
	CN	0.3084 (0.0011)	−1.2815 (−0.0099)
open dimer			
acid	CO	0.4111 (−0.0046)	0.0959 (−0.0506)
	CN	0.3416 (0.0082)	−0.8043 (−0.0334)
	NH_b	0.3561 (−0.0081)	−2.0244 (0.0042)
	OH_b	0.0205	0.0773
base	CO	0.4096 (−0.0061)	0.0999 (−0.0465)
	CN	0.3404 (0.0070)	−0.7850 (−0.0141)

[a] All values in au. Numbers in parentheses represent the change from the monomer value. H_b denotes the hydrogen-bonded hydrogen.

values of $\rho(r_c)$ together with the positive values for $\nabla^2\rho(r_c)$ for the hydrogen bond critical points are typical of closed-shell interactions for which charge is removed from the interatomic surface and concentrated separately in the basins of the interacting atoms, while the larger values of ρ and negative values for $\nabla^2\rho$ as found for the N–H and C–H bonds are typical of shared interactions for which charge density is contracted towards the bond path and accumulated in the interatomic surface [11]. The value of $\rho(r_c)$ for hydrogen bonds has been shown to increase with an increase in the hydrogen bond strength [7,12] and the value is greater for the cyclic than for the open dimer. Correspondingly, the changes in the values of $\rho(r_c)$, negative for the neighbouring N–H_b and C–O bonds and positive for the C–N bonds, are twice as large for the cyclic dimer as for its open form.

The two negative eigenvalues λ_i at r_c, i.e. the curvatures of ρ directed perpendicular to the bond path at the bond critical point, serve to define ϵ, the ellipticity of a bond [13]. This quantity provides a measure of the extent to which electronic charge is preferentially accumulated in a given plane and is defined as $\lambda_1/\lambda_2 - 1$, where λ_2 is the negative curvature of smallest magnitude. The axis of λ_2 defines the major axis of the elliptical contours of the charge density about the bond axis. In ethylene for example, the ellipticity of the carbon–carbon bond is 0.45 au with λ_2 being directed along the π axis, and electronic charge is preferentially accumulated in the π plane of the C–C bond in this molecule.

For homopolar bonds the ellipticity remains essentially constant over the valence regions of both atoms and the value of ϵ at the bond critical point is a useful measure of the preferred spatial arrangement of the valence density. This is illustrated in diagrams (a) and (b) of fig. 2, which show the variation in the magnitude of ϵ along the length of a carbon–carbon bond in ethylene and benzene. The value of ϵ goes through zero at 0.5 to 0.6 au from a carbon nucleus and the direction of the major axis flips by 90° so that the density of the core is very slightly polarized into the plane of the nuclei, a reflection of the dominant contribution of the sp^2 hybridized density to this region of space. For heteropolar bonds with significant charge transfer between the atoms, the value of ϵ at the bond critical point is not indicative of the preferred plane of polarization of the valence density. This is illustrated by diagrams (c) and (d) of fig. 2, which show the variation in ϵ along the C–N and C–O bonds of the formamide monomer. There is considerable charge transfer from C to both N and O, and consequently the associated bond critical points are found at distances from the C nucleus only slightly greater than the core radius of the carbon atom (figs. 1 and 2). The major axis of the relatively small ellipticity found in the region of the carbon is in the plane of the nuclei in both bonds but flips into the π plane just after the bond critical point is reached. Thus most of the π density lies within the basin of the N atom in the C–N bond. In the C–O bond the major axis undergoes a second flip and while the valence density in the central region of the bond is preferentially accumulated in the π plane, this direction changes back to the plane of the nuclei closer to the oxygen nucleus. The differing behaviour of the ellipticity over the basins of the N and O atoms is in accord with the locations of the regions of charge concentration in the valence shells of these atoms as determined by the Laplacian of the charge distribution, a function whose topology recovers the Lewis model of localized electron pairs [14]. This distribution shows that oxygen possesses two non-bonded charge concentrations in the plane of the nuclei while

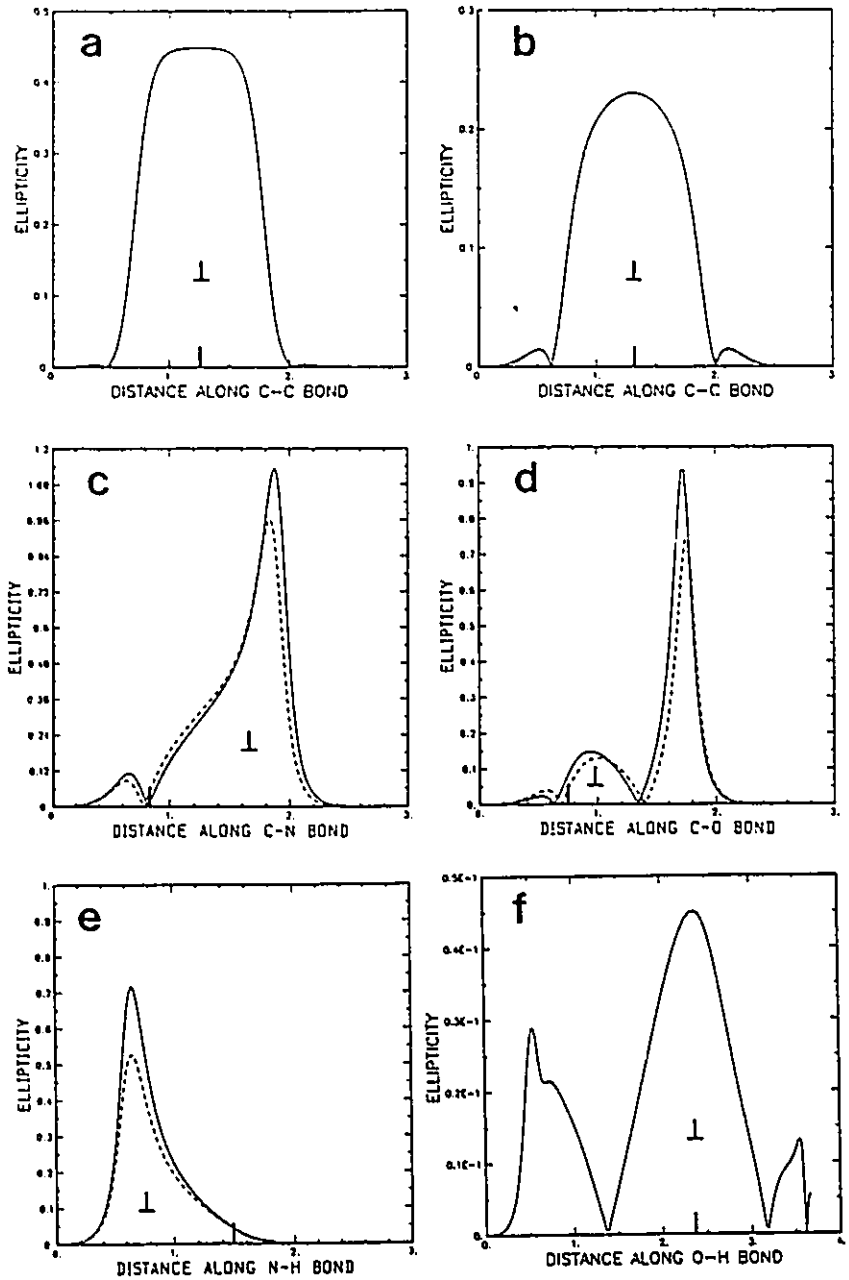

Fig. 2. Values of the bond ellipticity as a function of position along the bond. The bond critical point is denoted by a vertical bar. The presence or absence of the symbol ⊥ indicates that the major axis of ϵ is perpendicular to the plane of the nuclei or lies in this plane, respectively. The solid curves are for the monomer except for (f) which, along with the dashed curves, refer to the cyclic dimer. Note the changes in scale between the different plots. The left-hand nucleus is at the origin of each plot. Distances are in au.

the nitrogen has two smaller non-bonded maxima, one above and one below this plane [14]. The fact that the major axis of the ellipticity lies in the plane of the nuclei for the carbon atoms is also in accord with the properties of the Laplacian distribution, which shows the presence of regions of charge de-

ficiency above and below the plane of the nuclei for this atom. Because of the transfer of π charge to the N and O atoms, the carbon charge distribution is dominated by the sp^2 hybridization pattern.

A more detailed description of the π character of a charge distribution afforded by these parameters for the total charge density shows that the classical picture of a continuous delocalization of charge extending over a set of conjugated bonds is, in general, not correct. That the parameters used to define ε are indeed physically relevant is illustrated by fig. 3.

Other diagrams in fig. 2 illustrate the effect that the formation of a hydrogen bond has on the ellipticities of the C–N, C–O and N–H bonds for the case of the cyclic dimer. There is a significant decrease in the ellipticity across the basin of the N atom and in the in-plane ellipticity of the oxygen atom. The values of the ellipticity averaged along the bond path between pairs of points where ε goes through zero (see fig. 2) are given in table 3. The major axis of the ellipticity of the N–H bond is in the perpendicular plane and nearly the whole of the contribution comes from within the nitrogen basin. Its value decreases on formation of the H bond (fig. 2e). The ellipticity along a hydrogen bond is small in magnitude and its major axis, as in the C–O bond, flips both out of and back into the plane of the nuclei, fig. 2f.

Table 3
Average ellipticities along bond paths [a]

System	Bond	1	2	3
formamide	CO	0.009	0.100	0.241
	CN	0.039	0.343	
	NH_s	0.175		
	NH_a	0.183		
cyclic dimer	CO	0.016	0.089	0.188
	CN	0.031	0.341	
	NH_b	0.140		
	OH_b	0.012	0.026	0.008
open dimer				
acid	CO	0.011	0.092	0.235
	CN	0.034	0.327	
	NH_b	0.250		
	OH_b	0.115	0.017	
base	CO	0.013	0.092	0.219
	CN	0.037	0.342	

[a] The separate regions over which the ellipticity is averaged, are distinguished by a change in direction of the major axis along the bond path starting from the left-hand nucleus in each case (see fig. 2).

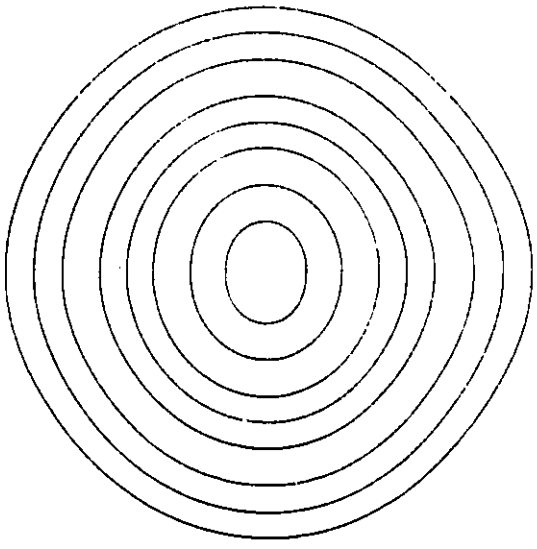

Fig. 3. Contour plot of the charge density perpendicular to the bond path of the C–N bond in the monomer at the point where ε attains its maximum value (see fig. 2c). The open crosses denote the positions of the out-of-plane nuclei and they define the molecular plane. The elliptical form of the inner contours reflect the properties of a charge distribution with noticeable π character.

Study of the ellipticities shows that there are substantial reorganization of electronic charge within the basins of the N and O atoms which correspond to a transfer of out-of-plane density into the plane of the molecule for the N atom, and to the reverse of this for oxygen. These changes are shown to correlate with the changes in the π populations of the N and O atoms.

3. Atomic properties

The atomic populations, energies and volumes for the formamide monomer are given in table 4, together with the changes in these properties on formation of the cyclic and open dimers. The net charges on the atoms are also listed. The C atom loses charge to both the N and O atoms and C bears a substantial net positive charge. The N atom withdraws charge

Table 4
Average electron populations, energies and volumes of formamide and changes following dimerization [a]

	Ω	$N(\Omega)$	$E(\Omega)$	$V(\Omega)$	$N_s(\Omega)$	$q(\Omega)$
monomer	O	9.3703	−75.58890	131.39	1.706	−1.370
	N	8.4805	−55.25862	120.67	1.846	−1.480
	C	4.0525	−36.57949	36.65	0.398	1.948
	H_s	0.5247	−0.42062	25.28	0.016	0.475
	H_a	0.5424	−0.43344	25.92	0.018	0.458
	H_c	1.0294	−0.65851	50.36	0.016	−0.029
	total	23.9998	−168.93958	390.27	4.000	
	SCF		−168.93953			
	Ω	$\Delta N(\Omega)$	$\Delta E(\Omega)$	$\Delta V(\Omega)$	$\Delta N_s(\Omega)$	$q(\Omega)$
cyclic dimer [b]	O	0.0291	8.5	−4.64	0.046	−1.399
	N	0.0724	−47.9	2.41	−0.030	−1.553
	C	−0.0020	−2.4	−0.87	−0.010	1.950
	H_b	−0.1048	38.3	−10.46	−0.004	0.580
	H_s	0.0077	−3.1	0.38	−0.001	0.450
	H_c	−0.0025	−0.1	−0.22	−0.001	−0.027
	total	−0.0002	−13.4	−26.80	0.001	
	SCF		−13.1			
open dimer [b]						
acid	O	0.0151	5.2	0.60	0.016	−1.385
	N	0.0522	−30.7	1.46	−0.012	−1.533
	C	−0.0065	2.5	−0.55	−0.002	1.954
	H_b	−0.0826	27.9	−8.63	−0.004	0.540
	H_s	0.0189	−7.0	1.22	0.002	0.456
	H_c	0.0123	−3.4	0.57	0.000	−0.042
base	O	0.0213	0.8	−2.58	0.024	−1.392
	N	0.0057	−10.5	−0.13	−0.008	−1.486
	C	0.0005	−2.3	−0.14	−0.012	1.947
	H_s	−0.0082	2.9	−0.43	−0.002	0.484
	H_a	−0.0110	3.9	−0.58	0.000	0.469
	H_c	−0.0182	4.4	−1.00	−0.002	−0.011
	total	−0.0005	−6.3	−10.19	0.000	
	SCF		−6.1			

[a] All values are in au except energy changes, which are in kcal mol^{-1}. The manner in which the energy of an atom is determined from its average kinetic energy via the atomic virial theorem is detailed in ref. [9]. The subscripts s and a denote the hydrogens which are syn and anti to the keto oxygen, respectively. The subscripts b and c denote the hydrogen-bonded hydrogen and the hydrogen bonded to carbon, respectively.

[b] Atomic property changes are given by subtracting the monomer values from the corresponding dimer values.

from two H atoms as well as from C and it bears the largest net negative charge. Of these two hydrogens, the one syn to oxygen has the largest positive charge and it forms the hydrogen bond in the cyclic dimer. The H atom bonded to C bears a small negative charge and the less contracted nature of its charge distribution compared to that of the amide hydrogens (fig. 1) is reflected in its volume being approximately twice as great.

The cyclic dimer is discussed first. Essentially all the changes in population, energy and volume are confined to the atoms of the N–H_b–O fragments. De-

noting N and O as the acid and base atoms respectively, H_b loses charge to both and as in the formation of H bonds in the neutral water and ammonia dimers [7], the acid atom gains more charge than does the base atom. The volume decrease accompanying the formation of the two H bonds in the cyclic dimer is 26.8 au, nearly all of which results from the formation of the new interatomic surfaces between the H_b and O atoms. The volumes of the N atoms increase slightly as a result of their increased populations.

The substantial loss of charge by the hydrogen causes its energy to increase. While both the acid and base atoms gain charge as in the water and ammonia dimers, unlike these latter systems, only the acid atom is stabilized and it is this stabilization which is responsible for the overall energy decrease accompanying the formation of the hydrogen bonds. The differing behaviour of the O and N atoms with respect to an increased electron population can be seen in the accompanying changes in their σ to π population ratios, changes which are anticipated on the basis of the behaviour of the ellipticities along the C–N and C–O bond paths. As suggested by the changes in the ϵ values, the π population of the O atom increases and this increase is greater than the charge transferred to this atom. Thus in addition to the charge transferred to its π population, there is an accompanying promotion of $0.017e$ from its σ to its π system and the O atom is destabilized. The N atom on the other hand, as again anticipated by the changes in the ϵ values of the C–N and N–H bonds, undergoes a decrease in its π population and hence the total increase in its σ population is the interatomic charge transfer plus the π to σ polarization, or $0.102e$. The C atom, while losing a small amount of charge, undergoes a π to σ polarization which is five times greater than its loss of charge and there is a small stabilizing energy change for this atom.

These changes in atomic charge distributions are characteristic of an interaction between two closed-shell systems with an accompanying transfer of charge leading to ionic binding [7,11]. Because of the Pauli principle and as reflected in the low value of $\rho(r_c)$, charge is removed from the interatomic surface where the hydrogen of the acid and the oxygen of the base molecule come into contact to form the new interaction. This results in the positive charge on the H of the acid increasing through a polarization of its charge density away from the negatively charged base to yield a σ charge transfer from H to N. The net negative charge on the base atom O is increased by a smaller transfer of charge to its π system. This π density is polarized towards the positively charged H of the acid, charge being removed from the σ system of O as a result of the contact of two closed-shell systems. The O atom is polarized towards C but because of the polarization of its density towards H in the dimer the magnitude of the first moment of the charge distribution of the O atom is reduced to 0.63 au from its value of 0.70 au in the monomer. Thus the positively charged H atom and the negatively charged O atom are polarized in a direction counter to the direction of charge transfer from acid to base, as characteristic of an ionic interaction.

The changes in atomic charge distributions of the NCO fragments correspond to opposing flows of σ and π charge, as coupled and initiated by the hydrogen bonds and these flows, together with the loss of charge by H, dominate the energy change. σ density is maximally concentrated in the plane of the nuclei and is bound more tightly by the nuclear–electron attractive force than is π density, which has a node in this plane. An atom which experiences a net gain in its σ over its π population, whether its total population increases or decreases, is stabilized, viz. the N and C atoms, while one which experiences a net loss in its σ relative to its π population is destabilized even though its total population is increased, albeit by a lesser amount, viz. the O atom. These are the energy changes resulting from the coupling of two conjugated systems via the formation of hydrogen bonds.

The patterns of change in the atomic properties for the formation of the open dimer are the same for corresponding atoms as for the formation of the cyclic dimer, but are, in general, of reduced magnitude. The increase in the π population of the oxygen atom of the base is only one-half as great as in the cyclic case and more nearly equal to the charge transferred to this atom. The near balance in charge gain and charge promotion results in a near-zero energy change for the oxygen atom. It is interesting to note that the N atom of the base and the O atom of the acid in the open dimer mimic on a smaller scale the changes in charge, in σ–π polarizations and in energy the

changes for the O and N atoms which are directly involved in the H bond formation. Clearly the formation of one hydrogen bond changes the system in such a way as to facilitate the formation of the second such bond.

References

[1] M.J. Wojcik, A.Y. Hirakawa, M. Tsuboi, S. Kato and K. Morokuma, Chem. Phys. Letters 100 (1983) 523.

[2] P. Hobza and C. Sandorfy, J. Am. Chem. Soc. 109 (1987) 1302;
E. Clementi, S. Chin and D. Logan, Israel J. Chem. 27 (1986) 127;
P. Otto, E. Clementi, J. Ladik and F. Martino, J. Chem. Phys. 80 (1984) 5294;
J.E. del Bene, J. Phys. Chem. 87 (1983) 367;
J. Maranon, H. Grinberg and N.S. Nudelman, Intern. J. Quantum Chem. 22 (1982) 69.

[3] R.F.W. Bader and T.T. Nguyen-Dang, Advan. Quantum Chem. 14 (1981) 63.

[4] R.F.W. Bader, T.T. Nguyen-Dang and Y. Tal, Rept. Progr. Phys. 44 (1981) 893.

[5] R.F.W. Bader, Accounts Chem. Res. 9 (1985) 18.

[6] F.W. Biegler-Konig, R.F.W. Bader and T.H. Tang, J. Comput. Chem. 3 (1982) 317.

[7] R.F.W. Bader, M.T. Carroll, J.R. Cheeseman and C. Chang, J. Am. Chem. Soc., to be published.

[8] K.B. Wiberg and J.J. Wendolowski, Proc. Natl. Acad. Sci. US 78 (1981) 6561.

[9] K.B. Wiberg, R.F.W. Bader and C.D.H. Lau, J. Am. Chem. Soc. 109 (1987) 1001.

[10] R.F.W. Bader, A. Larouche, C. Gatti, M.T. Carroll and P.J. MacDougall, J. Chem. Phys. 87 (1987) 1142.

[11] R.F.W. Bader and H. Essen, J. Chem. Phys. 80 (1984) 1943.

[12] R.J. Boyd and S.C. Choi, Chem. Phys. Letters 120 (1985) 80; 129 (1986) 62.

[13] R.F.W. Bader, T.S. Slee, D. Cremer and E. Kraka, J. Am. Chem. Soc. 97 (1983) 5061.

[14] R.F.W. Bader, P.J. MacDougall and C.D.H. Lau, J. Am. Chem. Soc. 106 (1984) 1594.

CHAPTER 3

Hydrogen Bonding in Weakly Bound Complexes

3.1 Introduction

The objective of this work is to characterize the nature of weakly bound hydrogen bonded complexes in terms of properties of the electronic charge distribution. The complexes studied here span the range of weak interactions and include the van der Waals complexes NeHCl, NeHF, ArHCl and ArHF and also the progressively stronger interactions found in NNHCN, NNHCl, NNHF, HCNHCN, HCNHCl and HCNHF. The electronic charge distribution contains the information necessary to discuss molecular systems in chemical terms; atoms, bonds and molecular structure.

For an acid-base interaction YB-HA, a hydrogen bond results from the mutual penetration of the van der Waals envelopes of the hydrogen of the acid HA and the B atom of the base YB. These interactions involve very small geometry changes and little charge transfer between the base and the acid and consequently produce relatively small changes in the monomer charge distributions upon complex formation. This redistribution of charge can be measured by an examination of the dipole and quadrupole polarizations of the charge distribution.

The total dipole moment of a neutral molecule can be expressed as a sum of contributions resulting from internal polarizations and intramolecular charge transfer among the atoms of the acid and base fragments and also intermolecular charge transfer

between the acid and base fragments upon complex formation. It is experimentally observed that the dipole moment of an acid-base complex is always greater than the vector sum of the dipole moments of the isolated acid and base, an effect known as dipole moment enhancement (Legon and Millen 1986). These enhancements have contributions from the polarization of the atoms in the fragments and from any charge transfer which occurs upon the formation of the complex. Separation of the total molecular dipole into acid and base polarization and charge transfer contributions reveals the origin of the dipole moment enhancement.

These interactions are interesting in the sense that they provide information and characterize the weak end of the spectrum of molecular interactions. These "limiting" interactions have been of considerable interest to spectroscopists over the past several years and much effort, both experimentally and theoretically has been expended despite the difficulties their study presents. Techniques such as molecular beam electric resonance spectroscopy, pulsed-nozzle Fourier transform microwave spectroscopy, and infrared spectroscopy have been used to observe the spectra of dimers under the required conditions of low pressure in the gas phase (Legon and Millen, 1986). The goal of both experimental and theoretical studies is to understand how charge is distributed in molecules and in particular how it is reorganized in the formation of a complex or interaction. Provided that a very good theoretical description of the charge distribution exists, this information can be obtained, in a more direct way, from accurate and easy observations of the theoretical charge density.

While the results for stronger hydrogen bonds are qualitatively the same with or without the inclusion of electron correlation, weaker interactions require a better approximation of the wave function. The results presented here were all obtained from large basis set calculations with the inclusion of some electron correlation. The calculated geometries, dissociation energies, dipole moments, and electric field gradients

compare well with the experimental values, indicating that these theoretically determined charge densities are accurate.

Calculations

The charge distributions and geometry optimizations of all molecules were determined at the 6-311G(2d,2p) basis set using second order Møller-Plesset perturbation theory (MP2) (Møller and Plesset 1934) using the program Gaussian 90 (Frisch et al, 1990). The 6-311G(2d,2p) basis set is the 6-311G basis (Krishnan et al. 1980; McLean and Chandler, 1980) with a second set of polarizing functions on all atoms. Møller-Plesset perturbation theory is a systematic procedure for finding the correlation energy, which is not variational but is size consistent[1] at each level. In this approach, the total Hamiltonian of the system is partitioned into two parts: a zeroth order part which is a sum of the one electron Fock operators which have known eigenfunctions and eigenvalues, and a perturbation consisting of the two-electron Hartree-Fock potential operator and the electron-electron repulsions. The exact energy is then expressed as an infinite sum of contributions of increasing complexity.

All analyses of the charge distributions were performed using the AIMPAC series of programs, developed in this laboratory. The atomic properties were calculated using the AIMPAC program PROAIMV (Keith, 1992; Bielger-König, 1982).

Dissociation Energies

These weak interactions, as illustrated by the data in Table 3.1, have dissociation energies which range from 0.10 to 6.13 kcal/mole. Dykstra (1988) defines weak hydrogen-bonded complexes as those which have dissociation energies less than 12

[1] A method is said to be size consistant when the energy of a many-particle system, even in the presence of interactions, becomes proportional to the number of particles (N) in the limit N --> ∞ (Szabo and Ostlund, 1989)

kcal/mol. The effect of MP2 on the dissociation energy of many hydrogen bonded complexes has been reviewed by Hobza and Zahradnik (1988). While the calculated results for the stronger hydrogen bonds are qualitatively the same with or without the inclusion of electron correlation, calculations for weaker interactions are sensitive to the effects of electron correlation. The dissociation energies (D_e) in the first column of Table 3.1 are calculated as the difference between the sum of the energies (MP2) of the monomers and the total energy (MP2) of the complex. The experimental dissociation energies (D_e) are determined from absolute well depths of intermolecular potentials obtained by least-squares fitting to rotational spectra.

A comparison of the dissociation energies in the first column with the experimental dissociation energies show, with the exception of the two argon complexes, the calculated values to be too large. This discrepancy is a result of a phenenomenon known as basis set superposition error (BSSE) (Hobza and Zahradnik 1988, Mo' et al 1988, Frisch et al 1986, Boys and Bernardi 1970). This error arises because the basis set used to describe each reactant is larger for the complex than for the isolated monomer, where in the complex use can be made of the basis functions centered on the other reactant. Boys and Bernardi (1970) introduced a method known as "function counterpoise" to correct for BSSE. In this method, the energies of the separated reactants are calculated with the full compliment of basis functions used in the calculation of the complex. This is accomplished for the calculation of each monomer by including ghost functions centered at locations of the other nuclei which are present in the complex. Dissociation energies which include correction for BSSE are given in the second column of Table 3.1 and are calculated by the following expression where E denotes the MP2 energy:

$$D_e(\text{BSSE}) = D_e - \sum_{\text{monomers}} [E(\text{monomer}) - E(\text{monomer + ghosts})]$$

Thus, the counterpoise correction always decreases the interaction energy. With the exception of the two complexes involving Ar, the dissociation energies which include a correction for BSSE are closer to the experimental values. The correction the dissociation energy for BSSE is not required for the two complexes, ArHCl and ArHF, due to the diffuse nature of argon.

Schwenke and Trular (1985) have shown that using large basis sets (though not including electron correlation), so that the counterpoise correction is small, does not guarantee accurate results for the interaction energy of two HF molecules. They have also shown that even for smaller basis sets the inclusion of counterpoise corrections does not systematically improve the accuracy of the calculations. Corrections using the counterpoise method here however give dissociation energies which are close to the experimentally determined values. The fact that these calculations, in general, reproduce the experimentally determined dissociation energies suggests that this basis set with the inclusion of electron correlation at the MP2 level provides a good description of the charge density.

Changes in Reactant Geometries

All of the geometries for these ten complexes were assumed to be linear in accord with experimental observation. Table 3.2 gives the values of the calculated and experimental geometric distances and also the changes which occur during complex formation. The changes in the original monomer bond lengths upon complexation are very small especially in the very weak van der Waals complexes. In NeHX, and ArHX where X is Cl or F, the H-X internuclear distance remains essentially the same. For the NNHX and HCNHX complexes, the H-X bond lengths increase according to the strength of the interaction. The N-N internuclear distance remains essentially the same in NNHCN and NNHCl and decreases by only 0.0018 au for NNHF. When HCN behaves

as a base, the C-N internuclear distance decreases and the H-C internuclear distance increases by a much smaller amount. When HCN behaves as an acid the H-C internuclear distance increases by 0.0030 and 0.0117 au for NNHCN and HCNHCN respectively, while the C-N distance also increases but by a much smaller amount. Except for the two Ar complexes, the calculated internuclear separations of the two heavy atoms on either side of the hydrogen bond underestimate the experimental values from 0.001 to 0.3 au. For ArHCl and ArHF, the calculated value of the Ar-X internuclear separation overestimates the experimental value by 0.1 and 0.04, respectively. The hydrogen bond length for these complexes (Tables 3.2 and 3.3) is found to decrease as the strength of the interaction increases within a given base series. For example, in NN-HCN, NNHCl and NNHF, the hydrogen bond lengths are 4.564, 4.327 and 3.922 au, respectively. The hydrogen bond lengths found in the van der Waals complexes are rather large, with the largest distance being 5.3 au for ArHCl.

3.2 Characterization of the Weak Hydrogen Bonded Interactions

For an acid-base complex YB-HA, a hydrogen bond results from the mutual penetration of the van der Waals envelopes of the H atom of the acid and the B atom of the base. Fig. (3.1) contains gradient vector field maps of the charge density for NeHCl, ArHF, NNHCN and HCNHF. Fig. (3.2) displays contour maps of the charge density out to the 0.001-au density envelope for these same molecules and the isolated reactants with the bond paths and interatomic surfaces overlaid. The 0.001-au density envelope contour for inert gases, hydrocarbons and hydrogen bonded complexes of ammonia and water is in agreement with the equilibrium diameters of these molecules as determined by second virial coefficient or viscosity data fitted with a Lennard-Jones 6-12 potential (Bader et al, 1987; Bader and Preston, 1970). It is apparent from these maps that the charge distributions of the complexes are the same as the monomer distributions out to the 0.02-

au contour and that only the four outermost contours (0.001, 0.002, 0.004, 0.008) are perturbed as a result of the mutual penetration.

As discussed in Chapter 1, a (3,-1) critical point is found between every pair of bonded nuclei which are considered to be linked by a chemical bond. The value of the charge density at the hydrogen bond critical point, denoted as $\rho(r_c)$ in Table 3.3, is very small for these weak interactions as compared to $\rho(r_c)$ between the remaining nuclei or in the isolated reactants (Table 3.5). As observed previously (Carroll et al 1988, Carroll and Bader 1988; Boyd and Choi, 1986), the value of the charge density at the hydrogen bond critical point increases with the strength of the interaction.

The sign of the Laplacian of ρ at the bond critical point is determined by the positive curvature (λ_3)[1] of ρ along the bond path (Chapter 1). When $\nabla^2\rho(r_c) < 0$, electronic charge is concentrated in the internuclear region as a result of the dominance of the perpendicular contractions of ρ towards the bond path. The result is a sharing of electronic charge by both nuclei, as is found for interactions usually characterized as covalent or polar, and are refered to as "shared interactions". For molecules with shared interactions, the ratio of the perpendicular contractions of ρ to its parallel expansion, as measured by the ratio $|\lambda_1|/\lambda_3$, is greater than unity. When $\nabla^2\rho(r_c) > 0$, the interaction is dominated by the contraction of charge away from the interatomic surface towards each of the nuclei. In this case, the ratio $|\lambda_1|/\lambda_3 < 1$ and the interaction is termed "closed-shell".

The value of the Laplacian at the hydrogen bond critical point is found to be positive for all of these interactions, implying that charge is removed from the new interatomic surface between hydrogen and the B atom of the base and concentrated in the individual atomic basins (Table 3.4). The values of the Laplacian at the remaining bond critical points in the complex and in the isolated reactants are negative, indicative of

[1] The interaction of two atoms leads to the formation of a critical point in the charge density at which the Hessian of ρ has one positive eigenvalue labeled λ_3 and two negative eigenvalues labeled λ_1 and λ_2.

shared interactions (Table 3.5). The kinetic energy density, $G(r_c)$, evaluated at the hydrogen bond critical point, is expressible in terms of three contributions along orthogonal axes. The relative values of the component parallel to the internuclear axis, ($G_{||}$) and one of the components perpendicular to this axis, ($G_{\perp}$) faithfully reflect the magnitudes of the corresponding curvatures of ρ at the position of the bond critical point. For these closed-shell hydrogen bonded interactions, $G_{\perp}(r_c) < G_{||}(r_c)$ while just the reverse situation is found for the shared interactions in the isolated reactants (Tables 3.4 and 3.5). As anticipated on the basis of the local virial theorem,

$$(\hbar^2/(4m))\nabla^2\rho(\mathbf{r}) = V(\mathbf{r}) + 2G(\mathbf{r})$$

where $V(\mathbf{r})$ is the potential energy density (its integral over all space yields the total electronic potential energy V), the ratio of the kinetic energy per electronic charge, $G(r_c)/\rho(r_c)$, is close to unity for these closed-shell hydrogen-bonded interactions and << 1 for the shared interactions (Tables 3.4 and 3.5)

Contour maps of the Laplacian of the charge density for the complexes: NeHCl, ArHF, NNHCN and HCNHF are displayed in Fig. 3.3, where the solid lines (negative values of the Laplacian) represent regions of charge concentration and dashed lines represent regions of charge depletion (positive values of the Laplacian). The negative regions of the Laplacian are separately localized in each acid or base fragment in a pattern similiar to that found in the isolated reactants. The Laplacian of ρ is positive over the entire region of the hydrogen bonded interaction as a result of the kinetic energy contribution to the virial from this region being greater than the contribution from the potential energy (Chapter 1). It is apparent from these maps that the (closed-shell) B-H interatomic surface where $\nabla^2\rho(r_c) > 0$ is much less curved than the (open-shell) H-X interatomic surface where $\nabla^2\rho(r_c) < 0$. This observation appears to be general for hydrogen-bonded systems (Bader 1990).

Fig. 3.4 displays profile plots of the Laplacian for the argon atom along a radial line from the nucleus and for ArHF along the internuclear axis. In the map for ArHF, the Ar atom possesses all three quantum shells of charge concentration and charge depletion. Only the outer region of charge depletion of argon is perturbed as a result of this weak interaction. Similiar results are also observed in the other van der Waals complexes.

As found previously (Bader, 1990), a hydrogen bond results from the interaction of two closed-shell systems. The properties of ρ at the associated bond critical point in these weakly bound complexes reflect all of the characterisities associated with closed-shell interactions: a low value for $\rho(r_c)$, $\nabla^2\rho(r_c) > 0$, $|\lambda_1|/\lambda_3 << 1$ and $G(r_c)/\rho(r_c) = 1$.

Carroll and Bader (1988) demonstrated a correlation between the relative penetration of the acid and base atoms and the strength of the interaction for several hydrogen bonded complexes. A measure of the extent of penetration is the difference between the bonded radii of the H and B atoms atom in the complex and their van der Waals non-bonded radius in the isolated reactant. The bonded radii of the B and H atoms (r_B and r_H respectively), the distance of a bond critical point to the corresponding nucleus, are given in Table 3.3. Each value is less than the corresponding van der Waals non-bonded radius, the distance of the H or B atom to its non-bonded 0.001-au contour in the isolated reactant. The extent of penetration of the van der Waals envelope for the acidic hydrogen,$|\Delta r_H|$, and the B atom of the base,$|\Delta r_B|$, as well as the sum of these two quantities, $\Sigma\,|\Delta r|$, are also given in Table 3.3. As observed previously, the extent of penetration is found to increase with the strength of the interaction.

Because these are very weak interactions, the value of the charge density at the point of penetration differs only slightly in magnitude from the value found at this same position in the isolated monomers. In Table 3.3, $\rho^\circ(r_H)$ and $\rho^\circ(r_B)$ are the values of the charge density in the isolated monomers at the point of penetration as determined by the bonded radius of H and B, respectively, and $\Sigma\rho^\circ$ is the sum of $\rho^\circ(r_H)$ and $\rho^\circ(r_B)$. This

sum is found to be very similar in magnitude to the actual value of the charge density at the hydrogen bond critical point, $\rho(r_c)$.

In the van der Waals complexes, argon, the softer of the two base atoms, is penetrated more by the hydrogen of HF and HCl than is Ne, the harder of the two bases, which penetrates the hydrogen atom's density to a greater extent than does Ar. Both argon and neon are penetrated more by H of the hard acid, HF, than the softer acid, HCl. Likewise, the hydrogen of HF is penetrated to a greater extent by the base atom than is H of HCl. For a given acid, the sum of the B and H penetrations are nearly equal. While the penetration of the argon atom by H is greater than that of the neon atom, the values of $\rho^{\circ}(r_c)$ at these penetrations are nearly equal, as the argon valence density is more diffuse than that of neon.

Unlike a shared interaction, there is no large increase in charge density at the bond critical point and in the interatomic surface relative to the unperturbed densities. The final density is instead determined primarily by the extent of penetration, the greater the penetration the larger the value of $\rho(r_c)$ and the stronger the hydrogen bond.

Charge Transfer

The formation of these weak hydrogen-bonded interactions are accompanied by a small amount of intermolecular charge transfer. With the exception of NeHCl, there is a net transfer of charge from the base to the acid, the amount increasing with the strength of the interaction, ranging from 0.001 au in NeHF to 0.030 au in HCNHF (Table 3.6).

Table 3.7 gives the changes in atomic populations which occur upon complex formation for hydrogen and the B atom of the base, while Table 3.8 gives the atomic populations and changes for all of the atoms in each complex. The changes in the atomic populations encountered in the formation of the van der Waals complexes are extremely small. The hydrogen of the acid loses charge in NeHCl, NeHF and ArHCl, while the B atom of the base loses charge in NeHF, ArHCl and ArHF. The hydrogen in ArHF and the

base atom in NeHCl both gain charge. In the remaining complexes, the hydrogen of the acid loses charge and the B atom of the base gains charge, these changes being an order of magnitude larger than the changes in atomic population encountered in the fomation of the van der Waals complexes. In general, there is a net transfer of charge from the tail of the base (Y group) to the head of the acid (Cl, F and N). This net transfer of charge, which is across the length of the molecule, gives rise to a dipole moment which will be discussed next.

3.3 Polarization of the Charge Distribution

It is experimentally observed that the dipole moment of a hydrogen-bonded complex is always greater than the vector sum of the dipole moments of the isolated reactants, an effect known as dipole moment enhancement (Legon and Millen 1986). These enhancements have contributions from the polarization of one subunit by the other and from any charge transfer on the formation of the dimer. Table 3.9 lists the magnitudes of the calculated and experimental dipole moments and dipole moment enhancements for these hydrogen bonded complexes[1]. The calculated results are found to overestimate the experimental values of the dipole moment except for HF and HCN. With the exception of ArHCl, the dipole moments of the complexes increase in magnitude with increasing dissociation energy. The dipole moment enhancements are also found to increase with the strength of the interaction with the exception of the last two complexes; HCNHCl and HCNHF.

The total dipole moment, μ, of a neutral molecule can be expressed as a sum of a polarization term μ_p and a charge transfer term μ_c.

---

[1] The dipole moments for all of the complexes are directed from the acid to the base.

$$\mu = \sum_{\Omega} Z_{\Omega} R_{\Omega} - \int r\rho(r)\, dr$$

where Z_{Ω} is the nuclear charge of atom Ω and $\mathbf{r}$ and R_{Ω} are the electronic and nuclear position vectors, respectively, measured from a common, arbitrary origin. The electronic position vector $\mathbf{r}$ can be re-expressed in terms of a position vector r_{Ω} with the nucleus Ω as its origin such that $\mathbf{r} = r_{\Omega} + R_{\Omega}$. The net charge of atom Ω can be expressed in terms of its nuclear charge, Z_{Ω}, and atomic population $N(\Omega)$:

$$q(\Omega) = (Z_{\Omega} - N(\Omega))$$

Using these relationships, the expression for the dipole moment becomes

$$\mu = \sum_{\Omega} \left[-\int_{\Omega} \rho\, r_{\Omega}\, dr + q(\Omega) R_{\Omega} \right]$$

The first term in the summation is just the definition of the first moment $\mathbf{m}(\Omega)$ of an atom's charge distribution (Chapter 1) and provides a measure of the extent and direction of the dipolar polarization of the atom's charge density. The total dipole moment can now be written as

$$\mu = \sum_{\Omega} [\mathbf{m}(\Omega) + q(\Omega)\mathbf{R}_{\Omega}] = \mu_p + \mu_c$$

which is a sum of a polarization term, which arises from the polarizations of the individual atomic distributions, and an origin-dependent charge transfer term resulting from intra- and/or intermolecular charge transfer (The removal of the origin dependence of $q(\Omega)\mathbf{R}_{\Omega}$ will be discussed later).

The relative changes in the atomic first moments, $m(\Omega)$, for the H and B atoms which occur upon complexation formation are given in Table 3.7. Table 3.8 contains the moments and their changes for all of the atoms in each complex. In HF, the atomic distribution of fluorine is polarized towards the hydrogen which is itself polarized away from fluorine, while in HCl chlorine is polarized away from hydrogen, which is itself polarized away from chlorine. In molecular nitrogen, each nitrogen atom is polarized into its non-bonded region and in HCN, nitrogen is polarized towards carbon which is polarized towards hydrogen which is itself polarized away from carbon.

The atoms in the molecular monomers retain their initial direction of polarization in the complexes, but the magnitudes change and this results in a net atomic polarization which is induced as a consequence of complex formation. In each case, the acid and base atoms polarize, so as to allow for mutual penetration of their van der Waals envelopes.

The changes in the atomic moments of the Ar and Ne atoms dominate the formation of the van der Waals complexes. The dipole polarizations of the noble gas atoms exceed in magnitude the corresponding changes for the base atoms in the stronger complexes and in each case they polarize towards the hydrogen atom by an almost equal amount as a result of complex formation.

The original polarization of nitrogen atom (B) into its non-bonded region is increased and as a result polarizes towards hydrogen in the formation of NNHCN and NNHCl, while in the formation of the slightly stronger interaction NNHF, nitrogen polarizes away from hydrogen. The extent to which the acid hydrogen is penetrated by nitrogen in NNHCN and NNHCl is roughly equal to the amount the nitrogen atom is penetrated by hydrogen. However, in NNHF the nitrogen is penetrated to a greater extent by hydrogen than hydrogen is by nitrogen. Nitrogen therefore polarizes away from hydrogen so as to facilitate the greater penetration of HF.

When HCN acts as the base the original polarization of nitrogen, which is towards carbon, becomes enhanced and as a result polarizes away from hydrogen in the formation

of HCNHCN, HCNHCl and HCNHF. The relative magnitudes of these polarizations are found to increase with the strength of the interaction and the extent to which nitrogen is penetrated by the acid hydrogen.

The initial polarization of the hydrogen-bonded hydrogen is decreased and as a result polarizes away from the B atom of the base for all the complexes except for ArHF, where the original polarization of hydrogen increases slightly. This differing behavior of hydrogen in ArHF is consistent with the large extent to which Ar is penetrated by the hydrogen of HF and the large change in polarization induced Ar upon forming the complex.

Upon formation of the complexes with HF and HCl, fluorine polarizes away from hydrogen and in ArHCl, chlorine also polarizes away from hydrogen by a small amount. In NeHCl and HCNHCl chlorine polarizes towards hydrogen upon complex formation. When HCN acts as an acid, carbon and nitrogen both polarize towards hydrogen. When HCN is the base, the terminal hydrogen polarizes towards carbon which itself polarizes away from nitrogen, their magnitudes increasing with the strength of the interaction. In NNHCN and NNHCl the terminal nitrogen atom polarizes towards the other nitrogen, while in NNHF the terminal nitrogen polarizes away from the other nitrogen.

Acid and Base Contributions to the Molecular Dipole Moment

In the study of these acid-base complexes, it is useful to separate the polarization and charge transfer contributions to the molecular dipole moment into separate contributions from both the acid and the base. In this context, the charge transfer contribution to the molecular dipole moment can be written as a sum of two terms: an intramolecular charge transfer term, μ_c^{intra}(acid or base), and an intermolecular charge transfer term, μ_c^{inter}(acid or base), to distinguish between charge which is redistributed within either the acid or the base fragment and the charge which is transferred between

the base and acid fragments, respectively. Using these new terms, the total molecular dipole moment can be expressed as follows:

$$\mu(\text{base}) = \mu_p(\text{base}) + \mu_c^{\text{intra}}(\text{base}) + \mu_c^{\text{inter}}(\text{base})$$
$$\mu(\text{acid}) = \mu_p(\text{acid}) + \mu_c^{\text{intra}}(\text{acid}) + \mu_c^{\text{inter}}(\text{acid})$$
$$\mu_{\text{total}} = \mu(\text{base}) + \mu(\text{acid})$$

In the following diagram of a hydrogen-bonded interaction B-HA [1], $\mathbf{R}_1$ and $\mathbf{R}_2$ are the position vectors of the critical points between B-H and H-A, respectively, and $\mathbf{R}_B$, $\mathbf{R}_H$, and $\mathbf{R}_A$ are the nuclear position vectors for B, H and A, respectively.

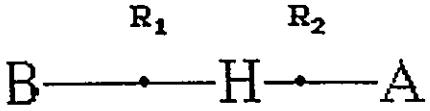

Origin independent atomic contributions to the total molecular dipole moment can be expressed as follows[2] for B, H and A:

$$\mu(B) = \mathbf{m}(B) + (\mathbf{R}_1 - \mathbf{R}_B)\,(q(H) + q(A))$$

$$= \mathbf{m}(B) + (\mathbf{R}_1 - \mathbf{R}_B)(-q(B))$$

$$\mu(H) = \mathbf{m}(H) + (\mathbf{R}_1 - \mathbf{R}_H)\,q(B) + (\mathbf{R}_2 - \mathbf{R}_H)\,q(A)$$

$$\mu(A) = \mathbf{m}(A) + (\mathbf{R}_2 - \mathbf{R}_A)\,((q(B) + q(H))$$

---

[1] B and A represent either single atoms or groups of atoms.

[2] This method works only if $\sum_{\Omega} q(\Omega) = 0$

where the total dipole moment is the sum of the atomic dipole moment contributions, consisting of polarization and charge transfer terms.

$$\mu_{total} = \mu(B) + \mu(H) + \mu(A)$$

These individual atomic contributions to the molecular dipole moment can be combined in a more interesting way so as to give separately, the polarization and charge transfer contributions originating from a particular fragment. The following is an example of the determination of the polarization, intramolecular and intermolecular contributions to a particular fragment where, in this case, B represents a single base atom (Ar for example) and H-A represents the acid fragment (HF for example). The polarization and charge transfer terms for the base can be written as:

$$\mu_p(\text{base}) = \mathbf{m}(B)$$

$$\mu_c^{intra}(\text{base}) = 0$$

$$\mu_c^{inter}(\text{base}) = (\mathbf{R}_1 - \mathbf{R}_B)\,(q(H) + q(A)) = -(\mathbf{R}_1 - \mathbf{R}_B)\,q(B)$$

$$\mu(\text{base}) = \mu_p(\text{base}) + \mu_c^{inter}(\text{base})$$

and the polarization and charge transfer terms for the acid fragment, H-A, can be written as:

$$\mu_p(\text{acid}) = \mathbf{m}(H) + \mathbf{m}(A)$$

$$\mu_c^{intra}(\text{acid}) = (\mathbf{R}_2 - \mathbf{R}_H)\,q(A) - (\mathbf{R}_2 - \mathbf{R}_A)\,q(A) = (\mathbf{R}_A - \mathbf{R}_H)\,q(A)$$

$$\mu_c^{inter}(acid) = -(R_1 - R_H)(q(H) + q(A))$$

$$\mu(acid) = \mu_p(acid) + \mu_c^{intra}(acid) + \mu_c^{inter}(acid)$$

where the total molecular dipole moment of the complex, B HA is:

$$\mu_{total} = \mu(base) + \mu(acid)$$

Table 3.10 gives the polarization and charge transfer contributions (μ_p, μ_c^{intra} and μ_c^{inter}) to the total molecular dipole moment from the acid and base fragments for each of the complexes, and Table 3.11 lists the polarization and charge transfer terms (μ_p and μ_c^{intra}) for the monomers.

The dipole moment of the acid fragment is roughly an order of magnitude larger than the dipole moment of the base fragment for the van der Waals complexes and for NNHCN. For NNHCl and NNHF, the dipole moment of the acid fragment is six times larger than the dipole moment of the base fragment and in HCNHCN they are equal. For the last two complexes, HCNHCl and HCNHF, the dipole moment of the base fragment is roughly twice as large as the acid dipole moment.

Dipole Moment Enhancements

It is useful to examine the changes in the polarization and charge transfer terms which occur upon complex formation in order to uncover the origin of the dipole moment enhancement. The changes in the polarization and charge transfer contributions to $\Delta\mu$(acid) and $\Delta\mu$(base) as a consequence of complex formation are given in Table 3.12. There is no intermolecular charge transfer in the isolated reactants, so the $\Delta\mu_c^{inter}$ terms

in Table 3.12 are the same as the μ_c^{inter} terms in Table 3.10. Also, the noble gas atoms and molecular nitrogen do not possess dipole moments, so the base fragment $\Delta\mu_p$(base), $\Delta\mu_c^{intra}$(base) and $\Delta\mu$(base) terms for the the first seven complexes are the same as μ_p(base), μ_c^{intra}(base) and μ(base) in Table 3.10.

The relative magnitudes of the dipole moment enhancement are found to increase with the strength of the interaction[1], ranging from 0.056 a.u. in NeHCl to 0.435 a.u. in HCNHCl. The contribution to the overall dipole moment enhancement from the base fragment increases with the strength of the interaction. In the van der Waals complexes, the acid fragment makes the same contribution to the dipole moment enhancement, while in the remaining complexes, its contribution increases with the strength of the interaction. In NeHCl, the acid and base contributions to the dipole moment enhancement are nearly equal. The patterns in the relative contributions of internal polarization and charge transfer to the total dipole moment enhancement fall into three groups: the first consisting of the van der Waals complexes, the second of NNHCN, NNHCl and NNHF, and the third consisting of HCNHCN, HCNHCl and HCNHF.

The principal source of the overall dipole moment enhancement in the van der Waals complexes comes from the internal polarization of the base atom. The contributions to the overall enhancement arising from internal polarization of the acid fragment, decrease with the strength of the interaction, reaching zero in ArHF. The contributions to the enhancement arising from intramolecular charge transfer in the acid fragment, decrease with increasing dissociation energy. The small intermolecular charge transfer contributions, which oppose the overall dipole moment enhancement in NeHCl parallel the strength of the interaction, making an increasingly larger contribution to the overall enhancement.

---

[1] The dipole moment enhancement in HCNHCl is larger than in the stronger interaction HCNHF.

In NNHCN, NNHCl and NNHF, the principal source of the dipole moment enhancement is the intramolecular charge transfer which occurs within the acid and base fragments. The much smaller contributions to the enhancement resulting from intermolecular charge transfer, increase with the strength of the interaction, the contributions from the base fragment being roughly twice that of the acid fragment. The contribution to the overall enhancement arising from internal polarization of the base fragment decreases with the strength of the interaction and actually opposes the overall dipole moment enhancement in NNHF. Just the opposite behavior is found for the enhancement contribution arising from internal polarizations of the acid fragment.

In HCNHCN, HCNHCl and HCNHF also, the principal source of the dipole moment enhancement is the intramolecular charge transfer which occurs within the acid and base fragments. The contribution to the dipole moment enhancement arising from intramolecular charge transfer within the acid fragment of HCNHF is much smaller in magnitude as compared to this contribution in HCNHCN and HCNHCl. This is reflected in the observation (both experimentally and theoretically) that the dipole moment enhancement, which occurs upon formation of HCNHF, is smaller in magnitude as compared to the enhancement in HCNHCl, despite the fact that HCNHF is the stronger of the two interactions. The smaller contributions to the enhancement arising from intermolecular charge transfer increase with increasing dissociation energy in both the acid and base fragments. The contribution arising from the internal polarization of the base fragment, which opposes the overall dipole moment enhancement in these three complexes, increases with the strength of the interaction. The internal polarization contribution of the acid fragment opposes the dipole moment enhancement in HCNHCN, while in HCNHCl and HCNHF it increases the overall enhancement.

Atomic Quadrupole Polarization

In addition to the dipole polarization, another important atomic polarization is measured by the axial component of the quadrupole moment (Chapter 1). All of the molecules here are oriented with their molecular axes along the z-axis, so Q_{zz} is the appropriate moment to examine and these are given in Tables 3.7 and 3.8. Before discussing the atomic quadrupole polarizations and changes as a result of complex formation, it is useful to first look at the atomic quadrupole polarizations of the monomers. In HCl, NN and HCN, each atom has a positive value for the quadrupole polarization along the internuclear axis, implying that the charge is distributed in a torus-like distribution about the internuclear axis. For HF, both atoms have quadrupole polarizations which are less than zero, implying that charge is accumulated along the intermolecular axis and depleted in a plane perpendicular to this axis.

Although the atomic quadrupole polarizations in the complexes are interesting in themselves, it is more useful to examine the changes in the polarization and how these changes facilitate the mutual penetration of the non-bonded densities in the formation of the complex. With the exception of Ne, the change in the quadrupole polarization with respect to the internuclear axis for the hydrogen bonded hydrogen and the base atoms B are positive, implying that charge is removed from along the axis of approach to facilitate maximum penetration. For NeHCl and NeHF, the change in quadrupole polarization of the base neon is less than zero, implying that in this case charge is accumulated along the intermolecular axis. This differing behavior of Ne as compared to Ar is consistent with the observation that Ne is the harder of these two base atoms.

In the complexes in which NN or HCN is the base, the terminal nitrogen in NN and the carbon and hydrogen in HCN polarize, so as to remove charge from along the internuclear axis. Chlorine and fluorine in all cases polarize so as to accumulate charge along the intermolecular axis. In NNHCN, the carbon and nitrogen of the HCN fragment polarize so as to remove charge from along the internuclear axis; however, in the stronger

HCNHCN complex, the carbon in the acid polarizes as it does in NNHCN, but to a much greater extent, while nitrogen in the acid fragment slightly polarizes so as to accumulate charge along the internuclear axis.

3.4 Nuclear Quadrupole Coupling Constants and Electric Field Gradients

Nuclear quadrupole hyperfine structure arises from the coupling of the angular momentum associated with a given nucleus to the overall rotational motion. The mechanism of the coupling is the interaction of the nuclear electric quadrupole moment with any electric field gradient that exists at the nucleus (Luken, 1969). For a linear dimer, the quantity obtained from the hyperfine structure is the diagonal component χ_{aa} of the nuclear quadrupole coupling tensor. This can be expressed as the coupling between the nuclear quadrupole moment and the electric field gradient as follows:

$$\chi_{zz} = -eQq_{zz}/h$$

where z is the molecular axis, eQ is the nuclear quadrupole moment and q_{zz} is the electric field gradient which is equal to $\partial^2 V / \partial z^2$ (where V is the electrostatic potential at the nucleus). The redistribution of charge which accompanies the formation of complexes is related to the change in the electric field gradient at that nucleus. The difference in χ_{zz} (for a nucleus which possesses a quadrupole moment, for example ^{14}N) before and after complex formation, therefore contains direct information about electric charge redistribution which occurs as a result of complex formation. Unfortunately, the observed quantity for a linear species is the diagonal component χ_{aa} (abbreviated as χ_a in the following discussion) in the zero-point vibrational state and there are difficulties in separating the contributions that the electrical and vibrational averaging effects make to

the changes in the observed χ_a values. Because of these difficulties in separating the vibrational and electrical effects, the HCN-HA complexes must be treated separately from the NN-HA complexes.

HCNHCN, HCNHCl and HCNHF

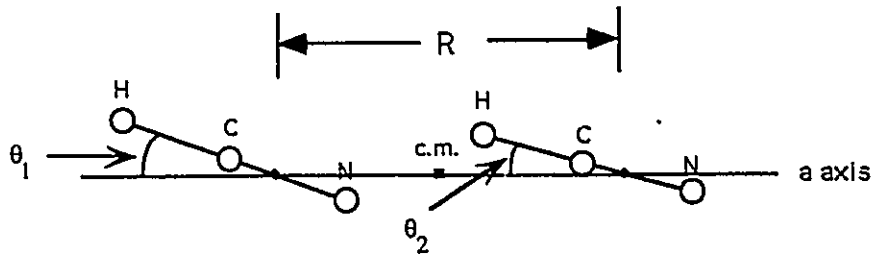

The torsional amplitudes θ_1 and θ_2 in the above diagram are determined using inertial analysis methods (Ruoff et al, 1987). This method is based upon an equation for the moment of inertia of isotopic dimers containing three unknowns: θ_1, θ_2 and R. Of these, the θ are insensitive to isotopic substitution; however, isotopic substitution in a monomer changes the position of its center-of-mass and therefore affects R. Experimentally measured values of the rotational constant are then fitted to these relationships to obtain values for θ. These values of θ are used in eqn. (2) along with the observed χ_a to determine χ_o^d, the (^{14}N) quadrupole coupling constant for the rigid, linear dimer.

(2) $$\chi_a = \tfrac{1}{2} < 3\cos^2\theta - 1 > \chi_o^d$$

The quantity, $\Delta\chi_o = \chi_o^d - \chi_o^m$, where χ_o^m is the quadrupole coupling constant for the free HCN molecule (= -4.7091 MHz, DeLucia and Gordy, 1969), gives the change in the quadrupole coupling constant produced by charge rearrangement upon dimer formation.

The experimental values of χ_o^d and $\Delta\chi_o$ for HCNHCN, HCNHCl and HCNHF are listed in Table 3.13 along with χ_a, $\Delta\chi_a = \chi_a - \chi_o^m$ and $(\%\Delta\chi_\rho) = 100(\Delta\chi_o / \Delta\chi_a)$. This later quantity is a measure of the changes in the ^{14}N quadrupole coupling constant produced by the charge rearrangement upon complex formation. Roughly 40% of the total change in the quadrupole coupling constant is due to charge rearrangement for both nitrogen atoms in HCNHCN and also HCNHCl, while in HCNHF, 57% of the changes in the observed quadrupole coupling constant is due to charge rearrangement. The actual charge redistribution which occurs upon complex formation is found to be quite small, ranging from roughly 2 to 7%, as compared to the isolated reactants:

(3) $$\% \text{ charge redistribution} = (\%\Delta\rho) = 100(\Delta\chi_o/\chi_o^m).$$

In the following discussion, N_1 refers to the hydrogen-bonded nitrogen and N_2 refers to the terminal nitrogen of HCNHCN. The experimentally determined $\%\Delta\rho$ values predict the order of increasing charge redistribution at nitrogen to be: HCNHCN(N_2) < HCNHCN(N_1) ≈ HCNHCl < HCNHF.

The calculated values of the electric field gradient component (q_{zz}), changes ($\Delta q_{zz} = q_{zz}^d - q_{zz}^m$) and charge redistribution $\%\Delta\rho = 100(\Delta q_{zz}/q_{zz}^m)$) are given in the second section of Table 3.13. The agreement between the experimental and calculated $\%\Delta\rho$ values is quite good for N_1 of HCNHCN and nitrogen of HCNHF, both predicting the charge rearrangement effects for nitrogen in HCNHF to be greater than the rearrangement effects for N_1 in HCNHCN. The calculated $\%\Delta\rho$ values predict the charge rearrangement effects at the N_2 nucleus in HCNHCN to be negligible and the order of increasing charge redistribution at nitrogen to be: HCNHCN(N_1), HCNHCN, HCNHF. This is in contrast to the experimentally determined values which predict N_1 of HCNHCN and nitrogen of HCNHCl to undergo the same charge redistribution upon

complex formation. Reference to Table 3.9 shows that although the change in population and first moments of these two atoms in HCNHCN are nearly the same, the change in quadrupole polarization of N_1 is much larger than for N_2 (0.1796 as compared to 0.0061). The change in atomic population, first moments and quadrupole moments also increase in accordance with the calculated percent charge redistribution obtained from electric field gradient changes. These results suggest that experimental values overestimate the charge rearrangement contributions to N_2 of HCNHCN, and underestimate the charge rearrangement contributions for nitrogen of HCNHCl

NNHCN, NNHCl and NNHF

If the coupling constant for the nitrogen nucleus in molecular nitrogen, χ_o^m, were known, it could be used to obtain $\Delta\chi_o$ for the corresponding nitrogen nuclei in NNHCN, NNHCl and NNHF in a manner analogous to the above complexes; however, for these three complexes, the vibrational averaging effects are somewhat isolated because the angle for N_1 is identical with that for N_2 in the NN subunit of N_1N_2HX, as a result of their strong covalent interaction. The difference in ^{14}N nuclear quadrupole coupling constants, $\Delta\chi_a = \chi_a(N_2) - \chi_a(N_1)$, is therefore a direct sign of charge rearrangement effects and these are given in the first section of Table 3.14.

The calculated values of the electric field gradient component, q_{zz}, for each nitrogen nucleus and the differences, $\Delta q_{zz} = q_{zz}(N_2) - q_{zz}(N_1)$, are listed in the second section of Table 3.14. The calculated electric field gradients are used to determine $\%\Delta\rho$ (as for HCNHCN, HCNHCl and HCNHF), and these are also listed in Table 3.14. The calculated $\%\Delta\rho$ values predict the charge rearrangement effects at the N_2 nucleus in each of the complexes to be small (< 1%) and the order of increasing charge redistribution at N_2 to be: NNHCN ≈ NNHCl < NNHF. Although N_1 loses more charge than N_2 gains, the change in the atomic first moment and quadrupole moment is much larger for N_2 than

for N_1 in each of these complexes, being smallest for NNHCN and largest for NNHF (Table 3.9).

In order to compare the calculated values of the electric field gradients with the experimentally determined nuclear quadrupole coupling constants, it is useful to compare ratios of the coupling constants (which results in a ratio of electric field gradients) with ratios of the calculated electric field gradients. The ratios,

$$\frac{\chi_a(N_1) - \chi_a(N_2)}{\chi_a(N_1) + \chi_a(N_2)} \text{ and } \frac{q_{zz}(N_1) - q_{zz}(N_2)}{q_{zz}(N_1) + q_{zz}(N_2)}$$

are given in the fourth column of Table 3.14. The agreement between the experimental ratios and the calculated ratios is quite good with the calculated ratios being slightly larger in each case. The magnitudes for both the experimental and calculated ratios are similar for NNHCN and NNHCl but are larger for NNHF.

Calculated Nuclear Quadrupole Coupling Constants

The calculated electric field gradients along with the measured nuclear quadrupole moment of the nitrogen nucleus can be used to obtain calculated values for the nuclear quadrupole moment. The calculated and experimental values of the quadrupole coupling constants, χ^d_{calc} and χ^d_o, along with $\Delta\chi^d_{calc}$ and $\Delta\chi^d_o$ for each of these complexes are given in Table 3.15. For HCNHCN, HCNHCl and HCNHF, the calculated values of χ^d are between 10-15% smaller in magnitude as compared to the experimental values. With the exception of N_2 in HCNHCN, $\Delta\chi^d_{calc}$ and $\Delta\chi^d_o$ are similar for these three complexes, with the calculated values being slightly larger than the experimental values. These results suggest that experimental values underestimate the vibrational contributions to the nuclear quadrupole coupling constant for the terminal nitrogen in HCNHCN.

For NNHCN and NNHCl, the calculated values of χ^d for N_1 and N_2 are between 2-5% larger than the experimental values, while in NNHF the calculated χ^d values are

smaller than the experimental values by 2-3%. $\Delta\chi^{d}_{calc}$ and $\Delta\chi^{d}_{o}$ are similar in magnitude, both being smallest in NNHCN and largest in NNHF.

3.5 Conclusions

In stronger hydrogen-bonded complexes as well as these weak interactions, a hydrogen atom links an acid to a base fragment with a shared and a closed-shell interaction, respectively. The formation of these complexes (YB-HA) results from the mutual penetration of the non-bonded van der Waals radii of the H atom of the acid and of the terminal B atom of the base to yield a value for the density at the H-B critical point which is only slightly greater than the sum of the unperturbed densities.

The changes in atomic populations encountered in the formation of these weak interactions are very small. There is a predicted transfer of 0.001 electrons from the base to the acid in NeHF[1] and a transfer of 0.008 electrons in ArHF, the strongest of the van der Waals interactions. There is a predicted transfer of charge from the base to the acid fragment ranging from 0.005 au in NNHCN to 0.030 au in HCNHF. Although the net transfer of charge between the fragments is small, there are significant changes in the first and second moments of the atoms in these complexes.

There are two patterns of atomic polarization that result from the mutual penetration of closed-shell systems, with little or no accompanying charge transfer. The first of these patterns is observed in the formation of the van der Waals complexes, where the noble gas atoms are polarized to a greater extent upon complex formation than is a base atom in the stronger hydrogen bonds. Unlike the polarization of the base atom in other hydrogen bond interactions, the dipolar polarization of a noble gas atom is towards the hydrogen, and this polarization increases with the strength of the interaction. While the dipole and quadrupole polarizations of argon are greater than those of neon, the latter

[1] The error in the integrated atomic populations for these complexes is ≤ 0.0001 au.

atom penetrates and perturbs the hydrogen atom to a greater extent. Thus, the effect on the binding energy of the greater penetration of hydrogen by neon is offset by the greater polarizability of argon. In the relatively weak complex of HCN with N_2, the change in the polarization of the base atom, which is toward hydrogen, is very small. This polarization of the B atoms towards the hydrogen which is induced upon complex formation is reduced further in the formation of the slightly stronger interaction, NNHCl.

The second pattern of atomic polarization is observed in the formation of the stronger interactions found in: NNHF, HCNHCN, HCNHCl and HCNHF, where the B atom polarizes away from the hydrogen. In this case, the B atom is penetrated to a greater extent than the H atom, and the strength of the interaction increases with the degree of mutual penetration. In these molecules, the H and B atoms polarize so as to facilitate the mutual penetration of their non-bonded densities.

The changes in atomic population, first moments and quadrupole moments also increase in accordance with the calculated charge redistribution effects obtained from electric field gradient changes at the nitrogen nucleus. The comparison of these results with the data obtained from experimentally determined nuclear quadrupole coupling constants indicates that experimental values overestimate the charge rearrangement effects at the terminal nitrogen of HCNHCN and underestimate the charge rearrangement effects for nitrogen of HCNHCl.

The principal source of the overall dipole moment enhancement in the van der Waals complexes comes from the internal polarization of the base atom. In NNHCN, NNHCl, NNHF, HCNHCN, HCNHCl and HCNHF the principal source of the dipole moment enhancement is the intramolecular charge transfer which occurs within the acid and base fragments. The intramolecular charge transfer contribution to the overall dipole moment enhancement is larger for the latter three as compared to the former three complexes.

Table 3.1. Dissociation Energies of the Complexes.[a]

	D_e	D_e(BSSE)	D_e(experimental)
NeHCl	1.04	0.1	0.20[c]
NeHF	1.28	0.17	
ArHCl	0.47	0.27[b]	0.52[c]
ArHF	0.59	0.18[b]	0.60[d]
NNHCN	1.98	1.22	
NNHCl	2.12	1.35	
NNHF	3.03	1.88	1.77[e]
HCNHCN	5.44	4.33	4.40[f]
HCNHCl	5.75	4.55	3.43[g]
HCNHF	7.76	6.13	6.24[h]

[a] All values are in kcal/mole. D_e is the calculated dissociation energy of the complex. D_e(BSSE) is the calculated dissociation energy of the complex corrected for basis set superposition errors using the counterpoise method.

[b] Correction for BSSE is not required for these complexes.

[c] Hutson and Howard (1982). Well depth of potential energy surfaces from molecular beam rotational spectra and far infrared line broadening cross sections.

[d] Hutson (1992). Well depth of potential energy surface from high-resolution microwave, far-infrared and infrared spectroscopy.

[e] Soper et al (1982). Well depth of potential energy surface from pulsed Fourier transform microwave spectroscopy.

[f] Buxton et al (1981). Well depth of potential energy surface from pulsed Fourier transform microwave spectroscopy.

[g] Legon et al (1982). Well depth of potential energy surface from pulsed Fourier transform microwave spectroscopy.

[h] Legon et al (1980). This is the only value of D_e determined by rotational spectroscopy so far.

Table 3.2. Bond Lengths and Changes.[a]

	Parameter[b]	R	ΔR	$R_{experimental}$
NeHCl	r(NeH)	4.5000		
	r(NeCl)	6.9000		7.256[c]
	r(HCl)	2.4000	-0.0004	
NeHF	r(NeH)	3.9887		
	r(NeF)	5.7170		
	r(HF)	1.7283	-0.0004	
ArHCl	r(ArH)	5.3069		
	r(ArCl)	7.7079		7.570[d]
	r(HCl)	2.4010	0.0006	
ArHF	r(ArH)	4.8412		
	r(ArF)	6.5701		6.535[e]
	r(HF)	1.7289	0.0002	
NNHCN	r(NN)	2.1016	-0.0007	
	r(NH)	4.5637		4.82[f]
	r(NC)	6.5723		6.83[f]
	r(HC)	2.0086	0.0030	
	r(CN)	2.2013	0.0001	
NNHCl	r(NN)	2.1016	-0.0007	
	r(NH)	4.3267		4.567[f]
	r(NCl)	6.7318		
	r(HCl)	2.4051	0.0047	
NNHF	r(NN)	2.1005	-0.0018	
	r(NH)	3.9219		
	r(NF)	5.6544		5.833[g]
	r(HF)	1.7325	0.0038	
HCNHCN	r(HC)	2.0063	0.0007	
	r(CN)	2.1978	-0.0034	
	r(NH)	4.1508		4.203[f]
	r(NC)	6.1681		6.212[f]
	r(HC)	2.0173	0.0117	
	r(CN)	2.2019	0.0007	

References follow on next page.

Table 3.2 (Cont'd.).

	Parameter[b]	R	ΔR	$R_{experimental}$
HCNHCl	r(HC)	2.0066	0.001	
	r(CN)	2.1967	-0.0045	
	r(NH)	3.8083		
	r(NCl)	6.2332		6.434[h]
	r(HCl)	2.4248	0.0244	
HCNHF	r(HC)	2.0061	0.0005	
	r(CN)	2.1946	-0.0066	
	r(NH)	3.553		
	r(NF)	5.2978		5.299[g]
	r(HF)	1.7447	0.016	
Monomers				
HCl	r(HCl)	2.4004		2.426[h]
HF	r(HF)	1.7287		1.7325[i]
NN	r(NN)	2.1023		2.074[i]
HCN	r(HC)	2.0056		2.010[c]
	r(CN)	2.2012		2.185[c]

[a] All values are in atomic units.
[b] r(XY) is the geometrical distance between atom X and Y.
[c] Barton et al (1980)
[d] Novick et al (1973)
[e] Harris et al (1974)
[f] Goodwin and Legon (1985)
[g] Legon and Millen (1986)
[h] Legon et al (1982)
[i] Huber and Herzberg (1979)

Table 3.3. Properties of the Hydrogen Bond.[a]

	R	$\rho(r_c)$	$\nabla^2\rho(r_c)$	r_H	r_B	$\lvert\Delta r_H\rvert$	$\lvert\Delta r_B\rvert$	$\Sigma\lvert\Delta r\rvert$	$\rho^\circ(r_H)$	$\rho^\circ(r_B)$	$\Sigma\rho^\circ$	D_e
Ne-HCl	4.500	0.0060	0.0287	1.836	2.664	0.48	0.19	0.67	0.0033	0.0020	0.0053	0.10
Ne-HF	3.989	0.0099	0.0483	1.519	2.470	0.56	0.38	0.94	0.0050	0.0040	0.0090	0.17
Ar-HCl	5.307	0.0051	0.0199	1.963	3.344	0.36	0.39	0.74	0.0024	0.0024	0.0048	0.47
Ar-HF	4.841	0.0077	0.0311	1.669	3.172	0.41	0.56	0.97	0.0033	0.0037	0.0069	0.59
NN-HCN	4.564	0.0090	0.0340	1.737	2.827	0.60	0.64	1.25	0.0045	0.0045	0.0090	1.22
NN-HCl	4.327	0.0117	0.0434	1.605	2.721	0.71	0.75	1.46	0.0058	0.0057	0.0116	1.35
NN-HF	3.922	0.0169	0.0648	1.359	2.563	0.72	0.91	1.63	0.0079	0.0083	0.0161	1.88
HCNHCN	4.151	0.0154	0.0551	1.512	2.639	0.83	0.93	1.76	0.0078	0.0080	0.0158	4.33
HCN-HCl	3.808	0.0228	0.0740	1.323	2.485	1.00	1.08	2.08	0.0118	0.0111	0.0229	4.55
HCN-HF	3.553	0.0285	0.0921	1.163	2.390	0.92	1.18	2.10	0.0135	0.0138	0.0273	6.13

[a] All values are in atomic units except for D_e which is in kcal/mol. **R** is the length of the hydrogen bond. $\rho(r_c)$ is the value of the charge density at the bond critical point. $\nabla^2\rho(r_c)$ is the Laplacian of the charge density at the bond critical point. r_H is the bonded radius of hydrogen. r_B is the bonded radius of the base atom. $\lvert\Delta r_H\rvert$ and $\lvert\Delta r_B\rvert$ are the measures of the extent of penetration of the van der Waals envelope to yield the bonded radii found in the complex. $\rho^\circ(r_H)$ and $\rho^\circ(r_B)$ are the values of the charge density in the isolated acid and base molecules at the point of penetration, i.e. at the position determined by the bonded radius r_H and r_B.

Table 3.4. Properties at the Hydrogen Bond Critical Point.[a]

	λ_1	λ_3	$\lvert\lambda_1\rvert / \lambda_3$	$G(r_c)_\perp$	$G(r_c)_{\parallel}$	$G_\perp / G_{\parallel}$	$G(r_c)/r(r_c)$
NeHCl	-0.0069	0.0424	0.162	0.0002	0.0055	0.042	0.997
NeHF	-0.0135	0.0754	0.180	0.0005	0.0098	0.053	1.097
ArHCl	-0.0043	0.0285	0.150	0.0002	0.0035	0.047	0.755
ArHF	-0.0080	0.0470	0.169	0.0003	0.0058	0.049	0.828
NNHCN	-0.0093	0.0525	0.177	0.0001	0.0066	0.018	0.761
NNHCl	-0.0123	0.0681	0.181	0.0003	0.0084	0.031	0.765
NNHF	-0.0216	0.1080	0.200	0.0005	0.0132	0.037	0.837
HCNHCN	-0.0178	0.0907	0.196	0.0002	0.0112	0.022	0.762
HCNHCl	-0.0123	0.0681	0.181	0.0003	0.0084	0.031	0.765
HCNHF	-0.0413	0.1748	0.236	0.0010	0.0210	0.046	0.807

[a] All values are in atomic units.

Table 3.5. Critical Point Properties in the Reactants.[a]

	R	$\rho(r_c)$	$\nabla^2\rho(r_c)$	λ_1	λ_3
HCl	2.4004	0.2478	-0.6953	-0.5867	0.4782
HF	1.7287	0.3827	-3.2804	-2.5908	1.9012
NN	2.1023	0.6648	-2.6048	-1.8160	1.0272
HCN (HC)	2.0056	0.2944	-1.1937	-0.8589	0.5241

	$\lvert\lambda_1\rvert / \lambda_3$	$G(r_c)_\perp$	$G(r_c)_{\parallel}$	$G_\perp / G_{\parallel}$	$G(r_c)/ \rho(r_c)$
HCl	1.227	0.0243	0.0161	1.509	0.261
HF	1.363	0.0368	0.0266	1.384	0.261
NN	1.768	0.2567	0.0486	5.285	0.845
HCN (HC)	1.639	0.0155	0.0067	2.313	0.128

[a] All values are in atomic units.

Table 3.6. Charge Transfer from Base to Acid.

	Charge Transfer
Ne-HCl	-0.003
Ne-HF	0.001
Ar-HCl	0.003
Ar-HF	0.008
NN-HCN	0.005
NN-HCl	0.006
NN-HF	0.015
HCN-HCN	0.013
HCN-HCl	0.021
HCN-HF	0.030

Table 3.7. Changes in the Atomic Populations and First and Second Moments of the H and B atoms upon formation of the complex YB-HX.[a]

	ΔN(H)	ΔN(B)	Δ|m(H)|	Δ|m(B)|	ΔQzz(H)	ΔQzz(B)
NeHCl	-0.0088	0.0026	-0.0167	0.0370	0.0720	-0.0670
NeHF	-0.0054	-0.0009	-0.0105	0.0391	0.0435	-0.0488
ArHCl	-0.0015	-0.0032	-0.0074	0.0310	0.0664	0.0861
ArHF	0.0036	-0.0084	0.0005	0.0438	0.0318	0.1220
NNHCN	-0.0178	0.0254	-0.0139	0.0099	0.0729	0.0609
NNHCl	-0.0236	0.0245	-0.0217	0.0063	0.0938	0.0844
NNHF	-0.0038	0.0288	-0.0092	-0.0041	0.0640	0.1108
HCNHCN	-0.0540	0.0341	-0.0213	0.0053	0.0708	0.1796
HCNHCl	-0.0737	0.0333	-0.0368	0.0172	0.1045	0.2212
HCNHF	-0.0127	0.0376	-0.0187	0.0336	0.0938	0.2281

[a] All values are in atomic units.

Table 3.8. Atomic Populations, First and Second Moments and their Changes upon Complex Formation.[a]

	Ω	N(Ω)	ΔN(Ω)	m(Ω)	Δ|m(Ω)|	Qzz	ΔQzz
NeHCl	Ne	10.0026	0.0026	-0.0370	0.0370	-0.0670	-0.0670
	H	0.7762	-0.0088	0.0972	-0.0167	0.4107	0.0720
	Cl	17.2212	0.0061	-0.0653	-0.0008	3.9165	-0.0251
NeHF	Ne	9.9991	-0.0009	-0.0391	0.0391	-0.0488	-0.0488
	H	0.2615	-0.0054	0.1093	-0.0105	-0.0351	0.0435
	F	9.7393	0.0062	0.4427	-0.0001	-0.0427	-0.0052
ArHCl	Ar	17.9968	-0.0032	-0.0310	0.0310	0.0861	0.0861
	H	0.7834	-0.0015	0.1065	-0.0074	0.4051	0.0664
	Cl	17.2199	0.0048	-0.0669	0.0008	3.9229	-0.0187
ArHF	Ar	17.9916	-0.0084	-0.0438	0.0438	0.1220	0.1220
	H	0.2705	0.0036	0.1203	0.0005	-0.0468	0.0318
	F	9.7379	0.0047	0.4424	-0.0004	-0.0384	-0.0009
NNHCN	N	6.9698	-0.0302	0.6120	-0.0012	1.3477	-0.0211
	N	7.0254	0.0254	-0.6231	0.0099	1.4297	0.0609
	H	0.7966	-0.0178	0.0992	-0.0139	0.4594	0.0729
	C	5.2046	0.0112	0.9482	0.0250	2.9885	-0.0365
	N	8.0036	0.0113	0.3781	0.0029	0.6321	-0.0013
NNHCl	N	6.9695	-0.0305	0.6130	-0.0002	1.3486	-0.0202
	N	7.0245	0.0245	-0.6195	0.0063	1.4532	0.0844
	H	0.7614	-0.0236	0.0921	-0.0217	0.4325	0.0938
	Cl	17.2454	0.0303	-0.0548	-0.0112	3.8278	-0.1138
NNHF	N	6.9564	-0.0436	0.6141	0.0009	1.3448	-0.0240
	N	7.0288	0.0288	-0.6091	-0.0041	1.4796	0.1108
	H	0.2631	-0.0038	0.1106	-0.0092	-0.0146	0.0640
	F	9.7521	0.0190	0.4391	-0.0037	-0.0467	-0.0092

Table 3.8 (Cont'd.).

	Ω	N(Ω)	ΔN(Ω)	m(Ω)	Δ|m(Ω)|	Qzz	ΔQzz
HCNHCN	H	0.7973	-0.0170	0.1106	-0.0025	0.3725	-0.0140
	C	5.1632	-0.0302	0.9397	0.0165	2.8734	-0.1515
	N	8.0264	0.0341	0.3805	0.0053	0.8130	0.1796
	H	0.7603	-0.0540	0.0919	-0.0213	0.4573	0.0708
	C	5.2228	0.0294	0.9964	0.0732	2.8945	-0.1305
	N	8.0298	0.0375	0.3829	0.0078	0.6395	0.0061
HCNHCl	H	0.7960	-0.0183	0.1106	-0.0025	0.3707	-0.0158
	C	5.1575	-0.0359	0.9425	0.0193	2.8546	-0.1704
	N	8.0256	0.0333	0.3924	0.0172	0.8546	0.2212
	H	0.7112	-0.0737	0.0770	-0.0368	0.4432	0.1045
	Cl	17.3097	0.0946	-0.0326	-0.0335	3.6038	-0.3379
HCNHF	H	0.7928	-0.0216	0.1100	-0.0031	0.3684	-0.0181
	C	5.1469	-0.0465	0.9476	0.0244	2.8180	-0.2070
	N	8.0300	0.0376	0.4088	0.0336	0.8615	0.2281
	H	0.2542	-0.0127	0.1011	-0.0187	0.0151	0.0938
	F	9.7774	0.0443	0.4288	-0.0140	-0.0632	-0.0257
HCl	H	0.7850		0.1138		0.3387	
	Cl	17.2151		-0.0661		3.9416	
HF	H	0.2669		0.1198		-0.0786	
	F	9.7331		0.4428		-0.0375	
NN	N	7		0.6132		1.3688	
	N	7		-0.6132		1.3688	
HCN	H	0.8143		0.1131		0.3865	
	C	5.1934		0.9233		3.0250	
	N	7.9923		0.3752		0.6334	

[a] All values are in atomic units. N(Ω), m(Ω) and Q_{zz}(Ω) are the atomic population, first moment, and quadrupole moment, respectively for atom Ω.

Table 3.9. Calculated and Experimental Values for the Molecular Dipole Moment and Dipole Moment Enhancement.

	$\|\mu_{calc}\|$	$\|\mu_{exp}\|$	$\|\Delta\mu_{calc}\|$	$\|\Delta\mu_{exp}\|$
NeHCl	0.5245	0.475[b]	0.056	0.039[b]
NeHF	0.7681	0.749[c]	0.063	0.030[c]
ArHCl	0.5366	0.319[d]	0.068	
ArHF	0.7975	0.525[e]	0.093	
NNHCN	1.2983		0.153	
NNHCl	0.6490	0.489[f]	0.180	0.098[f]
NNHF	0.8985	0.783[g]	0.194	0.098[g]
HCNHCN	2.6207	2.58[h]	0.330	0.36[h]
HCNHCl	2.0492	1.90[i]	0.435	0.37[i]
HCNHF	2.2114	2.21[j]	0.362	0.315[j]
Monomers				
HCl	0.4688	0.436[k]		
HF	0.7047	0.719[l]		
HCN	1.1452	1.174[b]		

[a] All values are in atomic units.
[b] Barton et al (1980)
[c] Liu and Dykstra (1987)
[d] Novick et al (1973)
[e] Frazer and Pine (1986)
[f] Altman et al (1983)
[g] Jucks et al (1987)
[h] Ruoff -Thesis (1988)
[i] Legon and Millen (1986)
[j] Legon et al (1980)
[k] Hutson and Howard (1982)
[l] Legon et al (1982)

Table 3.10. Acid and Base Contributions to the Dipole Moment of the Complex.[a]

	Base				Acid			
	μ_p	μ_c^{intra}	μ_c^{inter}	μ	μ_p	μ_c^{intra}	μ_c^{inter}	μ
NeHCl	-0.037		0.007	-0.030	0.032	-0.531	0.005	-0.494
NeHF	-0.039		-0.002	-0.041	0.552	-1.278	-0.001	-0.727
ArHCl	-0.031		-0.011	-0.042	0.040	-0.528	-0.006	-0.495
ArHF	-0.044		-0.027	-0.070	0.563	-1.276	-0.014	-0.727
NNHCN	-0.011	-0.064	-0.014	-0.088	1.426	-2.627	-0.008	-1.210
NNHCl	-0.007	-0.065	-0.018	-0.090	0.037	-0.589	-0.010	-0.561
NNHF	0.005	-0.092	-0.039	-0.126	0.550	-1.303	-0.020	-0.773
HCNHCN	1.431	-2.691	-0.034	-1.294	1.471	-2.778	-0.020	-1.326
HCNHCl	1.446	-2.708	-0.052	-1.315	0.044	-0.751	-0.028	-0.734
HCNHF	1.466	-2.744	-0.075	-1.353	0.530	-1.355	-0.035	-0.860

[a]All values are in atomic units.

Table 3.11. Charge Transfer and Polarization Contributions to the Dipole Moments of the Reactants.[a]

	μ_p	μ_c^{inter}	μ^{total}
HCl	0.048	-0.516	-0.469
HF	0.563	-1.267	-0.705
HCN	1.412	-2.557	-1.145

[a] All values are in atomic units.

Table 3.12. Changes in the Acid and Base Contributions to the Dipole Moment of the Complex.[a]

	Base				Acid			
	$\Delta\mu_p$	$\Delta\mu_c^{intra}$	$\Delta\mu_c^{inter}$	$\Delta\mu$	$\Delta\mu_p$	$\Delta\mu_c^{intra}$	$\Delta\mu_c^{inter}$	$\Delta\mu$
NeHCl	-0.037		0.007	-0.030	-0.016	-0.015	0.005	-0.026
NeHF	-0.039		-0.002	-0.041	-0.011	-0.011	-0.001	-0.023
ArHCl	-0.031		-0.011	-0.042	-0.008	-0.012	-0.006	-0.026
ArHF	-0.044		-0.027	-0.070	0.000	-0.009	-0.014	-0.022
NNHCN	-0.011	-0.064	-0.014	-0.088	0.014	-0.071	-0.008	-0.065
NNHCl	-0.007	-0.065	-0.018	-0.090	-0.010	-0.073	-0.010	-0.093
NNHF	0.005	-0.092	-0.039	-0.126	-0.013	-0.035	-0.020	-0.068
HCNHCN	0.019	-0.134	-0.034	-0.149	0.060	-0.221	-0.020	-0.181
HCNHCl	0.034	-0.151	-0.052	-0.170	-0.003	-0.235	-0.028	-0.266
HCNHF	0.055	-0.188	-0.075	-0.208	-0.033	-0.087	-0.035	-0.155

[a]All values are in atomic units.

Table 3.13. Measured ^{14}N-Nuclear Quadrupole Coupling Constants and Calculated Electric Field Gradients for HCNHCN, HCNHCl and HCNHF [a].

	χ_a	χ_o^d	$\Delta\chi_a = \chi_a - \chi_o^m$	$\Delta\chi_o = \chi_o^d - \chi_o^m$	$\%\,\Delta\chi\rho$ $((\Delta\chi_o/\chi_o)100)$	$\%\Delta\rho$ $((\Delta\chi_o/\chi_o^m)100)$
HCNHCN (N_1)[b]	-4.106	-4.480	0.603	0.229	38	4.9
HCNHCN (N_2)[b]	-4.434	-4.603	0.275	0.106	39	2.3
HCNHCl[c]	-4.080	-4.479	0.629	0.230	37	4.9
HCNHF[d]	-4.098	-4.363	0.611	0.346	57	7.3

	q_{zz}^d	$\Delta q_{zz} = q_{zz}^d - q_{zz}^m$	$\%\Delta\rho$ $((\Delta q_{zz}/q_{zz}^m)100)$
HCNHCN N(1)	0.857	-0.055	6.0
HCNHCN N(2)	0.910	-0.001	0.1
HCNHCl	0.839	-0.072	7.9
HCNHF	0.832	-0.079	8.7

a ^{14}N-nuclear quadrupole coupling constants, χ, are expressed in MHz and calculated electric field gradients, q_{zz}, are in atomic units. χ_a is the measured quadrupole coupling constant for the dimer, χ_o^d is the nitrogen quadrupole coupling constant for the rigid, linear dimer and χ_o^m is the coupling constant for nitrogen in the HCN monomer which equals -4.7091 MHz (DeLucia and Gordy 1969). q_{zz}^m is the calculated electric field gradient for nitrogen in the HCN monomer which equals 0.911 au.

b Ruoff et al (1987).

c Legon et al (1982). d Legon and Millen (1986).

Table 3.14. Measured ^{14}N-Nuclear Quadrupole Coupling Constants and Calculated Electric Field Gradients for NNHCN, NNHCl and NNHF.[a]

	χ_a (N1)	χ_a (N2)	$\Delta\chi_a=\chi_a(N2)-\chi_a(N1)$
NNHCN[a]	-4.728	-4.544	0.184
NNHCl[b]	-4.611	-4.447	0.164
NNHF[c]	-4.978	-4.697	0.281

	$q_{zz}(N1)$	$q_{zz}(N2)$	$\Delta q_{zz}=q_{zz}(N2)-q_{zz}(N1)$
NNHCN	1.074	1.023	-0.051
NNHCl	1.072	1.020	-0.052
NNHF	1.075	1.004	-0.071

	$\Delta q_{zz}(N1) = q_{zz} - q_{zz}^m$	$\Delta q_{zz}(N2) = q_{zz} - q_{zz}^m$	$\%\Delta\rho$ $((\Delta q_{zz}/q_{zz}^m)100)$	
			N(1)	N(2)
NNHCN	0.008	-0.043	0.8	4.0
NNHCl	0.006	-0.046	0.6	4.3
NNHF	0.009	-0.062	0.8	5.8

	$\frac{\chi_a(N1)-\chi_a(N2)}{\chi_a(N1)+\chi_a(N2)}$	$\frac{q_{zz}(N1)-q_{zz}(N2)}{q_{zz}(N1)+q_{zz}(N2)}$
NNHCN	-0.020	-0.024
NNHCl	-0.018	-0.025
NNHF	-0.029	-0.034

a ^{14}N-nuclear quadrupole coupling constants, χ_a, are expressed in MHz and calculated electric field gradients, q_{zz}, in atomic units. N1 is the first nitrogen in each complex as written. q_{zz}^m is the calculated elecric field gradient of nitrogen in N_2 which is equal to 1.066 au.

b Goodwin and Legon (1985).

c Altman et al (1983).

d Soper et al (1982)

Table 3.15. Calculated and Experimental Nuclear Quadrupoie Coupling Constants.[a]

	χ^{d}_{calc}	χ^{d}_{o}	% difference	$\Delta\chi^{d}_{calc}$ $(\chi^{d}_{calc} - \chi^{m}_{calc})$	$\Delta\chi^{d}_{o}$ $(\chi^{d}_{o} - \chi^{m}_{o})$
HCNHCN N_1	-3.886	-4.480	-13	0.245	0.229
HCNHCN N_2	-4.127	-4.603	-10	0.005	0.106
HCNHCl	-3.805	-4.479	-15	0.327	0.230
HCNHF	-3.773	-4.363	-14	0.358	0.346

	$\chi^{d}_{calc}(N_1)$	$\chi^{d}_{calc}(N_2)$	$\chi^{d}_{o}(N_1)$	$\chi^{d}_{o}(N_2)$	% difference		$\Delta\chi^{d}_{calc}$ $(\chi^{d}_{calc}(N_2) - \chi^{d}_{calc}(N_1))$	$\Delta\chi^{d}_{o}$ $(\chi^{d}_{o}(N_2) - \chi^{d}_{o}(N_1))$
					N_1	N_2		
NNHCN	-4.870	-4.639	-4.728	-4.544	+3	+2	0.231	0.184
NNHCl	-4.861	-4.625	-4.611	-4.447	+5	+4	0.236	0.164
NNHF	-4.875	-4.553	-4.978	-4.679	-2	-3	0.322	0.281

[a] All values are expressed in MHz. A positive value for the "% difference" means that the calculated value is larger than the experimental value while a negative value means that the calcualted value is smaller than the experimental value. The quadrupole moment for the nitrogen nucleus is 1.93×10^{-26} cm^2 (Legon and Millen, 1986). If the electric field gradient is expressed in atomic units, $Q = (0.4256 \times 10^{-26}) \times (eQq \text{ MHz}/q) \text{cm}^2$

Figure 3.1

A display of the gradient vector field of ρ for NeHCl, ArHF, NNHCN and HCNHF. All of the trajectories of $\nabla\rho$ in the vicinity of a given nucleus terminate at that nucleus, in all three dimensions, thereby defining the basin of the atom.

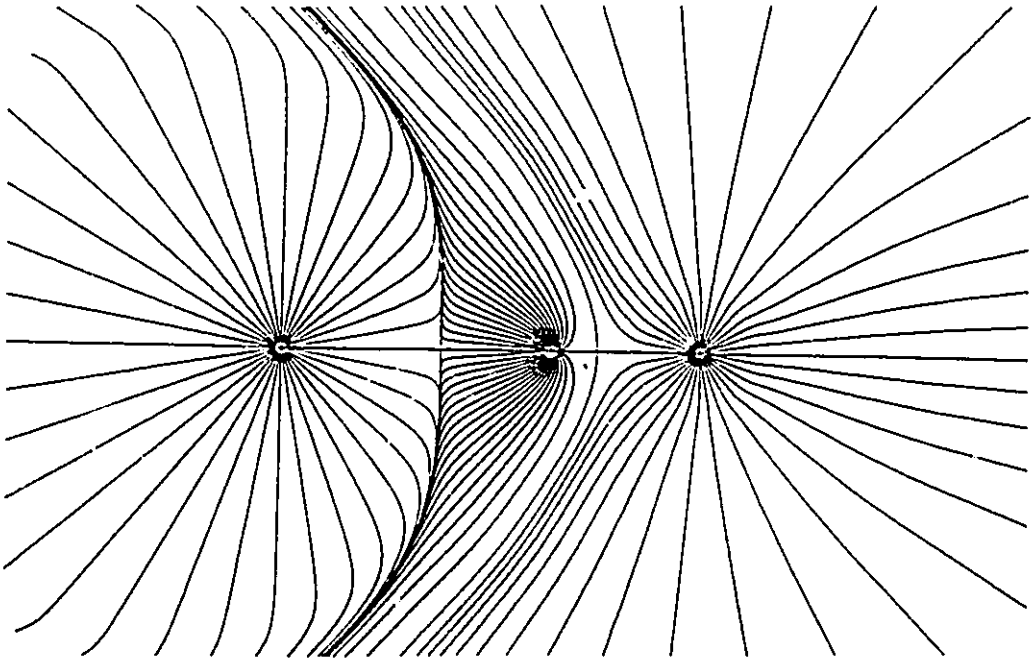

NeHCl

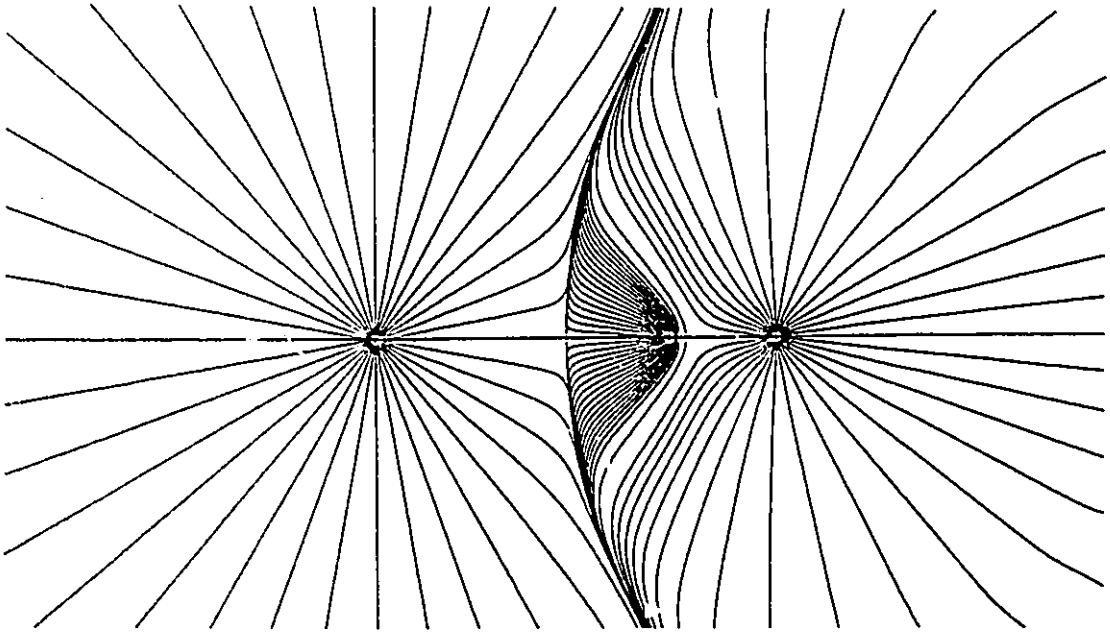

ArHF

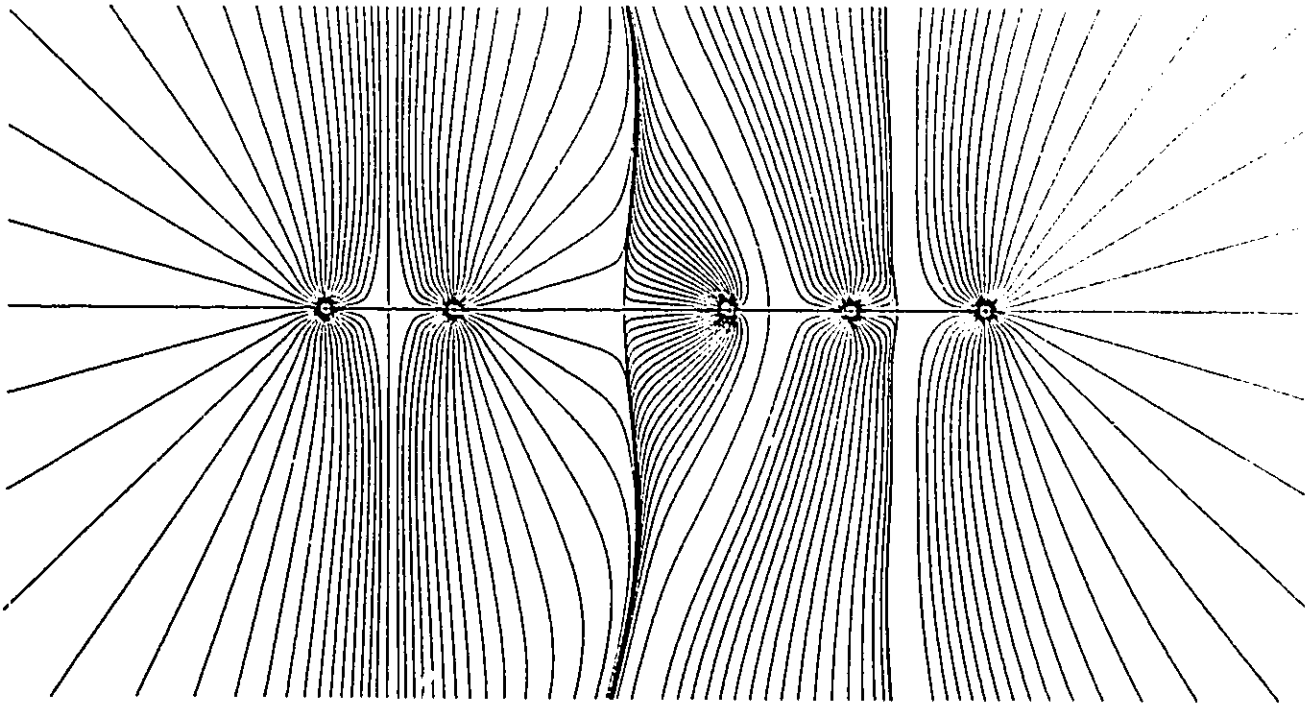

NNHCN

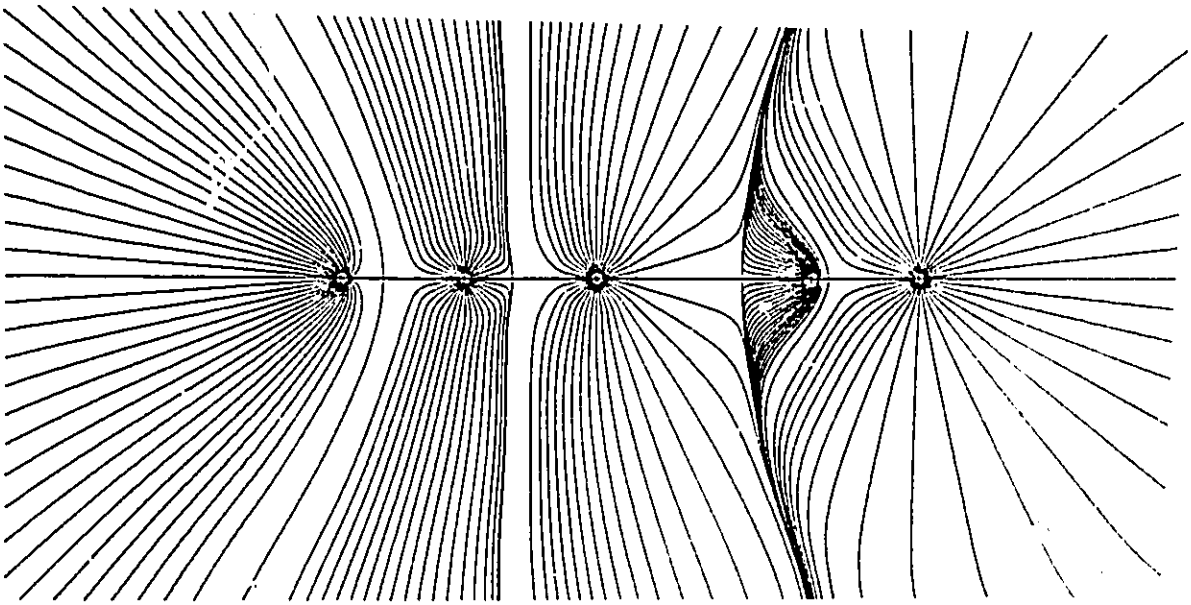

HCNHF

Figure 3.2

Contour maps of the charge density for NeHCl, ArHF, NNHCN, HCNHF, HF, HCl, NN and HCN with bond paths and atomic boundaries overlaid. The outermost charge density contour equals 0.001 au. The contours increase in order 2×10^n, 4×10^n, 8×10^n, with n increasing in steps of unity from n = -3.

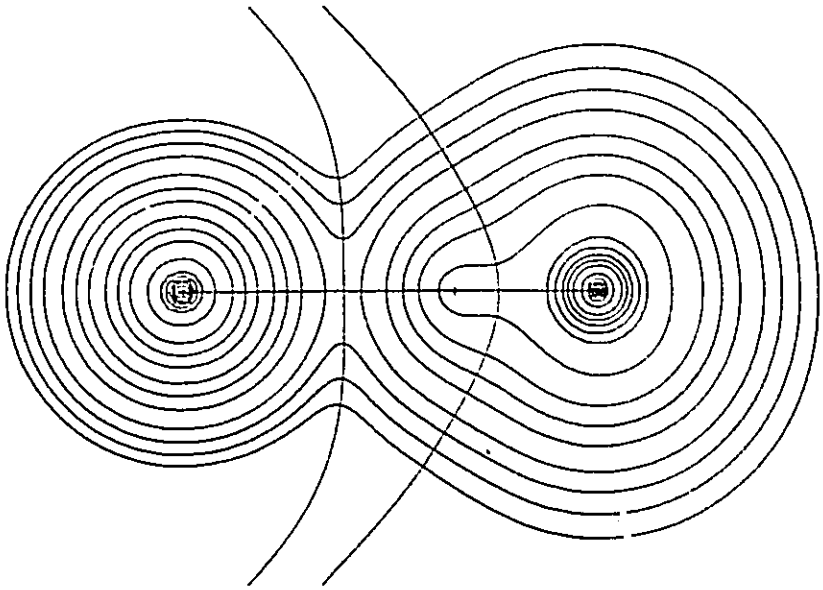

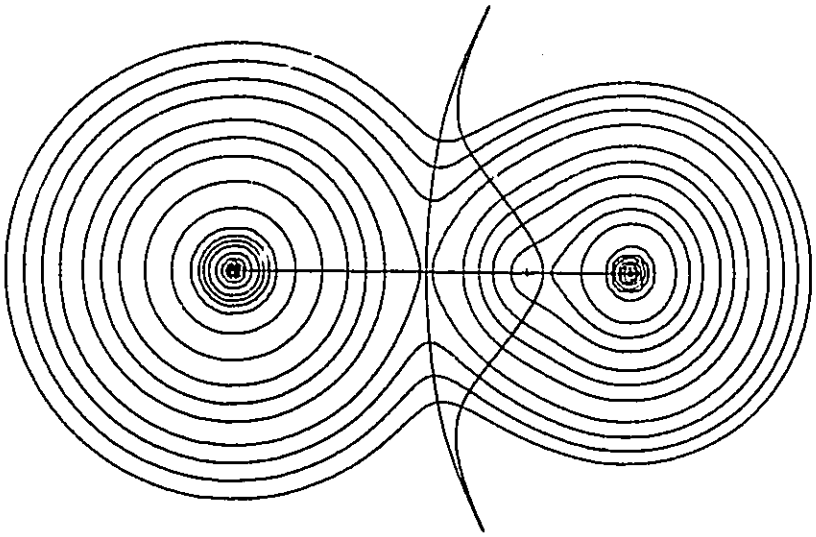

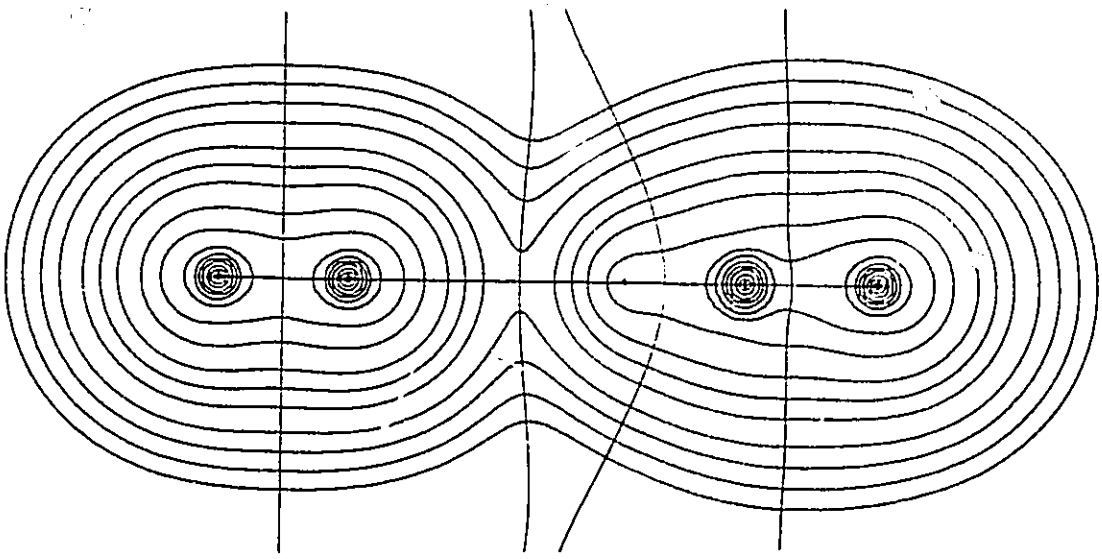

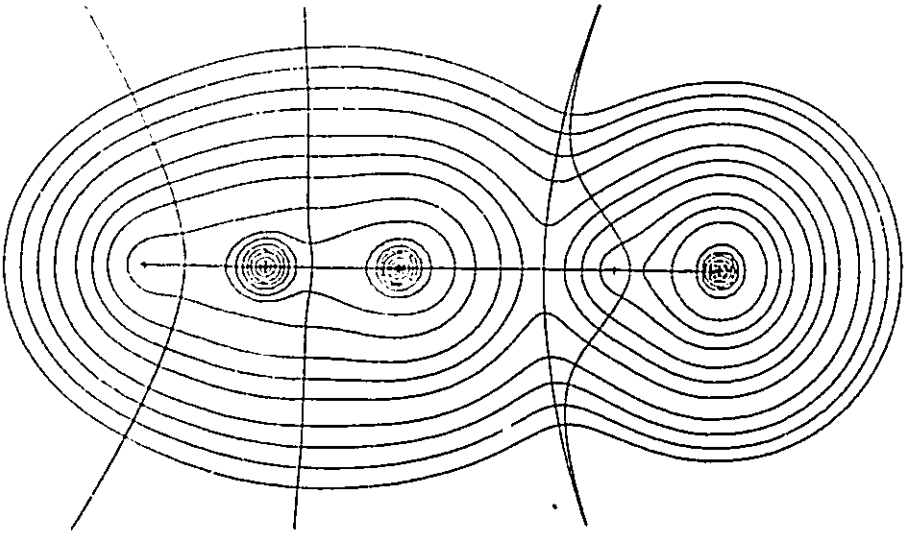

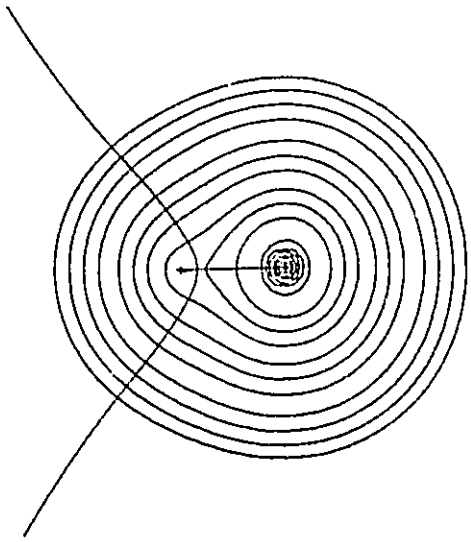

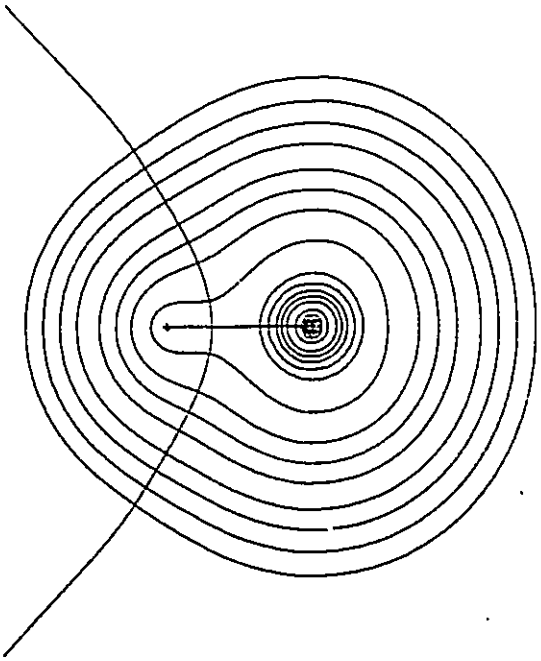

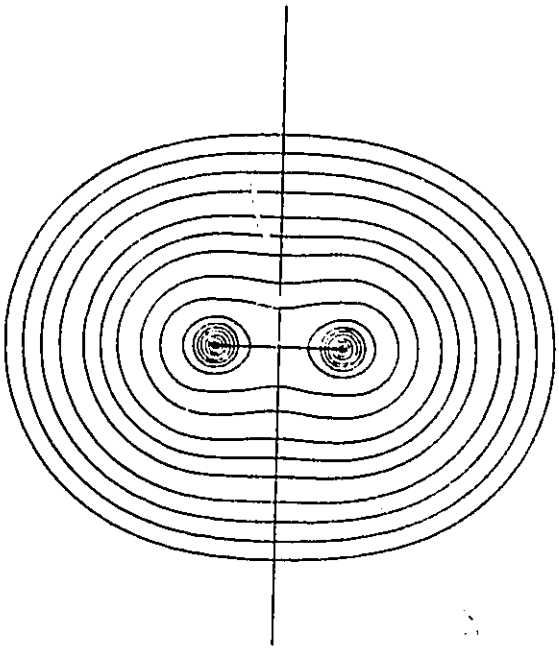

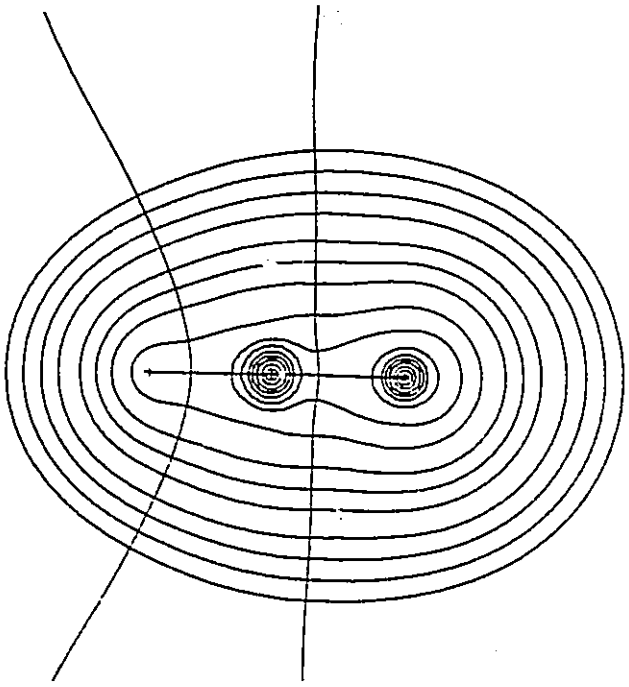

Figure 3.3

Contour map of the Laplacian of the charge density for NeHCl, ArHF, NNHCN and HCNHF with bond paths and the atomic boundaries overlaid. The contours of the Laplacian of the electronic charge density (solid contours $\nabla^2\rho < 0$, dashed contours $\nabla^2\rho > 0$) increase and decrease froma zero contour in steps $\pm 2 \times 10^n$, $\pm 4 \times 10^n$, $\pm 8 \times 10^n$, begining with $n = -3$ and increasing in steps of unity. The innermost solid contour encompassing a nucleus with $Z > 1$ encloses the innermost region of charge concentration.

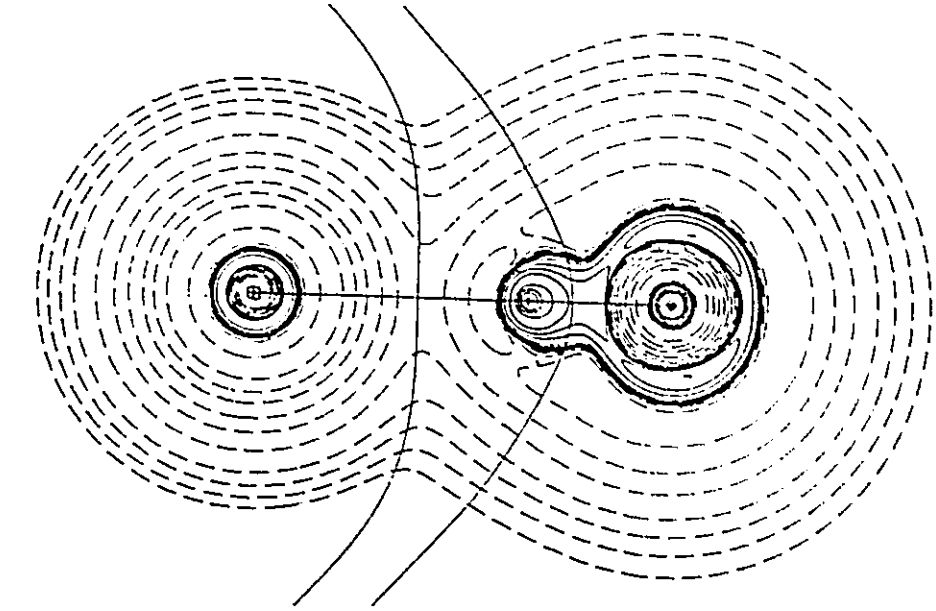

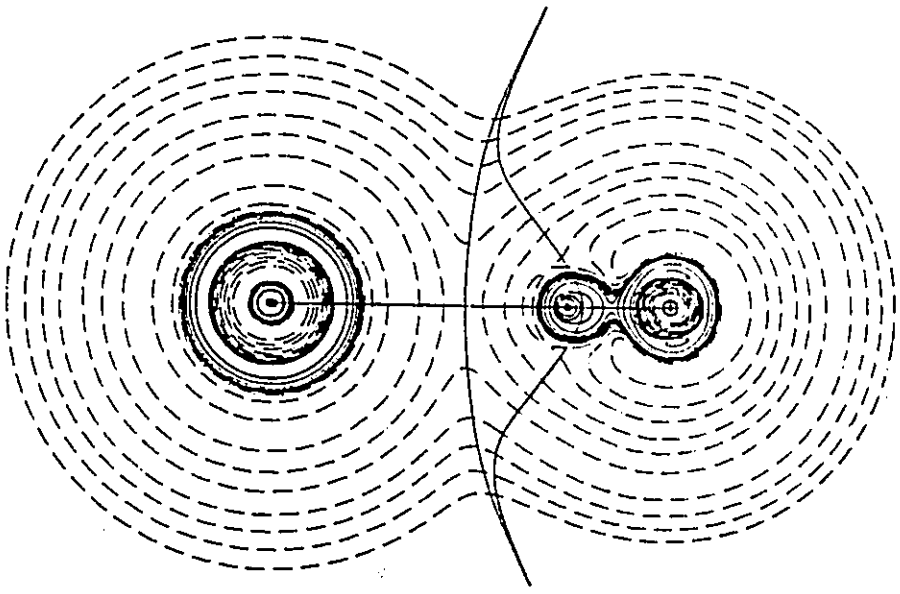

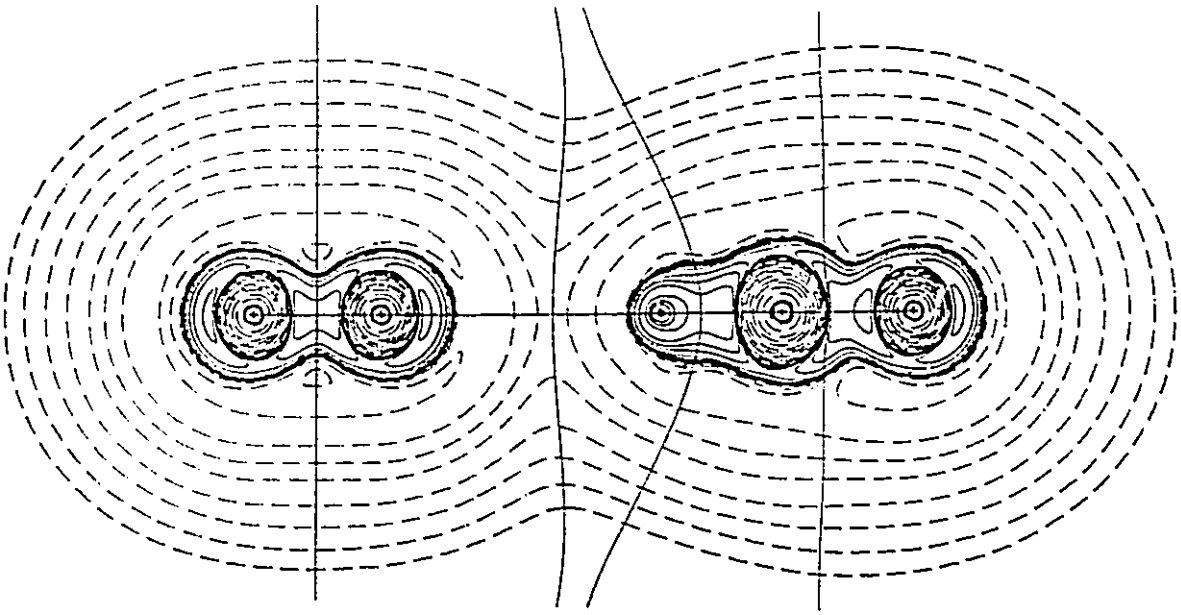

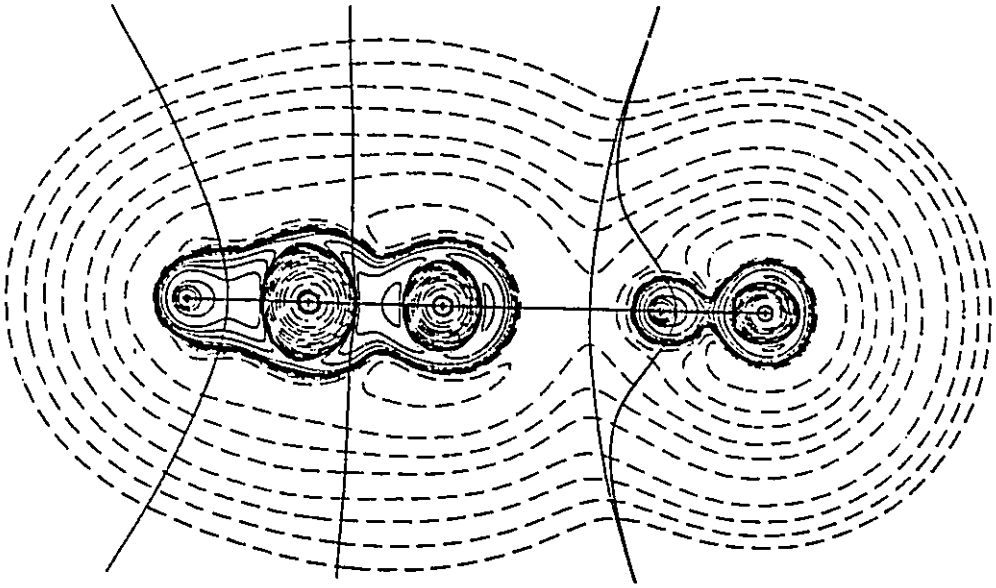

Figure 3.4

Profile maps of the Laplacian for the free argon atom along a radial line from the nucleus (left side) and for ArHF along the internuclear axis (right side). The distance "R" from the argon nucleus is in au.

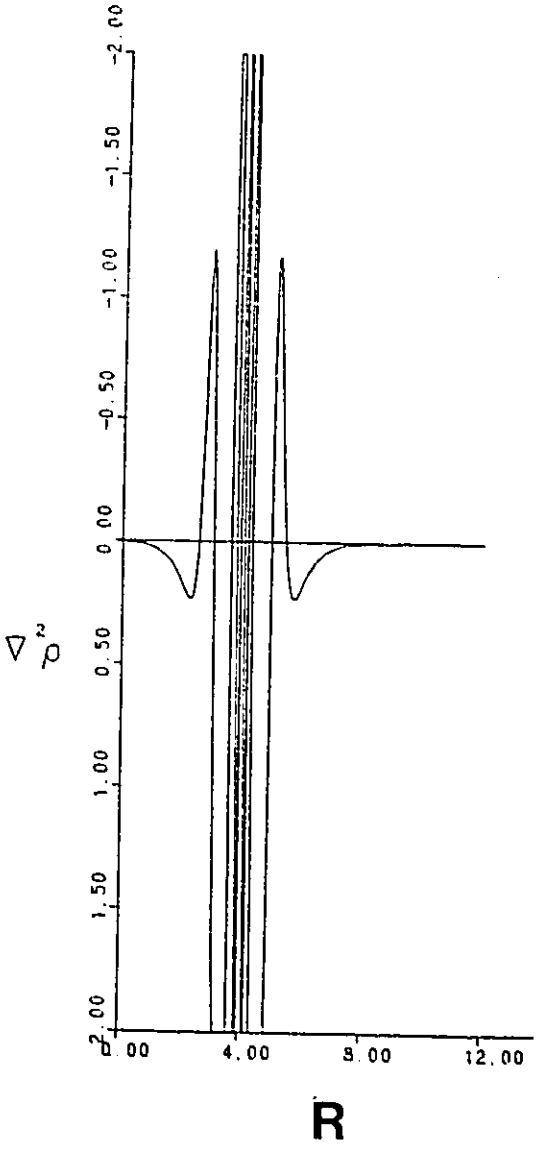
$\nabla^2\rho$
-2.00
-1.50
-1.00
-0.50
0.00
0.50
1.00
1.50
2.00
0.00
4.00
8.00
12.00
R

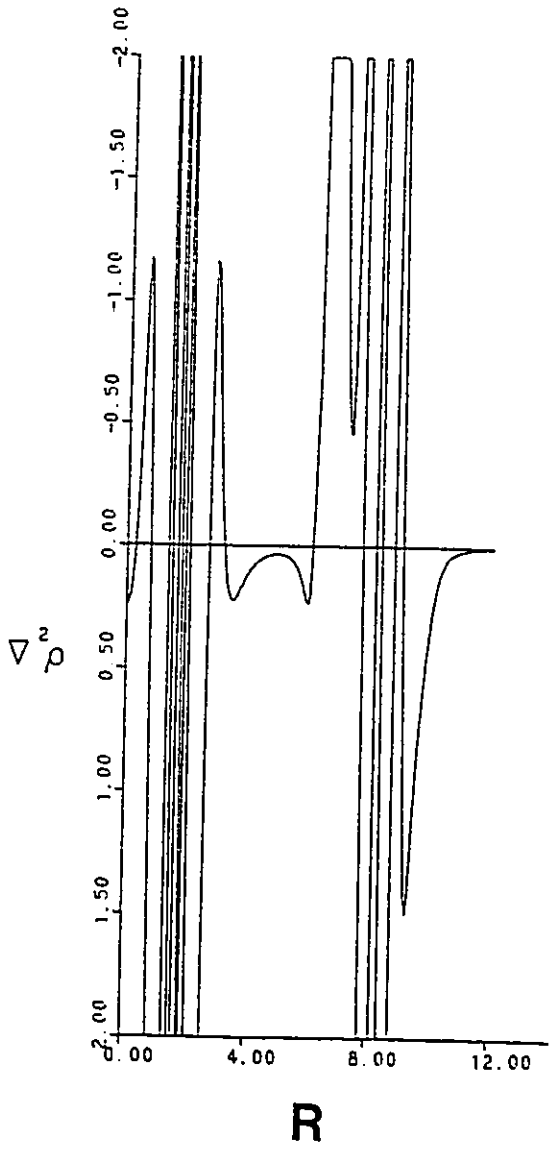
$\nabla^2\rho$
-2.00
-1.50
-1.00
-0.50
0.00
0.50
1.00
1.50
2.00
0.00
4.00
8.00
12.00
R

CHAPTER 4

Rotation and Inversion Barriers

This chapter addresses the origin of the barriers to rotation and inversion through the relative changes in the attractive and repulsive potential energies using the virial theorem. The redistribution of charge that determines these energy changes is also examined. The rotation barriers in ethane, methanol and methylamine are found to result from an increase in the attractive potential energy in spite of a decrease in the repulsive potential energy, while just the opposite is found for the inversion barriers in NH_3, PH_3 and H_3O^+ and for the barrier to bending in H_2O. Since the theory of atoms in molecules enables one to calculate all well-defined mechanical properties, new emphasis is placed on the study of these energies. This method of analysis, which is developed in detail here, is applied in Chapter 5 where it is used to address the hydrolytic cleavage of the P-O-P and P-O-C linkages.

Reprinted from the Journal of the American Chemical Society, 1990, 112.

Origin of Rotation and Inversion Barriers

R. F. W. Bader,*[†] J. R. Cheeseman,[†] K. E. Laidig,[†] K. B. Wiberg,[‡] and C. Breneman[‡]

Contribution from the Department of Chemistry, McMaster University, Hamilton, Ontario, L8S 4M1 Canada, and Department of Chemistry, Yale University, New Haven, Connecticut 06511. *Received November 1, 1989*

Abstract: This paper discusses the origin of barriers to rotation and inversion at the SCF and CI levels by use of the theory of atoms in molecules. The barriers are related to the changes in the attractive and repulsive potential energies through the use of the virial theorem. Rotation barriers in C_2H_6, CH_3OH, and CH_3NH_2 are shown to result from an increase in the attractive potential energy and in spite of a decrease in the repulsive energy. Just the opposite behavior is found for the inversion barriers in NH_3, PH_3, and H_3O^+ and for the barrier to bending in H_2O. The relative changes in energy found for the rotation barriers are anticipated for conformational changes dominated by an increase in internuclear separations, while those for the inversion barriers are typical of changes accompanied by decreases in these separations. The origins of the barriers are given in terms of the mechanical properties of the atoms. In ethane, the transformation of a S_3 to a C_3 symmetry axis in attaining the eclipsed geometry induces a quadrupole polarization of the density in the C–C bond, causing it to lengthen. This lengthening leads to a decrease in the magnitude of the attractive interaction of each carbon nucleus for the electronic charge in the basin of the other carbon atom, and this is the origin of the barrier. The changes in the charge distribution that determine these changes in atomic properties are not consistent with a model that relates the barrier in this molecule to Pauli-like exchange repulsions between localized C–H bond orbitals.

Introduction

The prediction and understanding of changes in energy are among the most important challenges in chemistry. Quantum mechanics predicts the change in energy accompanying a change in state for the total system and for every atom in the system.[1,2] The atomic view of a system's properties increases our understanding of the mechanics of a process and aids in our attempts to construct predictive models. In addition to predicting the total energy, quantum mechanics enables one to calculate the average values of the kinetic and potential energy contributions, the latter consisting of the nuclear–electron attractive potential energy (V_{ne}) and the electron–electron and the nuclear–nuclear repulsive energies (V_{ee} and V_{nn}, respectively). These energies, along with the contribution to the potential energy of the electrons arising from the virials of the external forces exerted on the nuclei,[1] are the only energy quantities defined in terms of the usual fixed-nucleus Hamiltonian in the absence of external fields. Model-independent predictions and interpretations of energy changes are, therefore, restricted to these quantities and the atomic contributions to these quantities. The theory of atoms in molecules, since it enables one to calculate all well-defined mechnical properties at the atomic level, places new emphasis on the study of these energies.

The electron–nuclear interaction energy is the only attractive interaction in a molecular system, and it is the decrease in the potential energy resulting from this interaction that is responsible for the formation of a bound molecular state from the separated atoms. In the absence of external forces acting on the nuclei, the virial theorem states that the total energy E equals $(1/2)V$, where $V = V_{ne} + V_{ee} + V_{nn}$ is the total potential energy. Similarly, the change in energy ΔE between two states free of external forces equals $(1/2)\Delta V$. Energy changes associated with relatively large reductions in internuclear separations, such as those enountered in the formation of molecules from atoms, lead to a decrease in the attractive potential energy and to increases in the electron–electron and nuclear–nuclear energies of repulsion. The attractive potential energy, however, does not necessarily decrease when the total energy decreases. Thus, it is possible for the total energy to decrease and for a system to become more stable in spite of an increase in attractive potential energy because of an even larger reduction in the energies of repulsion. Correspondingly, it is possible for the energy to increase and for a system to become less stable in spite of a decrease in the attractive energy.

One anticipates that the changes in the electron–electron and nuclear–nuclear repulsions will, in general, parallel one another. It is frequently found, as anticipated on simple grounds, that the changes in the repulsive energies V_{ee} and V_{nn} are nearly equal and that each is approximately half the magnitude of the change in the attractive potential energy. Consider the formation of AB from neutral atoms A and B. The new interactions, without charge transfer, are as follows: nuclear repulsion, Z_aZ_b/R; electron repulsion, $\approx N_aN_b/R$ $(=Z_aZ_b/R)$; electron–nuclear attractive energy, which is approximately equal to the negative sum of the two interactions, $\approx -(Z_aN_b/R + Z_bN_a/R)$. The same near-cancellation occurs when there is a transfer of charge A → B, but to the same order of approximation, one must include the change in the internal energies, a change that is approximated by $-I_a + A_b$ where I is an ionization potential and A an electron affinity. Thus, whether a nuclear displacement results in an increase or a decrease in the total energy is determinated by the difference in larger competing changes in the attractive and repulsive potential energies, changes that are approximately equal in magnitude.

Other decompositions of the total energy have been suggested. Allen[3a] introduced the terms attractive and repulsive dominant in the classification of barriers, with the attractive and repulsive contributions defined, respectively, as V_{ne} and $(T + V_{ee} + V_{nn})$. Payne and Allen[3b] discuss this and other partitionings of the energy in a review of barrier calculations done in the seventies. Csizmadia[4] has discussed the separate contributions of V_{nn} and the remaining energy terms $(T + V_{ne} + V_{ee})$, which he calls the electronic contribution, to energy barriers. These early results were criticized[3b,5] because of an apparent dependence of the resulting interpretation on the basis set. These sets were small, and difficulties in interpreting these early studies were further compounded by the use of unoptimized geometries. As is demonstrated here, these criticisms do not apply when one uses basis sets of a size sufficient to describe the accompanying relaxations in the charge density and optimized geometries are employed for the energy maxima and minima. In addition, the use of the virial theorem for the basis of the partitioning, as is done in the present study, enables one to isolate and include the contribution to the virial arising from the forces exerted on the nuclei for other

[†] McMaster University.
[‡] Yale University.

(1) Bader, R. F. W.; Nguyen-Dang, T. T. *Adv. Quantum Chem.* **1981**, *14*, 63.
(2) Bader, R. F. W. *Pure Appl. Chem.* **1988**, *60*, 145.
(3) (a) Allen, L. C. *Chem. Phys. Lett.* **1968**, *2*, 597. (b) Payne, P. W.; Allen, L. C. *Applications of Electronic Structure Theory*; Schaefer, H. F., Ed.; Plenum: New York, 1977; pp 29–108.
(4) Csizmadia, I. G. *Theory and Practice of MO Calculations on Organic Molecules*; Elsevier: New York, 1976.
(5) Veillard, A. *Internal Rotation in Molecules*; Orville-Thomas, W. J., Ed.; Wiley: New York, 1974; pp 385–424.

0002-7863/90/1512-6530$02.50/0

Table I. Dissociation, Rotation, and Inversion Barriers[a]

molecule	E, au	$\gamma = -V/T$	ΔE	ΔV_a, au	ΔV_r, au	ΔV_{nn}, au	ΔV_{ee}, au	ΔE(exptl)
				Dissociation[b]				
N_2	−109.298 81	1.998 74	8.0	48.1548	−47.5673	−24.2972	−23.2701	9.91[d]
BF	−124.438 59	2.000 73	6.9	38.0201	−37.5096	−19.1076	−18.4019	7.90[d]
LiF	−107.222 69	2.000 88	5.5	20.6530	−20.2499	−9.1466	−11.1032	5.97[d]
				Internal Rotation[c]				
C_2H_6	−79.257 33	2.000 26	3.0	0.3321	−0.3223	−0.1687	−0.1537	2.93[e]
CH_3NH_2	−95.251 67	2.000 34	2.0	0.1627	−0.1562	−0.0840	−0.0722	1.98[f]
CH_3OH	−115.086 44	2.000 54	1.0	0.0938	−0.0906	−0.0492	−0.0414	1.07[g]
				Inversion[j]				
NH_3	−56.436 95	1.999 50	5.4	−0.2058	0.2232	0.1043	0.1189	5.8[h]
PH_3	−342.649 92	1.999 97	34.2	−0.4875	0.5965	0.3429	0.2536	31.5[i]
H_3O^+	−76.569 23	1.999 89	2.1	−0.1028	0.1094	0.0335	0.0759	
H_2O	−76.293 26	2.000 08	33.0	−0.2345	0.3399	0.1237	0.2162	

[a] The potential energies have been scaled by a factor close to unity to satisfy the virial theorem. [b] 6-311++G(2d,2p)/6-311++G(2d,2p) CI singles and doubles. ΔE values in electronvolts. [c] 6-311++G(2d,2p)/6-311++G(2d,2p). ΔE values in kilocalories per mole. [d] Huber, K. P.; Herzberg, G. *Molecular Spectra and Molecular Structure*; Van Nostrand: New York, 1979. [e] Weiss, S.; Leroi, G. *J. Chem. Phys.* 1968, *48*, 962. [f] Lide, D. R., Jr. *J. Chem. Phys.* 1941, *27*, 343. [g] Ivash, E. V.; Dennison, D. M. *J. Chem. Phys.* 1953, *21*, 1804. [h] Dumbacker, B. *Theor. Chim. Acta* 1972, *23*, 346. [i] Weston, R. E. *J. Am. Chem. Soc.* 1954, *76*, 2645. [j] 6-311++G(2d,2p)/6-311++G(2d,2p) CI singles and doubles. ΔE values in kilocalories per mole.

geometries. The interpretations so obtained are stable to changes in the basis set and to the addition of correlation, and no contributions to the electronic potential energy are ignored.

We denote the electron–nuclear attractive potential energy as V_a and the sum of the electron–electron and nuclear–nuclear repulsive energies as V_r. The two possible origins of a barrier as determined by their relative changes are summarized in Figure 1. In case I, there is an increase in total energy E as a result of an increase in V_a and a smaller decrease in V_r, while in case II the increase in E is a result of a decrease in V_a accompanied by an even larger increase in V_r. Also indicated in the figure is the reverse of each process. The reverse of case I, as noted above, is generally associated with significant decreases in internuclear separations, such as the formation of a molecule from separated atoms. Thus, one anticipates that a case I barrier will result from an increase in internuclear separations. Table I lists values of ΔV_a and ΔV_r for the barrier to dissociation of N_2, BF, and LiF obtained from CI calculations that give dissociation energies close to the observed values. The magnitudes of ΔV_{nn} and ΔV_{ee} are nearly equal and each is approximately half of ΔV_{ne}, but overall the increase in V_a exceeds the decrease in V_r and $\Delta E > 0$. The value of V_{nn} is larger for N_2 than for isoelectronic BF, since Z_aZ_b is a maximum when $Z_a = Z_b$. Following similar arguments, one would expect a case II barrier to result from an overall decrease in internuclear separations, leading to the dominance of the repulsive energy increase in such instances.

Considered from the point of view of $\Delta E > 0$, case I is exemplified by barriers to internal rotation and case II by barriers to inversion. We shall discuss the barriers to internal rotation in ethane, methylamine, and methanol as examples of case I and the inversion or bending barriers in NH_3, PH_3, H_3O^+, and H_2O as examples of case II.

Theoretical Calculations

Calculations at the single-determinant level with use of the 6-311++G(2d,2p) basis set[6a] for both geometry optimization and energy determination were performed for all of the molecules. The above basis is the 6-311G** basis[6b] with an extra diffuse s and p set on the heavy atoms and an extra diffuse s function on H, together with a second set of polarizing functions on all atoms. The total energies obtained by Cade and Wahl[7a] for N_2 and by Cade and Huo[7b] for BF and LiF using a very extended set of STO's in calculations that are close to the Hartree–Fock limit are more negative than the SCF energies obtained here by 0.0116 au for N_2, 0.0164 au for BF, and 0.0115 au for LiF. The results reported here for NH_3, PH_3, H_2O, H_3O^+, N_2, BF, and LiF are obtained from configuration interaction calculations, with all single and double configurations generated from the large set of basis functions. In addition, MP2 calculations with the 6-31G** basis were performed for ethane, methylamine, and methanol to ensure that the results obtained for these molecules are also stable to the addition of electron correlation.

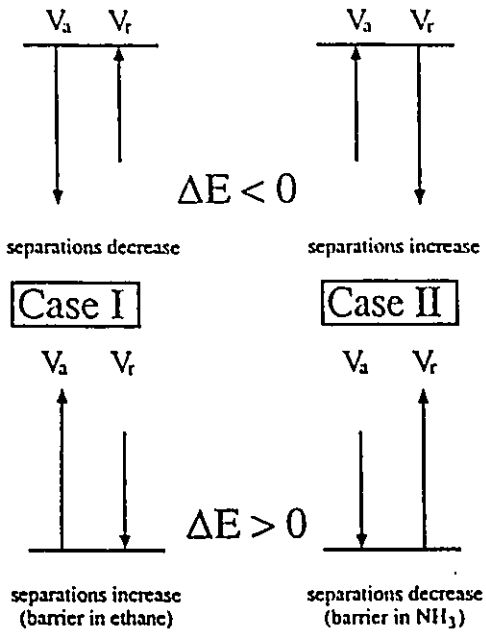

Figure 1. Diagramatic representation of the relative contributions of the changes in the attractive (V_a) and repulsive (V_r) energies to barriers characterized by an increase or decrease in internuclear separations.

The calculated total energies are reported in Table I. Good agreement of the values for rotation and inversion barriers obtained at the SCF level with the experimental values is anticipated on the basis of previous results.[3b] The SCF and correlated energy hypersurfaces for closed-shell systems parallel one another for nuclear motions such as inversions and rotations that do not involve large bond extentions,[8] implying that the correlation energy stays relatively constant for such motions. It is necessary to include polarizing functions in the calculation of inversion barriers because of the significant changes in hybridization that accompany such nuclear motions.[3b,9] The relative values of the contributions to ΔE reported in Table I, as well as the values of ΔE themselves, are stable to changes in basis set or level of calculation. The use of the 6-31G** basis with optimized geometries already recovers all of the results and conclusions reported here; results that are obtained with a much larger basis set and that include electron correlation.

(6) (a) Frisch, M. J.; Pople, J. A.; Binkley, J. S. *J. Chem. Phys.* 1984, *80*, 3265. Clark, T.; Chandrasekhar, J.; Spitznagel, G. W.; Schleyer, P. v. R. *J. Comput. Chem.* 1983, *4*, 294. (b) Krishnan, R.; Binkley, J. S.; Seeger, R.; Pople, J. A. *J. Chem. Phys.* 1980, *72*, 650. McLean, A. D.; Chandler, G. S. *J. Chem. Phys.* 1980, *72*, 5639.

(7) (a) Cade, P. E.; Wahl, A. C. *At. Data Nucl. Data Tables* 1974, *13*, 339. (b) Cade, P. E.; Huo, W. M. *At. Data Nucl. Data Tables* 1973, *12*, 415.

(8) Stanton, R. E. *J. Chem. Phys.* 1962, *36*, 1298.

(9) Rauk, A.; Allen, L. C.; Clementi, E. *J. Chem. Phys.* 1970, *52*, 4133.

Table II. Changes in Bond Lengths (Å) and Bond Angles (deg) upon Rotation or Inversion

molecule		bond length or bond angle	Δ[b]
C_2H_6	C–C	1.5247	0.0140
	C–H$_e$	1.0835	−0.0010
	∠H$_e$CC	111.19	0.42
CH_3NH_2[a]	C–N	1.4531	0.0064
	C–H	1.0877	−0.0049
	C–H$_e$	1.0820	0.0012
	N–H	0.9974	−0.0025
	∠HCN	114.36	−3.72
	∠H$_e$CN	109.36	2.28
	∠CNH	111.07	0.83
CH_3OH[a]	C–O	1.3999	0.0035
	C–H$_e$	1.0791	0.0039
	C–H	1.0850	−0.0030
	O–H	0.9383	−0.0018
	∠H$_e$CO	107.31	4.63
	∠HCO	111.79	−2.12
	∠COH	110.03	0.60
NH_3	N–H	0.9984	−0.0130
	∠HNH	107.98	12.02
PH_3	P–H	1.4042	−0.3500
	∠HPH	95.47	24.53
H_3O^+	O–H	0.9593	−0.0040
	∠HOH	113.30	6.7
H_2O	O–H	0.9410	−0.0180
	∠HOH	106.31	73.69

[a] Methyl hydrogens that become eclipsed in the rotated conformer are denoted by H$_e$. [b] A positive value denotes an increase in length or angle in attaining the transition-state geometry.

Discussion

Rotational Barriers. The dominant geometry change encountered in the formation of a rotationally eclipsed conformer from a staggered one is an increase in the length of the bond about which rotation occurs. In ethane, the C–C separation increases in forming the eclipsed conformer, and this increase is more than 10 times larger than the accompanying decreases in the C–H separations. The CCH bond angles open by 0.4°, and there is an overall decrease of 0.0069 Å in the separations of the hydrogens on a given carbon. In methylamine and methanol, the C–N and C–O separations also increase upon rotation to the eclipsed conformation, although by smaller amounts than the C–C bond in ethane. The bond lengths of the methyl hydrogens that become eclipsed (labeled as H$_e$ in Table II) increase in both molecules, as do the angles they make with the C–N or C–O axis, while the bonds and corresponding angles to the noneclipsed hydrogens undergo a decrease upon rotation. The N–H and O–H bond lengths also undergo a decrease. Unlike ethane, all of the changes in bond lengths are of roughly the same magnitude in methylamine and methanol. Both the predicted pattern of geometrical changes and their magnitudes are maintained at the MP2/6-31G** level of calculation. The MP2 calculations predict increases in the C–C, C–N, and C–O bond lengths upon rotation of 0.0134, 0.0068, and 0.0048 Å, respectively (compare Table II). Reference to Table I shows that these rotational barriers result from an increase in the attractive potential energy and a decrease in the repulsive potential energy, in agreement with the general arguments given above. The atomic origin of the barrier in ethane is presented next.

Rotational Barrier in Ethane. The increase in the C–C separation dominates the changes in V_{nn} and V_{ee} in ethane, as both these quantities undergo decreases of similar magnitude when the staggered (S) is rotated into the eclipsed (E) conformer. The same geometrical increase results in a lessening of the attractive interactions within the molecule, with the increase in V_{ne} exceeding the decrease in the repulsive interactions. Thus, the barrier to internal rotation in ethane results from a reduction in the attractive interactions between the nuclei and the electrons and in spite of an accompanying reduction in the electron–electron and nuclear–nuclear repulsions. The energy changes that give rise to the rotation barrier are characteristic of case I and represent a small reversal of the process of C–C bond formation (Figure 2).

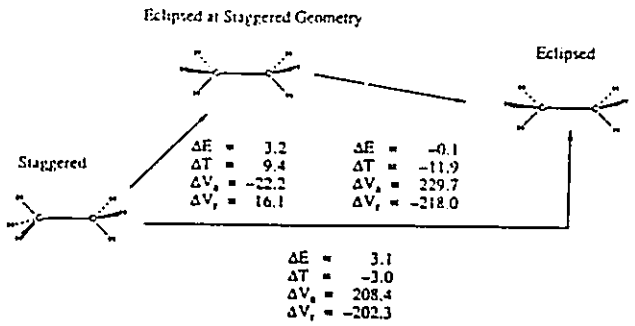

Figure 2. Energy changes for the rotation of the staggered conformer (S) into the eclipsed conformer (E) and into the frozen eclipsed conformer (FE).

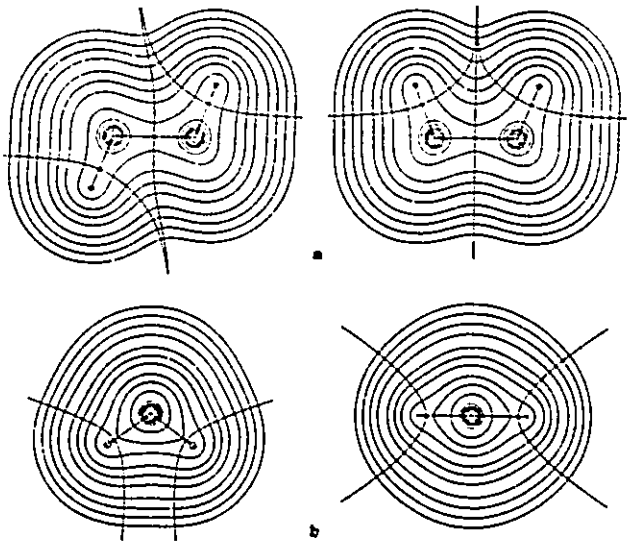

Figure 3. Contour maps of the electronic charge density for the staggered and eclipsed conformers of ethane and for the bent and linear conformers of water. The outermost contour has the value 0.001 au. The remaining contours increase in value in the order 2×10^n, 4×10^n, and 8×10^n beginning with $n = -3$ and increasing in steps of unity to give a maximum contour of 20 au. The bond paths, the interatomic surfaces, and the bond critical points are also indicated.

The changes in the charge distribution of ethane caused by the internal rotation are relatively small (Figure 3). The principal change is the replacement of the slightly curved C–C interatomic surface in the S conformer with the planar one of the E conformer, a consequence of the replacement of a threefold alternating axis of symmetry with a simple threefold axis. With reference to Figure 3, one sees that the upper arm of the atomic surface of an eclipsed hydrogen atom is moved inward relative to its form in the S conformer and the volume of a hydrogen atom that equals 38.44 au in the S geometry is slightly decreased, by 0.24 au. The remainder of the basin of a hydrogen atom is nearly unperturbed by the rotation. The changes in ρ at the bond critical points[10] are small, being largest for the C–C bond for which the value of ρ_b decreases by 0.0071 au from a value of 0.2495 au in the S conformer. Its value for the C–H bond increases by 0.0008 au from its value of 0.2908 au. The C–H bond critical point shifts by 0.0017 au toward the proton in the eclipsed geometry, a harbinger of the small transfer of charge from H to C that accompanies the rotation. The C–H bonds in ethane exhibit a small ellipticity[10] with major axes directed so as to be tangent to the cone obtained by rotation of the C–H bonds of a methyl group about the C–C axis. This ellipticity approximately doubles in value to 0.014 when the group is rotated into the eclipsed geometry.

(10) Bader, R. F. W.; Slee, T.; Cremer, D.; Kraka, E. *J. Am. Chem. Soc.* 1983, *105*, 5061.

Table III. Atomic Contributions to Barriers[a]

molecule	Ω	$E(\Omega)$	$q(\Omega)$	$\Delta E(\Omega)$	$\Delta N(\Omega)$	$\Delta V_a(\Omega)$	$\Delta V_r(\Omega)$	$\Delta V_a°(\Omega)$	r_H[b]	Δr_H
N_2	N	−54.649 40	0.000	92.2	0.000	24.0774	−23.7836	1.4239		
	$\sum_\Omega \Delta E(\Omega)$			184.4						
BF	B	−24.212 99	0.902	−239.3	0.902	10.8928	−11.6554	−2.2924		
	F	−100.225 59	−0.902	399.4	−0.902	27.1239	−25.8508	5.7786		
	$\sum_\Omega \Delta E(\Omega)$			160.1						
LiF	Li	−7.362 70	0.932	−43.5	0.932	5.4975	−5.6362	−0.7821		
	F	−99.859 95	−0.932	170.0	−0.932	15.1559	−14.6141	5.1026		
	$\sum_\Omega \Delta E(\Omega)$			126.5						
C_2H_6	C	−37.672 15	0.184	2.6	0.010	0.0878	−0.0802	−0.0135		
	H	−0.652 24	−0.0612	−0.3	−0.003	0.0261	−0.0270	0.0012	0.7766	−0.0017
	$\sum_\Omega \Delta E(\Omega)$			3.4						
NH_3	N	−54.917 46	−1.005	−36.5	0.145	−0.8874	0.7711	−0.5634		
	H	−0.506 49	0.335	14.0	−0.048	0.2274	−0.1829	0.0468	0.5112	−0.0226
	$\sum_\Omega \Delta E(\Omega)$			5.5						
PH_3	P	−340.271 67	1.546	3.2	0.131	−0.9957	1.0060	−0.4207		
	H	−0.792 91	−0.515	10.3	−0.044	0.1696	−0.1367	0.0426	1.2958	−0.0422
	$\sum_\Omega \Delta E(\Omega)$			34.1						
H_3O^+	O	−75.765 05	−1.222	−18.9	0.047	−0.3720	0.3117	−0.2668		
	H	−0.268 05	0.741	7.0	−0.016	−0.0898	−0.0675	0.0220	0.2959	−0.0071
	$\sum_\Omega \Delta E(\Omega)$			2.1						
H_2O	O	−75.539 33	−1.172	−101.1	0.310	−1.8776	1.5552	−1.3985		
	H	−0.376 97	0.586	67.1	−0.155	0.8223	−0.6085	0.2066	0.3447	−0.0604
	$\sum_\Omega \Delta E(\Omega)$			33.1						

[a] All results in atomic units except for ΔE values which are in kilocalories per mole. [b] r_H is the bonded radius of hydrogen.

Thus, the extent to which electronic charge is accumulated in the tangent plane containing the C–H bond as opposed to the one perpendicular to it, while small, is increased when the molecule attains the staggered geometry.

The atomic contributions to the energy changes are given in Table III. The changes in the energies of the individual atoms are small, a reflection of the small perturbations of the atomic charge distributions that accompany the internal rotation. The net charge on a H atom in the staggered form is $q(H) = -0.061e$. On changing to the eclipsed geometry, there is a transfer of 0.003e from each hydrogen to the carbons. Each H atom is stabilized by a small amount in the eclipsed geometry in spite of the small decrease in its population. Each carbon atom is destabilized by an amount nine times the magnitude of the stabilization of the hydrogens bonded to it, and this is the source of the barrier at the atomic level. The transfer of charge to C leads to a decrease in $V_a°(C)$, the potential energy of interaction of the C nucleus with its own charge distribution, with $\Delta V_a°(C) = -8.5$ kcal/mol. The energy change for C, however, is dominated by the increase in the C–C separation. This increase, while leading to a reduction in the repulsive interactions between the two C atoms, gives rise to an even greater reduction in the attractive interaction of each C nucleus with the charge density on the other C atom. ($\Delta V_a(C)$ consists of $\Delta V_a°(C)$, which is less than zero, and the interaction of each of the other nuclei with the charge density of the carbon atom in question. Since the C–H bond lengths have decreased in the eclipsed geometry and only the C–C length has increased, the increase in $V_a(C)$ is the result of the latter effect.) Thus, the carbon atoms are destabilized in the eclipsed geometry as a result of a decrease in the attractive interactions of each carbon nucleus with the charge density of the other. These energy changes of the carbon atom dominate the change in energy for the total system, and hence the barrier in ethane is an example of case I.

Orbital arguments concerning the origin of the barrier to rotation in ethane have been reviewed and discussed by Pitzer.[11] The explanation favored by him is based on a model in which the molecular orbitals for the staggered geometry are first frozen in form and the nuclear framework of the staggered geometry is rotated without change into the eclipsed geometry. This leads to a small negative barrier, a result that is interpreted to mean that simple electrostatic interactions between the ends of the molecule are not important in the ethane barrier. The freezing of the orbitals destroys their orthogonality, which is required by the Pauli principle, and the change in ρ obtained from their reorthogonalization results in so-called overlap or exchange repulsion contributions to the energy,[12] that is, to so-called "Pauli repulsions" between the C–H bond orbitals. Changes in the nuclear–electron and Coulomb integrals make the largest contributions to the potential energy change, resulting from this change in density.[11] The energy change could, therefore, be the result of an increase in V_a or of a decrease in V_r. Equating a repulsive interaction to the overlap of occupied orbitals and an attractive one to the overlap between filled and vacant orbitals has been used by a number of authors to account for rotational barriers.[13,14] This interpretation has been recently used by Dorigo et al.[15a] and by Carpenter and Weinhold.[15b,c] The two latter papers include extensive discussions of the effects of geometry optimization on rotation barriers.

Imposing orthogonality on some initial set of model orbitals and equating the changes in the model density to the requirements of the Pauli principle have been used previously to define "Pauli repulsions"[16] as found, for example, in the He_2 repulsive interaction or as evisaged in the VSEPR model of molecular geometry.[17] The difficulty with such models is that the answer one obtains is determined by one's choice of the original set of orbitals. This is illustrated by the work of Corcoran and Weinhold,[18] who showed that it is possible to pick a set of C–H bond orbitals almost identical with the set used in the Pauli repulsion model[11,12] in their final orthogonalized form, but predicting an ethane rotation barrier of incorrect sign when used in an antisymmetric wave function assuming a tetrahedral rigid-rotor geometry.

While, as shown in Figure 3, the charge distribution of ethane changes so that the basins of the eclipsed hydrogen atoms do not overlap in forming the E conformer, these changes in ρ do not correspond to a compression of the hydrogen atoms. A pair of eclipsed hydrogens do not share a common interatomic surface, and thus they do not touch as occurs in a closed-shell repulsion.

(11) Pitzer, R. M. *Acc. Chem. Res.* 1983, *16*, 207.

(12) Sovers, O. J.; Kern, C. W.; Pitzer, R. M.; Karplus, M. *J. Chem. Phys.* 1968, *49*, 2592.

(13) Gimarc, B. M. *Molecular Structure and Bonding*; Academic: New York, 1979, p 148ff.

(14) Lowe, J. P. *Prog. Phys. Org. Chem.* 1968, *6*, 1. Lowe, J. P. *Science (Washington, D.C.)* 1973, *179*, 527. Brunck, T. K.; Weinhold, F. *J. Am. Chem. Soc.* 1979, *101*, 1700.

(15) (a) Dorigo, A. E.; Pratt, D. W.; Houk, K. N. *J. Am. Chem. Soc.* 1987, *109*, 6591. (b) Carpenter, J. E.; Weinhold, F. *J. Phys. Chem.* 1988, *92*, 4306. (c) Carpenter, J. E.; Weinhold, F. *J. Mol. Struct. THEOCHEM* 1988, *169*, 41.

(16) Bader, R. F. W.; Preston, H. J. T. *Can. J. Chem.* 1966, *44*, 1131.

(17) Gillespie, R. J. *Molecular Geometry*; Van Nostrand Reinhold: London; 1972.

(18) Corcoran, C. T.; Weinhold, F. *J. Chem. Phys.* 1980, *72*, 2866.

This is reflected in the decrease in the repulsive contributions to their energy (Table III). Instead, the spatial extent of each hydrogen atom is diminished by a transfer of a small portion of its space and its contained charge to the carbon atoms, each of whose volumes increases by 0.47 au.

To demonstrate that the increased C–C bond length in the E conformer and hence the barrier are not a result of repulsions between eclipsed hydrogens, one can inquire into the origin of the barrier resulting from an internal rotation of the rigid nuclear framework of ethane from its staggered to an eclipsed geometry, and do so without recourse to a model state. Such a configuration of the nuclei, while physically realizable, does not lie on the reaction path, and it possesses an energy slightly in excess of the eclipsed transition-state geometry. Forces act on the nuclei in this constrained geometry such as to move them into the positions they occupy in the eclipsed transition state. Since the major geometrical change between the staggered and eclipsed equilibrium geometries is a lengthening of the C–C bond, one anticipates that the principle forces operative in the frozen eclipsed geometry are forces of repulsion acting on the two carbon nuclei. The changes in the potential and kinetic energies for the nuclear motions staggered to frozen eclipsed, S → FE, frozen eclipsed to eclipsed, FE → E, and S → E are summarized in Figure 2.

Because forces act on the nuclei in the FE conformation, the general statements of the virial theorem, which include the contributions of the virials of the nuclear forces to the total electronic energy, must be used.[19] The contribution of nucleus α to the virial of the forces acting on the electrons is equal to $-\mathbf{X}_\alpha\cdot\mathbf{F}_\alpha$, where $\mathbf{X}_\alpha$ is the position vector of nucleus α and $\mathbf{F}_\alpha = -\nabla_\alpha E$, the net force acting on it. The general statement of the virial theorem is

$$2T = -A = -V + \sum_\alpha \mathbf{X}_\alpha\cdot\mathbf{F}_\alpha \tag{1}$$

where A, the virial of the forces exerted on the electrons, is the potential energy of the electrons. When the forces on the nuclei vanish, $A = V = V_a + V_r$, and one obtains the corresponding statements of the virial theorem, $T = -E$ and $E = (1/2)V$. The general statement corresponding to $T = -E$ is

$$T = -E + \sum_\alpha \mathbf{X}_\alpha\cdot\mathbf{F}_\alpha \tag{2}$$

When the nuclear virial is positive, T must exceed $|E|$ to balance the contribution to the virial arising from the repulsive forces acting on the nuclei. Since we are taking differences between a state where the forces do not vanish and one where they do, the total nuclear virial for the nonequilibrium state appears in the difference. Thus, for the reaction S → FE, the change in kinetic energy equals minus the change in total energy plus the nuclear virial:

$$\Delta T = -\Delta E + \sum_\alpha \mathbf{X}_\alpha\cdot\mathbf{F}_\alpha \tag{3}$$

Since ΔT is positive for the reaction S → FE (Figure 2) and exceeds the magnitude of ΔE, the nuclear virial is positive, showing that this contribution to the potential energy of the electrons is dominated by repulsive forces acting on the nuclei. The corresponding expression for the change in potential energy is

$$\Delta V = \Delta V_a + \Delta V_r = 2\Delta E - \sum_\alpha \mathbf{X}_\alpha\cdot\mathbf{F}_\alpha \tag{4}$$

In this case, V_a decreases and V_r increases, both quantities changing in the direction opposite to that for the overall reaction S → E, but the increase in repulsive energy arising from the nuclear–nuclear and electron–electron forces is less than the decrease in the attractive potential energy, and overall the change in the potential energy is less than zero; i.e., the attractive contributions dominate. *Thus, the increase in energy encountered in the formation of the frozen eclipsed conformer comes not from an increase in the usual potential energy contributions but from the virials of the repulsive forces acting on the carbon nuclei in the nonequilibrium geometry.* This is also evident in the expression for the total energy change expressed as $\Delta E = \Delta T + \Delta V$. The fact that $\Delta T > \Delta E$ shows that ΔT includes the contribution of a repulsive nuclear virial. The atomic contributions to the change S → FE, like those for S → E, come primarily from the carbon atoms, $\Delta T(C) = 4.0$ kcal/mol and $\Delta V_a(C) = -35.8$ kcal/mol, while $\Delta T(H) = 0.2$ kcal/mol.

The geometry changes encountered in the reaction FE → E result in a decrease of only 0.1 kcal/mol in the total energy. However, the relaxation in the geometry, particularly the lengthening of the C–C internuclear separation, causes sizable changes in the potential energy contributions, primarily those of the carbon atoms. The contribution from the nuclear virial vanishes in reaching this metastable geometry, and the attractive and repulsive potential energy contributions change in the direction dictated by case I for the partial unmaking of the C–C bond, with $\Delta V_a > 0$ and $\Delta V_r < 0$, the kinetic energy undergoes a decrease that, aside from the small ΔE value, equals the loss of the nuclear virial. The value of $\Delta T(H)$ is only 0.1 kcal/mol for this change, showing that essentially the whole of the decrease in T comes from the carbon atom contributions. Thus, the energy increase associated with the rigid rotation of one methyl with respect to another to give the frozen eclipsed geometry arises from the contribution of the virials of the repulsive forces generated on the carbon nuclei, and this change in energy overides the decrease in the potential energy V.

One can investigate further the nature of the changes in the charge density over the basins of the carbon atoms to better understand the accompanying changes in energy. The first moment of an atom is defined as

$$\mu(\Omega) = -e\int_\Omega \mathbf{r}_\Omega \rho(\mathbf{r})\, d\tau \tag{5}$$

where the position vector $\mathbf{r}_\Omega$ is defined with the nucleus of Ω as origin. The z component of the traceless quadrupole moment tensor for atom Ω is defined as

$$Q_{zz}(\Omega) = -e\int_\Omega (3z_\Omega^2 - r_\Omega^2)\rho(\mathbf{r})\, d\tau \tag{6}$$

In the S conformation of ethane, each carbon atom is polarized toward the other with $|\mu_z(C)| = 0.030$ au. This value decreases to 0.025 au in the FE conformation. Thus, electronic charge is shifted from the binding to the antibinding regions of the carbon nuclei[20] (where these regions are defined with respect to the carbon nuclei) when the molecule is rotated without the possibility of relaxing the C–C separation. These counterpolarizations contribute to the forces of repulsion acting on the carbon nuclei in the FE conformation. They are destroyed and replaced by an even larger polarization of each carbon atom into its binding region, $|\mu_z(C)| = 0.039$ au, when the FE conformation is allowed to relax to the force-free E conformation. The value of $Q_{zz}(\Omega)$ for a carbon atom in the S conformation is +0.031 au, a polarization that corresponds to the transfer of charge from along the C–C axis to a toruslike distribution about this axis. (For comparison, the same moment for a carbon atom in acetylene has the value of 4 au.) This moment is increased to 0.074 au in the FE conformation and undergoes a further increase to 0.092 au in the E conformation. The effect is a progressive transfer of charge density from along the C–C internuclear axis to a torus of density about this axis, a polarization that contributes to the lengthening of the C–C bond and to the shortening of the C–H bonds as occur in the E conformation.

The explanations of the barriers for S → FE and for S → E, stated in terms of the associated changes in the atomic potential and kinetic energies and in terms of the forces exerted on the nuclei, are at variance with those based on the consequences of an assumed nonorthogonality of localized C–H bond orbitals.[11,12] First, the principal physical change accompanying the internal rotation, the lengthening of the C–C internuclear separation, appears not to have been included in the model calculations. Second, as a result of the dominance of this geometry change, the principal changes in the charge distribution occur along the C–C bond path and within the basins of the carbon atoms, with

(19) Slater, J. C. *J. Chem. Phys.* **1933**, *1*, 687.

(20) Berlin, T. *J. Chem. Phys.* **1951**, *19*, 208.

only relatively small changes occurring along the C–H bond paths and within the basins of the hydrogen atoms. It is difficult to rationalize the changes in density anticipated to result from the requirements of orthogonality, in this case on the localized C–H bond orbitals, with the changes in the charge density that are found to occur. One might argue that the greater C–C separation found in the E conformation is a consequence of the exchange repulsions between the C–H bond orbitals. However, the changes in density and energy for the reaction S → FE do not correspond to those anticipated on the basis of the overlap of occupied bond orbitals, as even here the primary changes in density are along the C–C axis and within the basins of the carbon atoms, and the change in potential energy is attractive rather than repulsive. The barrier in this case, which is of almost the same size as the equilibrium barrier, results from the creation of repulsive forces on the carbon nuclei whose presence increases the total energy of the system by increasing the electronic kinetic energy of the carbon atoms. Relaxing the geometry by lengthening the C–C separation to its value in th E geometry replaces these forces of nuclear repulsion with a barrier arising from an increase in the attractive potential energy of the carbon atoms.

To understand the origin of the barrier in ethane, one must understand why the C–C bond is lengthened in the eclipsed geometry. The change S → E transforms an alternating axis of symmetry into a threefold axis. The alternating field of the protons exerted the length of the C–C axis in the Hamiltonian of the S conformation is replaced by a more pronounced field with a threefold symmetry in the Hamiltonian for the E conformation. This change in the Hamiltonian has the effect of increasing the quadrupolar polarization of the electronic charge density along the C–C axis, removing charge from this axis and concentrating it in a toruslike distribution about the axis. As a consequence, the electronic charge in the C–C binding region is less effective in binding these nuclei and the C–C separation increases. This same quadrupolar polarization slightly increases the binding of the protons.

Inversion Barriers. The A–H internuclear separations in NH_3, PH_3, H_3O^+, and H_2O decrease when the pyramidal or bent geometry is transformed into the planar or linear form, respectively, with an accompanying increase in the HAH bond angles to 120° or 180° (Table II). The approach of the protons toward the A nucleus, while resulting in a lowering of the electron–nuclear attractive potential energy (Table I) in the planar or linear geometry, leads to an even greater increase in the repulsive interactions. The inversion barrier in these molecules is thus a consequence of an increase in the repulsive interactions that outweighs an accompanying decrease in the attractive potential energy, an example of a case II energy change. Rauk et al.,[9] in the first successful calculation of the barrier in ammonia, give the same explanation for its origin. The decreases in internuclear separations in these molecules result in an increase rather than a decrease in the total energy of the system, a behavior opposite to that found for case I.

The hybridization model predicts an increase in the electronegativity of the A atom relative to hydrogen in the attainment of the planar or linear geometries. This is a consequence of the increase in the s character of its bonds to hydrogen, from sp^3 to sp^2 or from p to sp, coupled with the fact that s electrons are more tightly bound than are p electrons. On this basis, one predicts a transfer of charge from H to A to accompany the shortening of the A–H bonds in the formation of the planar or linear geometries. This prediction and the associated energetic consequences are found to be correct, as indicated by the data in Table III.

The molecular charge distributions of the pyramidal and bent molecules undergo larger perturbations during inversion or linearization as a consequence of the accompanying change in hybridization than does a charge distribution for a molecule undergoing internal rotation. This greater reorganization of the charge is reflected in the larger changes in the atomic energies, changes that are a direct measure of the extent of change in the distribution of charge over the basin of each atom. The sizable redistribution of charge caused by the change in hybridization of the N atom in attaining the planar form of ammonia is reflected in the value of $Q_{zz}(N)$ changing from −2.92 au in the pyramidal molecule to −4.15 au in the planar geometry. Table III also lists the bonded radius of hydrogen in the equilibrium geometry and the change in this radius when the barrier is attained. The shifts in the A–H interatomic surface toward the proton associated with these changes are much larger for the inversion barriers than for the rotation barrier in ethane (Figure 3). Note that the decrease in the radius of the hydrogen atom parallels the increase in the electronegativity of the A atom to which it is bonded, r_H decreasing in the order A = P, C, N, O, and O^+.

The change in the relative electronegativities of N and H and the associated changes in their stabilities resulting from the change in hybridization upon inversion have a direct parallel with the changes in the properties of the carbon and hydrogen atoms of the methylene group of a normal hydrocarbon when it is transferred to a cyclic system with geometric strain. As pointed out by Walsh[21] and by Coulson and Moffit,[22] the orbital model predicts an increase in the carbon s character of the C–H bonds of a methylene group in cyclopropane compared to the unstrained group, as a result of the decrease in the C–C–C bond angle and the associated increase in p character of the C–C bonds. The transfer of the standard transferable methylene group of the normal hydrocarbon series into the cyclopropane ring structure leads to a transfer of 0.05e from each of its hydrogens to carbon, to an opening of the HCH angle and to a shortening of the C–H bonds.[23] The increased s character and the resulting increase in population of the carbon atom lead to an increase of 15.6 kcal/mol in its stability and to a corresponding decrease of 12.6 kcal/mol in the stability of each of the hydrogen atoms. Overall, the transfer of charge within the CH_2 group leads to a 9.6 kcal/mol increase in its energy relative to the standard methylene group and to a total strain energy three times this, or 28.8 kcal/mol, a value in agreement with experiment. In the same manner, the theory successfully accounts for the strain energies in cyclobutane and cyclopentane and correctly predicts cyclohexane to be strain-free. The destabilization of the hydrogens also exceeds the stabilization of the nitrogen atom in the formation of planar ammonia. In terms of the mechanical properties of atoms, the strain energy of a methylene group in a cyclic hydrocarbon and the inversion barrier in ammonia have a common origin.

The transfer of charge from H to A is larger in the linearization of water than in the pyramidalization of ammonia, and the energy barrier and changes in atomic energies are correspondingly greater for H_2O than for NH_3. The pattern of energy changes and their contributions, however, is the same for the barrier in water as it is for the barrier in ammonia, with the hydrogens being destabilized to a greater extent than the oxygen atom is stabilized. The pattern of atomic contributions is also the same for the barrier in the hydronium ion, but the charge transfer from the hydrogens to the oxygen is considerably less than in water or ammonia. The energy changes are correspondingly smaller and more evenly matched; the destabilization of the hydrogens is predicted to exceed the stabilization of the oxygen by less than 2 kcal/mol. The small transfer of charge in this case is understandable, as the hydrogens already bear a net charge of +0.74e in the pyramidal geometry of H_3O^+ and the remaining charge density on the protons is relatively tightly bound. The repulsive contributions to the energy changes of the hydrogen atoms decrease in all these molecules, and the increase in the repulsive interactions that dominates the barriers is localized within the A atoms.

The change in $V_s^o(\Omega)$—the change in the attractive interaction of the nucleus of atom Ω with its own charge density—is stabilizing for the A atom and destabilizing for the hydrogens in each of the molecules. The observation that the magnitude of the decrease in $V_s^o(A)$ is considerably greater than is its increase for all the

(21) Walsh, A. D. *Nature (London)* **1947**, *159*, 167, 712.
(22) Coulson, C. A.; Moffitt, W. E. *Philos. Mag.* **1949**, *40*, 1.
(23) Wiberg, K. B.; Bader, R. F. W.; Lau, C. D. H. *J. Am. Chem. Soc.* **1987**, *109*, 1001.

hydrogens in a given molecule shows that the binding of the charge transferred to the A atom is significantly increased and is one of the principal contributors to the attractive energy contributions to the barriers in these molecules.

The phosphorus atom is slightly destabilized in the planar geometry in spite of being the recipient of a transfer of charge from the hydrogen atoms. While small changes in the charge distribution of an atom lead to small changes in its energy, it is possible that a change in the distribution can be such as to result in a near-cancellation of the changes in the attractive and repulsive contributions, as occurs for the phosphorus atom in the inversion of PH_3. This differing behavior of a second- and third-row atom can be accounted for in terms of the larger size of the latter atom. The magnitude of the decrease in the value of V_a° for the second-row atoms is greater than half the total decrease in $V_a(\Omega)$ (Table III). The charge transferred to the P atom, however, is relatively less effective at stabilizing the atom, since the added density is further from the attractive force of the nucleus. There is a smaller increase in stability per added electron for P than for N or O. The diffuse nature of the phosphorus charge distribution is reflected in the very large increase in its quadrupole polarization that accompanies the transfer of charge to this atom in the attainment of the planar structure, $Q_{zz}(P)$ changing from −4.2 to −13.1 au. The decrease in the A–H bond length in attaining the planar geometry is largest in PH_3, and this atom has the largest relative increase in its repulsive energy contributions. Both the A and H atoms are destabilized in PH_3, and the inversion barrier in this molecule is six times larger than the barrier in NH_3.

Conclusions

The observations made here regarding the changes in energy and geometry associated with internal rotations and inversions should be of general applicability. For example, the same observations apply to the origin of the barrier to internal rotation about the C–O bond in carboxylic acids and esters, as studied by Wiberg and Laidig.[24] Their calculations predict formic acid, methyl formate, acetic acid, and methyl acetate to possess a minimum energy planar Z conformation. Like the rotational barriers studied here, they find the principal geometry change associated with the attainment of the nonplanar conformation to be a lengthening of the bond about which the rotation occurs, and the barriers to arise from an increase in the attractive potential energy and in spite of a decrease in the repulsive interactions. The largest energy changes occur for the C and O atoms of the rotated bond, the carbon being stabilized and the oxygen being destabilized in the nonplanar rotamer.

The origin of the barrier for the rotation of planar formamide by 90° or 270° was also investigated.[24] This is an interesting case, as here the rotation about the C–N bond results in the pyramidalization of the N atom and its formal hybridization changes from sp^2 to sp^3. Thus, as for the inversion barriers discussed above, the N atom is found to gain electronic charge from its bonded neighbors and to increase in stability when the amide group is rotated from a nonplanar into its planar form. In this molecule, however, the destabilization of the atoms that donate charge to the N atom in the planar geometry is less than the stabilization achieved by the N atom, and the equilibrium geometry of this molecule is planar. Here again, the principal geometrical change is a lengthening of the bond about which rotation occurs (as in the inversion of ammonia, the bonds to N are shortest when its s character is greatest), and the predicted barrier of 16.0 kcal/mol is a result of an increase in the attractive potential energy and a decrease in the repulsive energies. Because of the transfer of charge from N to C that accompanies the loss of planarity, most of the lengthening of the C–N bond, which equals 0.15 au, is taken up by an increase in the bonded radius of the carbon atom, from 0.83 to 1.04 au. The resonance model accounts for the relative stability of the planar geometry by invoking a resonance structure wherein the N atom donates charge to the carbonyl oxygen atom, a resonance interaction that is lost upon rotation. The resonance model is, therefore, in direct contradiction with the hybridization model for these systems, which predicts the N to be most electronegative in the planar structure. The theory of atoms in molecules shows the resonance model to be wrong in this instance.[24] Not only is the direction of the charge transfer for N incorrect, the properties of the oxygen atom, including its geometrical parameters, are found to change by only small amounts compared to the changes undergone by the C and N atoms, the magnitude of its energy change being 20–30 times smaller. This conclusion is not some artifact of the theory of atoms in molecules. It is a result of the observation that the distribution of charge over the basin of the oxygen atom—a well-defined region of real space extending to within 0.74 au of the carbon nucleus—is only slightly perturbed by a rotation about the C–N axis. Siggel et al.[25] make the same criticism of the resonance model with regard to its explanation of the relative acidities of carboxylic acids and alcohols. The enhanced acidity of the former over the latter is accounted for by the inductive effect, as measured by spatially determined atomic populations, rather than increased resonance stabilization of the carboxylate anion.

An atomic property and its change are determined by the distribution of electronic charge and its change over the basin of the atom and are model-independent. Because of this, the theory may be used to test existing models and aid in the construction of new ones.

(24) Wiberg, K. B.; Laidig, K. E. *J. Am. Chem. Soc.* 1987, *109*, 5935.

(25) Siggel, M. R. F.; Streitwieser, A.; Thomas, T. D. *J. Am. Chem. Soc.* 1988, *110*, 8022.

CHAPTER 5

Energetics of the Hydrolysis Reactions of Diphosphoric Acid, Methyldiphosphoric Acid and Phosphoenolpyruvate.

5.1 "High-Energy" Phosphate Compounds

Adenosine triphosphate (ATP) plays an important role as the energy source in various biochemical processes. The energy released by the hydrolysis of ATP to adenosine diphosphate (ADP) and inorganic phosphate is used in biosynthesis, active transport, contraction of muscle, etc. Biologically important phosphorylated compounds with unusually large and negative free energies of hydrolysis at physiological pH have been described as "high-energy" compounds. Table 5.1 shows the ΔG° values for the hydrolysis of a number of important phosphate compounds, arranged in order of increasingly positive values. Compounds with the more negative values undergo more complete hydrolysis at equilibrium and therefore tend to lose phosphate groups more readily than those near the bottom of the scale. ATP is unique because it has an intermediate value in this thermodynamic scale. Two classes of phosphorylated compounds have a standard free energy of hydrolysis substantially more negative than ATP. This first class includes 1,3-diphosphoglycerate and phosphoenolpyruvate, generated during enzymatic breakdown of fuel molecules. The second class of phosphorylated compounds include the phosphogens which consist mainly of phosphocreatine and phosphoarginine and serve as storage reservoirs of phosphate bond energy. Most low-energy phosphate compounds are phosphoric acid esters of organic alcohols.

Phosphorylated compounds found in cells were originally classified into high-energy and low-energy compounds, according to the magnitude of the ΔG° values for their hydrolysis, but these terms are rather misleading since they fail to indicate an important and fundamental energetic relationship between ATP and other phosphorylated compounds in the cell. It is the whole function of the ATP-ADP system to serve as an intermediate carrier of phosphate compounds above ATP on the thermodynamic scale to acceptor molecules that form low-energy phosphate compounds below ATP on the scale.

The P-O-P linkage plays a role of supreme importance in the chemistry of phosphorus compounds, somewhat analogous to the role of C-C bonds in the chemistry of carbon compounds. Because of its high susceptibility to hydrolysis, the P-O-P linkage is not found in nature except as produced by living systems. The P-O-P linkage has been assigned a central role in energy storage and transport in living cells, via the putative "high-energy phosphate bonds" as in ADP and ATP. The term phosphate-bond energy used by the biochemist must not be confused with the term bond energy which denotes the energy required to break the bond. The term phophate-bond energy specifically denotes the difference in the free energy of the reactants and products when a phosphorylated compound is hydrolyzed to yield inorganic phosphate.

Review of Previous Work

Because of their importance in processes fundamental to the maintenance of life, these compounds have been the subject of study both experimentally and theoretically. The earliest explanation for the observed large free energy of hydrolysis had as its basis the reduction of electrostatic repulsions. At pH 7.0, ATP molecules have on the average about 3.8 closely spaced negative charges which repel each other and this electrical stress is removed when the terminal phosphate bond is hydrolyzed. Kalckar (1941) suggested that "opposing resonance", the inability of a single central oxygen to satisfy the electron demand of two P=O groups as well as when each P=O group can draw electrons from its

own -O- , plays an important role in the large negative free energy of hydrolysis of ATP, ADP, and phosphoenolpyruvate by stabilizing the products relative to the reactants. Hill and Morales (1951) suggested that although opposing resonance was of crucial importance in most high-energy compounds, electrostatic repulsions were also very important. This conclusion was supported by π electron calculations done by Pullman and Pullman (1963) and extended Hückel calculations carried out by Boyd and Lipscomb (1969).

George et al (1970) measured accurately ΔH°_{298} and ΔG°_{298} for the hydrolysis of different pH forms of pyro- and tripolyphosphoric acids, ATP,ADP, phosphoenolpryvuate and acetyl phosphate and observed that the free energy of hydrolysis was very nearly the same for charged as for uncharged species (Table 5.2). He concluded that the predominant free-energy contributions to the large negative free energies of hydrolysis of these compounds were the differences in solvation energy of the reactants and products and that intramolecular effects such as opposing resonance and electrostatic repulsions were of secondary importance. Their tentative estimate of the solvation energy of $H_4P_2O_7$ suggests that the gas-phase reaction may be nearly thermoneutral, the favorable value of $\Delta H^{\circ} = -7.6$ kcal/mol arising largely from the greater solvation energy of the products.

Hayes et al (1977, 1978) determined the relative contributions of intramolecular (opposing resonance) and intermolecular (solvation) effects in the hydrolysis reactions of the various ionizations states of phosphoric acid anhydrides, phosphoenolpyruvate, acetyl phosphates, phosphoguanidines, enol phosphates, thiol esters, and amino acid esters from electronic structure calculations using the STO-3G* and 4-31G basis sets. Their results for phosphoenolpyruvate suggested, in agreement with the π calculations of Pullman and Pullman (1963), that a substantial contribution to the "high-energy" nature of this compound was due to the energy gain from enol -> keto tautomerism in the product and that the only high-energy reaction dominated by resonance effects is the hydrolysis of

acetic anhydride. They concluded that for the hydrolysis of phosphoenolpyruvate; 1) the solvation energy must be crucial in dampening the large negative ΔH calculated in the gas phase to its solution value of -6 to -12 kcal/mol in the reactions where both the phosphate and carboxylate are charged; 2) internal electrostatic effects between the CO_2^- and the phosphate oxygens account for the more exothermic hydrolysis energies observed when both the carboxylate and phosphate groups are charged; 3) solvation effects change an intrinsically very "low- energy" N-P bond in phosphocreatine (ΔG and ΔH, >> 0) to a high-energy bond (ΔG, ΔH ca. -10 kcal/mol). Hayes et al (1978) conclude in agreement with George et al (1970) that for biologically important high-energy compounds in which there is no charge separation, the key energy terms are the large intramolecular electrostatic terms strongly modulated by solvation effects but that intramolecular electrostatic effects are not the "key" to the high-energy nature because ΔG does not become more exothermic with increasing ionization states.

Role of Magnesium

There have been many studies on the role of Mg^{2+} in the enzyme-catalyzed hydrolysis of ATP to ADP and inorganic phosphate (Yoshikawa, 1987 and references there within) but its precise function, especially in the specific cleavage of the terminal phosphoryl group of the ATP molecule is still unknown. Terada et al (1984) carried out a ^{31}P-NMR spectroscopic study on the interaction of ATP with Mg^{2+} and measured the exchange rate between free ATP and Mg^{2+}-bound ATP at various temperatures. Their results indicated that Mg^{2+} binds asymmetrically to the terminal (P_γ) and penultimate (P_β) phosphoryl groups of ATP and that the binding to the penultimate phosphoryl group is tighter than to the terminal phosphoryl group of ATP. They proposed that this asymmetric location of Mg^{2+} weakens the chemical bond of the terminal bridged phosphoryl group and this is why cleavage takes place between O and P_γ and not O and P_β. Yoshikawa et al (1987) performed molecular orbital calculations at the STO-3G level

on the magnesium-bound tetravalent anionic form of methyl triphosphate as a model of ATP. Their results showed Mg^{2+} to coordinate asymmetrically and concluded, based upon molecular orbital arguments, that this asymmetric location weakens the terminal phosphorus-oxygen bond. Tajima and Honda (1991) showed, using MNDO-generated potential energy surfaces, that a metal cation makes it possible for the hydroxide ion to attack the terminal phosphorus atom of methyldiphosphate, and then extrapolated these results to ADP.

Reaction Mechanism

The hydrolysis of ATP has been shown to proceed through the attack of nucleophiles such as H_2O and OH^- at the terminal phosphorus (Senter et al, 1983). The reaction proceeds by the cleavage of the adjacent bond to oxygen.

$$-P\text{-}O^*\text{-}P(O_3) + H_2O \;\text{--->}\; -P\text{-}O^*\text{----}P(O_3)\text{-}OH_2^+ \;\text{--->}\; -P\text{-}O^{*-} + (O_3)POH_2^+$$

$$-P\text{-}O^*\text{-}P(O_3) + OH^- \;\text{--->}\; -P\text{-}O^*\text{---}P(O_2)\text{-}OH \;\text{--->}\; -P\text{-}O^{*-} + (O_2)POH$$

The -O* oxygen is then protonated by either $-OH_2^+$ or any other acid in solution, either directly or via several protonation and deprotonation steps. This mechanism is also the same in the hydrolysis of phosphoenolpyruvate (with the adjacent phosphorus being replaced by carbon). In this case, once the O* atom in pyruvic acid is protonated, it tautomerizes to the more stable keto form.

An investigation into this reaction mechanism was attempted by positioning OH^- near the phosphorus of phosphoenolpyruvate and searching for the transition state. Although the actual transition state was not located, the O*-P distance was found to increase as the oxygen of OH^- came closer to P.

Reactions

Since the P-O-P and P-O-C linkages have been assigned a central role in energy storage and transport in living cells, a detailed examination of the reactions for the neutral and charged forms of diphosphoric acid, methyldiphosphoric acid and phosphoenolpyruvate with the two nucleophiles, water and hydroxide ion, is presented here. The hydrolysis reaction of the magnesium complex $P_2O_7Mg^{2-}$ is also presented in order to address the role magnesium ion plays in reactivity. Table 5.3 lists the reactions which were studied along with the calculated energies of hydrolysis. The calculated energies of hydrolysis obtained here differ from those of Hayes et al (1978) which were determined from smaller basis set calculations employing only partial geometry optimizations.

The standard definition of "high-energy" molecules are those with large negative *free* energies of hydrolysis. In virtually all of the cases studied by George et al (1970) the enthalpy parallels the free energy and thus is an appropriate index of a high energy molecule (Table 5.2). Only for the very highly charged $P_2O_7^{4-}$ is the enthalpy of hydrolysis very different from the free energy of hydrolysis, presumably due to the release of tightly bound water to the highly charged ion (George et al, 1970). Since the reactions studied here are isodesmic, the difference between ΔH_{298} and ΔE should be on the order of a few kcal/mol resulting mainly from zero-point energy differences for these gas-phase reactions. (Radom et al, 1971).

The remainder of this section discusses the calculations and method used to include solvation effects. Section 5.2 characterizes the interaction of phosphorus and the bridging oxygen in relation to the P-O-P and P-O-C bonds and also addresses the effect of electon-electron repulsions between the phosphoryl oxygens. The origin of the reaction energy changes are uncovered in section 5.3 though a detailed examination of individual atomic contributions. The conclusions are presented in section 5.3.

Calculations

Calculations were performed at the single-determinant level with use of the 6-311++G** basis set for both geometry optimization and energy determination for all of the molecules except for methyldiphosphoric acid (trianion) and the corresponding hydrolysis products. The above basis is the 6-311G** basis (Krishnan et al, 1980) with an extra diffuse s and p set of the heavy atoms and an extra diffuse s function on H. The 6-31G** basis set was used for both geometry optimization and energy determination for methyldiphosphoric acid and the corresponding hydrolysis products. All of the calculations were done using Gaussian90 (Frisch et al, 1990), Gaussian92 (Frisch et al, 1992) and GAMESS (Schmidt et al, 1990). All of the reactions studied here are isodesmic reactions and should be well-treated at the single determinant level. The structures for each molecule are displayed in Table A, along with the numbering of the atoms, and geometric parameters for these are given in Table B of the Appendix.

Initial geometry optimizations for diphosphoric acid ($H_4P_2O_7$, $H_2P_2O_7^{2-}$ and $P_2O_7^{4-}$) were done without any use of symmetry to assure a local minimum structure. The minimum energy configurations for $H_4P_2O_7$ and $H_2P_2O_7^{2-}$ were found to have C_s symmetry while $P_2O_7^{4-}$ was found to have D_{3d} symmetry. The P-O-P bond angle is 122.5° in $H_4P_2O_7$ and 153.2° in $H_2P_2O_7^{2-}$. Crystal structure determinations of a number of pyrophosphate salts have shown that both linear and non-linear ions can exist, with P-O-P bond angles in the range of 130°-180° (Corbridge, 1974). Ewig and van Wazer (1988) found that the STO-3G* basis set predicted an asymmetric staggered structure for $H_4P_2O_7$ to be slightly lower in energy by about 2.3 kcal than a C_2 structure. The C_2 structure found by Ewig and van Wazer differs from the minimum energy structure here. In their case, the O_2-P-O_1-P dihedral angle is nearly 180° and the O_3-P-O_1-P dihedral angle is roughly 52°. In the C_2 structure determined here using the larger 6-311++G** basis, the O_2-P-O_1-P dihedral angle is 51.27 and the O_3-P-O_1-P dihedral angle is 176.98 degrees. The smaller 6-31G** basis set predicts $P_2O_7^{4-}$ to have a P-O-P angle of 171.1°.

Uncontracting the basis on the central oxygen reduces this angle to 161.4° (The difference in energy between this structure and the non-equilibrium D_{3d} structure with a uncontracted basis on the central oxygen is only 0.2 kcal/mol). This suggests that these charged species require extra diffuse s and p functions to properly describe the molecular geometry.

Initial geometry optimizations for the magnesium complexes of $P_2O_7^{4-}$ and HPO_4^{2-} were done without the use of symmetry. In both cases the magnesium ion was placed in an asymmetric position and the optimization process allowed to proceed. $P_2O_7Mg^{2-}$ eventually converged to a structure which had C_{2v} symmetry and HPO_4Mg to a structure with C_s symmetry.

Initial geometry optimizations for phosphoenolpyruvate (trianion) were done assuming C_s symmetry for all of the atoms except for the phosphoryl group, which was allowed to rotate freely until it eventually converged on a near C_s structure, at which time the symmetry was fixed. This same procedure was followed for the geometry optimization of phosphoenolpyruvate (neutral). The minimum energy configuration for this molecule has only C_1 symmetry . This molecule would have C_s symmetry if it were not for the orientation of the phosphoryl hydrogens which destroy this symmetry. The hydrolysis products (various pyruvic acid forms) were assumed to have C_s symmetry.

The lowest energy C_s conformer from Tajima and Honda (1991) was used as a starting geometry for methyldiphosphoric acid trianion. The hydrolysis products (methylmonophosphate forms) were also assumed to have C_s symmetry. As noted above, these were the only structures determined using the 6-31G** basis set. The P-O-P angle in the minimum energy structure for methyldiphosphoric acid was found to be 147.31°. The crystal structure of ATP (Kennard et al, 1971) gives the terminal P-O-P angle to be 135.5° and the penultimate P-O-P angle to be 131°.

Table C (in the Appendix) gives the atomic populations, $N(\Omega)$, energies $E(\Omega)$, volumes $Vol(\Omega)$, attractive potential energies, $V_a(\Omega)$, repulsive potential energies $V_r(\Omega)$

and also the potential energy associated with the interaction of a given nucleus with its own charge distribution, $V_a^*(\Omega)$ for each atom Ω in all of the reactant and product molecules. The atomic potential energies have been scaled by a factor close to unity to satisfy the virial theorem ($V(\Omega)_{cor} = 2V(\Omega)(1+ \varepsilon^{-1})$ where $\varepsilon = V/T$ is obtained from the SCF calculation). The sum of these properties over each atom in a given molecule is also given along with the values obtained from the SCF calculation (the potential energies from the SCF calculation are not scaled to satisfy the virial theorem). The difference between the sum of atomic contributions and the SCF values are an indication of the quality of the atomic integrations. Many of the atoms in these molecules required the use of the new program PROMEGA (Keith and Cheeseman, 1992) to preform the atomic integrations. This new program is a modified version of PROAIMV (Biegler-König et al, 1982; Keith, 1992) in which the interatomic surfaces are determined in a different way. The atomic surfaces are located by determining where on a ray (from the nucleus of interest) the gradient paths passing through this ray change attractors. This procedure bypasses many of the problems encountered with the surface routines used in PROAIMV in cases where the charge density in the region of the interatomic surface is very flat. No knowledge or use of critical points is required as the surface is found using essentially local conditions.

The Effects of Solvation

There are likely to be large solvation energy effects associated with the hydrolytic reactions discussed above when there are charge separations in going from reactant to product. George et al (1970) demonstrated that the free energy of these types of reactions in aqueous solution is due almost entirely to differential heats of solution of the various species involved in the reaction, and not to the relative energies of the isolated molecules *in vacuo*. Of all solvents likely to participate in living systems, only water gives rise to solvation energies large enough to stabilize multi-charged phosphate and phosphate

anhydride ions in solution. The reaction field stabilization in water can be estimated using the simple reaction field equation for the solvation of ions (Beveridge and Schnuelle 1975, Hayes et al 1978):

$$-\Delta E_{solv} = \frac{\varepsilon - 1}{2\varepsilon} \frac{q^2}{a_0} \quad (1)$$

where ε is the solvent dielectric constant (ε=80 for H_2O), q is the solute charge, and a_0 is the cavity radius. The solvation energy for water is calculated using:

$$-\Delta E_{solv} = \left[\frac{\varepsilon - 1}{2\varepsilon + 1}\right] \frac{\mu^2}{a_o^3} \quad (2)$$

where μ is the dipole moment for H_2O. Hayes et al (1978) found that the relative solvation energies calculated in this manner are sensitive to the cavity radius and therefore must be interpreted only qualitatively. The determination of the cavity radius is somewhat arbitrary and there have been several methods used to estimate this quantity (Hayes et al, 1978; Onsagar, 1936; Rivail et al, 1985; Tapia, 1982 and Wong et al, 1991).

Bader et al (1987) have shown that the 0.001 au density envelope gives molecular volumes which compare with experimentally determined van der Waals contact distances. The total molecular volume is given by the sum of the individual atomic volumes, where an atomic volume is defined to be a measure of the region of space enclosed by the intersection of the atomic surface of zero flux and a particular envelope of the charge density (Bader et al, 1978). Wong et al (1992) have used these sums of atomic volumes in their estimates of the cavity radius required for *ab inito* self-consistent reaction field theory (Wong et al, 1991). They obtain very good estimates of solvation effects by determining the molecular volume out to the 0.001 au density envelope and then scaling the molecular volume by 1.33. The spherical radius is then determined using $V=\frac{4}{3}\pi a^3$ and adding 0.5 Å to the final a_0 values to account for the nearest approach of solvent

molecules. This method was used here to determine the cavity radii. Estimates of the solvation energy for the reactant and product molecules , ΔE_{solv}, were obtained using eqns. (1) and (2). Table 5.4 lists the calculated molecular volumes, cavity radii and solvation energies for the charged species studied here. The solvation energy associated with a given reaction, ΔE^{rxn}_{solv}, is calculated using eqn. (3) and the estimated energy of hydrolysis in water, ΔE_{H_2O}, is calculated using eqn. (4).

(3) $$\Delta E^{rxn}_{solv} = \Sigma \Delta E_{solv}(\text{products}) - \Sigma \Delta E_{solv}(\text{reactants})$$

(4) $$\Delta E_{H_2O} = \Delta E_{gas} + \Delta E^{rxn}_{solv}$$
$$\text{where } \Delta E_{gas} = \Sigma E_{SCF}(\text{products}) - \Sigma E_{SCF}(\text{reactants})$$

Table 5.5 gives ΔE_{gas}, ΔE^{rxn}_{solv} and ΔE_{H_2O}, the estimated solvation energies for each of the reactions involving charge species along with the experimentally determined ΔH values. This simple solvation model brings the calculated energy differences into the same range as the experimentally determined ΔH values.

The hydrolytic cleavage of the P-O-P bond of $H_4P_2O_7$ *in vacuo* is essentially thermoneutral (calculated and experimental). In solution, ΔH is -7.6 kcal/mol, so the effect of the solvent is to stabilize the products relative to the reactants. In the hydrolysis reactions of charged diphosphoric acid ($H_2P_2O_7^{2-}$ and $P_2O_7^{4-}$), the calculated hydrolysis energy is much more exothermic than the solution value. In this case, the effect of solvation is to stabilize the reactants relative to the products.

There are no experimental data available for the hydrolytic cleavage of the P-O-P bond in methyldiphosphoric acid, but since it is a good model for ADP, it has been suggested (Tajima and Honda, 1991) that ΔH should be very close to -6.8, the observed value for the hydrolysis of ADP (George et al , 1970).

$$ADP^{3-} + H_2O \text{ --> } AMP^{2-} + H_2PO_4^-$$

In the hydrolysis of methyldiphosphoric acid (rxn. (9)), the solvent stabilizes the reactants relative to the products and reduces the large exothermic (calculated) hydrolysis energy to -6.6 kcal/mol.

The hydrolytic cleavage of the P-O-P bond in $P_2O_7Mg^{2-}$ is calculated to be +108.9 kcal/mol. The effect of solvation in this case is to stabilize the products relative to the reactants.

The hydrolytic cleavage of the P-O-C bond in neutral phosphoenolpyruvate is calculated to be -15.7 kcal/mol, while in solution ΔH is measured to be -14.3 kcal/mol. This result indicates that in solution, the relative stabilizations of the reactant and product molecules are roughly of equal magnitude. The calculated hydrolysis energy of charged phosphoenolpyruvate (trianion) is much more exothermic than the solution value. As in the case of charged diphosphoric acid and methyldiphosphoric acid, the effect of solvation is to stabilize the reactants relative to the products.

5.2 Atomic Properties of the Reactants and Products.

Figs. 5.1a, 5.2a and 5.3a are displays of the gradient vector field of the charge density for neutral diphosphoric acid, phosphoenolpyruvate and methyldiphosphoric acid (trianion), respectively and Figs. 5.1b, 5.2b and 5.3b are contour maps of the charge density of these same molecules out to the 0.001 au density envelope with the bond paths and interatomic surfaces overlaid. These displays of the charge density illustrate the similarity between phosphorus and the bridging oxygen atoms constituting the P-O-P and P-O-C linkages in different molecules. This section begins with a discussion of the atomic and topological properties of phosphorus in the neutral and charged forms of diphosphoric acid, methyldiphosphate, phosphoenolpyruvate and their respective hydrolysis products. The behavior of the bridging oxygen in the P-O-P and P-O-C

linkages is discussed next and this section concludes with a discussion of the electron-electron repulsions originating from the non-bridging oxygen atoms.

Phosphorus

Table 5.6 lists the atomic properties of phosphorus for the range of molecules studied here. The electron population of phosphorus remains relatively constant in the neutral and charged forms of diphosphoric acid, phosphoenolpyruvate and phosphoric acid, having a minimum value of 11.041 in $H_4P_2O_7$ and a maximum value of 11.106 in HPO_4^{2-}. The atomic volume of phosphorus is very small, relative to carbon and oxygen, as a result of losing nearly 4 electrons and remains relatively constant in these molecules ranging from 19.68 to 22.06 in $H_4P_2O_7$ and HPO_4^{2-}, respectively. Figs. 5.4 and 5.5 are three-dimensional representations of the density envelope out to the 0.001 au contour of the phosphorus atom in neutral diphosphoric acid and phosphoenolpyruvate and provide a pictorial explanation as to its small atomic volume. As a result of its interaction with four oxygen atoms, much of the valence shell of phosphorus is stripped away, leaving mainly the core with a small amount of density which is squeezed out between the neighboring oxygen atoms.

Despite the relative consistency of the atomic electron populations and volumes of phosphorus, its energy varies by 156 kcal/mol, being most stable in HPO_4Mg and least stable in $P_2O_7^{4-}$. The energy $E(\Omega)$ of atom Ω in a molecule is equal to $(1/2)V(\Omega)$ where $V(\Omega)$ is a sum of attractive interactions, $V_a(\Omega)$, and repulsive interactions, $V_r(\Omega)$ (Chapter 4). The electron-nuclear interaction energy is the only attractive interaction in a molecular system, while both the nuclear-nuclear and electron-electron interactions contribute to $V_r(\Omega)$. Although the energy of phosphorus varies by 156 kcal/mol throughout these molecules, the attractive and repulsive potential energies each vary by nearly 100 au (1au = 627.51 kcal/mol). The sum, $V_a(\Omega) + V_r(\Omega)$, and thus the energy $E(\Omega)$, remain relatively constant despite the large changes in each of the components.

$V_{ii}^{*}(P)$, the measure of the interaction between the phosphorus nucleus and the charge density contained within its basin varies by roughly 350 kcal/mol.

The above discussion also applies to the trends in the atomic properties of phosphorus in methyldiphosphoric acid, methylmonophosphoric acid and the neutral and charged forms of phosphoric acid obtained using the smaller 6-31G** basis set, although the electron populations and volumes are, in general, slightly smaller.

Fig. 5.6a is a profile map of the Laplacian of the charge density for a free phosphorus atom showing the presence of three shells, and Figs. 5.6b and c are profile maps of the Laplacian along the bridging oxygen-phosphorus bond in $H_4P_2O_7$ (all of the phosphorus-oxygens bonds exhibit this same behavior). This latter figure shows that the valence shell of charge concentration (VSCC) of phosphorus in the region of the phosphate-oxygen bonds becomes part of the valence shell of oxygen, implying that phosphorus does not contain a bonded maximum within in its basin. This is also evident in Figs. 5.7, 5.8 and 5.9 which are contour and relief maps of the Laplacian for the P-O-P and/or P-O-C planes in $H_4P_2O_7$, phosphoenolpyruvate (neutral) and methyldiphosphate (trianion), respectively. Similar behavior has been observed for phosphorus when it is bound to other electronegative atoms such as F in PF_4^-, OPF_3 and OPF_4^- (Bytheway, private communication).

The value of $\nabla^2\rho$ at the bond critical point for all of the phosphorus-oxygen bonds is positive, indicative of closed shell interactions, implying that these interactions are dominated by the contraction of charge away from the interatomic surface and towards each of the nuclei (Chapter 1). The values of $\rho(r_c)$ and $\nabla^2\rho(r_c)$ are smaller in magnitude at the bond critical points between the bridging oxygen-phosphorus than for the remaining P-O bonds. Table C (Appendix) lists the values of ρ and $\nabla^2\rho$ at the bond (3,-1) critical points between all of the bonded nuclei for the molecules studied here.

The bonded radius of phosphorus, the distance between the phosphorus nucleus and the bridging oxygen-phosphorus critical point, increases by 0.006 Å from its value of

0.6260 Å in $H_4P_2O_7$ each time a pair of protons is removed, forming $H_2P_2O_7^{2-}$ and $P_2O_7^{4-}$ (Table 5.7). The electron population of phosphorus also increases, but by a very small amount, as diphosphoric acid becomes deprotonated with $H_4P_2O_7$ and $P_2O_7^{4-}$, differing by only 0.035 electrons. Despite these small increases in electron population, phosphorus is less stable relative to $H_4P_2O_7$ in $H_2P_2O_7^{2-}$ and $P_2O_7^{4-}$ by 12 and 62 kcal/mol, respectively. Although both the attractive and repulsive interactions decrease as diphosphoric acid becomes deprotonated, the charge density contained in the basin of phosphorus is able to interact most favorably with its own nucleus in $H_2P_2O_7^{2-}$ ($V_a^{\circ}(P)$ is largest in magnitude for this species).

The two phosphorus atoms in methyldiphosphoric acid have the same electron population and differ in energy by only 1 kcal/mol, which is roughly the error in the sum of the atomic energies. Both the attractive and repulsive interactions are greater in magnitude by nearly 13 au for P_2 as compared to P_1, but V_a° is greater in magnitude by 7 kcal/mol for P_2.

The bonded radius of phosphorus increases by 0.06Å from its value in neutral phosphoenolpyruvate as a result of the removal of three protons to form the trianion. The electron population of phosphorus is larger by 0.061 au and its energy is more stable by 9 kcal/mol in the trianion, relative to the neutral species, and phosphorus is able to interact more favorably with the charge density contained in its own basin in the trianion.

Fig. 5.10 displays both the gradient vector field and the Laplacian maps for the complex $P_2O_7Mg^{2-}$ in the plane containing both phosphorus atoms, Mg, O_1 and O_2. Each of the four O_3 oxygens which are bonded to magnesium donate a small amount of charge, which results in magnesium having an electron population of 10.212 au. The value of ρ at the O_3-Mg critical point is very low (0.04 au) and $\nabla^2\rho$ is positive, indicating that this is a relatively weak closed shell interaction ($\rho(r_c)$ for N-H is 0.02 au in HCN-HF, Chapter 3). The presence of these new interactions holds the P-O-P bond in a bent configuration, preventing it from becoming linear. The electron population of

phosphorus increases by 0.013 electrons and it becomes more stable by 100 kcal/mol, relative to phosphorus in $P_2O_7^{4-}$. In addition, the V_a° interactions increase by 225 kcal/mol. In HPO_4Mg, magnesium is bonded to only three oxygens and has an electron population of 10.189 au. Magnesium pushes these oxygens back as if opening an umbrella. The electron population of phosphorus is decreased relative to phosphorus in HPO_4^{2-}, but it is more stable by 80 kcal/mol.

The presence of Mg^{2+} has been experimentally observed to be essential in the enzyme-catalyzed hydrolysis of ATP (Yoshikawa et al, 1987) but its precise function, especially in the specific cleavage of the terminal phosphoryl group of ATP is still unknown. It has been shown that sites of electrophilic attack in a molecule correlate respectively with the sites of maximum charge depletion; the greater the charge depletion, the greater susceptibility to nucleophilic attack (Bader and MacDougal, 1985; Carroll et al, 1989). The extent of charge depletion is measured by the value of the minimum in $-\nabla^2\rho$. The valence shell of charge concentration (VSCC) of a free atom possesses a spherical surface over which the charge is maximally concentrated. The curvature of $-\nabla^2\rho$ normal to this surface, the radial curvature, is negative. The remaining two curvatures, those tangential to the surface, are equal to zero. In general this surface persists when this atom is in chemical combination, but the surface is no longer one of uniform concentration as the tangential curvatures assume either positive or negative values. If a local minimum is formed on the surface, then the two tangential curvatures assume positive values, resulting in the formation of (3,+1) critical points. The positions of three (3,+1) critical in the VSCC of phosphorus in $P_2O_7^{4-}$ are displayed in Fig. 5.11a. These critical points, which correspond to regions of local charge depletion, are 0.813Å from the phosphorus nucleus and form angles with the P-O_1 bond axis of 124°. The value of $\nabla^2\rho$ at these critical points is 0.0953 au. Since these are the only regions of local charge depletion in the VSCC of phosphorus which allow easy access for a nucleophile, it is likely that nucleophilic attack occurs at these positions. The phosphorus in $P_2O_7Mg^{2-}$

exhibits two corresponding (3,+1) critical points which are 0.814Å from the phosphorus nucleus and form angles with the P-O_1 bond of 126°, each having a $\nabla^2\rho$ value of 0.0912 au. In addition to these two critical points, two more (3,+1) critical points are found in the O_3-P-O_3 angle which are 0.809Å from the phosphorus nucleus and form an angle with the P-O_1 bond of 108°. The value of $\nabla^2\rho$ at these two critical points, 0.1340 au, is much larger than the value of $\nabla^2\rho$ at the other two critical points, implying greater susceptibility to nucleophilic attack at these positions (Fig. 5.11b). Although there are no available experimental data available for the relative susceptibility to hydrolysis of $P_2O_7Mg^{2-}$ as compared to $P_2O_7^{4-}$, it is reasonable to conclude, based upon the above observations, that the magnesium complex has a greater susceptibility towards nucleophilic attack.

The Bridging Oxygen in the P-O-P and P-O-C Linkage

Table 5.8 lists the atomic properties for the bridging oxygen atoms in the P-O-P and P-O-C linkages. The value of the charge density at the O_1-P bond critical point, which is smaller than for the other oxygen-phosphorus bonds, decreases from its value in $H_4P_2O_7$ as diphosphoric acid becomes deprotonated. In $P_2O_7Mg^{2-}$, the value of ρ at the P-O_1 bond critical point is slightly greater than in $P_2O_7^{4-}$, implying that the presence of magnesium does not weaken the P-O_1 bond.

The bonded radius of oxygen, the distance between the oxygen nucleus and the oxygen-phosphorus bond critical point is the same for both $H_4P_2O_7$ and $H_2P_2O_7^{2-}$, and increases by 0.02 Å in $P_2O_7^{4-}$ as the bond becomes linear and then again by another 0.02 Å in $P_2O_7Mg^{2-}$ (Table 5.7). The volume of this oxygen also becomes larger as the P-O-P angle increases, which occurs as diphosphoric acid becomes deprotonated. Relative to $H_4P_2O_7$, oxygen is less stable in $H_2P_2O_7^{2-}$ and $P_2O_7^{4-}$ by 19 and 94 kcal/mol, respectively. Despite these changes in volume and energy, the electron population remains relatively constant, changing by only 0.030 electrons. Oxygen behaves similarly

to phosphorus in the sense that both the attractive and repulsive interactions decrease as diphosphoric acid becomes deprotonated, but the oxygen nucleus is able to interact most favorably with the charge density contained in its own basin in $H_2P_2O_7^{2-}$ ($V_a^{\circ}(O_1)$ is largest in magnitude for this species).

The electron population of the central oxygen in the P-O-C bond of neutral phosphoenolpyruvate is reduced by 0.15 au and is less stable by 34 kcal/mol relative to oxygen in $H_4P_2O_7$. Upon removal of three protons, the P-O-C bond angle decreases by 2°, oxygen loses 0.038 electrons but increases its volume by 7 au and becomes less stable by 101 kcal/mol. Unlike phosphorus, the interaction of the oxygen nucleus with the charge density contained in its basin is reduced in the trianion relative to the neutral species. The 0.2 Å increase in the P-O bond is accompanied by a 0.1 Å increase of the bonded radius of oxygen to phosphorus and a 0.2 Å decrease in the bonded radius of oxygen to carbon. The values of the charge density at the oxygen-carbon and oxygen-phosphorus critical points, $\rho(r_c^{O-C})$ and $\rho(r_c^{O-P})$, respectively, are smaller than the values at the remaining bond critical points. The value of the charge density at the oxygen-carbon critical point is greater than at the oxygen-phosphorus critical point in both neutral phosphoenolpyruvate and the trianion. Relative to the neutral species, $\rho(r_c^{O-P})$ becomes smaller while $\rho(r_c^{O-C})$ becomes larger upon deprotonation to form the trianion.

The electron population of the oxygen (O_2) in the P-O-P linkage in methyldiphosphoric acid is greater than the population of the oxygen (O_1) in P-O-C by 0.161 electrons and it is more stable by 32 kcal/mol, despite the fact that the V_a° interaction is increased for O_1 relative to O_2 by 486 kcal/mol. The volume of O_2 is also greater than the volume of O_1 by 7 au. As in phosphoenolpyruvate, the values of the charge density at the oxygen-carbon and oxygen-phosphorus critical points are smaller than the values at the remaining bond critical points, with $\rho(r_c^{O-P})$ being smaller than $\rho(r_c^{O-C})$. The value of the charge density at the critical point between the terminal

oxygen-phosphate bond (O_2-P_2) is much smaller than at the critical point between the penultimate oxygen-phosphorus bond (O_2-P_1). This indicates that the terminal oxygen-phosphorus bond, the one which is cleaved upon hydrolysis, is the weaker interaction.

Electron-Electron Repulsions

Table 5.9 contains the atomic electron-electron repulsion potential energy terms, V_{ee}, for the non-bridging oxygens in the neutral and charged forms of diphosphoric acid and phosphoenolpyruvate. The sum of the electron-electron repulsions coming from these non-bridging oxygens are also listed for each molecule. The sum of the electron-electron repulsions coming from these oxygens is largest in $H_4P_2O_7$ and becomes smaller by 16 and 21 au in $H_2P_2O_7^{2-}$ and $P_2O_7^{4-}$, respectively. In each case, these oxygens contribute roughly 54% of the total electron-electron potential energy. Although the sum of the electron-electron repulsions coming from the non-bridging oxygens is the largest in $P_2O_7Mg^{2-}$, they contribute only 49% of the total electron-electron repulsion energy. In phosphoenolpyruvate, the sum of the electron-electron repulsions coming from the non-bridging oxygens is greater in the trianion than the neutral species by 0.20 au. In both cases, these oxygens contribute roughly 50% of the total electron-electron potential energy.

The changes in the sum of non-bridging oxygen electron-electron repulsive potential energies which occur upon hydrolysis are given in Table 5.9 along with the total molecular change. In each of these molecules which undergo hydrolysis, the reduction in the electron-electron repulsions is greater for the neutral species than for the charged species. These results demonstrate that electrostatic repulsions between these non-bridging oxygens are not responsible for the calculated decrease in ΔE as diphosphoric acid and phosphoenolpyruvate become deprotonated.

The non-bridging oxygen atoms are most stable in neutral diphosphoric acid and phosphoenolpyruvate as compared to the charged species. In $H_4P_2O_7$ and neutral

phosphoenolpyruvate, the protonated oxygens are more stable than the unprotonated one, but in $H_2P_2O_7^{2-}$ the protonated oxygen is the least stable.

5.3 Origins of Reaction Energy Changes

Attractive and Repulsive Contributions to the Total Energy

The total energy E of a molecule is equal to (1/2)V where V is a sum of attractive interactions, V_a, and repulsive interactions, V_r (Chapter 3). The electron-nuclear interaction energy is the only attractive interaction in a molecular system, while both the nuclear-nuclear and electron-electron interactions contribute to V_r. A rearrangement of atoms in going from reactants to products which results in a value of ΔE which is less than zero can either come about by a reduction in the repulsive interactions ($\Delta V_r < 0$) accompanied by a smaller loss of attractive interactions ($\Delta V_a > 0$) or by an increase in the attractive interactions ($\Delta V_a < 0$) despite a smaller increase in the repulsive interactions ($\Delta V_r > 0$). The latter case is observed for the following four reactions while the former case is observed in all the remaining reactions studied in this work.

(4) $P_2O_7^{4-} + Mg^{2+} \rightarrow P_2O_7Mg^{2-}$

(5) $HPO_4^{2-} + Mg^{2+} \rightarrow HPO_4Mg$

(13) $CH_2{=}C(O)COOH^- + H_3O^+ \rightarrow CH_2{=}C(OH)COOH + H_2O$

(14) $CH_2{=}C(O)COO^{2-} + H_3O^+ \rightarrow CH_2{=}C(OH)COO^{1-} + H_2O$.

A rearrangement of atoms during a reaction which results in ΔE being greater than zero can come about either by a decrease in the attractive interactions ($\Delta V_a > 0$) coupled with a smaller decrease in the repulsive interactions, or by an increase in the repulsive interactions despite a smaller increase in the attractive interactions. The only reaction in this section which results in a change of energy greater than zero is for the hydrolysis of

$P_2O_7Mg^{2-}$ (rxn. (7)), and in this case, the former condition is observed. Table 5.10 lists the changes in total energy, volume, and attractive and repulsive energies for each of the twenty reactions.

These same conditions also exist for the atomic contributions. For the atoms of H_2O and OH^-, and most of the atoms involved in the above four reactions, both the attractive and repulsive interactions are increased, their relative magnitudes depending on whether the atom becomes more or less stable in its new environment. For most of the other atoms in these reactions, both the attractive and repulsive interactions are decreased, their relative magnitudes again depending on whether the atom becomes more or less stable in its new environment.

$V_a^\circ(\Omega)$ is the potential energy associated with the interaction of the nucleus of atom Ω with the charge distribution contained within its basin. In most cases, the $\Delta V_a^\circ(\Omega)$ values for a reaction parallel the changes in atomic energy. If the atom becomes more stable, then the interaction of the nucleus of this atom with its own charge distribution is increased. The molecular value, V_a°, is just the sum of all the atomic values, $V_a^\circ(\Omega)$ and can be treated as any other potential energy contribution.

The atomic changes in the energy, volume, attractive and repulsive potential energies are listed along with the corresponding reaction diagram for each of the reactions in Table E of the Appendix. In the following discussion of the changes in atomic properties which occur in going from reactants to products, the atom listed first always refers to the atom in the reactant. The atoms in H_2O, OH^- or the products will be referenced to the appropriate molecule.

Diphosphoric Acid Reactions

The calculated energy change for the prototype hydrolytic cleavage of the P-O-P linkage, rxn. (1), is 0.9 kcal/mol (see Table E1 of the appendix).

(1) $H_4P_2O_7 + H_2O \rightarrow 2H_3PO_4$

George et al (1970) suggested, based upon tentative estimates of the solvation energy of $H_4P_2O_7$, that this gas-phase reaction may be nearly thermoneutral.

The volume change accompanying this reaction is an increase of 18 au. ΔV_a° for this reaction is less than zero, which implies that more of the nuclei can interact better with their own charge distribution in the products than in the reactants. Phosphorus gains only 0.008 electrons and becomes more stable by 13 kcal/mol as a result of this reaction. The bridging oxygen, O_1, in losing 0.181 electrons, increases its volume by nearly 21 au and becomes less stable by 126 kcal/mol in becoming O_2 of H_3PO_4. This atom makes the single largest destabilizing contribution to the reaction energy. O_2 and O_3, which become O_1 and O_2, respectively, in H_3PO_4 retain their original electron populations but become less stable by 5 and 11 kcal/mol, respectively, while O_4 loses 0.020 electrons and becomes less stable by 19 kcal/mol. H_1 and H_2, the hydrogens of O_3 and O_4, respectively, gain 0.012 and 0.032 electrons and become more stable in H_3PO_4 by 5 and 14 kcal/mol, respectively. Oxygen in H_2O, which becomes O_2 in H_3PO_4 gains 0.227 electrons, becoming smaller in volume by 20 au and becoming more stable by 179 kcal/mol, making the largest stabilizing contribution to the total energy change. Each hydrogen of H_2O loses 0.057 electrons and becomes less stable by 23.50 kcal/mol.

In all of the atoms of $H_4P_2O_7$, both the attractive and repulsive interactions are reduced as a result of the reaction, their relative magnitudes changing according to whether the atom becomes more or less stable in its new environment ($\Delta V_a(\Omega) > 0$ and $\Delta V_r(\Omega) < 0$). The atoms of H_2O behave differently in this respect. For these atoms, the attractive and repulsive interactions both increase ($\Delta V_a(\Omega) < 0$ and $\Delta V_r(\Omega) > 0$). For oxygen, the increase in the attractive interactions is greater in magnitude than the increase in the repulsive interactions, the opposite being true for hydrogen. The atoms which become more stable in the products exhibit an increase in their respective V_a°

interactions, the attractive interaction being between the density contained within the basin of the atom and its own nucleus ($\Delta V_a^\circ(\Omega) < 0$).

In summary, the atoms which undergo the largest atomic changes in energy for this reaction are the bridging oxygen (O_1) of $H_4P_2O_7$ and the oxygen of H_2O. All of the oxygen atoms in $H_4P_2O_7$ become less stable in the products, their sum being 196 kcal/mol, with 52% of this total coming from O_1 of $H_4P_2O_7$. The sum of the destabilizing contributions is 243 kcal/mol, while the sum of the stabilizing contributions is 242 kcal/mol, 74% of this coming from oxygen of H_2O.

The calculated energy change for rxn. (2) is -66.8 kcal/mol, where hydroxide ion is the nucleophile.

(2) $H_4P_2O_7 + OH^- \text{---> } H_3PO_4 + H_2PO_4^-$

The decreases in both the attractive and repulsive interactions are larger relative to rxn. (1), but the increase in the V_a° interactions is roughly 5.5 times greater in comparison to rxn. (1). This reaction leads to a total decrease in volume of 6 au.

The phosphorus which ends up in $H_2PO_4^{1-}$ gains 0.025 electrons and becomes more stable by 12.4 kcal/mol, while the phosphorus which ends up in H_3PO_4 gains only 0.008 electrons but becomes more stable by the same amount. Although both of these phosphorus atoms become more stable by the same amount, the phosphorus nucleus in $H_2PO_4^{1-}$ is able to interact more favorably with its own charge distribution as compared to phosphorus in H_3PO_4 ($\Delta V_a^\circ(P)$ is 2.5 times greater in magnitude in $H_2PO_4^{2-}$ as compared to H_3PO_4). O_1, which becomes O_1 of $H_2PO_4^{1-}$, gains only 0.005 electrons, becoming larger in volume by 50 au and becoming less stable by 171 kcal/mol.

All of the other atoms of $H_4P_2O_7$ which end up in H_3PO_4 undergo the same changes as in rxn. (1). The remaining oxygen atoms of diphosphoric acid all become less

stable in the product $H_2PO_4^{1-}$. The oxygen of OH^-, which becomes O_2 of H_3PO_4, becomes smaller in volume by 86 au, gaining 0.018 electrons and becoming more stable by 419 kcal/mol, thereby making the largest stabilizing contribution to the total energy change. The oxygen and hydrogen of hydroxide ion exhibit the same behavior with respect to changes in the attractive and repulsive potential energy contributions as do the atoms of H_2O in rxn. (1).

The calculated energy change for rxn. (3), the hydrolysis of diphosphoric acid (dianion), is -70.2 kcal/mol.

(3) $$H_2P_2O_7^{2-} + H_2O \dashrightarrow 2H_2PO_4^{1-}$$

Relative to rxn. (1), the reductions in both the attractive and repulsive interactions which occur upon hydrolysis are smaller in magnitude, but the increase in the V_a° interactions is greater for rxn. (3) by 37 kcal/mol. This reaction leads to a total decrease in volume of 6 au.

The electron population of phosphorus remains unchanged, but it becomes more stable by 24 kcal/mol in the product $H_2PO_4^{1-}$. O_1, the bridging oxygen which becomes O_2 in $H_2PO_4^{1-}$, loses 0.220 electrons, becoming larger by 23 au and becoming less stable by 160 kcal/mol. These changes are larger in magnitude than the corresponding changes for this atom in rxn. (1), the hydrolysis of neutral diphosphoric acid.

Each of the remaining oxygen nuclei in $H_2P_2O_7^{2-}$ are able to interact more favorably with the density contained in their respective basins in the product $H_2PO_4^-$, becoming more stable as a result of the reaction. These oxygen atoms exhibit differing behavior in this reaction as compared to rxn. (1), where they all become less stable in the products, relative to the reactants. The electron populations of O_2 and O_4, which become O_1 in $H_2PO_4^{1-}$, essentially remain unchanged but become more stable by 7.5 and 12

kcal/mol, respectively. O_3, which becomes O_2 in $H_2P_2O_7^{1-}$, gains 0.014 electrons and becomes more stable by 14 kcal/mol, while its hydrogen loses 0.012 electrons and becomes less stable by 4 kcal/mol.

The oxygen of H_2O, which becomes O_2 of $H_2PO_4^{1-}$, gains 0.220 electrons and becomes more stable by 126 kcal/mol, making the dominant stabilizing contributions to the total energy change. The hydrogens of H_2O which become the hydrogens in $H_2PO_4^{1-}$ lose only 0.006 electrons and become less stable by only 1.80 kcal/mol. This is in contrast to rxn. (1) where these hydrogens became less stable by 24 kcal/mol.

The calculated energy change for rxn. (4), the hydrolysis of diphosphoric acid (tetraanion) , is -280.5 kcal/mol.

(4) $\quad P_2O_7^{4-} + H_2O \text{ --> } 2HPO_4^{2-}$

The decreases in both the attractive and repulsive interactions are smaller in magnitude relative to rxns. (1) and (2), but the increases in the V_a° interactions which accompany this reaction are larger by nearly 450 kcal/mol as compared to rxn. (1). The total volume decreases by 12 au as a result of this reaction.

In this reaction, all of the atoms in the reactants, with the exception of the bridging oxygen, become more stable in the products. Phosphorus, which gains 0.030 electrons and becomes more stable by 75 kcal/mol, makes the single largest stabilizing contribution to the total energy change. The change in energy of phosphorus which occurs as a result of this hydrolysis reaction is roughly six times larger in magnitude here than in rxn. (1), and roughly three times greater than in rxn. (3). The interaction of the phosphorus nucleus with its own charge density is increased significantly in the product HPO_4^{2-}, relative to the reactant (ΔV_a°=-0.4282 au for this reaction as compared to -0.0833 au for rxn. (1) and -0.0985 for rxn. (3)). The bridging oxygen of $P_2O_7^{4-}$, which becomes O_3 in

HPO_4^{2-}, loses 0.229 electrons, increasing its volume by 24 au and becoming less stable by 142.75 kcal/mol.

The oxygen of H_2O, which becomes O_3 in HPO_4^{2-}, gains 0.205 electrons and becomes more stable by only 50 kcal/mol, no longer making the dominant stabilizing contribution to the total reaction energy change.

Summary of Diphosphoric Reaction Energy Changes

The calculated energy for hydrolytic cleavage of the P-O-P linkage in neutral diphosphoric acid is essentially thermoneutral. As diphosphoric acid becomes more charged as a result of deprotonation, the calculated hydrolysis energies become more exothermic.

In the hydrolysis of neutral diphosphoric acid, the bridging oxygen makes the dominant destabilizing contribution (126 kcal/mol), and the oxygen of water makes the dominant stabilizing contribution (179 kcal/mol) to the total reaction energy change. Phosphorus becomes more stable by 12 kcal/mol and the other oxygens of $H_4P_2O_7$ all become less stable (5-20 kcal/mol).

In the hydrolysis of $H_2P_2O_7^{2-}$, the bridging oxygen again makes the dominant, and even larger, destabilizing contribution (160 kcal/mol) and the oxygen of water makes a smaller, but still the largest, stabilizing contribution (126 kcal/mol) to the total reaction energy change. All of the other oxygens of $H_2P_2O_7^{2-}$ become more stable (8-12 kcal/mol) and phosphorus becomes more than twice as stable (24 kcal/mol) as compared to rxn. (1).

In the hydrolysis of $P_2O_7^{4-}$, the bridging oxygen makes the largest destabilizing contribution (143 kcal/mol) to the total reaction energy change. The oxygen of water no longer makes the dominant stabilizing contribution, becoming more stable by only 50 kcal/mol. All of the other oxygens become more stable (30-35 kcal/mol) and phosphorus

becomes more stable by 76 kcal/mol, making the single largest contribution to the total reaction energy change.

In summary, the bridging oxygen makes the dominant destabilizing contribution to the total reaction energy change for the hydrolytic cleavage of the P-O-P bond in neutral and charged diphosphoric acid. As diphosphoric acid becomes more charged, the stabilizing contribution from phosphorus is increased while at the same time the stabilizing contribution of the oxygen of water is reduced.

Complexation with Magnesium Ion

The energy for the complexation of $P_2O_7^{4-}$ with Mg^{2+} (5) is calculated to be -955 kcal/mol.

(5) $P_2O_7^{4-} + Mg^{2+} \rightarrow P_2O_7Mg^{2-}$

The total attractive, repulsive, and V_a° interactions are increased, relative to the reactants, in the complex. ΔV_a° for this reaction is nearly -4 au, indicating that the individual nuclei are able to interact much more favorably with the charge density contained in their respective basins in the complex. This reaction is accompanied by a substantial decrease in volume of 138 au.

Every atom in $P_2O_4^{4-}$ becomes more stable in the complex with the exception of the bridging oxygen, which becomes less stable by only 2 kcal/mol. Each phosphorus gains 0.013 electrons and becomes more stable by 100 kcal/mol and the remaining oxygen atoms become more stable by 85 kcal/mol. Magnesium, which gains 0.212 electrons, becomes more stable in the complex by 249 kcal/mol. The individual atomic attractive and repulsive interactions are increased in the complex relative to $P_2O_7^{4-}$. Excluding the bridging oxygen, the attractive interactions increase more than the repulsive interactions increase, resulting in a net stabilization.

The energy of complexation of HPO_4^{2-} with Mg^{2+} (6) is calculated to be -565 kcal/mol.

(6) $HPO_4^{2-} + Mg^{2+} \rightarrow HPO_4Mg$

As in rxn. (5), the total attractive, repulsive and V_a° interactions increase in the products, relative to the reactants, as a result of this complexation reaction. ΔV_a° for this reaction is -2.5 au, indicating that the individual nuclei are able to interact much more favorably with the charge density contained in their respective basins in the complex. This reaction is accompanied by a decrease in volume of 23 au.

All atoms in the reactants, with the exception of hydrogen in HPO_4^{2-}, become more stable in the complex. Phosphorus loses 0.032 electrons and becomes more stable by 80 kcal/mol and Mg^{2+} gains 0.189 electrons and becomes more stable by 210 kcal/mol. Hydrogen loses 0.093 electrons and becomes less stable by 37 kcal/mol. As in rxn. (5), both the attractive and repulsive interactions are increased for each atom in the complex, relative to HPO_4^{2-}.

The calculated energy change for rxn. (7), the hydrolysis of the magnesium complex of diphosphoric acid, is +109 kcal/mol.

(7) $P_2O_7Mg^{2-} + H_2O \rightarrow HPO_4Mg + HPO_4^{2-}$

The decreases in both the attractive and repulsive interactions which occur upon hydrolysis are larger in magnitude, relative to rxn. (4), but in this case, the loss of attractive interactions is greater in magnitude than the loss of repulsive interactions, resulting in a total energy change greater than zero. The V_a° interactions are reduced in

the products, relative to the reactants by nearly 450 kcal/mol. The total volume decreases by 56 au as a result of this reaction.

The phosphorus atom which forms HPO_4^{2-} gains 0.017 electrons and becomes less stable by 25 kcal/mol while the phosphorus which forms HPO_4Mg loses 0.014 electrons and becomes more stable by 56 kcal/mol. The bridging oxygen of $P_2O_7Mg^{2-}$ can become O_3 of either HPO_4^{2-} or HPO_4Mg. If it becomes O_3 of HPO_4Mg, then it loses 0.180 electrons and becomes less stable by 15 kcal/mol. If this oxygen becomes O_3 of HPO_4^{2-}, it loses 0.202 electrons and becomes less stable by 141 kcal/mol. Mg^{2+} loses 0.023 electrons and becomes less stable by 39 kcal/mol.

In summary, the presence of magnesium in these complexes, in addition to effecting geometrical changes, induces a stabilizing effect on most of the atoms. The atoms in $P_2O_7Mg^{2-}$ which become more stable in the product HPO_4^{2-} upon hydrolysis, become even more stable in the product HPO_4Mg. Atoms in $P_2O_7Mg^{2-}$ which become less stable in the product HPO_4^{2-} also become less stable in the product HPO_4Mg, but by a smaller amount.

Methyldiphosphoric Acid Reactions

The calculated energy changes (using the 6-31G** basis) for rxns. (8) and (9), the hydrolysis of methyldiphosphoric acid (MDP^{3-}) to methylphosphate (MP^{-x}) and phosphoric acid are -134 and -142 kcal/mol, respectively.

(8) $CH_3OP(O_2)OPO_3^{3-} + H_2O \rightarrow CH_3OPO_3H^{1-} + HPO_4^{2-}$

(9) $CH_3OP(O_2)OPO_3^{3-} + H_2O \rightarrow CH_3OPO_3^{2-} + H_2PO_4^{1-}$

In accord with the hydrolysis reaction mechanisms discussed in Section 5.1, the proton of H_2O which is initially transferred to methylphosphate (rxn. (8)), is then subsequently transferred to phosphoric acid resulting in an additional stabilization of 10 kcal/mol. In

the overall rxn. (9), both the attractive and repulsive interactions are reduced but the V_a° interactions are increased in the products, relative to the reactants. The total volume decreases by 8 au as a result of this reaction.

In rxn. (9), all four atoms in the terminal $-PO_3$ group of MDP^{3-} lose charge but become significantly more stable in the product $H_2PO_4^{2-}$. P_2, the terminal phosphorus, loses 0.013 electrons and becomes more stable by 80 kcal/mol, making the largest contribution to the total energy change of all the atoms in MDP^{3-}. P_1 retains its electron population but becomes more stable by 5 kcal/mol. O_2, the terminal bridging oxygen, gains 0.064 electrons and becomes less stable by 79 kcal/mol, making the single largest destabilizing contribution to the total energy change. O_1, the penultimate bridging oxygen, retains its electron population but becomes less stable by 21 kcal/mol.

It is not possible to assign a direct 1:1 correspondence between O_4 and the two equivalent O_5 oxygens of MDP^{3-} and the oxygens of H_2PO_4. It is therefore assumed that O_4 of MDP^{3-} is the oxygen which is protonated and becomes O_2 in $H_2PO_4^{1-}$, while the two equivalent O_5 oxygens become the two equivalent (unprotonated) O_1 oxygens in $H_2PO_4^{1-}$. Because O_4 and O_5 of MDP^{3-} only differ in electron population and energy by 0.002 au and 3.6 kcal/mol, these relative assignments, although arbitrary, are not particularly important. Using these assignments, O_4 loses 0.246 electrons but becomes more stable by 21 kcal/mol, while O_5 loses 0.036 electrons and becomes more stable by 45 kcal/mol. O_3, which becomes O_3 in MP^{2-}, gains 0.020 electrons and becomes less stable by 20 kcal/mol, even though the interaction between the charge density contained within this atom and its nucleus is increased in MP^{2-} relative to MDP^{3-}. (ΔV_a° = -0.0224 au) The atomic properties of C_1, H_1 and H_2, the atoms of the methyl group, change by very small amounts with the carbon atom becoming less stable by only 6 kcal/mol.

The oxygen of H_2O gains 0.227 electrons and becomes more stable by 98 kcal/mol, making the dominant stabilizing contribution to the total energy change.

The hydrogens of water which become the hydrogens in $H_2PO_4^{1-}$ become less stable by only 2.5 kcal/mol.

The calculated energy change for rxn. (10), where hydroxide ion is the nucleophile is -89 kcal/mol.

(10) $CH_3OP(O_2)OPO_3^{3-} + OH^- \rightarrow CH_3OPO_3^{2-} + HPO_4^{2-}$

The reductions in the attractive and repulsive interactions which occur in going from reactants to products are much greater in magnitude in this reaction as compared to rxns. (8) and (9). The relative increase in the V_a° interactions is of greater magnitude as compared to the previous two reactions.

All four atoms in the terminal $-PO_3$ group of MDP^{3-} become less stable in the product HPO_4^{2-}. P_2 loses 0.01 electrons and becomes less stable by only 1.5 kcal/mol, while O_4 loses 0.013 electrons and becomes less stable by 12.9 kcal/mol; nevertheless, the interaction between the charge density contained within these atoms and their own respective nuclei are increased ($\Delta V_a^\circ = < 0$ for these atoms). The changes for the remaining atoms in MDP^{3-} are identical to the rxn. (9).

The oxygen of hydroxide ion gains 0.072 electrons and becomes more stable by 319 kcal/mol, while the hydrogen loses 0.205 electrons and becomes less stable by 61 kcal/mol, resulting in a net stabilizing contribution of 258 kcal/mol from hydroxide ion.

Phosphoenolpyruvate (neutral) Reactions

The calculated energy change for rxn. (11), hydrolysis of neutral phosphoenolpyruvate (PEP) to the keto form of pyruvic acid (keto) and phosphoric acid, is -15.7 kcal/mol. This is the prototype reaction for the cleavage of the P-O-C linkage.

(In solution, the relative stabilizations of the reactant and product molecules are roughly of equal magnitude (Section 5.1)).

(11) $CH_2=C(OPO_3H_2)COOH + H_2O \rightarrow CH_3COCOOH + H_3PO_4$

The attractive, repulsive and V_a° interactions are all reduced in the products, relative to the reactants, and this reaction is accompanied by a decrease in volume of 14 au.

As a result of the hydrolytic cleavage of the P-O-C linkage, phosphorus gains 0.011 electrons and becomes more stable by 6 kcal/mol in the product H_3PO_4. The bridging oxygen loses 0.243 electrons and becomes less stable by 77 kcal/mol.

O_1', which becomes O_1 in H_3PO_4, retains its same electron population but becomes less stable by 12 kcal/mol. Each of the O_2' oxygens which become O_2 in H_3PO_4 also retain their electron population and becomes less stable by 3 kcal/mol. H' gains a small amount of charge (0.005 electrons) and becomes more stable by 2 kcal/mol.

The labels for the remaining atoms are the same in both phosphoenolpyruvate and pyruvic acid (keto form). C_1 loses 0.813 electrons and becomes less stable by 304 kcal/mol, making the single largest contribution to the total energy change. C_2 gains 0.086 electrons and becomes more stable by 29 kcal/mol. H_1 and H_2 both gain charge and become more stable by 19 and 14 kcal/mol, respectively. C_3 gains 0.055 electrons and becomes more stable by 21 kcal/mol. O_2 and O_3, the carboxylic acid oxygens, become more stable by only a few kcal/mol.

The oxygen of H_2O which becomes O_2 in H_3PO_4 gains 0.227 electrons and becomes more stable by 179 kcal/mol, making the largest stabilizing contribution to the total energy change. The hydrogen of H_2O which ends up in H_3PO_4 loses 0.057 electrons and becomes less stable by 24 kcal/mol, while the hydrogen of H_2O which becomes H_1 of pyruvic acid loses 0.598 electrons and becomes more stable by 162

kcal/mol. The atoms of water make the dominant contributions to the total energy change just as previously observed in the neutral diphosphoric acid reaction.

The calculated energy change for rxn. (12), where hydroxide acts as the nucleophile to form pyruvic acid (PA^-) and phosphoric acid, is -51 kcal/mol.

(12) $CH_2=C(OPO_3H_2)COOH + OH^- \rightarrow CH_2=COCOOH^{1-} + H_3PO_4$

The reductions in attractive and repulsive interactions which occur as a result of this reaction are greater in magnitude, as compared to rxn. (11), but the V_a^* interactions are reduced by a smaller amount. The volume decreases by only 4 au as compared to 14 au in rxn. (11).

The changes of the atoms in the phosphoryl group $-PO_3H_2$ are the same as in the previous reaction. The bridging oxygen gains 0.075 electrons but becomes less stable by 169 kcal/mol, which is over twice the amount by which it becomes destabilized in the reaction with water. C_1 loses 0.651 electrons and becomes less stable by 251 kcal/mol. The oxygen of hydroxide, which becomes O_2 in H_3PO_4, gains only 0.018 electrons but becomes more stable by 419 kcal/mol. As observed in rxn. (11), the dominant destabilizing contributions to the total energy change come from O_1 and C_1, while the dominant stabilizing contributions come from the oxygen of H_2O.

Enol-Keto Tautomerization (neutral)

The calculated energy change for rxn. (14), the enol-keto tautomerization, is -10.1 kcal/mol. 75% of the total energy change for the hydrolytic cleavage of the P-O-C linkage of (neutral) phosphoenolpyruvate comes from this enol-keto tautomerization. Although the relative solvation energies of these two molecules were not calculated, it is

likely that the relative stabilizations, due to the solvent water, are roughly of equal magnitude.

(14) $CH_2=C(OH)COOH \rightarrow CH_3COCOOH$

The attractive, repulsive and V_a° interactions are decreased in the keto form, relative to the enol form, as a result of this tautomerization.

The numbering system is the same in each of these molecules with the exception of H_4 in the enol form which becomes H_1 in the keto form of pyruvic acid. C_1 loses 0.698 electrons and becomes less stable by 279 kcal/mol, making the single largest contribution to the total reaction energy change. H_4, which becomes H_1 in the keto form of pyruvic acid, gains 0.618 electrons and becomes more stable by 169 kcal/mol, making the largest stabilizing contribution to the total energy change.

O_1 loses 0.021 electrons and becomes more stable by 62 kcal/mol. The interaction of the charge density in the basin of O_1 with its nucleus is reduced, despite the fact that it becomes more stable. C_2 gains 0.045 electrons and becomes more stable by 29 kcal/mol while C_3 gains 0.046 electrons and becomes more stable by 23 kcal/mol. H_1 loses 0.017 electrons and becomes less stable by 4.32 kcal/mol while H_2 gains 0.041 electrons and becomes more stable by 13.19 kcal/mol. O_2, O_3, and H_3 of the carboxylic acid group all change by less than 1.5 kcal/mol.

Phosphoenolpyruvate (trianion) Reactions

The calculated energy change for rxn. (15), the hydrolysis of phosphoenolpyruvate (trianion), is -134 kcal/mol:

(15) $CH_2=C(OPO_3)COO^{3-} + H_2O \rightarrow CH_3COCOO^{1-} + HPO_4^{2-}$.

As in rxn. (11), the attractive, repulsive and V_a° interactions are all reduced in the products, relative to the reactants. This reaction is accompanied by a decrease in volume of 24 au, as compared to 14 au for rxn. (11).

The bridging oxygen loses 0.131 electrons but becomes more stable by 11 kcal/mol as compared to the neutral hydrolysis reaction where it becomes less stable by nearly 80 kcal/mol. C_1 loses 0.435 electrons and becomes less stable by 143 kcal/mole, roughly half the amount this atom is destabilized in the neutral reaction. The hydrogen of H_2O which becomes H_1 of pyruvic acid gains 0.664 electrons and becomes more stable by 134 kcal/mol, making the largest stabilizing contribution to the total energy change.

All of the atoms in the phosphoryl group retain their same electron populations and become slightly less stable in the product HPO_4^{2-}. Phosphorus becomes less stable by only 2 kcal/mol while O_1' and O_2' becomes less stable by 10 and 6 kcal/mol respectively. Even though phosphorus becomes less stable in its new environment, the interactions between the charge distribution in its basin with its own nucleus is increased.

C_2 loses 0.128 electrons and becomes more stable by 13 kcal/mol while C_3 loses roughly the same number of electrons but becomes less stable by 16 kcal/mol. O_2 and O_3 lose 0.049 and 0.031 electrons and become more stable by 35 and 24 kcal/mol, respectively. In the neutral reaction, these atoms changed by only a few kcal/mol. H_1 gains 0.046 electrons and becomes more stable by 11 kcal/mol, while H_2 loses roughly twice the amount of electrons as H_1 and becomes less stable by 18 kcal/mol.

The oxygen of H_2O gains 0.205 electrons and becomes more stable by only 50 kcal/mol. In the neutral reaction, this atom became more stable by 179 kcal/mol and made the dominant stabilizing contribution. The hydrogen of H_2O which becomes the hydrogen in HPO_4^{2-} gains 0.031 electrons and becomes more stable by 12 kcal/mol.

As in the neutral reaction, the atoms which undergo the largest atomic changes in population and energy are C_1 and the proton of water, which becomes H_1 in the keto form of pyruvic acid. In this hydrolysis reaction of the trianion, the large stabilizing

contribution from the oxygen of water is reduced relative to the neutral phosphoenolpyruvate reaction. This trend was also observed in the diphosphoric acid reactions.

The calculated energy change for rxn. (16), where hydroxide acts as the nucleophile, is -64 kcal/mol.

(16) $CH_2=C(OPO_3)COO^{3-} + OH^- \rightarrow CH_2=COCOO^{2-} + HPO_4^{2-}$

As in rxn. (12), both the attractive and repulsive interactions are reduced in the products, relative to the reactants. In this case however, the V_a° interactions are greater in the products and the volume undergoes a substantial increase of 36 au.

The changes of the atoms in the phosphoryl group $-PO_3$ are the same as in the previous reaction. The labels for the remaining atoms are the same in both phosphoenolpyruvate and pyruvic acid (dianion). O_1, the bridging oxygen, retains its electron population and becomes less stable by 84 kcal/mol. C_1 loses 0.297 kcal/mol and becomes less stable by 119 kcal/mol, again making the largest destabilizing contribution to the total energy change. C_2 gains 0.219 electrons and becomes more stable by 6 kcal/mol. H_1 and H_2 become more stable and less stable respectively, although their relative magnitudes are reduced as compared to the changes these atoms make in the above reaction. C_3 gains 0.049 electrons and becomes more stable in this reaction. O_2 becomes more stable by 10 kcal/mol while O_3 actually becomes less stable by 5 kcal/mol. The oxygen of hydroxide ion retains its electron population but becomes more stable by 290 kcal/mol, making the largest of all the atomic contributions to the total energy change.

<u>Enol-Keto Tautomerization (anion)</u>

The calculated energy change for rxn. (18), the enol-keto tautomerization, is -17.5 kcal/mol. The relative solvation energies of these two molecules are calculated to be the same (Section 5.1).

(18) $CH_2=C(OH)COO^- \rightarrow CH_3COCOO^-$

As in rxn. (14) the attractive, repulsive and V_a° interactions are reduced in the products, relative to the reactants, but by a lesser amount. The relative atomic energy changes in this reaction are similar to the changes in the enol-keto tautomerization of the neutral species, but are of smaller magnitude.

Summary of Reaction Energy Changes

Table 5.11 summarizes the major energetic group and atomic contributions in the reactions of diphosphoric and methyldiphosphoric acid and phosphoenolpyruvate with water and hydroxide ion. In each of these reactions, the atoms of water or hydroxide ion make significant stabilizing contributions to the total energy change. In the diphosphoric acid and phosphoenolpyruvate reactions, the stabilizing contributions from water and hydroxide ion are reduced as the reactants become deprotonated.

In the diphosphoric acid reactions, the largest destabilizing contribution comes from the bridging oxygen (O_1). In the hydrolysis of neutral diphosphoric acid, the phosphoryl ($-PO_3H_x$) group contribution is slightly destabilizing (+7 kcal/mol) while in the hydrolysis of $H_2P_2O_7^{2-}$ and $P_2O_7^{4-}$, the phosphoryl group makes a stabilizing contribution of -100 and -350 kcal/mol, respectively.

In the hydrolysis of phosphoenolpyruvate, the largest destabilizing contribution comes from C_1, and the phosphoryl group makes a destabilizing contribution of 9 and 25 kcal/mol for the neutral and trianion, respectively. The bridging oxygen (O_1) also makes a destabilizing contribution of 77 kcal/mol in the hydrolysis of the neutral species, but a

stabilizing contribution of 11 kcal/mol in the trianion. The destabilizing contributions from C_1 and O_1 in the reactions with hydroxide ion are also reduced as phosphoenolpyruvate becomes deprotonated.

In the hydrolysis of methyldiphosphoric acid, the stabilizing contribution from water is smaller than in the reactions of diphosphoric acid and phosphoenolpyruvate. In rxn. (8), the phosphoryl group and the bridging oxygen make destabilizing contributions of 30 and 46 kcal/mol, respectively. In rxn. (9), the overall hydrolysis reaction, the phosphoryl group makes a stabilizing contribution of -190 kcal/mol and the bridging oxygen makes a destabilizing contribution of 78 kcal/mol. In rxn. (10), the phosphoryl group and O_1 make destabilizing contributions, while hydroxide ion makes the dominant stabilizing contribution of 258 kcal/mol.

Table 5.12 summarizes the major energetic group and atomic contributions to the total energy change for the protonation of pyruvic and phosphoric acid and the pyruvic acid enol-keto tautomerization. In the pyruvic acid protonation rxns. (13) and (17), the dominant stabilizing contribution comes from C_1. For rxn. (13), O_1 and H_3O^+ make stabilizing contributions of 29 and 39 kcal/mol, respectively, while in rxn. (17), O_1 and H_3O^+ make stabilizing contributions of 27 and 56 kcal/mol, respectively. In the protonation reactions of phosphoric acid, (19) and (20), the stabilizing contribution from the phosphoryl group is roughly six times greater than the stabilizing contribution from H_3O^+.

In the pyruvic acid enol-keto tautomerizations, (14) and (18), the proton which is transferred makes the dominant stabilizing contribution of 169 kcal/mol and C_1 makes the dominant destabilizing contribution (279 and 261 kcal/mol for rxns. (14) and (18), respectively). O_1 makes a smaller stabilizing contribution of 62 and 68 kcal/mol for rxns. (14) and (18), respectively.

5.4 Concluding Remarks

The hydrolysis of neutral diphosphoric acid (rxn. 1) is the prototype reaction for the hydrolytic cleavage of the P-O-P linkage. This reaction is observed, both experimentally and theoretically to be essentially thermoneutral *in vacuo*, while in solution, ΔH of hydrolysis is -7.6 kcal/mol (Tables 5.2 and 5.3). The solvent, water, therefore stabilizes the products relative to the reactants, resulting in the observed negative enthalpy of hydrolysis. The calculated (*in vacuo)* energies of hydrolysis for the di- and tetranion of diphosphoric acid are much more exothermic than the observed solution enthalpies of hydrolysis. Calculated values of the solvation energy (Section 5.1) show the solvent to preferentially stabilize the reactants, relative to the products (Table 5.5), the solvation energy of the tetraanion being much larger than for the dianion. This is consistent with the observed dispersal of charge from along the P-O-P bond as evidenced by smaller values of the charge density at the bond critical point between oxygen and phosphorus as diphosphoric acid becomes more highly charged.

The calculated hydrolysis energy is greater for the dianion, as compared to neutral diphosphoric acid, due to the increased stabilization of the atoms constituting the phosphoryl group in the products, relative to the reactants (Table 5.5). The increased stabilization of phosphorus in the products, relative to the reactants accounts for roughly 20% of the phosphoryl group contribution to the overall reaction energy change. This large increase in stabilization of the phosphoryl group is partially off-set by the increased destabilization of the bridging oxygen.

The hydrolysis of (neutral) phosphoenolpyruvate (rxn. 11) is the prototype reaction for the hydrolytic cleavage of the P-O-C linkage. For this reaction, the calculated (*in vacuo*) hydrolysis energy is very close to the experimental solution enthalpy value (ΔE= -15.7 kcal/mol and ΔH_{sol}= -14.3 kcal/mol). This good agreement between the calculated *in vacuo* and solution values implies that the solvent stabilizes the

reactants and the products to roughly the same extent. The calculated enol-keto tautomerization of pyruvic acid accounts for roughly 2/3 of the overall energy of hydrolysis. In this case, the relative solvation energies of the enol and keto form are expected to be very similar[1]. This energy change of -10 kcal/mol results from the cancellation of large individual atomic changes, coming mainly from C_1, O_1 and H_4, the hydrogen which is transferred. With the exception of C_1, the atoms in the enol form of pyruvic acid either become more stable or become less stable by a small amount in the keto form. The large destabilizing contribution to the tautomerization reaction energy made by C_1 is partially balanced by the increased stabilization of the hydrogen.

The calculated *in vacuo* hydrolysis energy of phosphoenolpyruvate (trianion) is much more exothermic than the observed solution value. As in the charged diphosphoric acid reactions, the calculated values of the solvation energy show the solvent to preferentially stabilize the reactants, relative to the products (Table 5.5). The calculated hydrolysis energy is greater for the trianion, as compared to neutral phosphoenolpyruvate, due to the increased stabilization of the bridging oxygen and C_1 in the products, relative to the reactants (Table 5.11).

In conclusion, this is a preliminary step in the study of the hydrolysis of the P-O-P and P-O-C linkages. In order to address the specific influence of the solvent on the atomic energy changes it will be necessary to include the effects of solvent in a more direct way using self-consistent reaction field theory (SCRF) (Wong et al, 1991).

[1] The solvation energies were not calculated for these two neutral molecules. In rxn (18), the charged analog of this reaction, the solvation energies of the reactants and products are nearly identical (Table 5.5).

Table 5.1. Standard Free Energy of Hydrolysis of Some Phosphorylated Compounds.[a]

	ΔG° (kcal/mol)
Phosphenolpyruvate	-14.80
1,3-Diphosphoglycerate	-11.80
Phosphocreatine	-10.30
Acetyl phosphate	-10.10
Phosphoarginine	-7.70
ATP	-7.30
Glucose 1-phosphate	-5.00
Fructose 6-phosphate	-3.80
Glucose 6-phosphate	-3.30
Glycerol 1-phosphate	-2.20

[a] Data taken from Lehninger (1970).

Table 5.2. Experimental Values of ΔG°, ΔH° and ΔS° for the Hydrolysis of Diphosphoric Acid, Phosphoenolpyruvate and Adenosine Diphosphate.[a]

Reaction	ΔG° (kcal/mol)	ΔH° (kcal/mol)	ΔS° (cal/degree per mol)
$H_4P_2O_7 + H_2O \text{ ---> } 2H_3PO_4$	-9.5	-7.6	+6
$H_3P_2O_7^- + H_2O \text{ ---> } H_2PO_4^- + H_3PO_4$	-7.5	-7.3	+1
$H_2P_2O_7^{2-} + H_2O \text{ ---> } 2H_2PO_4^-$	-7.7	-6.8	+3
$HP_2O_7^{3-} + H_2O \text{ ---> } HPO_4^{2-} + H_2PO_4^-$	-7.1	-5.8	+4
$P_2O_7^{4-} + H_2O \text{ ---> } 2HPO_4^{2-}$	-10.4	-3.7	+22
$CH_2=C(OPO_3H_2)COOH + H_2O \text{ ---> } CH_3COCOOH + H_3PO_4$	-15.2	-14.3	+3
$CH_2=C(OPO_3H)COOH^{1-} + H_2O \text{ ---> } CH_3COCOOH + H_2PO_4^-$	-13.4	-12.2	+2
$CH_2=C(OPO_3H)COO^{2-} + H_2O \text{ ---> } CH_3COCOO^{1-} + H_2PO_4^-$	-15.5	-8.8	+22
$CH_2=C(OPO_3)COO^{3-} + H_2O \text{ ---> } CH_3COCOO^{1-} + HPO_4^{2-}$	-14.8	-6.0	+30
$ADP + H_2O \text{ ---> } AMP^{2-} + H_2PO_4^{1-}$	-9.8	-6.8	+10

[a] Values are taken from George et al (1970).

Table 5.3. Reactions of Diphosphoric Acid, Methyldiphosphoric Acid and Phosphoenolpyruvate.[a]

	Reactions	ΔE (kcal/mol)
1)	$H_4P_2O_7 + H_2O$ ---> $2H_3PO_4$	+0.9
2)	$H_4P_2O_7 + OH^-$ ---> $H_3PO_4 + H_2PO_4^-$	-66.8
3)	$H_2P_2O_7^{2-} + H_2O$ ---> $2H_2PO_4^-$	-70.2
4)	$P_2O_7^{4-} + H_2O$ ---> $2HPO_4^{2-}$	-280.5
5)	$P_2O_7^{4-} + Mg^{2+}$ ---> $P_2O_7Mg^{2-}$	-954.7
6)	$HPO_4^{2-} + Mg^{2+}$ ---> HPO_4Mg	-565.3
7)	$P_2O_7Mg^{2-} + H_2O$ ---> $HPO_4Mg + HPO_4^{2-}$	+108.9
8)*	$CH_3OP(O_2)OPO_3^{3-} + H_2O$ ---> $CH_3OPO_3H^- + HPO_4^{2-}$	-134.0
9)*	$CH_3OP(O_2)OPO_3^{3-} + H_2O$ ---> $CH_3OPO_3^{2-} + H_2PO_4^-$	-142.4
10)*	$CH_3OP(O_2)OPO_3^{3-} + OH^-$ ---> $CH_3OPO_3^{2-} + HPO_4^{2-}$	-88.5
11)	$CH_2=C(OPO_3H_2)COOH + H_2O$ ---> $CH_3C(O)COOH + H_3PO_4$	-15.7
12)	$CH_2=C(OPO_3H_2)COOH + OH^-$ ---> $CH_2=C(O)COOH^- + H_3PO_4$	-51.4
13)	$CH_2=C(O)COOH^- + H_3O^+$ ---> $CH_2=C(OH)COOH + H_2O$	-185.4
14)	$CH_2=C(OH)COOH$ ---> $CH_3C(O)COOH$	-10.2
15)	$CH_2=C(OPO_3)COO^{3-} + H_2O$ ---> $CH_3C(O)COO^- + HPO_4^{2-}$	-134.0
16)	$CH_2=C(OPO_3)COO^{3-} + OH^-$ ---> $CH_2=C(O)COO^{2-} + HPO_4^{2-}$	-63.9
17)	$CH_2=C(O)COO^{2-} + H_3O^+$ ---> $CH_2=C(OH)COO^- + H_2O$	-283.9
18)	$CH_2=C(OH)COO^-$ ---> $CH_3C(O)COO^-$	-17.5
19)	$HPO_4^{2-} + H_3O^+$ ---> $H_2PO_4^- + H_2O$	-297.3
20)	$H_2PO_4^- + H_3O^+$ ---> $H_3PO_4 + H_2O$	-163.6

[a] The "*" indicates that the results were obtained using the 6-31G** rather than the 6-311++G** basis set.

Table 5.4. Molecular Volumes, Cavity Radii and Solvation Energies.[a]

Molecule	Volume atomic units	a_o atomic units	ΔE_{solv} kcal/mol
$H_2P_2O_7^{2-}$	1412.106	7.904	-156.79
$P_2O_7^{4-}$	1155.918	8.104	-611.68
$P_2O_7Mg^{2-}$	1065.444	7.913	-156.63
$CH_3OP(O_2)OPO_3^{3-}$	*1577.730	*8.167	*-341.45
$CH_3OPO_3H^-$	*753.114	*7.152	*-43.32
$CH_3OPO_3^{2-}$	*769.627	*7.197	*-172.21
$CH_2=C(COO^-)(OPO_3^{2-})$	1210.915	8.216	-339.39
$CH_2=C(O^-)COO^-$	790.104	7.252	-170.90
$CH_2=C(OH)COO^-$	723.950	7.070	-43.82
$CH_3C(O)COO^-$	720.373	7.060	-43.88
$H_2PO_4^-$	625.209	6.778	-45.71
	*583.213	*6.645	*-46.63
HPO_4^{2-}	664.394	6.898	-179.67
	*594.913	*6.682	*-185.46
HPO_4Mg	641.648	6.829	-58.43[b]
^cH_2O	184.604	4.829	-13.18[b]
	*174.813	*4.759	*-13.16[b]
H_3O^+	163.027	4.672	-66.32

[a] a_o is the estimated cavity radius. ΔE_{solv} is calcualted using equation (5.2.). A "*" indicates that the value was obtained using the 6-31G** basis set rather than the 6-311++G** basis set.
[b] This value was obtained using eqn. (5.2).

Table 5.5. Reaction Energies Including Solvation Effects.[a]

	Reaction	ΔE_{gas} (kcal/mol)	ΔE_{solv}^{rxn} (kcal/mol)	ΔE_{H_2O} kcal/mol	ΔH_{exp} kcal/mol
3)	$H_2P_2O_7^{2-} + H_2O \rightarrow H_2PO_4^-$	-70.2	78.6	8.4	-6.8
4)	$P_2O_7^{4-} + H_2O \rightarrow 2HPO_4^{2-}$	-280.5	265.5	-15.0	-3.7
5)	$P_2O_4^{4-} + Mg^{2+} \rightarrow P_2O_7Mg^{2-}$	-954.7	358.9	-595.8	
6)	$HPO_4^{2-} + Mg^{2+} \rightarrow HPO_4Mg$	-565.3	483.9	-81.4	
7)	$P_2O_7Mg^{2-} + H_2O \rightarrow HPO_4Mg + HPO_4^{2-}$	108.9	-68.3	40.6	
8)*	$CH_3OP(O_2)OPO_3^{3-} + H_2O \rightarrow CH_3OPO_3H^{1-} + HPO_4^{2-}$	-134.0	125.8	-8.2	
9)*	$CH_3OP(O_2)OPO_3^{3-} + H_2O \rightarrow CH_3OPO_3^{2-} + H_2PO_4^-$	-142.4	135.8	-6.6	-6.8[b]
15)	$CH_2=C(OPO_3)COO^{3-} + H_2O \rightarrow CH_3COCOO^- + HPO_4^{2-}$	-134.0	131.9	-2.1	-6.0
17)	$CH_2=C(O)COO^{2-} + H_3O^+ \rightarrow CH_2=C(OH)COO^- + H_2O$	-283.9	180.2	-103.7	
18)	$CH_2=C(OH)COO^- \rightarrow CH_3COCOO^-$	-17.5	-0.1	-17.5	
19)	$HPO_4^{2-} + H_3O^+ \rightarrow H_2PO_4^{1-} + H_2O$	-297.3	187.1	-110.2	

[a] A "*" indicates that the values were obtained using the 6-31G** rather than the 6-311++G** basis set. Experimental Values are from George et al (1970).

[b] Value for the hydrolysis of $ADP^{3-} + H_2O \rightarrow AMP^{2-} + H_2PO_4^-$.

Table 5.6. Atomic Properties of Phosphorus in Various Molecules.[a]

	N(P)	E(P)	Vol(P)	$V_a(P)$	$V_r(P)$	$V_a^*(P)$
$H_4P_2O_7$	11.041	-338.66935	19.678	-985.5257	308.1839	-784.0638
$H_2P_2O_7^{2-}$	11.065	-338.65029	21.663	-973.9230	296.6191	-784.1847
$P_2O_7^{4-}$	11.076	-338.57038	21.148	-966.1115	288.9682	-784.1651
$P_2O_7Mg^{2-}$	11.089	-338.73035	20.703	-1002.2632	325.1630	-784.5236
HPO_4Mg	11.074	-338.81911	20.217	-940.7827	263.1369	-784.5788
[b]PEP	11.038	-338.68023	19.859	-968.9818	291.6163	-784.0425
[c]PEP^{3-}	11.099	-338.69444	21.257	-959.5661	282.1733	-784.5375
H_3PO_4	11.049	-338.68922	20.707	-913.6415	236.2616	-784.1471
$H_2PO_4^-$	11.066	-338.68916	21.003	-910.4669	233.0863	-784.2832
HPO_4^{2-}	11.106	-338.69136	22.062	-907.5731	230.1894	-784.5933
6-31G**						
[d]MDP^{3-} P_1	10.974	-338.65471	18.940	-972.6670	295.2969	-783.3642
[d]MDP^{3-} P_2	10.975	-338.65317	20.241	-985.3431	307.9710	-783.3526
[e]MP^{1-}	10.969	-338.77283	18.249	-924.6018	247.0093	-783.5220
[f]MP^{2-}	10.971	-338.66077	18.475	-920.8507	243.4904	-783.3782
H_3PO_4	10.946	-338.82566	18.016	-911.4939	233.7951	-783.3983
$H_2PO_4^-$	10.961	-338.78165	18.206	-908.3374	230.7328	-783.4627
HPO_4^{2-}	10.964	-338.6523	18.403	-904.7166	227.3784	-783.8178

[a] N(P), E(P), Vol(P), $V_a(P)$, $V_r(P)$, are the electron population, energy, volume out to the 0.001 density envelope, total attractive potential energy, and total repulsive potential energy for phosphorus. $V_a^*(P)$ is the potential energy interaction of the phosphorus nucleus with the charge density contained within its own basin. [b] Phosphoenolpyruvate (neutral). [c] Phosphoenolpyruvate (trianion). [d] Methyldiphosphate (trianion). [e] Methylphosphate (monoanion). [f] Methylphosphate (dianion).

Table 5.7. The P-O-P and P-O-C Linkages.

				P-O-P or P-O-C	
	R	$\rho(r_c)$	$\nabla^2\rho(r_c)$	r_O	r_P
$H_4P_2O_7$					
P-O_1	1.6001	0.1707	0.9308	0.9744	0.6260
$H_2P_2O_7^{2-}$					
P-O_1	1.6056	0.1578	0.9070	0.9738	0.6322
$P_2O_7^{4-}$					
P-O_1	1.6386	0.1433	0.7575	0.9943	0.6443
$P_2O_7Mg^{2-}$					
P-O_1	1.6663	0.1459	0.6617	1.0192	0.6477
*MDP^{3-}					
P_2-O_2	1.7931	0.0967	0.3527	1.096	0.698
P_1-O_2	1.5430	0.1896	1.2735	0.933	0.610
P_1-O_1	1.7210	0.1268	0.5490	1.060	0.662
O_1-C	1.3683	0.2954	-0.4546	0.923	
PEP					
P-O_1	1.5692	0.1824	1.0685	0.953	0.617
O_1-C_1	1.3683	0.2571	0.2500	0.931	
PEP^{3-}					
P-O_1	1.7485	0.1176	0.4300	1.073	0.677
O_1-C_1	1.3162	0.3135	-0.0848	0.887	

[a] **R** is the geometric bond length, and r_O and r_P are the bonded radii of oxygen and phosphorus, respectively, in Å. $\rho(r_c)$ and $\nabla^2\rho(r_c)$ are the values of the charge density and the Laplacian of the charge density (in atomic units) evaluated at the bond critical point. A "*" indicates that the values were obtained using the smaller 6-31G** basis set.

Table 5.8. Atomic Properties of the Bridging Oxygen in P-O-P and P-O-C Linkages. [a]

Oxygen	N(O)	E(O)	Vol(O)	Va(O)	Vr(O)	Va°(O)
P-O-P						
$H_4P_2O_7$	9.634	-75.83323	103.989	-388.7977	237.1277	-187.0951
$H_2P_2O_7^{2-}$	9.665	-75.80348	106.435	-384.8411	233.2301	-187.2242
$P_2O_7^{4-}$	9.660	-75.65435	113.076	-376.3723	225.0605	-186.9052
$P_2O_7Mg^{2-}$	9.634	-75.65158	109.420	-400.1101	248.7979	-186.6870
*MDP^{3-} (O_2)	9.649	-75.56815	110.786	-387.1094	235.8960	-186.6598
P-O-C						
PEP	9.488	-75.77918	98.211	-365.8923	214.3282	-186.5836
PEP^{3-}	9.450	-75.61855	105.385	-353.0685	201.8269	-186.0669
*MDP^{3-} (O_1)	9.448	-75.51709	103.674	-350.3343	199.2368	-185.8851
*MP^{1-}	9.490	-75.57585	102.729	-311.8458	160.6408	-186.1546
*MP^{2-}	9.450	-75.48334	105.208	-305.7565	154.7461	-185.8342

[a] The "*" indicates that these values were obtained using the 6-31G** rather than the 6-311++G** basis set.

Table 5.9. Atomic Properties of the Non-Bridging Oxygens.

	E	V_a	V_r	V_a°	V_{ee}	ΔV_{ee}
$H_4P_2O_7$						
O_2	-75.62467	-353.0985	201.8462	-186.2773	115.2482	
$^aO_3$	-75.64920	-336.7190	185.4179	-186.1810	106.5748	
$^aO_4$	-75.66294	-346.6056	195.2769	-186.2702	111.5617	
ΣA(O)	-453.87362	-2072.8464	1165.0820	-1117.4569	666.7694	-159.2343
Molecular					1246.6525	-232.1460
$H_2P2O_7^{2-}$						
O_2	-75.54936	-340.0637	188.9619	-186.2681	110.4973	
$^aO_3$	-75.52597	-331.3897	180.3348	-185.8197	105.6942	
O_4	-75.54229	-337.1149	186.0272	-186.2445	109.0142	
ΣA(O)	-453.23524	-2017.1366	1110.6478	-1116.6647	650.4114	-142.0163
Molecular					1218.8915	-208.2441
$P_2O_7^{4-}$						
O_2	-75.40285	-331.0969	180.2887	-186.0995	107.7165	
ΣA(O)	-452.41707	-1986.5811	1081.7325	-1116.5973	646.2990	-136.7990
Molecular					1201.8648	-197.5466
$P_2O_7Mg^{2-}$						
O_2	-75.53767	-346.5654	195.4833	-186.2031	113.7520	
O_3	-75.53786	-373.2287	222.1451	-186.4047	127.0420	
ΣA(O)	-453.22676	-2186.0458	1279.5469	-1118.0251	735.6719	
Molecular					1507.7635	
PEP						
$O_{1'}$	-75.63465	-338.0742	186.8000	-186.2856	107.7884	
$^aO_{2'}$	-75.63750	-330.5321	179.2524	-186.1486	103.5767	
O_2	-75.68948	-306.9938	155.6109	-185.6084	92.1510	
O_3	-75.63666	-314.9494	163.6718	-185.6044	95.8405	
ΣA(O)	-378.23580	-1621.0816	864.5876	-929.7957	502.9333	-102.1058
Molecular					1022.4139	-181.4883
PEP^{3-}						
$O_{1'}$	-75.46615	-324.9693	174.0332	-186.1787	103.8827	
$O_{2'}$	-75.46794	-329.6303	178.6905	-186.1958	106.2135	
O_2	-75.52654	-302.2017	151.1454	-185.7464	92.1468	
O_3	-75.55662	-307.3095	156.1929	-185.6760	94.6752	
ΣA(O)	-377.48518	-1593.7410	838.7525	-929.9927	503.1317	-100.7915
Molecular					1010.3088	-175.5082

[a] The protonated oxygen.

Table 5.10. Changes in Molecular Properties.[a]

	Reaction	ΔE (kcal/mol)	ΔVolume (au)	ΔV_a (au)	ΔV_r (au)	ΔV_a° (au)
1)	$H_4P_2O_7 + H_2O$	0.9	18.40	465.5417	-465.5596	-0.1022
2)	$H_4P_2O_7 + OH^-$	-66.8	-6.01	475.3704	-475.5715	-0.5543
3)	$H_2P_2O_7^{2-} + H_2O$	-70.2	4.08	407.8701	-408.0884	-0.1609
4)	$P_2O_7^{4-} + H_2O$	-280.5	-11.73	377.5525	-378.4864	-0.8169
5)	$P_2O_7^{4-} + Mg^{2+}$	-954.7	-138.09	-489.1666	486.1563	-3.9256
6)	$HPO_4^{2-} + Mg^{2+}$	-565.3	-22.75	-258.5789	256.8200	-2.5369
7)	$P_2O_7Mg^{2-} + H_2O$	108.9	55.99	608.1403	-607.8227	0.5718
8)*	$MDP^{3-} + H_2O$	-134.0	-13.05	443.4148	-443.8546	-1.1586
9)*	$MDP^{3-} + H2O$	-142.4	-8.24	443.4518	-443.9106	-0.2484
10)*	$MDP^{3-} + OH^-$	-88.5	-6.86	454.4536	-454.6571	-1.1826
11)	$PEP + H_2O$	-15.7	14.15	362.8957	-362.9606	1.9818
12)	$PEP + OH^-$	-51.4	3.51	366.0819	-366.2549	0.1131
13)	$PA^{1-} + H_3O^+$	-185.4	-25.37	-9.0793	8.4820	-0.2422
14)	enol --> keto	-10.1	0.53	4.5614	-4.5956	1.9532
15)	$PEP^{3-} + H_2O$	-134.0	23.71	339.2147	-339.6607	1.5283
16)	$PEP^{3-} + OH^-$	-63.9	36.39	345.0174	-345.2255	-0.2002
17)	$PA^{2-} + H_3O^+$	-283.9	-44.58	-10.3088	9.3898	-0.1167
18)	enol --> keto	-17.5	-3.58	3.1745	-3.2329	1.6876
19)	$HPO_4^{2-} + H_3O^+$	-297.3	-17.61	-13.3074	12.3746	0.3678
20)	$H_2PO_4^- + H_3O^+$	-163.6	-11.07	-11.1604	10.6039	0.2944

[a] The "*" indicates that these values were obtained using the 6-31G** rather than the 6-311++G** basis set. The complete expresions for the reactions are given in Table 5.3.

Table 5.11. Group Contributions to the Calculated Hydrolysis Energies of Diphosphoric Acid, Methyldiphosphoric Acid and Phosphoenolpyruvate.[a]

Diphosphoric Acid Reactions					
	Reaction	ΔE (H_2O or OH^-)	ΔE ($-PO_3H_x$)[b]	ΔE (O_1)	ΔE (total)
1)	$H_4P_2O_7 + H_2O$	-132	7	126	0.9
2)	$H_4P_2O_7 + OH^-$	-340	102	171	-66.8
3)	$H_2P_2O_7^{2-} + H_2O$	-130	-100	160	-70.2
4)	$P_2O_7^{4-} + H_2O$	-74	-350	143	-280.5

Methyldiphosphate Reactions						
	Reaction	ΔE (H_2O or OH^-)	ΔE ($-PO_3H_x$)	ΔE (O_1)	ΔE (remaining)	ΔE (total)
8)*	$MDP^{3-} + H_2O$	-35	30	46	-175	-134.0
9)*	$MDP^{3-} + H_2O$	-93	-190	78	61	-142.4
10)*	$MDP^{3-} + OH^-$	-258	30	78	61	-88.5

Phosphoenolpyruvate Reactions							
	Reactions	ΔE (H_2O or OH^-)	ΔE ($-PO_3H_x$)[c]	ΔE (O_1)	ΔE (C_1)	ΔE (remaining)	E (total)
11)	$PEP + H_2O$	-318	9	77	304	-88	-15.7
12)	$PEP + OH^-$	-340	9	169	251	-140	-51.4
15)	$PEP^{3-} + H_2O$	-240	25	-11	144	-51	-134.0
16)	$PEP^{3-} + OH^-$	-247	25	84	119	-44	-63.9

[a] All values are in kcal/mol. The "*" indicates that these values were obtained using the 6-31G** rather than the 6-311++G** basis set.

[b] $-PO_3H_x$ is the phosphoryl group, where x = 2,1,0 for $H_4P_2O_7$, $H_2P_2O_7^{2-}$, and $P_2O_7^{4-}$, respectively.

[c] x = 2,0 for PEP and PEP^{2-}, respectively.

Table 5.12. Protonation and Tautomerization Reactions.[a]

Pyruvic Acid Protonation Reactions						
	Reaction	ΔE (H_3O^+)	ΔE (O_1)	ΔE (C_1)	ΔE (remaining)	ΔE (total)
13)	CH_2=C(O)$COOH^{1-}$ + H_3O^+	-39	-29	-226	109	-185.4
17)	CH_2=C(O)COO^{2-} + H_3O^+	-56	-27	-237	35	-283.9

Phosphoric Acid Protonation Reactions				
	Reactions	ΔE (H_3O^+)	ΔE (PO_3H_x)	ΔE (total)
19)	HPO_4^{2-} + H_3O^+	-45	-252	-297.3
20)	$H_2PO_4^{1-}$ + H_3O^+	-23	-141	-163.6

Pyruvic Acid enol-keto Tautomerizations						
	Reaction	ΔE (O_1)	ΔE (C_1)	ΔE[b] (H_x)	ΔE (remaining)	ΔE (total)
14)	enol->keto(neutral)	-62	279	-169	-58	-10.1
18)	enol-> keto (1-)	-68	261	-169	-42	-17.5

[a] All values are in kcal/mol. [b] H_4 in reaction (14) and H_3 in reaction (18).

Figure 5.1

A display of the gradient vector field (top) and a contour map (bottom) of the charge density for the P-O-P plane of diphosphoric acid (neutral). The bond paths and atomic boundaries are overlaid on the contour map. All of the trajectories of $\nabla\rho$ in the vicinity of a given nucleus terminate at that nucleus, in all three dimensions, thereby defining the basin of the atom. The outermost charge density contour equals 0.001 au. The contours increase in order 2×10^n, 4×10^n, 8×10^n, with n increasing in steps of unity from n = -3.

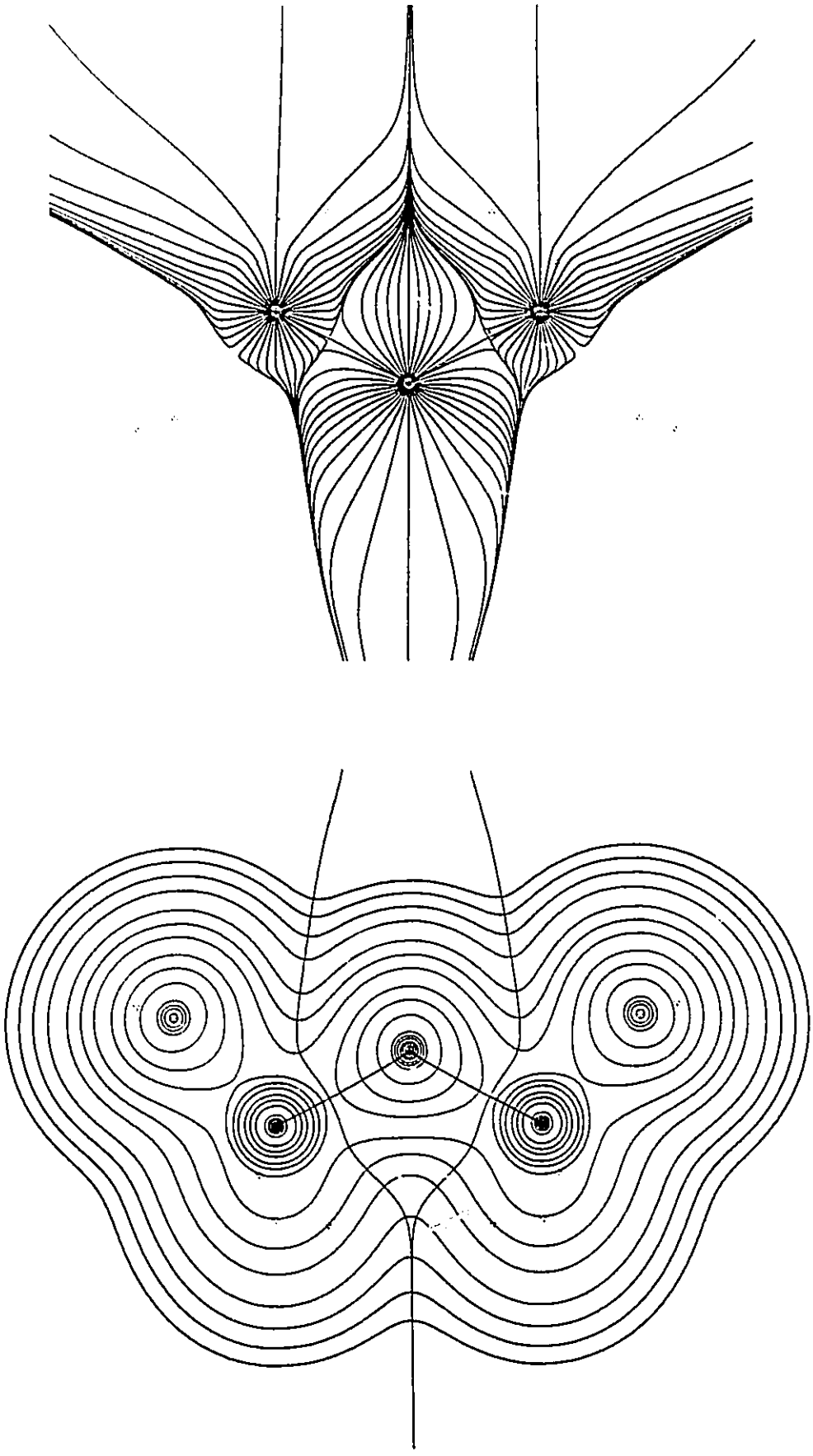

Figure 5.2

A display of the gradient vector field (top) and a contour map (bottom) of the charge density for the C_s symmetry plane of (neutral) phosphoenolpyruvate. The bond paths and atomic boundaries are overlaid on the contour map. Contour values are listed in Figure 5.1.

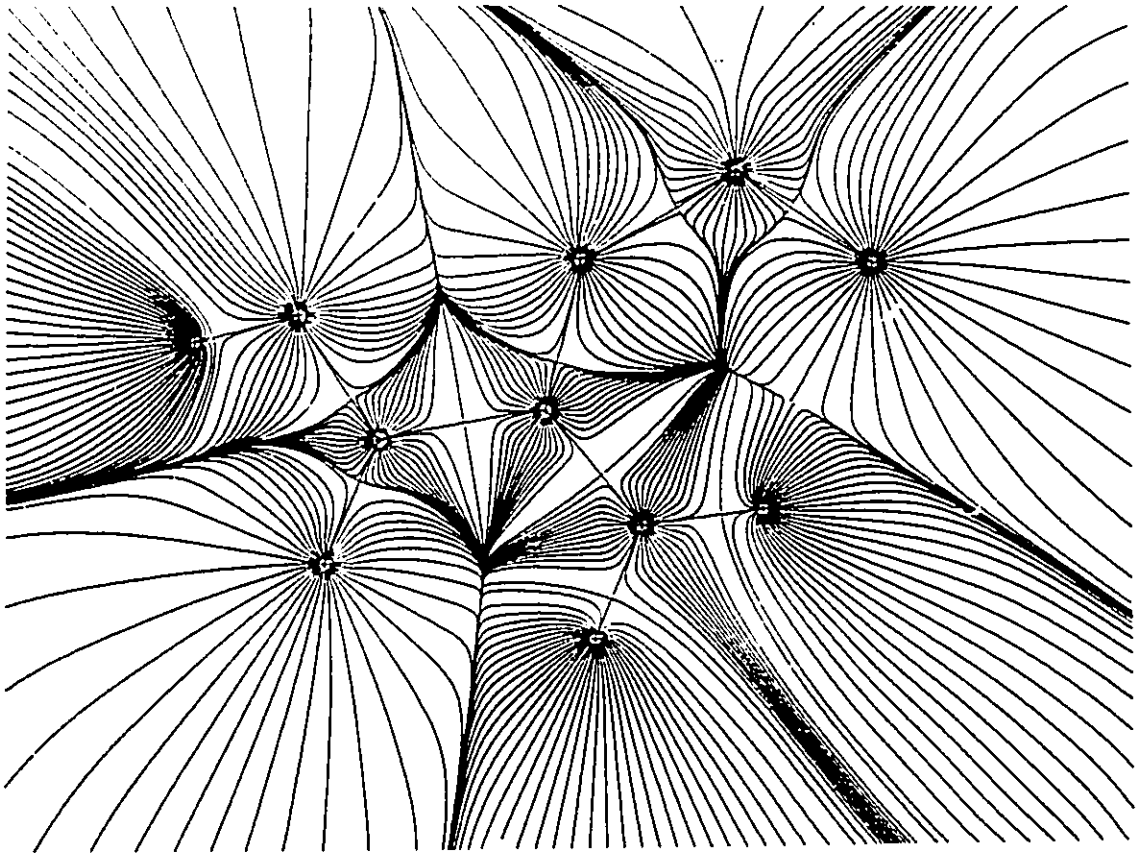

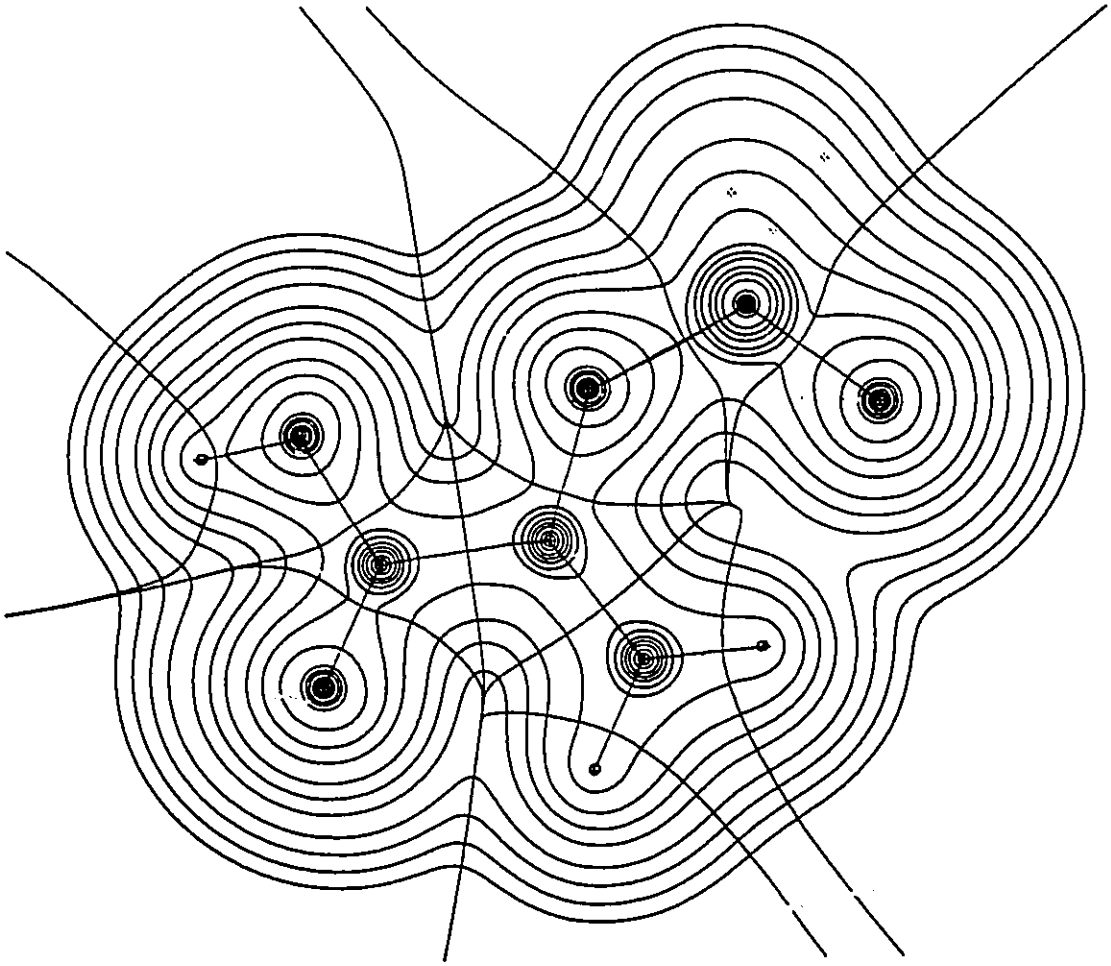

Figure 5.3

A display of the gradient vector field (top) and a contour map (bottom) of the charge density for the C_s symmetry plane of methyldiphosphoric acid (trianion).
The bond paths and atomic boundaries are overlaid on the contour map. Contour values are listed in Figure 5.1.

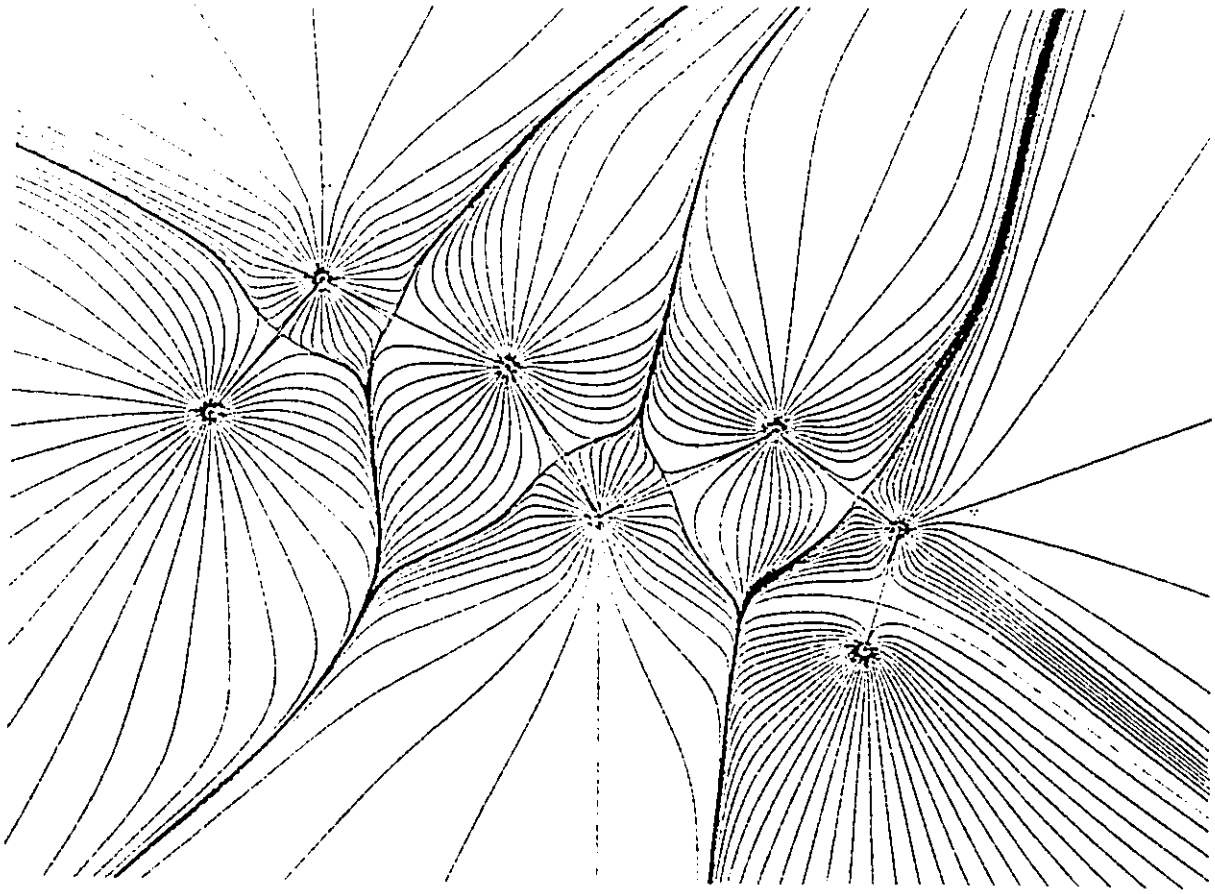

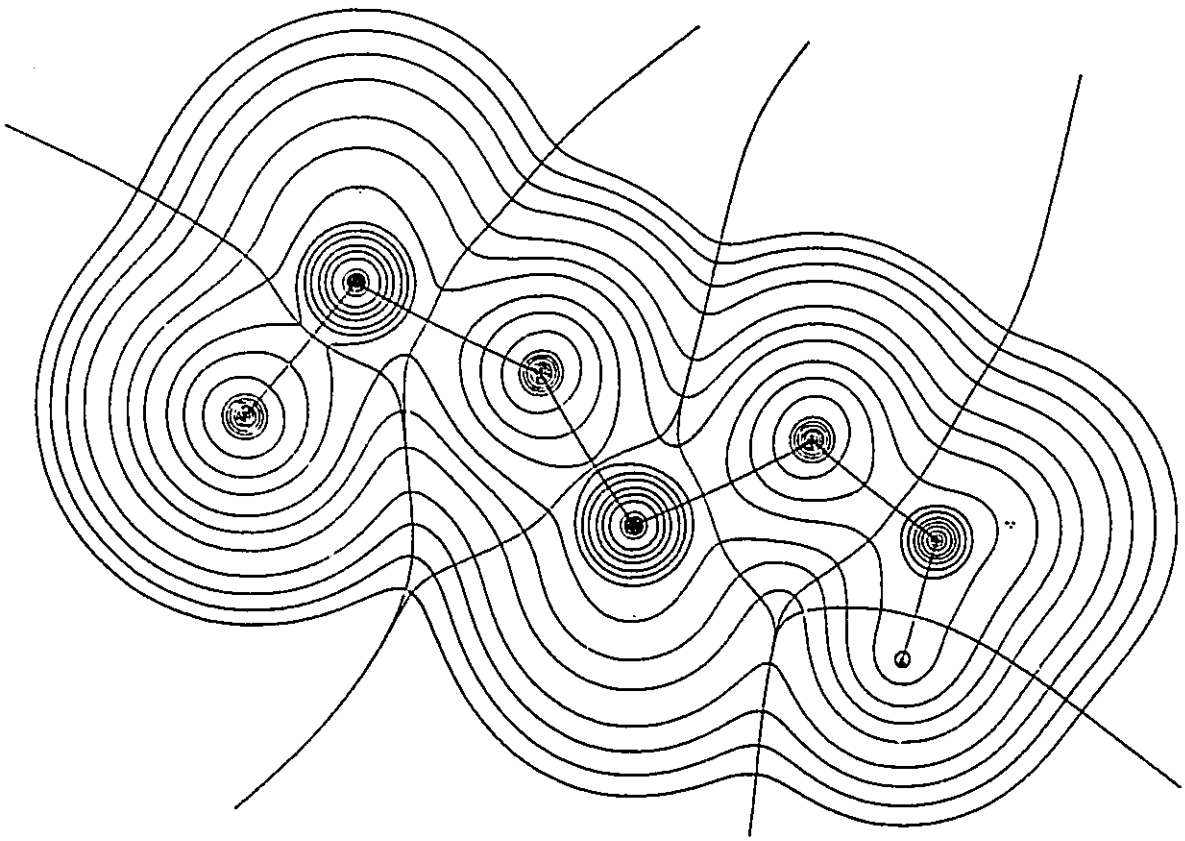

Figure 5.4

Three-dimensional density envelope out to the 0.001 au contour of the phosphorus atom in diphosphoric acid (neutral).

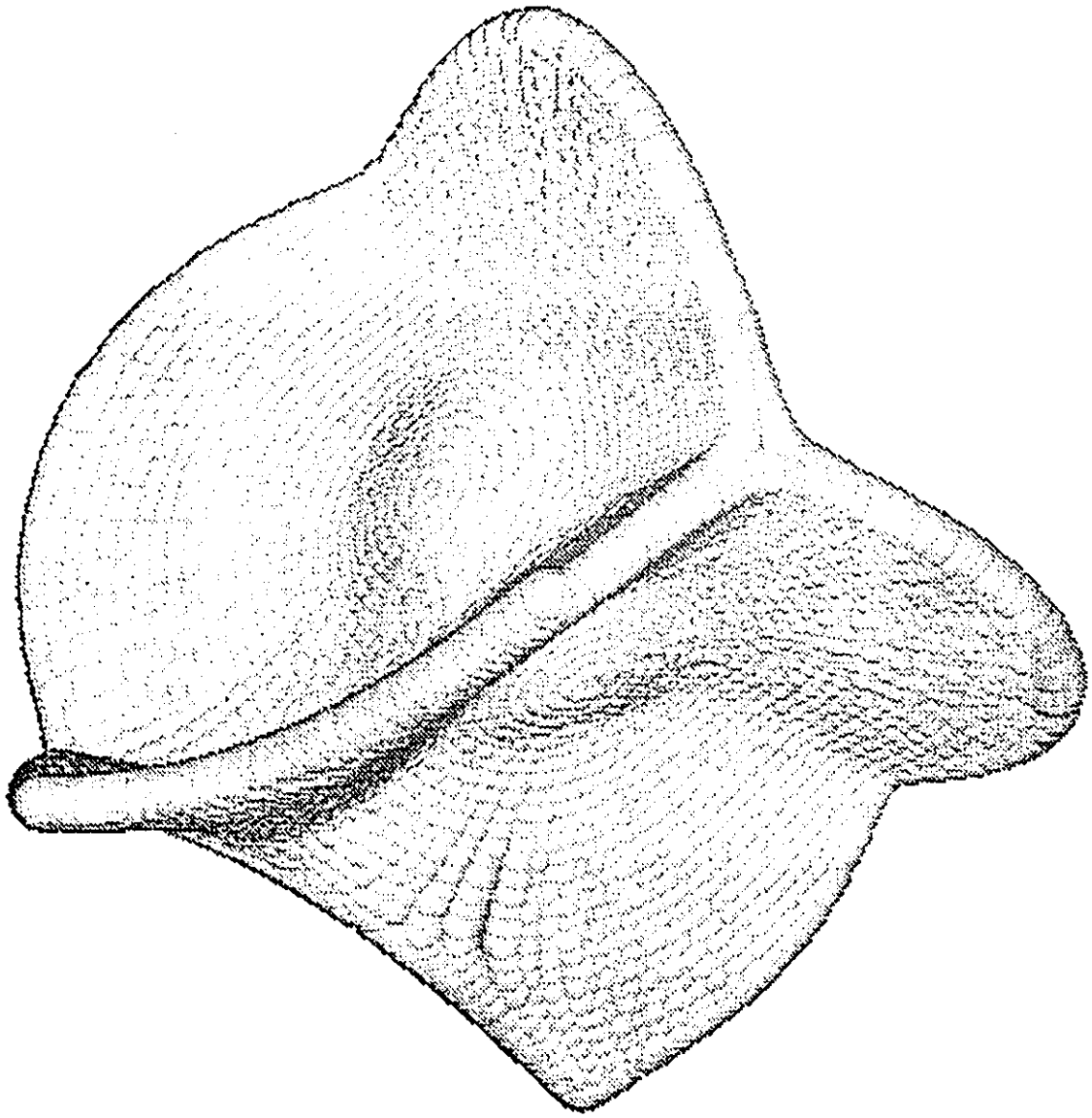

Figure 5.5

Three-dimensional density envelope out to the 0.001 au contour of the phosphorus atom in phosphoenolpyruvate (neutral).

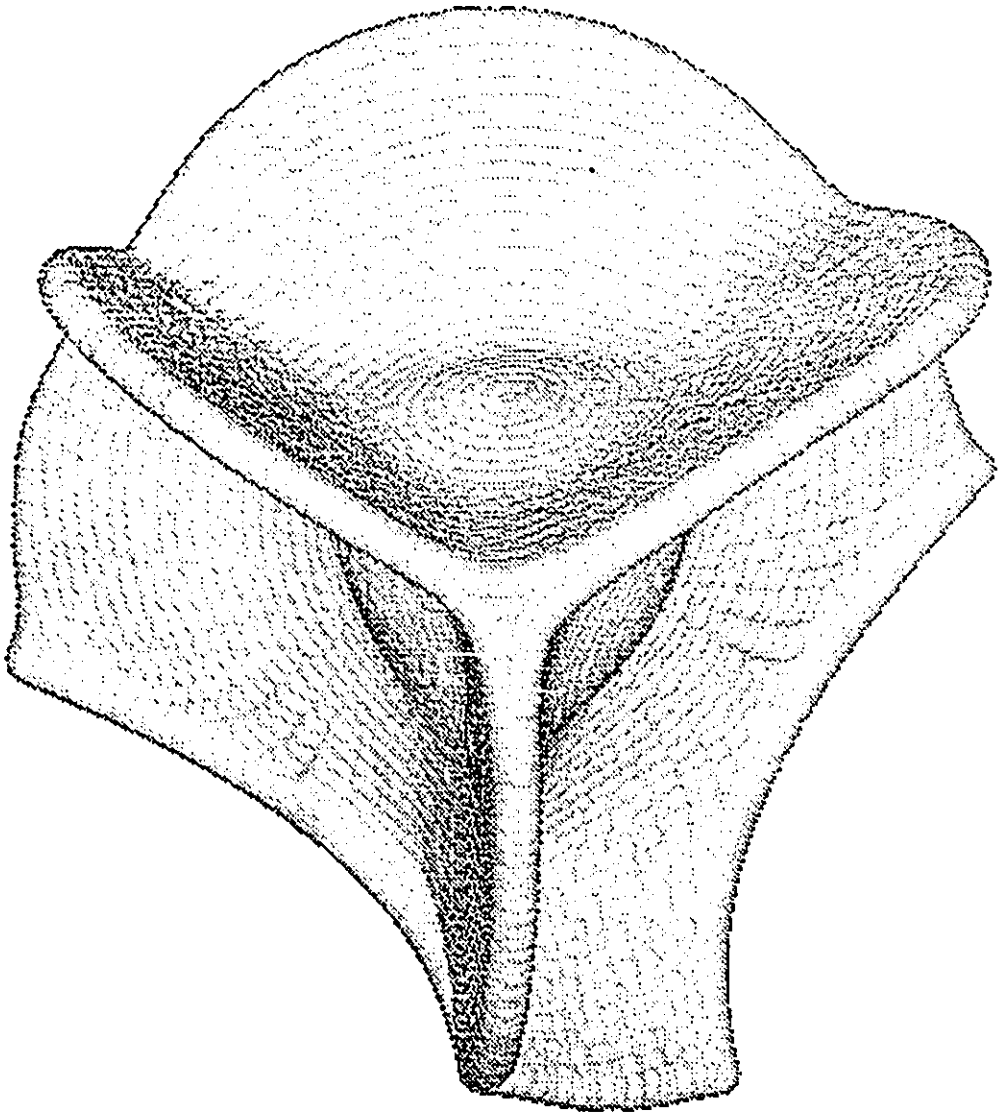

Figure 5.6

Profile maps of the Laplacian of the charge density for a) the free phosphorus atom and b) and c) along the P-O_1 bond in $H_4P_2O_7$. Note the change in scale for b). The vertical line in c) denotes the position of the interatomic surface. The distance "R" from the phosphorus nucleus is in Å.

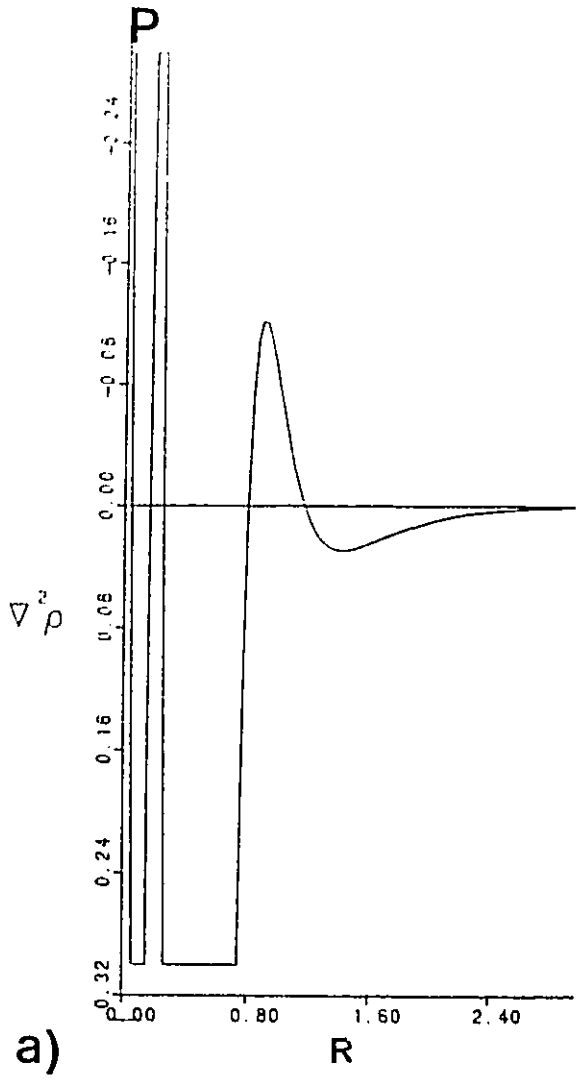
P
$\nabla^2\rho$
0.00
0.80
1.60
2.40
R
a)

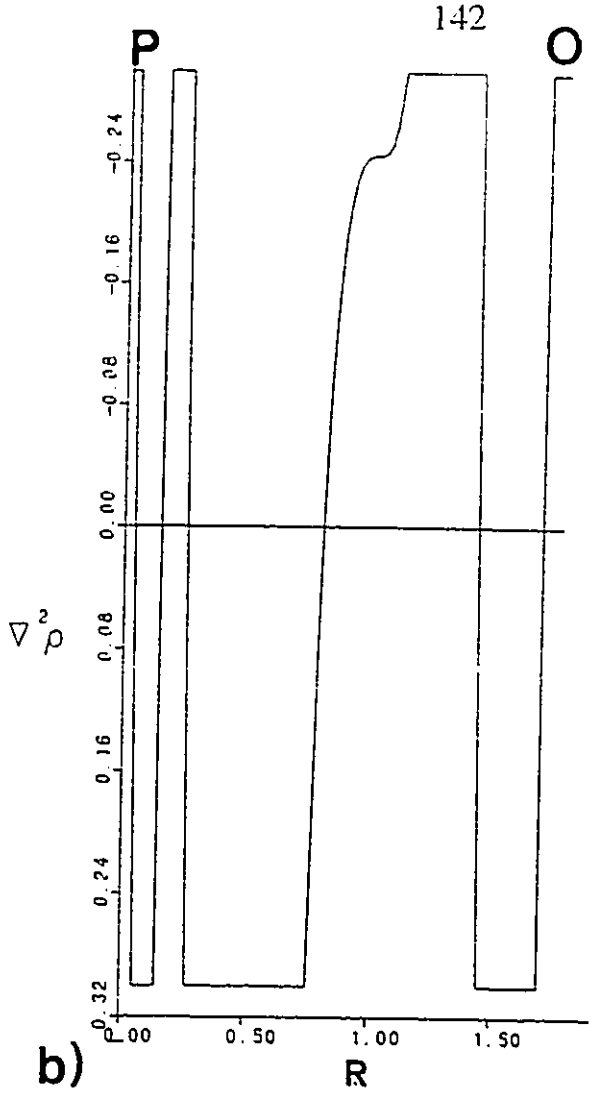
P
O
$\nabla^2\rho$
0.00
0.50
1.00
1.50
R
b)

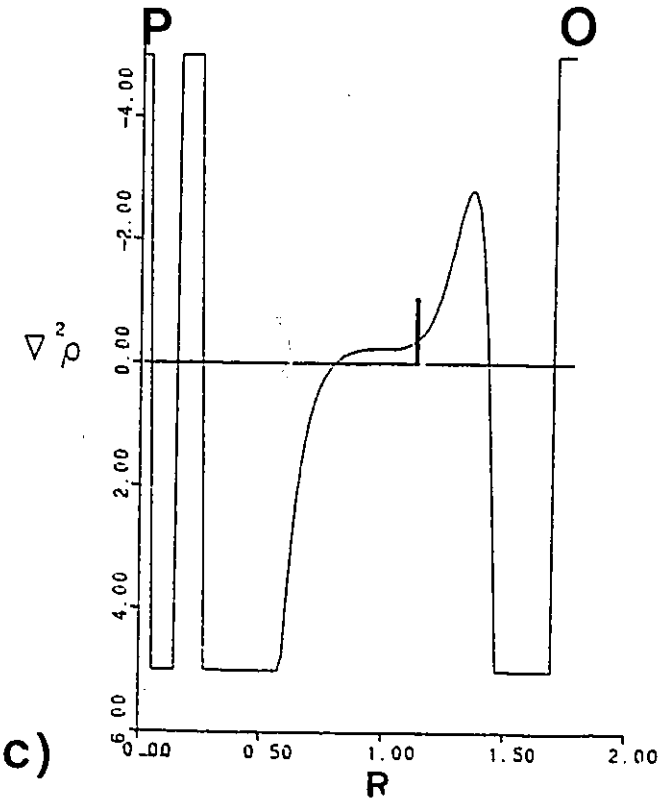
P
O
$\nabla^2\rho$
0.00
0.50
1.00
1.50
2.00
R
c)

Figure 5.7

Contour (top) and relief (bottom) maps of the Laplacian of the charge density for the P-O_1-P plane of diphosphoric acid (neutral). The bond paths and atomic boundaries are overlaid on the contour map. The contours of the Laplacian of the electronic charge density (solid contours $\nabla^2\rho < 0$, dashed contours $\nabla^2\rho > 0$) increase and decrease from a zero contour in steps $\pm 2 \times 10^n, \pm 4 \times 10^n, \pm 8 \times 10^n$, begining with n = -3 and increasing in steps of unity. The innermost solid contour encompassing a nucleus with Z > 1 encloses the innermost region of charge concentration.

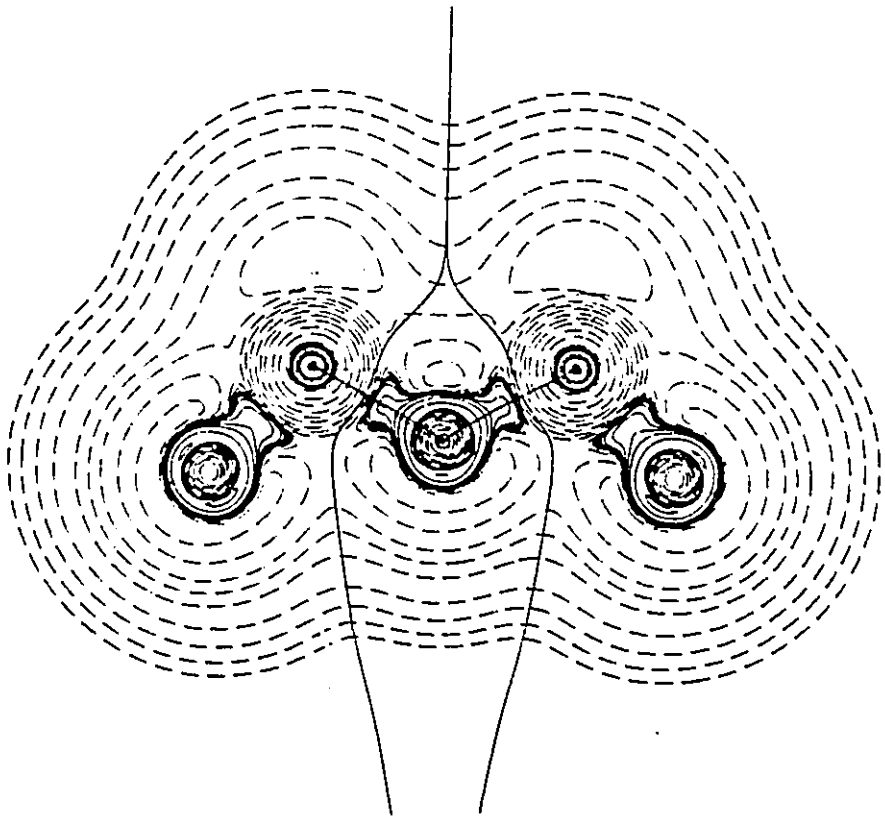

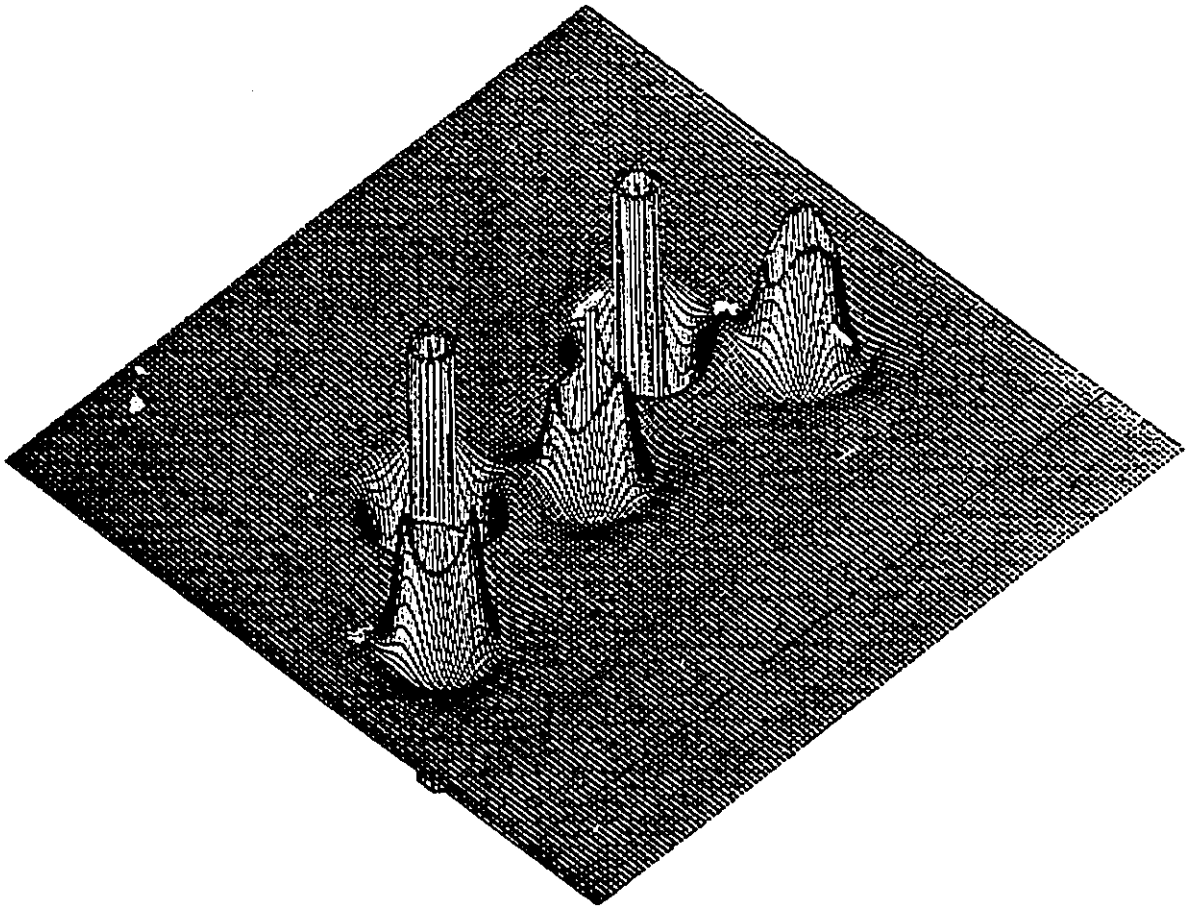

Figure 5.8

Contour (top) and relief (bottom) maps of the Laplacian of the charge density for the C_s symmetry plane of phosphoenolpyruvate (neutral). The bond paths and atomic boundaries are overlaid on the contour map. The contours of the Laplacian are listed in Figure 5.7.

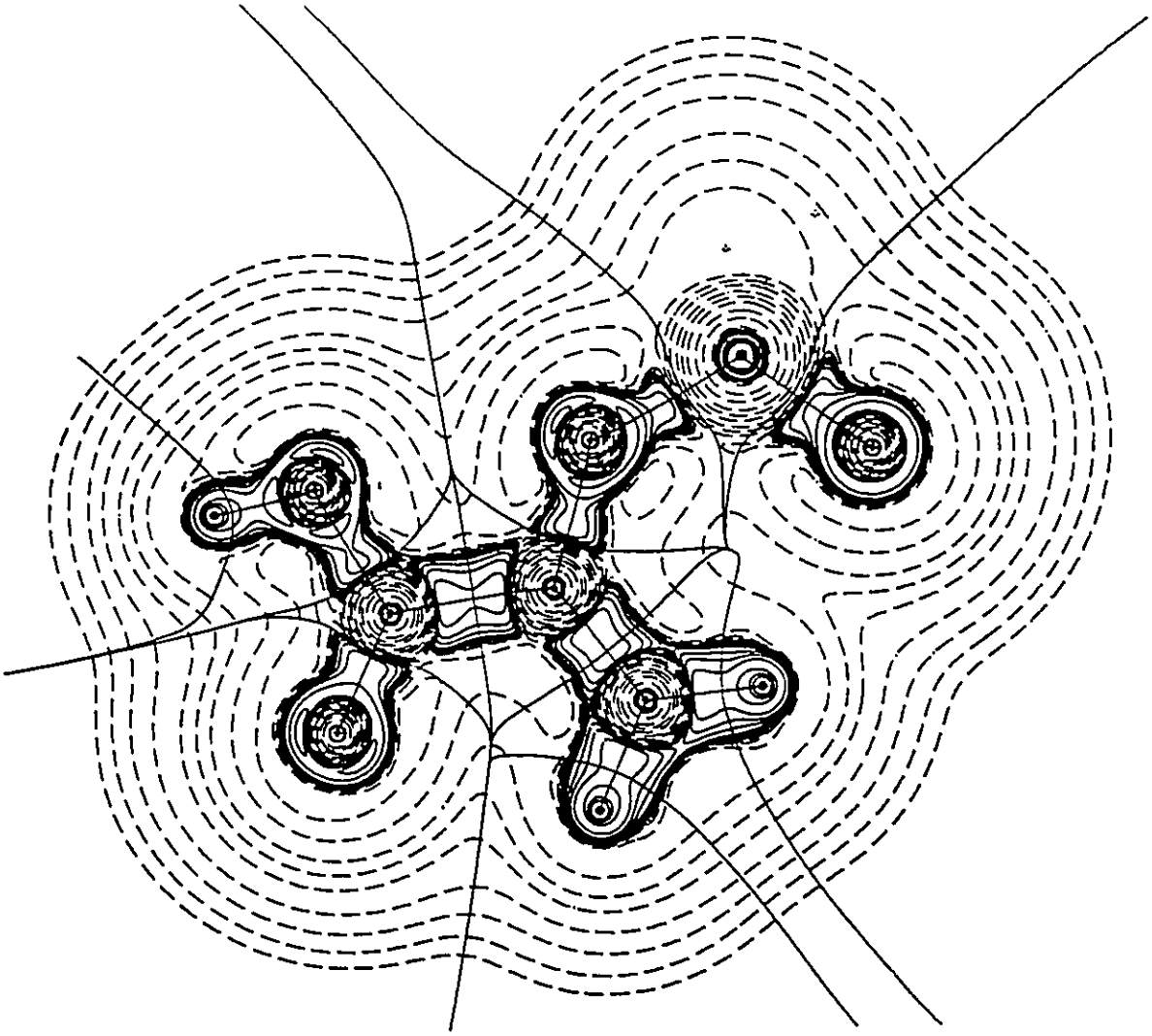

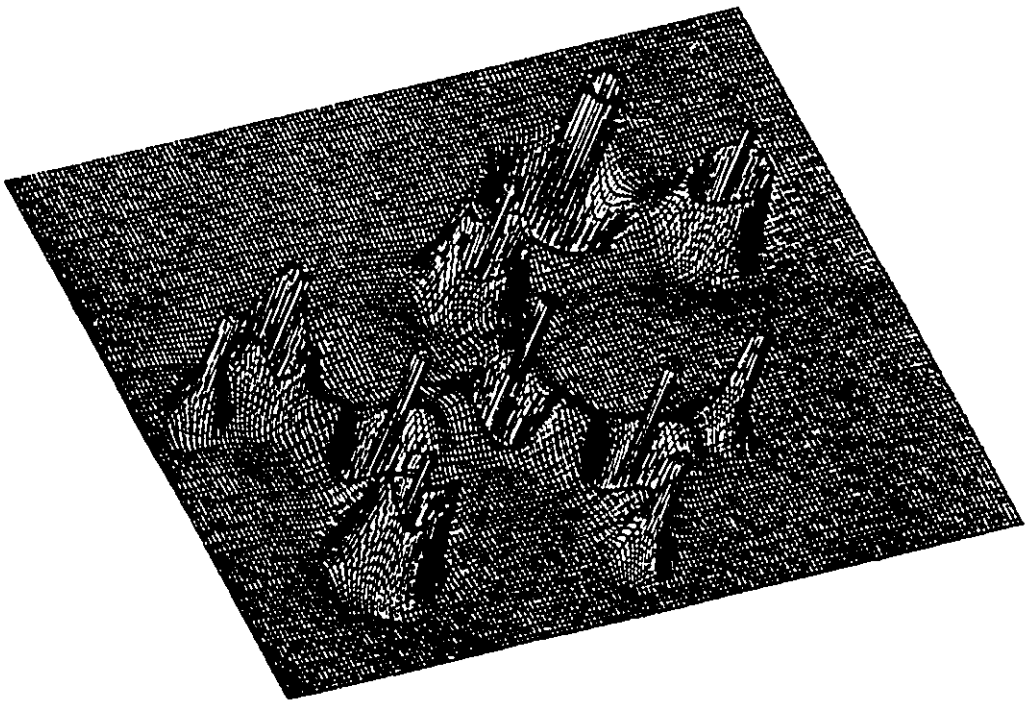

Figure 5.9

Relief map of the Laplacian of the charge density for the C_s symmetry plane in methyldiphosphoric acid (trianion).

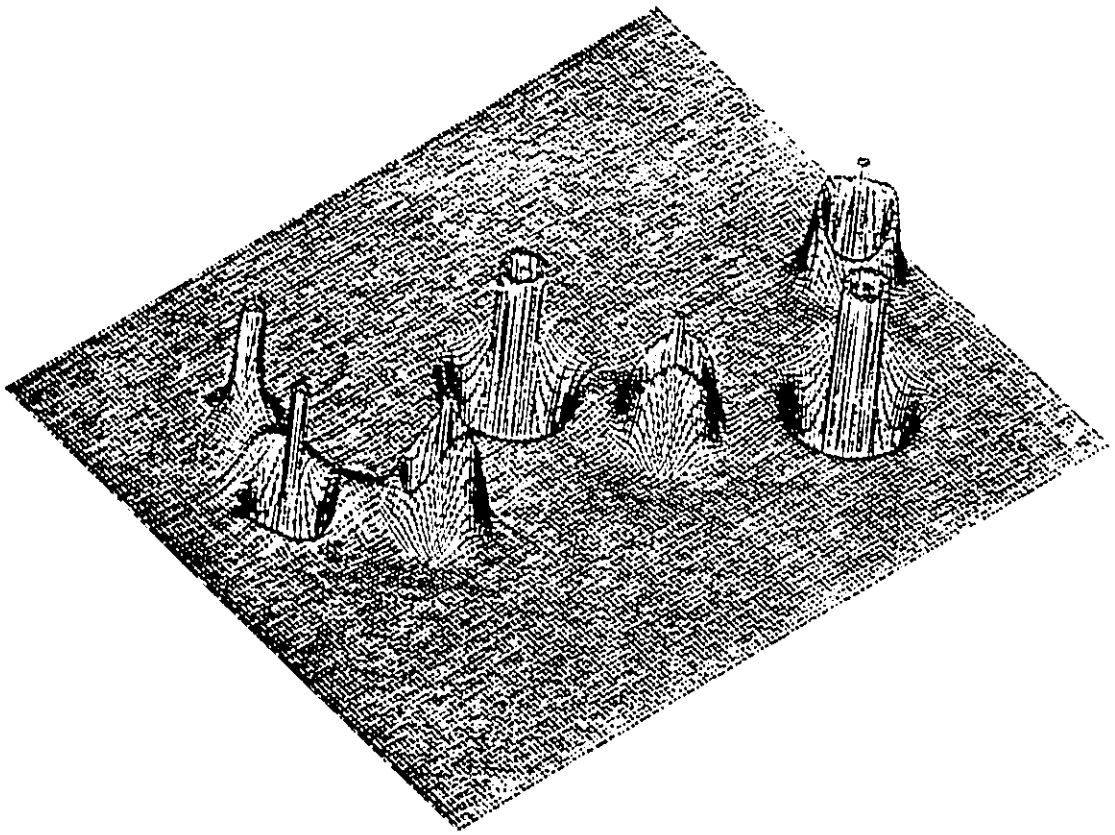

Figure 5.10

A display of the gradient vector field of the charge density (top) and a relief map (bottom) of the Laplacian of the charge density for $P_2O_7Mg^{2-}$ in a plane containing O_2-P-O_1-P-O_2(Mg).

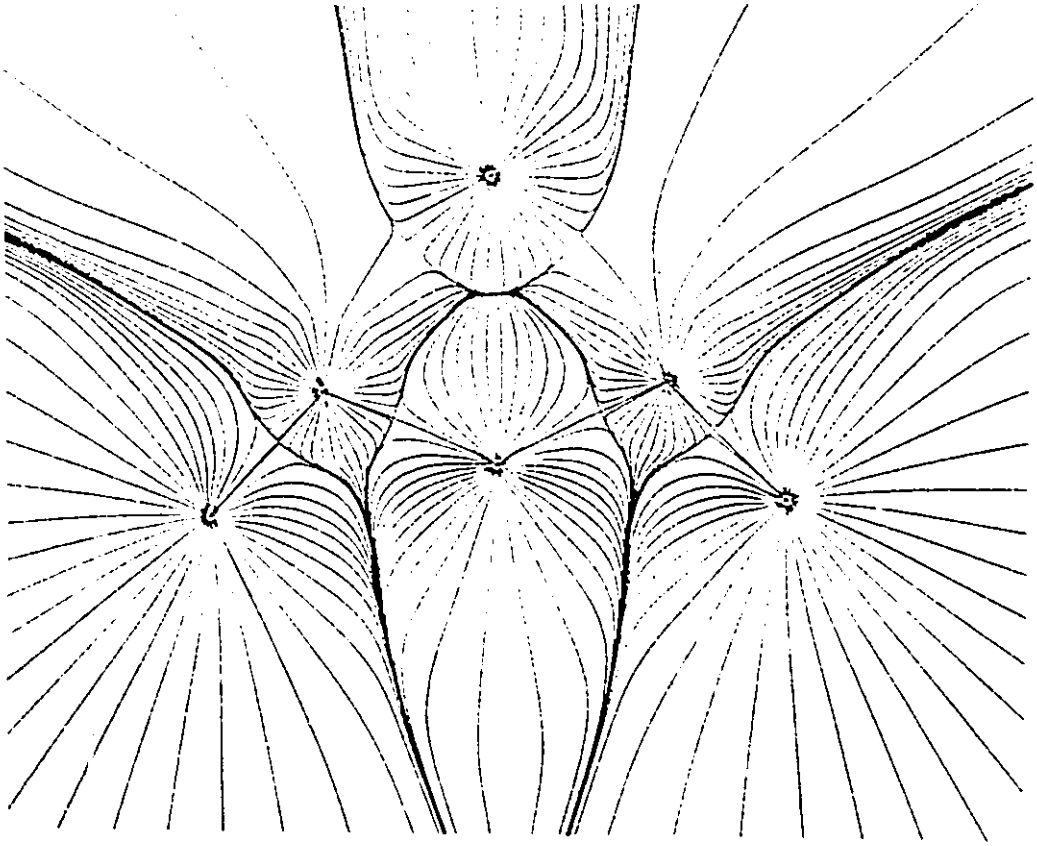

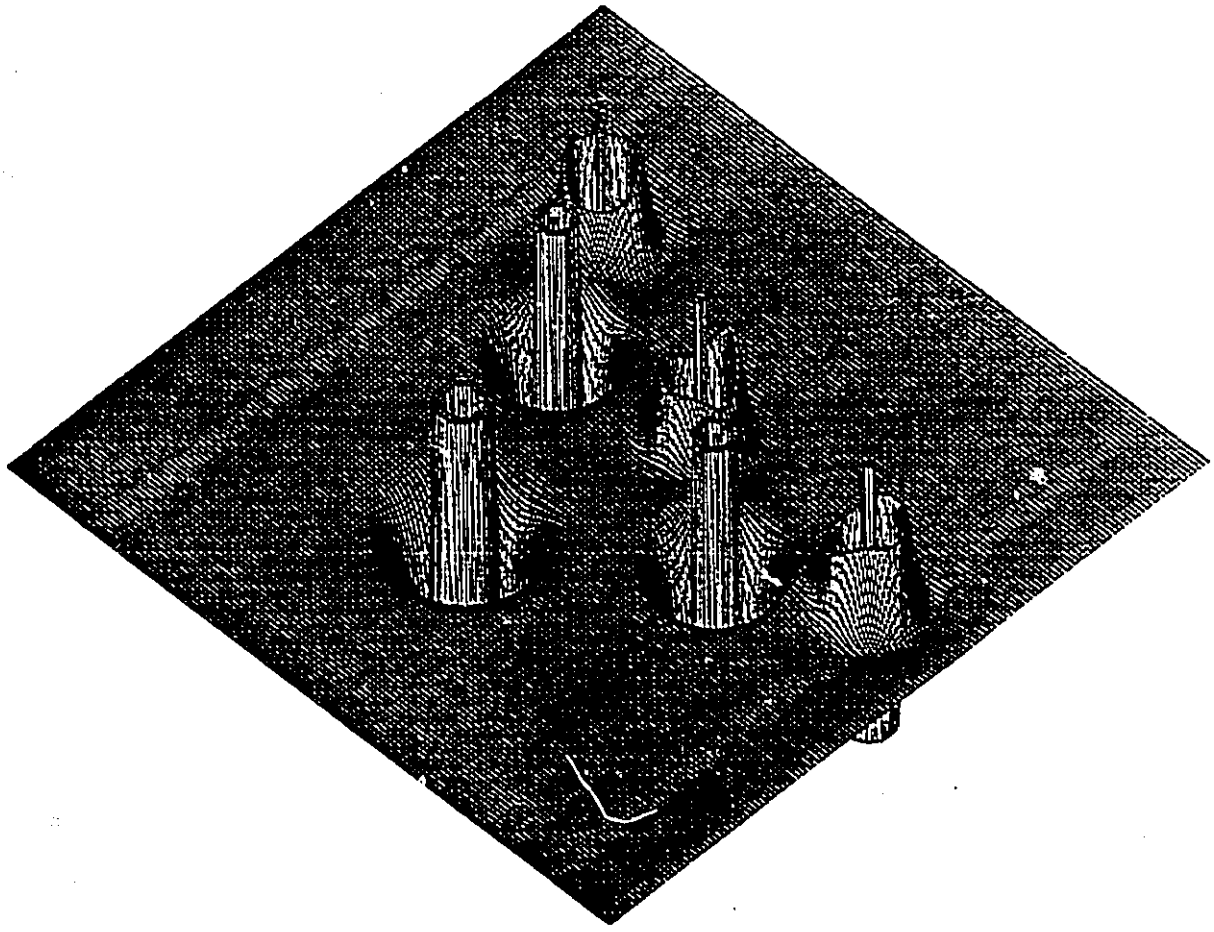

Figure 5.11

The relative positions of the (3,+1) critical points in the VSCC of phosphorus in a) $P_2O_7^{4-}$ and b) $P_2O_7^{2-}$ are indicated by black circles. The value of the Laplacian at the three (equivalent) (3,+1) critical points in $P_2O_7^{4-}$ is 0.0953 au. The value of the Laplacian at the two equivalent critical points closest to O_2 in $P_2O_7Mg^{2-}$ is 0.0912 au. and the value of the Laplacian at the two equivalent critical points in the O_3-P-O_3 angle of $P_2O_7Mg^{2-}$ is 0.1340 au.

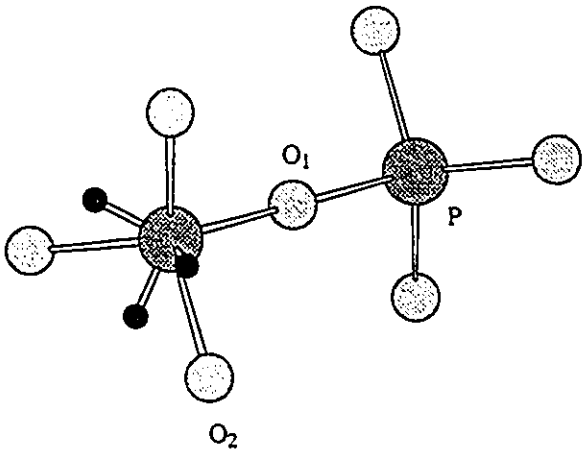

$P_2O_4^{4-}$

a)

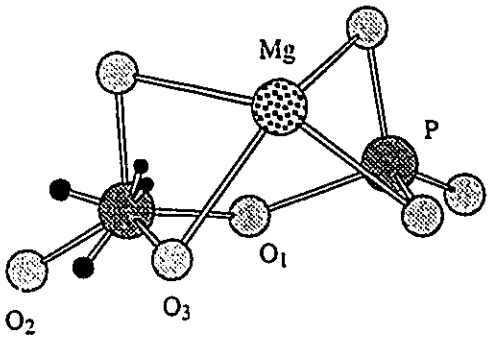

$P_2O_7Mg^{2-}$

b)

REFERENCES

Alcami, M.; Mo, O.; G.de Paz, J. J. and Yanez, M. (1990) *Theor. Chim. Acta* **77**, 1.

Altman, R. S.; Marshall, M. D. and Klemperer, W. (1983) *J. Chem. Phys.* **79**, 57.

Aray, Y. and Murgich, J. (1989) *J. Chem. Phys.* **91**, 293.

Bachrach, S. M. (1989) *J. Comput. Chem.* **10**, 392.

Bader, R. F. W. (1990) "Atoms in Molecules: A Quantum Theory" (Oxford University Press).

Bader, R. F. W. (1991) *Chem. Rev.* **91**, 893.

Bader, R. F. W. and Beddall, P. M. (1973) *J. Amer. Chem. Soc.* **95**, 305.

Bader, R. F. W.; Cade, P. E. and Beddall, P. M. (1971) *J. Amer. Chem. Soc.* **93**, 1831.

Bader, R. F. W.; Carroll, M. T.; Cheeseman, J. R.; Chang, C. (1987) *J. Amer. Chem. Soc.* **109**, 7968.

Bader, R. F. W. and Chang, C. (1989) *J. Phys. Chem.* **93**, 2946.

Bader, R. F. W. and Legare, D. A. (1992) *Can. J. Chem.* **70**, 657.

Bader, R. F. W. and MacDougall, P. J. (1985) *J. Amer. Chem. Soc.* **107**, 6788.

Bader, R. F. W. and Messer, R. R. (1974) *Can. J. Chem.* **52**, 2268.

Bader, R. F. W. and Preston, H. J. T (1970) *Theor. Chim. Acta.* **17**, 384.

Bader, R. F. W.; Tang, T.-H.; Biegler-König, F. W. (1982) *J. Amer. Chem. Soc.* **104**, 946.

Barton, A. E.; Howlett, D. J. B. and Howard, B. J. (1980) *Mol. Phys.* **41**, 619.

Beveridge, D. L.; Schnuelle, G. W. (1975) *J. Phys. Chem.* **79**, 2562.

Biegler-König, F. W.; Bader, R. F. W. and Tang, T.-H. (1982) *J. Comput. Chem.* **13**, 317.

Boyd, R. J. (1987) *Stud. Org. Chem.* **31**, 485.

Boyd, R. J. and Choi, S. C. (1986) *Chem. Phys. Lett.* **129**, 62.

Boyd, R. J. and Edgecombe, K. E. (1987) *J. Comput. Chem.* **8**, 489.

Boyd, R. J.; Knop, O.; Choi, S. C. (1988) *J. Amer. Chem. Soc.* **110**, 7299.

Boyd, D. B. and Lipscomb, W. N. (1969) *J. Theor. Biol.* **25**, 403.

Boys, S. F. and Bernardi, F. (1970) *Mol. Phys.* **19**, 553.

Buxton, L. W.; Campbell, E. J. and Flygare, W. H. (1981) *Chem. Phys.* **56**, 399.

Carroll, M. T. and Bader, R. F. W. (1988) *Mol. Phys.* **65**, 695.

Carroll, M. T.; Chang, C. and Bader, R. F. W. (1988) *Mol. Phys.* **63**, 387.

Carroll, M. T.; Cheeseman, J. R.; Osman, R. and Weinstein, H. (1989) *J. Phys. Chem.* **93**, 5120.

Choi, S. C.; Boyd, R. J. and Knop, O. (1987) *Can. J. Chem.* **65**, 1109.

Cioslowski, J. (1990a) *J. Phys. Chem.* **94**, 5496.

Cioslowski, J. (1990b) *J. Amer. Chem. Soc.* **112**, 6536.

Corbridge, D. E. C (1974) "The Structural Chemistry of Phosphorus" (Amsterdam: Elsevier Publ.).

DeLucia, F. and Gordy, W. (1969) *Phys. Rev.* **187**, 58.

Dykstra, C. E. (1988) *J. Comput. Chem.* **9**, 476.

Ewig, C. S. and Van Wazer, J. R. (1988) *J. Amer. Chem. Soc.* **110**, 79.

Fraser, G. T. and Pine, A. S. (1986) *J. Chem. Phys.* **85**, 2502.

Frenking, G.; Koch, W.; Cremer, D.; Gauss, J. and Leibman, J. F. (1989) *J. Phys. Chem.* **93**, 3397.

Frisch, M. J.; Del Bene, J. E.; Binkley, J. S. and Schaefer III, H. F. (1986) *J. Chem. Phys.* **84**, 2279.

Frisch, M. J.; Head-Gordon, M.; Trucks, G. W.; Foresman, J. B.; Schlegel, H. B.; Raghavachari, K.; Robb, M. A.; Binkly, J. S.; Gonzalez, C.; Defrees, D. J.; Fox, D. J.; Whiteside, R. A.; Seeger, C. F.; Melius, C. F.; Baker, J.; Martin, R. L.; Kahn, L. R.; Stewart, J. J. P.; Topiol, S. and Pople, J. A. (1990) *Gaussian 90* (Gaussian, Inc., Pittsburgh, PA)

Frisch, M. J.; Trucks, G. W.; Head-Gordon, M.; Gill, P. M. W.; Wong, M. W.; Foresman, J. B.; Johnson, B. G.; Schlegel, H. B.; Robb, M. A.; Replogle, E. S.; Gomperts,

R.; Andres, J. L.; Raghavachari, K.; Binkly, J. S.; Gonzalez, C.; Martin, R. L.; Fox, D. J.; Defrees, D. J.; Baker, J.; Stewart, J. J. P. and Pople, J. A. (1992) *Gaussian 92, Rev. A* (Gaussian, Inc., Pittsburgh, PA)

Gatti, C.; Barzaghi, M.; Pitea, D. (1988) *Stud. Phys. Theor. Chem.* **62**, 401.

George, P.; Witonsky, R. J.; Trachtman, M.; Wu, C. Dorwost, W.; Richman, L.; Richman, W.; Shurayh, F. and Lentz, B. (1970) *Biochim. Biophys. Acta* **223**, 1.

Glaser, R. J. (1990) *J. Comput. Chem.* **11**, 663.

Goodwin, E. J. and Legon, A. C. (1985) *J. Chem. Phys.* **82**, 4434.

Gronert, S.; Glaser, R.; Streitwieser, A. (1989) *J. Amer. Chem. Soc.* **111**, 3111.

Harris, S. J.; Novic, S. E. and Klemperer, W. (1974) *J. Chem. Phys.* **60**, 3208.

Hayes, D. M.; Kenyon, G. I. and Kollman, P. A. (1975) *J. Amer. Chem. Soc.* **97**, 4762.

Hayes, D. M.; Kenyon, G. I. and Kollman, P. A. (1978) *J. Amer. Chem. Soc.* **100**, 4331.

Hill, T. L. and Morales, M. F. (1951) *J. Amer. Chem. Soc.* **73**, 1606.

Hobza, P. and Zahradnik (1988) *Chem. Rev.* **88**, 871.

Huber, K. P. and Herzberg, G. (1979) "Molecular Spectra and Molecular Structure IV" (New York: Van Nostrand-Reinhold).

Hutson, J. M. (1992) *J. Chem. Phys.* **96**, 6752.

Hutson, J. M. and Howard, B. J. (1982) *Mol. Phys.* **45**, 769.

Jucks, K. W.; Huang, Z. S. and Miller, R. E. (1987) *J. Chem. Phys.* **86**, 1098.

Kalckar, H. M. (1941) *Chem. Rev.* **28**, 71.

Keith, T. A. (1992) *submitted to J. Comput. Chem.*

Keith, T. A. and Cheeseman, J. R. (1992) *to be submitted to J. Comput. Chem.*

Kennard, O.; Isaacs, N. W.; Motherwell, W. D. S.; Coppola, J. C.; Wampler, D. L. Larson, A. C. and Watson, D. G. (1971) *Proc. R. Soc. Lond. A.* **325**, 401.

Krishnan, R.; Binkley, J. S.; Seeger, R. and Pople, J. A. (1980) *J. Chem. Phys.* **72**, 650.

Lammertsma, K. and Leszczymski, J (1990) *J. Phys. Chem.* **94**, 5543.

Legon, A. C.; Campbell, E. J. and Flygare, W. H. (1982) *J. Chem. Phys.* **76**, 2267.

Legon, A. C.; Millen, D. J. (1986) *Chem. Rev.* **86**, 635.

Legon, A. C.; Millen, D. J. and Rodgers, S. C. (1980) *Proc. R. Soc. London, A* **370**, 213.

Lehninger, A. L. (1970) "Biochemistry" (New York: Worth Publ.).

Liu, S. Y. and Dykstra, C. E. (1987) *Chem. Phys. Lett.* **136**, 22.

Lucken, E. A. C (1969) "Nuclear Quadrupole Coupling Constants" (London: Academic Press).

McLean, A. D. and Chandler, G. S. (1980) *J. Chem. Phys.* **72**, 5639.

Mó, O.; de Paz, J. L. G. and Yanez, M. (1988) *Theor. Chim. Acta.* **73**, 307.

Møller, C. and Plesset, M. S. (1934) *Phys. Rev.* **46**, 618.

Novick, S. E. (1987) *Structure and Dynamics of Weakly Bound Molculear Complexes, NATO ASI Series C: Mathematical and Physical Sciences, Vol. 212* (ed.) Weber, A. (Dordrecht, Holland: Reidel Publ.).

Novick, S. E.; Davies, P.; Harris, S. J. and Klemperer, W. (1973) *J. Chem. Phys.* **59**, 2273.

Onsagar, L. (1936) *J. Amer. Chem. Soc.* **58**, 1486.

Pauling, L. "The Nature of the Chemical Bond" (1969) 3rd. edn. (Ithaca, NewYork: Cornell University Press).

Pullman, A. and Pullman, B. (1963) "Quantum Biology" (New York: Interscience).

Radom, L.; Hehre, W. J. and Pople, J. A. (1971) *J. Amer. Chem. Soc.* **93**, 289.

Rajca, A. and Streitwieser, A. (1988) *Organometallics* **7**, 2215.

Ritchie, J. P. (1986) *J. Comput. Chem.* **7**, 1.

Ritchie, J. P. and Bachrach, S. M. (1987). *J. Amer. Chem. Soc.* **109**, 5909.

Ritchie, J. P.; King, H. F. and Young, W. S. (1986) *J. Chem. Phys.* **85**, 5175.

Rivial, J. L.; Terryn, B. and Ruiz-Lopez, M. F. (1985) *J. Mol. Structure.: Theochem* **120**, 387.

Ruoff, R. S. (1988) Ph.D. Thesis (University of Illinois)

Ruoff, R.S; Emilsson, T.; Chuang, C.; Klots. T. D. and Gutowsky, H. S. (1987) *Chem. Phys. Lett.* **138**, 553.

Schmidt, M. W.; Baldridge, K. K.; Boatz, J. A.; Jensen, J. H.; Koseki, S.; Gordon, M. S.; Nguyen, K. A.; Windus, T. L. and Elbert, S. T. (1990) Program GAMESS *QCPE Bulletin* **10**, 52.

Schwenke, D. W. and Trular, D. G. (1985) *J. Chem. Phys.* **82**, 2418.

Senter, P.; Eckstein, F. and Kagawa, Y. (1983) *Biochemistry* **22**, 5514.

Soper, P. D.; Legon, A. C.; Read, W. G.; Flygare, W. H. (1982) *J. Chem. Phys.* **76**, 292.

Streitwieser, A.; Collins, J. B.; McKelvey, J. M.; Grier, D.; Sender, J. and Toczko, A. G. (1979) *Proc Natl. Acad. Sci. U.S.A.* **76**, 2499.

Szabo, A. and Osdand, N. S. (1989) "Modern Quantum Chemistry" 1st ed., revised (McGraw-Hill Publ.).

Tajima, M. and Honda, M. (1991) *J. Mol. Structure (Theochem)* **228**, 201.

Tapia, O. (1982) "Molecular Interactions" (ed.) Orville-Thomas, W. J. (New York: Wiley).

Terada, H.; Ikuno, M.; Shinohara, Y. and Yoshikawa, K. (1984) *Biochimica et Biophysica. Acta.* **767**, 648.

Thom, R. (1975) *Structural Stability and Morphogenesis*; (eds.) W. A. Benjaman: Reading, MA.

Wiberg, K. B. (1991) *J. Org. Chem.* **56**, 544.

Wiberg, K. B. and Breneman, C. (1990) *J. Amer. Chem. Soc.* **56**, 544.

Wiberg, K. B.; Breneman, C. M. and LaPage, T. J. (1990) *J. Amer. Chem. Soc.* **112**, 61.

Wiberg, K. B. and Laidig, K. E. (1987) *J. Amer. Chem. Soc.* **109**, 5935.

Wiberg, K. B.; Nakaji, D. and Breneman, C. M. (1989) *J. Amer. Chem. Soc.* **111**, 4178.

Wong, M. W.; Wiberg, K. B. and Frisch, M. J. (1991) *J. Chem. Phys.* **95**, 8991.

Wong, M. W.; Wiberg, K. B. and Frisch, M. J. (1992) *J. Amer. Chem. Soc.* **114**, 1645.

Yoshikawa, K.; Shinohara, Y.; Terada, H. and Kato, S. (1987) *Biophys. Chem.* **27**, 251.

Table A.

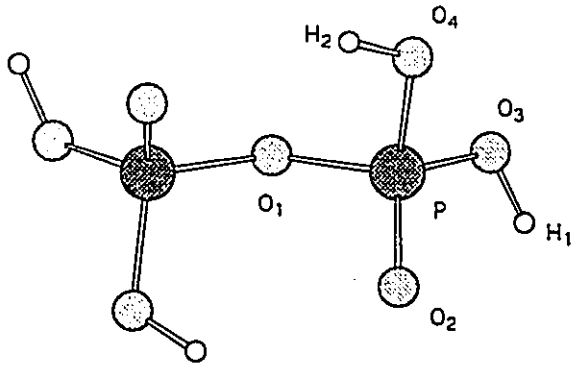

$H_4P_2O_7$

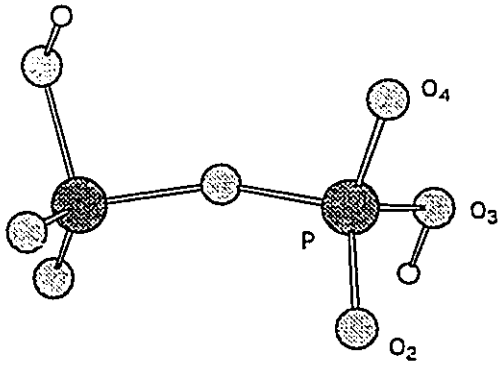

$H_2P_2O_7^{2-}$

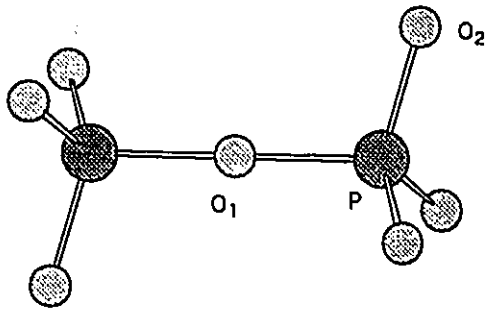

$P_2O_7^{4-}$

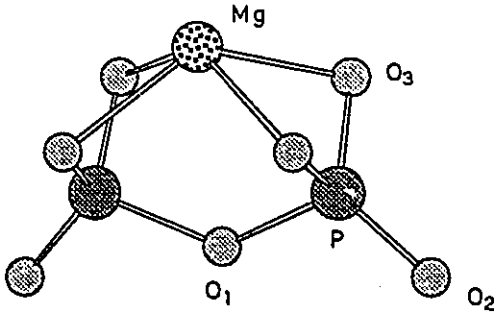

$P_2O_7Mg^{2-}$

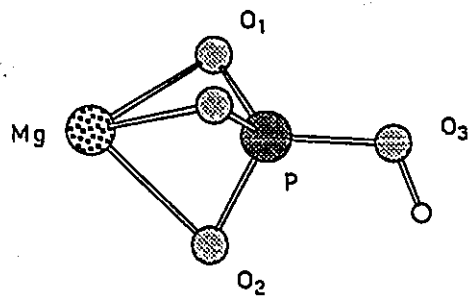

HPO_4Mg

Table A (Cont'd.).

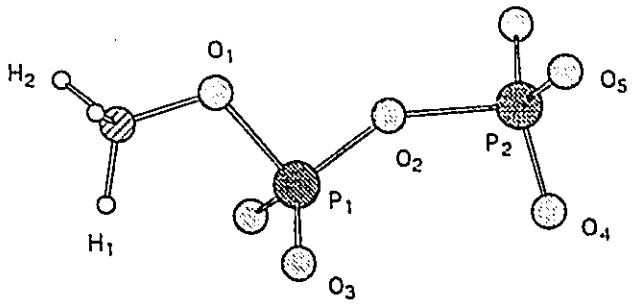

methyldiphosphoric acid (3-)

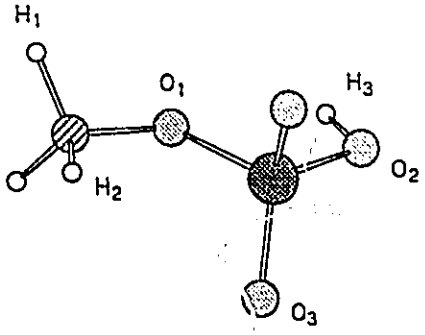

methyphosphate (1-)

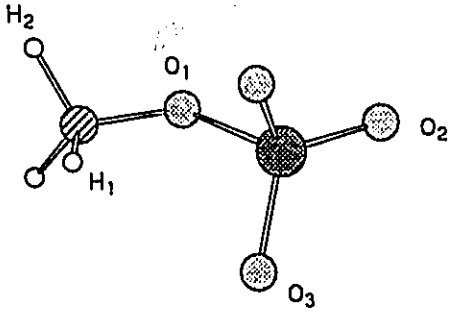

methylphosphate (2-)

Table A (Cont'd.).

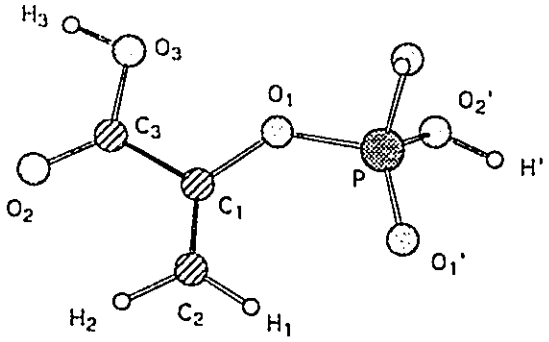

phosphoenolpyruvate (neutral)

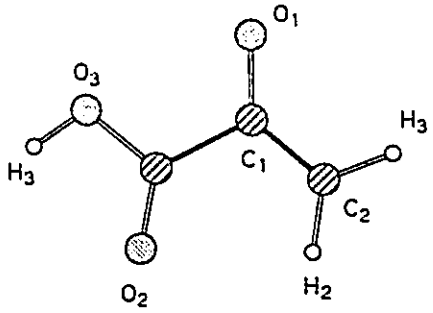

pyruvic acid (1-)

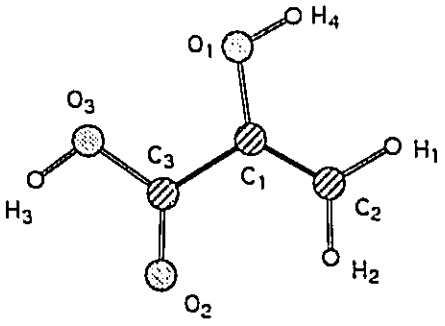

pyruvic acid (enol form)

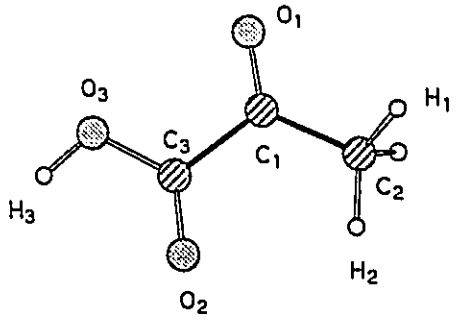

pyruvic acid (keto form)

Table A (Cont'd.).

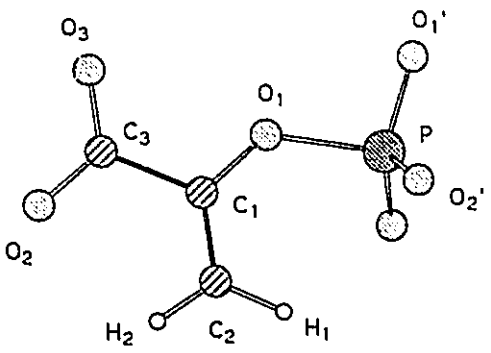

phosphoenolpyruvate (3-)

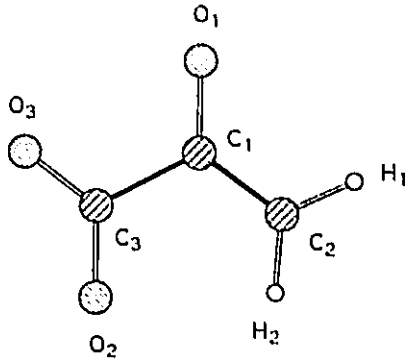

pyruvic acid (2-)

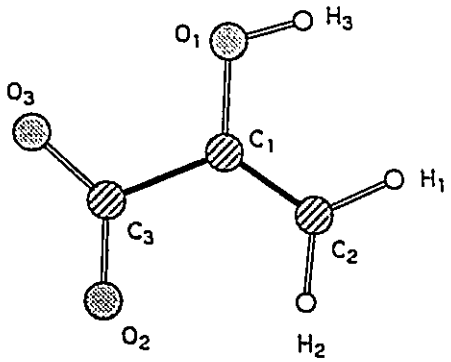

pyruvic acid (1- enol form)

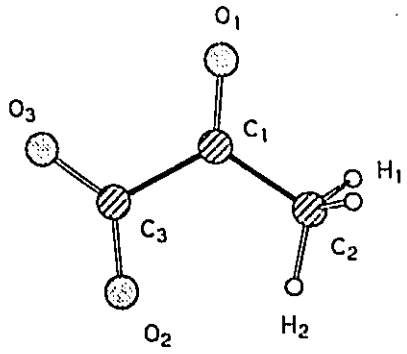

pyruvic acid (1- keto form)

Table A (Cont'd.).

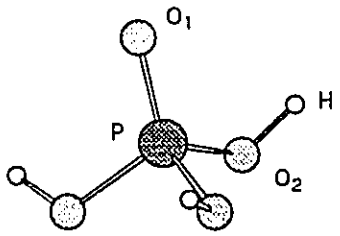

H_3PO_4

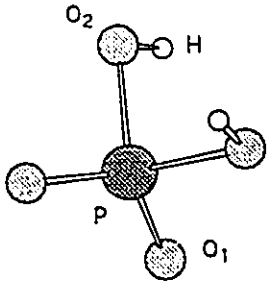

$H_2PO_4^{1-}$

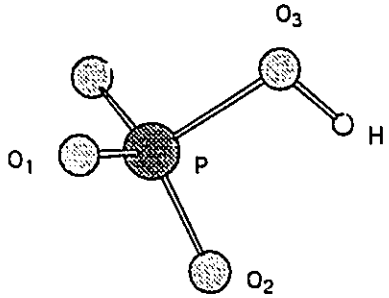

HPO_4^{2-}

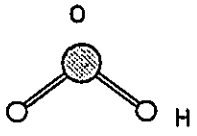

H_2O

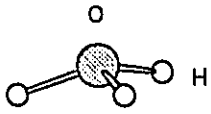

H_3O^+

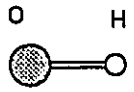

OH^-

Table B1. Diphosphoric Acid Geometric Parameters.[a]

A)

Parameter	$H_4P_2O_7$	$H_2P_2O_7^{2-}$
P-O_1	1.6001	1.6056
P-O_2	1.4494	1.4757
P-O_3	1.5550	1.6426
P-O_4	1.5552	1.4735
O_3-H_1	0.9444	0.9413
O_4-H_2	0.9504	
∠ P-O_1-P	122.46	153.23
∠ O_2-P-O_1	109.34	110.53
∠ O_3-P-O_1	104.34	97.95
∠ O_4-P-O_1	104.74	109.69
∠ O_2-P-O_3	116.84	107.33
∠ O_2-P-O_4	118.28	122.15
∠ O_3-P-O_4	101.80	106.30
∠ H_1-O_3-P	115.09	108.57
∠ H_2-O_4-P	114.87	
tor∠ O_2-P-O_1-P	51.27	29.84
tor∠ O_3-P-O_1-P	176.98	141.76
tor∠ O_4-P-O_1-P	-76.43	-107.69
tor∠ H_1-O_3-P-O_2	18.36	51.14
tor∠ H_2-O_4-P-O_2	-66.05	

B)

Parameter	$P_2O_7^{4-}$
P-O_1	1.6386
P-O_2	1.5335
∠ P-O_1-P	180.00
∠ O_1-P-O_2	107.14
∠ O_2-P-O_2	111.70

[a] Geometric bond lengths are in Angstroms and angles are in degrees.

Table B2. Diphosphoric Acid Geometric Parameters using an Uncontracted Basis on the Bridging Oxygen[a].

A)

Parameter	$P_2O_7^{4-}$	$P_2O_7^{4-}$ uncontracted basis on O_1
P-O_1	1.6612	1.6638
P-O_2	1.5311	1.5291
P-O_3	1.5339	1.5355
P-O_4	1.5326	1.5328
∠ P-O_1-P	171.13	161.42
∠ O_2-P-O_1	107.95	108.77
∠ O_3-P-O_1	105.82	104.87
∠ O_4-P-O_1	106.86	106.86
∠ O_2-P-O_3	111.93	111.98
∠ O_2-P-O_4	112.08	112.37
∠ O_3-P-O_4	111.79	111.54
tor∠ O_2-P-O_1-P	29.05	29.80
tor∠ O_3-P-O_1-P	149.05	149.75
tor∠ O_4-P-O_1-P	-91.68	-91.73

B)

Parameter	$P_2O_7^{4-}$ uncontracted basis on O_1 contrained linear
P-O_1	1.6569
P-O_2	1.5326
∠ P-O_1-P	180.00
∠ O_1-P-O_2	106.89
∠ O_2-P-O_2	111.93

[a] Geometric bond lengths are in Angstroms and angles are in degrees. Data are obtained using the 6-31G** basis set. In the second column of part A, data are obtained using an uncontracted basis on the bridging oxygen. In part B, the same uncontracted basis was used on the bridging oxygen, but the structure was constrained linear. Please refer to the text for explanation. The energy difference between the two structures with the uncontracted bais set on oxygen is only 0.3 kcal/mole.

Table B3. Geometric Parameters[a] for Diphosphoric Acid and Phosphoric Acid Complexed with $Mg^{(+2)}$.

$P_2O_7Mg^{2-}$	
P-O_1	1.6663
P-O_2	1.4700
P-O_3	1.5145
O_3-Mg	2.0582
∠ O_1-P-O_2	109.35
∠ O_1-P-O_3	102.60
∠ O_2-P-O_3	119.93
∠ O_3-P-O_3	99.88
∠ P-O_1-P	131.69
∠ O_3-Mg-O_3 [b]	70.14
∠ O_3-Mg-O_3 [c]	89.19
tor∠ O_3-P-O_1-P	51.65
tor∠ Mg-O_3-P-O_3	42.41
tor∠ Mg-O_3-P-O_2	175.63

HPO_4Mg	
P-O_1	1.5339
P-O_2	1.5384
P-O_3	1.5634
O_3-H	0.9436
O_1-Mg	2.0533
O_2-Mg	2.0743
∠ O_1-P-O_3	116.12
∠ O_2-P-O_3	114.20
∠ O_1-P-O_1	102.62
∠ O_1-P-O_2	102.96
∠ P-O_3-H	114.15
∠ O_1-Mg-O_1	71.34
∠ O_1-Mg-O_2	71.23
tor∠ O_1-P-O_3-O_2	120.00
tor∠ O_2-P-O_3-H	0.00
tor ∠ Mg-O_1-P-O_1	52.98
tor∠ Mg-O_2-P-O_1	53.22

[a] Geometric bond lengths are in Angstroms and angles are in degrees. [b] O_3 is bonded to the same phosphorus atom. [c] O_3 is bonded to two different phosphorus atoms.

Table B4. Methyldiphosphoric Acid and Methylmonophosphoric Acid Geometric Parameters.[a]

Parameter	$CH_3OP(O_2)OPO_3^{3-}$	$CH_3OPO_3^{2-}$	$CH_3OPO_3H^{1-}$
P_2-O_2	1.7931		
P_2-O_4	1.5037		
P_2-O_5	1.5072		
P_1-O_2	1.5430	1.5039	1.6322
P_1-O_3	1.4944	1.5107	1.4733
P_1-O_1	1.7210	1.7499	1.6584
O_2-H_3			0.9423
O_1-C	1.3683	1.3666	1.3934
C-H_1	1.0865	1.0862	1.0839
C-H_2	1.1013	1.1035	1.0880
∠ O_2-P_2-O_4	104.19		
∠ O_2-P_2-O_5	101.95		
∠ O_4-P_2-O_5	115.63		
∠ O_5-P_2-O_5	114.66		
∠ P_2-O_2-P_1	147.31		
∠ O_2-P_1-O_3	116.09	116.34	110.32
∠ O_2-P_1-O_1	96.59	101.00	94.14
∠ O_3-P_1-O_3	116.57	114.43	121.52
∠ O_3-P_1-O_1	103.63	102.71	108.52
∠ P_1-O_2-H_3			108.86
∠ P_1-O_1-C	115.49	116.20	117.56
∠ O_1-C-H_1	113.18	113.18	112.31
∠ O_1-C-H_2	111.38	111.67	109.84
∠ H_1-C-H_2	107.12	107.05	108.13
∠ H_2-C-H_2	106.28	105.78	108.48
tor∠ O_5-P_2-O_2-P_1	120.63		
tor∠ O_3-P_1-O_1-C	61.08	59.52	66.96
tor∠ H_2-C-O_2-H_1	120.77	120.89	120.38

[a] Geometric bond lengths are in Angstroms and angles are in degrees.

Table B5. Phosphoenolpyruvate (neutral) and Pyruvic Acid Geometric Parameters[a].

Parameter	$CH_2=C(O)PO_3H_2)COOH$	$CH_2=C(O)COOH^-$	$CH_2=C(OH)COOH$	$CH_3COCOOH$
P-O_1	1.5692			
P-O_1'	1.4464			
P-O_2'	1.5685			
O_2'-H	0.9439			
O_1-C_1	1.3683	1.2435	1.3447	1.1789
C_1-C_2	1.3153	1.3640	1.3184	1.5084
C_2-H_1	1.0717	1.0767	1.0760	1.0845
C_2-H_2	1.0717	1.0724	1.0710	1.0789
C_1-C_3	1.4980	1.5478	1.5017	1.5446
C_3-O_2	1.1828	1.1951	1.1828	1.1810
C_3-O_3	1.3173	1.3363	1.3182	1.3123
O_3-H_3	0.9462	0.9437	0.9461	0.9466
O_1-H_4			0.9414	
∠ O_1-P-O_1'	116.30			
∠ O_1-P-O_2'	102.42			
∠ O_1'-P-O_2'	115.42			
∠ O_2'-P-O_2'	102.87			
∠ P-O_2'-H	114.85			
∠ P-O_1-C_1	132.51			
∠ O_1-C_1-C_2	126.90	130.47	126.43	123.68
∠ C_1-C_2-H_1	122.36	119.16	121.62	108.28
∠ C_1-C_2-H_2	117.57	121.41	119.69	112.51
∠ O_1-C_1-C_3	112.52	116.20	113.82	119.49
∠ C_2-C_1-C_3	120.58	113.34	119.76	116.83
∠ H_1-C_2-H_2	120.07	119.43	118.68	109.92
∠ H_1-C_2-H_1				107.81
∠ C_1-C_3-O_2	123.07	127.64	123.51	122.72
∠ C_1-C_3-O_3	113.48	113.47	113.16	112.77
∠ O_2-C_3-O_3	123.45	118.89	123.33	124.51
∠ C_3-O_3-H_3	108.28	105.77	108.35	109.06
∠ C_1-O_1-H_4			110.57	
tor∠ O_2'-P-O_1-C_1	126.81			
tor∠ H-O_2'-P-O_1'	31.59			
tor∠ H_1-C_2-C_1-O_1				58.32

[a] Geometric bond lengths are in Angstroms and angles are in degrees.

Table B6. Phosphoenolpyruvate (trianion) and Pyruvic Acid Geometric Parameters.[a]

Parameter	$CH_2=C(OPO_3)COO^{3-}$	$CH_2=C(O)COO^{2-}$	$CH_2=C(OH)COO^{1-}$	CH_3COCOO^{1-}
$P\text{-}O_1$	1.7485			
$P\text{-}O_{1'}$	1.5063			
$P\text{-}O_{2'}$	1.5100			
$O_1\text{-}C_1$	1.3162	1.2505	1.3555	1.1902
$C_1\text{-}C_2$	1.3405	1.3896	1.3271	1.5242
$C_2\text{-}H_1$	1.0739	1.0837	1.0813	1.0873
$C_2\text{-}H_2$	1.0736	1.0733	1.0708	1.0783
$C_1\text{-}C_3$	1.5711	1.5935	1.5585	1.5806
$C_3\text{-}O_2$	1.2486	1.2437	1.2273	1.2305
$C_3\text{-}O_3$	1.2298	1.2349	1.2212	1.2162
$O_1\text{-}H_3$			0.9403	
$\angle O_1\text{-}P\text{-}O_{1'}$	101.08			
$\angle O_1\text{-}P\text{-}O_{2'}$	104.62			
$\angle O_{1'}\text{-}P\text{-}O_{2'}$	114.93			
$\angle O_{2'}\text{-}P\text{-}O_{2'}$	114.43			
$\angle P\text{-}O_1\text{-}C_1$	130.19			
$\angle O_1\text{-}C_1\text{-}C_2$	125.76	124.94	122.05	119.19
$\angle C_1\text{-}C_2\text{-}H_1$	120.44	118.92	121.89	108.26
$\angle C_1\text{-}C_2\text{-}H_2$	118.63	121.36	119.08	112.17
$\angle H_1\text{-}C_2\text{-}H_2$	120.93	119.73	119.03	110.21
$\angle H_1\text{-}C_2\text{-}H_1$				107.60
$\angle O_1\text{-}C_1\text{-}C_3$	115.72	118.26	114.78	122.69
$\angle C_2\text{-}C_1\text{-}C_3$	118.51	116.80	123.17	118.12
$\angle C_1\text{-}C_3\text{-}O_2$	116.25	117.39	114.16	113.39
$\angle C_1\text{-}C_3\text{-}O_3$	118.01	116.77	115.20	115.44
$\angle O_2\text{-}C_3\text{-}O_3$	125.73	125.84	130.63	131.17
$\angle C_1\text{-}O_1\text{-}H_3$			108.70	
$tor\angle O_{2'}\text{-}P\text{-}O_1\text{-}C_1$	60.33			
$tor\angle H_1\text{-}C_2\text{-}C_1\text{-}O_1$				58.18

[a] Geometric bond lengths are in Angstroms and angles are in degrees.

Table B7. Phosphoric Acid Geometric Parameters[a].

H_3PO_4	6-311++G**	6-31G**
P-O_1	1.4461	1.4500
P-O_2	1.5708	1.5765
O-H	0.9438	0.9459
∠ O_1-P-O_2	115.47	115.58
∠ O_2-P-O_2	102.87	102.74
∠ P-O_2-H	115.04	113.78
tor∠ O_1-P-O_2-O_2	120.00	120.00
tor∠ O_1-P-O_2-H	36.54	34.69

$H_2PO_4^{1-}$	6-311++G**	6-31G**
P-O_1	1.4711	1.4746
P-O_2	1.6335	1.6389
O_2-H	0.9406	0.9432
∠ O_1-P-O_2	106.73	106.04
∠ O_1-P-O_1	125.07	124.87
∠ O_2-P-O_2	101.08	100.93
∠ P-O_2-H	109.11	106.65
tor∠ O_1-P-O_2-O_1	126.28	126.66
tor∠ H-O_2-P-O_1	-20.38	-12.55

HPO_4^{2-}	6-311++G**	6-31G**
P-O_1	1.5092	1.5110
P-O_2	1.5203	1.5212
P-O_3	1.7184	1.7271
O_3-H	0.9389	0.9423
∠ O_1-P-O_3	104.47	104.50
∠ O_2-P-O_3	100.25	99.53
∠ O_1-P-O_1	113.97	113.95
∠ O_1-P-O_2	115.59	115.85
∠ P-O_3-H	103.10	99.32
tor∠ O_1-P-O_3-O_2	120.00	120.00
tor∠ O_2-P-O_3-H	0.00	0.00

[a] Geometric bond lengths are in Angstroms and angles are in degrees.

Table B8. Geometric Parameters[a] for H_2O, $H_3O^{(1+)}$ and $OH^{(-1)}$

H_2O	6-311++G**	6-31G**
O-H	0.9412	0.9432
∠ H-O-H	106.25	106.05

H_3O^+	6-311++G**	6-31G**
O-H	0.9605	0.9613
∠ H-O-H	114.25	114.74

OH^-	6-311++G**	6-31G**
O-H	0.9447	0.9582

[a] Geometric bond lengths are in Angstroms and angles are in degrees.

Table C1. Values of ρ and $\nabla^2\rho$ at Bond Critical Points and Bonded Radii of Phosphorus and Oxygen in the P-O-P Linkage in Diphosphoric Acid.

			P-O-P	
	$\rho(r_c)$	$\nabla^2\rho(r_c)$	r_O	r_P
$H_4P_2O_7$				
P-O_1	0.1707	0.9308	0.9744	0.6260
P-O_2	0.2528	1.8736		
P-O_3	0.1958	1.1346		
P-O_4	0.1970	1.1283		
O_3-H_1	0.3729	-2.8259		
O_2-H_2	0.3641	-2.7776		
$H_2P_2O_7^{2-}$				
P-O_1	0.1578	0.9070	0.9738	0.6322
P-O_2	0.2381	1.6446		
P-O_3	0.1585	0.7408		
P-O_4	0.2390	1.6565		
O_3-H	0.3874	-2.8346		
$P_2O_7^{4-}$				
P-O_1	0.1433	0.7575	0.9943	0.6443
P-O_2	0.2097	1.2189		
$P_2O_7Mg^{2-}$				
P-O_1	0.1459	0.6617	1.0192	0.6477
P-O_2	0.2388	1.6919		
P-O_3	0.2046	1.1855		
O_3-Mg	0.0410	0.3004		

ρ and $\nabla^2\rho$ are in au, radii expressed in Å.

Table C2. Critical Point Data for Methyldiphosphoric Acid and Methylphosphoric Acid.

			P-O-P and P-O-C	
	$\rho(r_c)$	$\nabla^2\rho(r_c)$	r_O	r_P
MDP^{3-}				
P_2-O_2	0.0967	0.3527	1.096	0.698
P_2-O_4	0.2178	1.5781		
P_2-O_5	0.2160	1.5534		
P_1-O_2	0.1896	1.2735	0.933	0.610
P_1-O_3	0.2230	1.6473		
P_1-O_1	0.1268	0.5490	1.060	0.662
O_1-C	0.2954	-0.4546	0.923	
C-H_1	0.2963	-1.1455		
C-H_2	0.2788	-1.0029		
MP^{-}				
P-O_1	0.1480	0.7648	1.018	0.641
P-O_2	0.1590	0.8724		
O_2-H_3	0.3870	-2.4190		
P-O_3	0.2338	1.8088		
O_1-C	0.2652	-0.1642	0.948	
C-H_1	0.2985	-1.1653		
C-H_2	0.2923	-1.1098		
MP^{2-}				
P-O_1	0.1170	0.4724	1.078	0.673
P-O_2	0.2172	1.5812		
P-O_3	0.2144	1.5370		
O_1-C	0.2979	-0.4871	0.921	
C-H_1	0.2966	-1.1490		
C-H_2	0.2768	-0.9880		

Table C3. Bond Critical Point Data for Phosphoenolpyruvate and Pyruvic Acid.

			P-O-C	
	$\rho(r_c)$	$\nabla^2\rho(r_c)$	r_O	r_P
PEP				
P-O_1	0.1824	1.0685	0.953	0.617
P-O_1'	0.2538	1.9021		
P-O_2'	0.1906	1.0587		
O_2'-H	0.3740	-2.8200		
O_1-C_1	0.2571	0.2500	0.931	
C_1-C_2	0.3620	-1.2279		
C_2-H_1	0.2970	-1.1322		
C_2-H_2	0.2959	-1.1178		
C_1-C_3	0.2825	-0.8656		
C_3-O_2	0.4449	1.0239		
C_3-O_3	0.3191	-0.1131		
O_3-H_3	0.3820	-2.9070		
PA$^-$				
C_1-C_2	0.3342	-1.0610		
C_2-H_1	0.2804	-0.9961		
C_2-H_2	0.2850	-1.0201		
C_1-O_1	0.3889	-0.2863		
C_1-C_3	0.2527	-0.7422		
C_3-O_2	0.4299	0.0792		
C_3-O_3	0.3011	-0.0413		
O_3-H_3	0.3904	-2.9205		
PA(enol form)				
C_1-C_2	0.3605	-1.2115		
C_2-H_1	0.2883	-1.0621		
C_2-H_2	0.2946	-1.1042		
C_1-O_1	0.2956	-0.0398		
C_1-C_3	0.2812	-0.8657		
C_3-O_2	0.4446	0.1136		
C_3-O_3	0.3182	-0.1056		
O_3-H_3	0.3824	-2.9079		
O_1-H_4	0.3888	-2.9227		
PA(keto form)				
C_1-C_2	0.2679	-0.7749		
C_2-H_2	0.2910	-1.0719		
C_2-H_1	0.2828	-1.0164		
C_1-O_1	0.4388	0.4557		
C_1-C_3	0.2643	-0.7795		
C_3-O_2	0.4439	0.2154		
C_3-O_3	0.3218	-0.0792		
O_3-H_3	0.3813	-2.9005		

Table C3 (Cont'd.).

			P-O-C	
	$\rho(r_c)$	$\nabla^2\rho(r_c)$	r_O	r_P
PEP^{3-}				
$P\text{-}O_1$	0.1176	0.4300	1.073	0.677
$P\text{-}O_1'$	0.2218	1.4099		
$P\text{-}O_2'$	0.2200	1.3849		
$O_1\text{-}C_1$	0.3135	-0.0848	0.887	
$C_1\text{-}C_2$	0.3481	-1.1334		
$C_2\text{-}H_1$	0.2881	-1.0521		
$C_2\text{-}H_2$	0.2853	-1.0300		
$C_1\text{-}C_3$	0.2493	-0.6829		
$C_3\text{-}O_2$	0.3818	-0.2122		
$C_3\text{-}O_3$	0.3974	-0.1069		
PA^{2-}				
$C_1\text{-}C_2$	0.3205	-0.9836		
$C_2\text{-}H_1$	0.2709	-0.9329		
$C_2\text{-}H_2$	0.2822	-0.9991		
$C_1\text{-}O_1$	0.3778	-0.1726		
$C_1\text{-}C_3$	0.2413	-0.6426		
$C_3\text{-}O_2$	0.3849	-0.1586		
$C_3\text{-}O_3$	0.3917	-0.1005		
PA^-(enol form)				
$C_1\text{-}C_2$	0.3560	-1.1759		
$C_2\text{-}H_1$	0.2783	-0.9928		
$C_2\text{-}H_2$	0.2912	-1.0730		
$C_1\text{-}O_1$	0.2820	0.0839		
$C_1\text{-}C_3$	0.2497	-0.7086		
$C_3\text{-}O_2$	0.4025	-0.1741		
$C_3\text{-}O_3$	0.4072	-0.1179		
$O_1\text{-}H_3$	0.3953	-2.9162		
PA^-(keto form)				
$C_1\text{-}C_2$	0.2627	-0.7373		
$C_2\text{-}H_2$	0.2914	-1.0750		
$C_2\text{-}H_1$	0.2783	-0.9872		
$C_1\text{-}O_1$	0.4250	0.4088		
$C_1\text{-}C_3$	0.2451	-0.6728		
$C_3\text{-}O_2$	0.3977	-0.1222		
$C_3\text{-}O_3$	0.4105	-0.0651		

Table C4. Bond Critical Point Data for Phosphoric Acid, H_2O, H_3O^+ and OH^-.

	6-311++G**		6-31G**	
	$\rho(r_c)$	$\nabla^2\rho(r_c)$	$\rho(r_c)$	$\nabla^2\rho(r_c)$
H_3PO_4				
P-O_1	0.2543	1.9017	0.2472	2.0035
P-O_2	0.1887	1.0519	0.1822	1.1323
O_2-H	0.3753	-2.8258	0.3779	-2.4918
$H_2PO_4^-$				
P-O_1	0.2390	1.7211	0.2332	1.8022
P-O_2	0.1612	0.8191	0.1564	0.8543
O_2-H	0.3870	-2.8513	0.3881	-2.4154
HPO_4^{2-}				
P-O_3	0.1320	0.4938	0.1266	0.5450
O_3-H	0.3924	-2.8406	0.3921	-2.3430
P-O_2	0.2152	1.3191	0.2098	1.4673
P-O_1	0.2205	1.3894	0.2142	1.5325
HPO_4Mg				
P-O_3	0.1894	1.0981		
O_3-H	0.3745	-2.8217		
P-O_2	0.2100	1.2312		
P-O_1	0.2123	1.2531		
O_2-Mg	0.0415	0.2973		
O_1-Mg	0.0435	0.3174		
H_2O				
O-H	0.3892	-2.8850	0.3909	-2.4416
H_3O^+				
O-H	0.3495	-2.8315	0.3519	-2.8224
OH^-				
O-H	0.3844	-2.4657	0.3708	-1.8365

Table D1. Molecular and Atomic Properties of Diphosphoric Acid.

	N	E	Volume	V_a	V_r	V_a^*
$H_4P_2O_7$						
O_1	9.634	-75.83323	103.99	-388.7977	237.1277	-187.0951
P	11.041	-338.66935	19.68	-985.5257	308.1839	-784.0638
O_2	9.602	-75.62467	142.06	-353.0985	201.8462	-186.2773
O_3	9.452	-75.64920	124.21	-336.7190	185.4179	-186.1810
H_1	0.318	-0.30747	16.03	-5.5598	4.9448	-0.5813
O_4	9.473	-75.66294	122.84	-346.6056	195.2769	-186.2702
H_2	0.298	-0.29281	14.24	-5.9574	5.3717	-0.5534
$\Sigma A(\Omega)$	90.004	-1208.24609	982.13	-4455.7299	2039.2106	-2874.9492
RHF	90.000	-1208.24640		-4455.4754	2039.0654	
Δ	0.004	0.2 kcal/mol		-0.2546	0.1452	
V/T = -2.0000686						
$H_2P_2O_7^{2-}$						
O_1	9.665	-75.80348	106.43	-384.8411	233.2301	-187.2242
P	11.065	-338.65029	21.66	-973.9230	296.6191	-784.1847
O_2	9.645	-75.54936	153.83	-340.0637	188.9619	-186.2681
O_3	9.431	-75.52597	128.67	-331.3897	180.3348	-185.8197
H	0.394	-0.35653	20.44	-7.1484	6.4352	-0.6789
O_4	9.640	-75.54229	153.05	-337.1149	186.0272	-186.2445
$\Sigma A(\Omega)$	90.014	-1207.05237	1061.73	-4364.1203	1949.9866	-2873.6162
RHF	90.000	-1207.05345		-4363.6708	1949.6595	
Δ	0.014	0.7 kcal/mol		-0.4495	0.3271	
V/T = -2.0000792						
$P_2O_7^{4-}$						
O_1	9.660	-75.65435	113.08	-376.3723	225.0605	-186.9052
P	11.076	-338.57038	21.15	-966.1115	288.9682	-784.1651
O_2	9.699	-75.40285	166.76	-331.0969	180.2887	-186.0995
$\Sigma A(\Omega)$	90.006	-1205.21218	1155.92	-4295.1765	1884.7294	-2871.8326
RHF	90.000	-1205.21248		-4294.9264	1884.5815	
Δ	0.006	0.2 kcal/mol		-0.2501	0.1479	
V/T = -2.0000665						

$\Sigma A(\Omega)$ is the sum of atomic contributions, RHF is the molecular value, and V/T is the virial ratio.

Table D2. Molecular and Atomic Properties of Diphosphoric Acid and Phosphoric Acid Complexed with Magnesium.

	N	E	Volume	V_a	V_r	V_a^*
$P_2O_7Mg^{2-}$						
O_1	9.634	-75.65158	109.42	-400.1101	248.7979	-186.6870
P	11.089	-338.73035	20.70	-1002.2632	325.1630	-784.5236
O_2	9.635	-75.53767	154.16	-346.5654	195.4833	-186.2031
O_3	9.676	-75.53786	141.44	-373.2287	222.1451	-186.4047
Mg	10.212	-199.21985	40.54	-662.8369	264.3896	-471.9354
$\sum A(\Omega)$	99.997	-1405.55890	1065.44	-5253.5191	2443.0604	-3345.6948
RHF	100.000	-1405.55724		-5253.8872	2443.0068	
Δ	-0.003	-1.0 kcal/mol		0.3681	0.0536	
V/T = -2.0001666						
HPO_4Mg						
P	11.074	-338.81911	20.22	-940.7827	263.1369	-784.5788
O_1	9.648	-75.55711	143.52	-318.3656	167.2436	-186.3106
O_2	9.657	-75.55036	144.56	-318.4630	167.3545	-186.3260
O_3	9.454	-75.62713	127.10	-302.0229	150.7617	-186.1185
H	0.326	-0.31329	16.56	-4.7018	4.0749	-0.5922
Mg	10.189	-199.15714	46.17	-584.2695	185.9491	-471.6521
$\sum A(\Omega)$	59.996	-840.58126	641.65	-2786.9711	1105.7643	
RHF	60.000	-840.58064		-2786.7272	1105.7565	
Δ	-0.004	-0.4 kcal/mol		-0.2439	0.0078	
V/T = -2.0002267						
Mg^{2+}						
Mg	10.000	-198.82334	47.62	-469.9365	72.2898	-469.9365
RHF	10.000	-198.82333		-469.7942	72.2691	
Δ	0.000	0.0 kcal/mol		-0.1423	0.0208	
V/T = -2.0006060						

Table D3. Molecular and Atomic Properties for Methyldiphosphoric and Methylphosphoric Acid.

	N	E	Volume	V_a	V_r	V_a^*
MDP^{3-}						
O_1	9.448	-75.51709	103.67	-350.3343	199.2368	-185.8851
P_1	10.975	-338.65317	20.24	-985.3431	307.9710	-783.3526
O_3	9.698	-75.47612	143.00	-350.3206	199.3054	-186.4071
O_2	9.649	-75.56815	110.79	-387.1094	235.8960	-186.6598
P_2	10.974	-338.65471	18.94	-972.6670	295.2969	-783.3642
O_4	9.713	-75.45702	145.38	-345.6587	194.6836	-186.4185
O_5	9.715	-75.45134	144.63	-340.9450	189.9830	-186.4225
C	5.018	-37.19345	48.47	-159.7646	85.3507	-85.8908
H_1	1.061	-0.66715	47.39	-18.2068	16.8662	-1.3546
H_2	1.171	-0.70342	58.05	-17.8207	16.4077	-1.4345
$\Sigma A(\Omega)$	98.006	-1244.97249	1186.26	-4637.2562	2146.6935	
RHF	98.000	-1244.97416		-4633.5976	2145.5418	
Δ	0.006	1.0 kcal/mol		-3.6586	1.1517	
V/T = -2.0015224						
MP^-						
O_1	9.490	-75.57585	102.73	-311.8458	160.6408	-186.1546
P	10.969	-338.77283	18.25	-924.6018	247.0093	-783.5220
O_3	9.674	-75.51516	142.52	-304.3088	153.2287	-186.3566
O_2	9.467	-75.49426	124.12	-297.8213	146.7851	-185.9327
H_3	0.365	-0.33660	17.16	-5.3551	4.6801	-0.6468
C_1	5.124	-37.27194	52.57	-143.6623	69.0956	-86.3359
H_1	1.042	-0.65948	48.09	-14.2728	12.9486	-1.3405
H_2	1.096	-0.67962	52.58	-13.3742	12.0101	-1.3823
$\Sigma A(\Omega)$	57.999	-680.50051	753.11	-2332.9251	971.6371	-1619.4102
RHF	58.000	-680.50090		-2331.0553	971.1641	
Δ	-0.001	0.2 kcal/mol		-1.8699	0.4729	
V/T = -2.0016348						
MP^{2-}						
O_1	9.450	-75.48334	105.21	-305.7565	154.7461	-185.8342
P	10.971	-338.66077	18.48	-920.8507	243.4904	-783.3782
O_2	9.713	-75.44345	145.05	-299.3801	148.4521	-186.4034
O_3	9.718	-75.44449	143.42	-302.3013	151.3702	-186.4294
C_1	5.010	-37.18317	48.27	-141.7116	67.3263	-85.8506
H_1	1.058	-0.66571	47.27	-14.5199	13.1838	-1.3519
H_2	1.180	-0.70578	59.26	-14.0998	12.6838	-1.4400
$\Sigma A(\Omega)$	57.998	-679.73697	769.63	-2315.0211	955.3067	
RHF	58.000	-679.73735		-2313.4080	954.9036	
Δ	-0.002	0.2kcal/mol		-1.6131	0.4030	
V/T = -2.0014296						

Table D4. Molecular and Atomic Properties of Phosphoenolpyruvate (neutral) and Pyruvic Acid.

	N	E	Volume	V_a	V_r	V_a^*
PEP						
P	11.038	-338.68023	19.86	-968.9818	291.6163	-784.0425
O_1'	9.602	-75.63465	142.37	-338.0742	186.8000	-186.2856
O_2'	9.451	-75.63750	124.42	-330.5321	179.2524	-186.1486
H'	0.325	-0.31231	16.67	-5.4320	4.8073	-0.5911
O_1	9.488	-75.77918	98.21	-365.8923	214.3282	-186.5836
C_1	5.617	-37.56507	69.39	-191.0243	115.8909	-88.0201
C_2	5.803	-37.70318	89.40	-176.0996	100.6905	-88.9623
H_1	0.896	-0.58116	39.62	-15.2820	14.1192	-1.1986
H_2	0.924	-0.59154	42.77	-14.5267	13.3432	-1.2224
C_3	4.105	-36.61461	31.12	-154.0213	80.9449	-81.8614
O_2	9.342	-75.68948	133.10	-306.9938	155.6109	-185.6084
O_3	9.289	-75.63666	117.08	-314.9494	163.6718	-185.6044
H_3	0.344	-0.32492	17.98	-5.4012	4.7512	-0.6160
$\sum A(\Omega)$	86.000	-906.70031	1083.07	-3523.1748	1709.8864	-2163.4849
RHF	86.000	-906.70031		-3523.1748	1709.8864	
V/T = -2.0001239						
PA^-						
O_1	9.413	-75.51023	146.87	-266.3479	115.3234	-185.5185
C_1	4.966	-37.16527	52.26	-143.3518	69.0186	-85.4935
C_2	6.110	-37.72811	115.96	-144.3044	68.8455	-89.6878
H_1	1.078	-0.64098	55.25	-10.9239	9.6414	-1.3360
H_2	1.050	-0.63756	50.50	-11.5318	10.2562	-1.3207
C_3	4.317	-36.72654	37.16	-135.8801	62.4246	-82.6047
O_2	9.395	-75.67593	138.00	-269.2111	117.8550	-185.7459
O_3	9.280	-75.60337	119.35	-268.5032	117.2922	-185.4718
H_3	0.386	-0.35162	20.31	-4.5575	3.8541	-0.6687
$\sum A(\Omega)$	45.996	-340.03960	735.67	-1254.6116	574.5112	-817.8475
RHF	46.000	-340.03873		-1254.5555	574.5431	
Δ	-0.004	-0.5 kcal/mol		-0.0561	-0.0320	
V/T = -2.0001915						

Table D4 (Cont'd).

	N	E	Volume	V_a	V_r	V_a^*
PA(enol form)						
O_1	9.267	-75.55685	117.07	-268.4090	117.2904	-185.3832
H_4	0.367	-0.34184	19.32	-4.2979	3.6140	-0.6473
C_1	5.502	-37.52532	65.48	-153.3589	78.3046	-87.6500
C_2	5.844	-37.70352	92.88	-143.1157	67.7056	-89.0644
H_1	1.002	-0.61864	49.80	-10.5170	9.2792	-1.2844
H_2	0.931	-0.59322	43.31	-10.4494	9.2625	-1.2271
C_3	4.114	-36.61078	31.76	-133.8645	60.6403	-81.9290
O_2	9.342	-75.69579	133.37	-270.5058	119.1093	-185.6124
O_3	9.289	-75.64083	117.50	-271.0880	119.8013	-185.6048
H_3	0.346	-0.32619	18.24	-4.1251	3.4726	-0.6185
$\Sigma A(\Omega)$	46.004	-340.61297	688.72	-1269.7312	588.4798	-819.0212
RHF	46.000	-340.61339		-1269.5408	588.3885	
Δ	0.004	0.3 kcal/mol		-0.1904	0.0912	
V/T = -2.0002188						
PA(keto form)						
O_1	9.245	-75.65597	131.57	-268.5102	117.1935	-185.1159
C_1	4.804	-37.08052	44.92	-142.4492	68.2852	-84.8363
C_2	5.890	-37.74926	68.72	-143.4699	67.9684	-89.4849
H_1	0.985	-0.61176	48.18	-10.5325	9.3085	-1.2683
H_2	0.972	-0.61423	44.57	-11.0474	9.8184	-1.2670
C_3	4.160	-36.64747	33.53	-134.1640	60.8664	-82.0828
O_2	9.326	-75.69335	133.01	-270.4033	119.0118	-185.5276
O_3	9.288	-75.64171	118.35	-269.9211	118.6329	-185.6020
H_3	0.343	-0.32434	18.24	-4.0659	3.4170	-0.6151
$\Sigma A(\Omega)$	45.999	-340.63037	689.26	-1265.0959	583.8106	-817.0680
RHF	46.000	-340.62956		-1264.9795	583.7929	
Δ	-0.001	-0.5 kcal/mol		-0.1164	0.0176	
V/T = -2.0002130						

Table D5. Molecular and Atomic Properties of Phosphoenolpyruvate (trianion) and Pyruvic Acid.

	N	E	Volume	V_a	V_r	V_a°
PEP^{3-}						
P	11.099	-338.69444	21.26	-959.5661	282.1733	-784.5375
O_1'	9.675	-75.46615	159.87	-324.9693	174.0332	-186.1787
O_2'	9.679	-75.46794	160.06	-329.6303	178.6905	-186.1958
O_1	9.450	-75.61855	105.39	-353.0685	201.8269	-186.0669
C_1	5.356	-37.36570	61.63	-182.3687	107.6348	-86.9368
C_1	6.043	-37.73750	107.84	-178.7074	103.2300	-89.5849
H_1	1.005	-0.61922	47.62	-16.9356	15.6967	-1.2844
H_2	1.062	-0.64328	50.51	-16.3416	15.0547	-1.3313
C_3	4.031	-36.50168	31.91	-148.8047	75.7996	-81.4826
O_2	9.480	-75.52654	151.34	-302.2017	151.1454	-185.7464
O_3	9.445	-75.55662	118.98	-307.3095	156.1929	-185.6760
$\Sigma A(\Omega)$	86.002	-904.66555	1176.45	-3449.5336	1640.1684	-2161.2172
RHF	86.000	-904.66597		-3449.3424	1640.1085	
Δ	0.002	0.3 kcal/mol		-0.1912	0.0599	
V/T = -2.0001083						
PA^{2-}						
O_1	9.446	-75.48459	151.78	-264.1224	113.1493	-185.5372
C_1	5.059	-37.17581	54.15	-143.6522	69.2978	-85.7509
C_2	6.262	-37.72821	133.38	-144.7080	69.2490	-89.9686
H_1	1.158	-0.66161	62.43	-11.4994	10.1757	-1.3859
H_2	1.075	-0.64065	53.44	-11.5325	10.2507	-1.3319
C_3	4.079	-36.53435	32.97	-130.6246	57.5514	-81.6802
O_2	9.477	-75.54212	150.64	-266.2241	115.1358	-185.7504
O_3	9.457	-75.54827	151.31	-266.1374	115.0368	-185.6889
$\Sigma A(\Omega)$	46.014	-339.31563	790.10	-1238.5006	559.8465	-817.0940
RHF	46.000	-339.31711		-1238.0677	559.4999	
Δ	0.014	0.9 kcal/mol		-0.4329	0.3466	
V/T = -2.0001958						

Table D5 (Cont'd).

	N	E	Volume	V_a	V_r	V_a^*
PA^-(cnol form)						
O_1	9.260	-75.52788	118.89	-265.9045	114.8445	-185.2723
H_3	0.410	-0.36879	20.98	-4.7444	4.0066	-0.7005
C_1	5.580	-37.55270	66.26	-153.3889	78.2803	-87.8409
C_2	5.969	-37.72956	101.41	-143.7769	68.3151	-89.4059
H_1	1.099	-0.65312	55.19	-11.3627	10.0559	-1.3577
H_2	0.968	-0.60579	45.99	-10.6810	9.4689	-1.2549
C_3	3.863	-36.43007	27.89	-128.2149	55.3526	-80.8820
O_2	9.438	-75.58702	143.79	-267.9114	116.7331	-185.7464
O_3	9.419	-75.59323	143.55	-268.4820	117.2912	-185.6817
$\Sigma A(\Omega)$	46.004	-340.04815	723.95	-1254.4667	574 3483	-818.1423
RHF	46.000	-340.04871		-1254.2825	574.2531	
Δ	0.004	0.4 kcal/mol		-0.1841	0.0952	
V/T = -2.0002000						
PA^-(keto form)						
O_1	9.319	-75.63643	138.04	-266.7406	115.4637	-185.3425
C_1	4.921	-37.13675	48.19	-143.3297	69.0535	-85.1978
C_2	5.915	-37.75836	68.23	-143.4149	67.8956	-89.5481
H_1	1.051	-0.63728	51.81	-11.1055	9.8304	-1.3218
H_2	0.975	-0.61528	44.47	-10.9796	9.7486	-1.2681
C_3	3.913	-36.47676	29.30	-128.7908	55.8352	-81.0908
O_2	9.431	-75.58210	142.83	-268.3151	117.1468	-185.7022
O_3	9.413	-75.59539	145.69	-267.3083	116.1135	-185.6617
$\Sigma A(\Omega)$	45.989	-340.07564	720.37	-1251.0900	570.9177	
RHF	46.000	-340.07656		-1251.1081	571.0202	
Δ	-0.011	0.6 kcal/mol		0.0181	-0.1025	
V/T = -2.0001919						

Table D6. Molecular and Atomic Properties of Phosphoric Acid, H_2O, H_3O^+ and OH^-.

	N	E	Volume	V_a	V_r	V_a°
H_3PO_4						
P	11.049	-338.68922	20.71	-913.6415	236.2616	-784.1471
O_1	9.603	-75.61611	147.10	-293.8505	142.6166	-186.2381
O_2	9.453	-75.63245	124.71	-291.3560	140.0895	-186.1464
H	0.330	-0.31545	16.87	-4.3809	3.7500	-0.5973
$\Sigma A(\Omega)$	50.001	-642.14901	592.57	-2094.7029	810.3967	-1530.6163
RHF	50.000	-642.14923		-2094.6341	810.3728	
Δ	0.001	0.1 kcal/mol		-0.0689	0.0239	
V/T = -2.0000579						
$H_2PO_4^-$						
P	11.066	-338.68916	21.00	-910.4669	233.0863	-784.2832
O_1	9.640	-75.56138	153.11	-291.3747	140.2496	-186.2750
O_2	9.445	-75.54856	129.41	-287.1482	136.0487	-185.9082
H	0.381	-0.35004	19.58	-5.0707	4.3705	-0.6648
$\Sigma A(\Omega)$	50.000	-641.60912	625.21	-2077.6541	794.4239	-1529.9792
RHF	50.000	-641.60938		-2077.5676	794.4055	
Δ	0.000	0.2 kcal/mol		-0.0864	0.0184	
V/T = -2.0000883						
HPO_4^{2-}						
P	11.106	-338.6914	22.06	-907.5731	230.1894	-784.5933
O_1	9.679	-75.4579	161.54	-287.6386	136.7217	-186.1737
O_2	9.686	-75.4500	160.99	-288.1239	137.2229	-186.1871
O_3	9.431	-75.4269	137.10	-281.8791	131.0244	-185.5789
H	0.418	-0.3725	21.17	-5.5288	4.7839	-0.7085
$\Sigma A(\Omega)$	49.999	-640.8565	664.39	-2058.3822	776.6639	
RHF	50.000	-640.8564		-2058.3542	776.6675	
Δ	-0.001	0.0 kcal/mol		-0.0280	-0.0036	
V/T = -2.0000124						
H_2O						
O	9.226	-75.34762	144.78	-194.9516	44.2557	-184.8386
H	0.387	-0.35291	19.91	-2.1994	1.4936	-0.6713
$\Sigma A(\Omega)$	10.000	-76.05343	184.60	-199.3504	47.2428	
RHF	10.000	-76.05345		-199.3345	47.2398	
Δ	0.000	0.0 kcal/mol		-0.0160	0.0030	
V/T = -2.0001613						

Table D6 (Cont'd).

	N	E	Volume	V_a	V_r	V_a^*
H_3O^+						
O	9.276	-75.57887	125.63	-200.8022	49.6422	-185.6931
H	0.241	-0.25126	12.47	-1.4922	0.9896	-0.4732
$\Sigma A(\Omega)$	10.000	-76.33264	163.03	-205.2788	52.6110	-187.1128
RHF	10.000	-76.33266		-205.2405	52.6033	
Δ	0.000	0.0 kcal/mol		-0.0383	0.0077	
V/T = -2.0003675						
OH^-						
O	9.435	-74.96422	210.35	-189.2378	39.3094	-184.2351
H	0.565	-0.44171	31.31	-2.8574	1.9739	-0.8569
$\Sigma A(\Omega)$	10.000	-75.40593	241.66	-192.0952	41.2833	-185.0921
RHF	10.000	-75.40578		-192.0967	41.2844	
Δ	0.000	-0.1 kcal/mol		0.0015	-0.0010	
V/T = -1.9999894						

Table D7. Molecular and Atomic Properties of Phosphoric Acid, H_2O, H_3O^+ and OH^- (6-31G** Basis).

	N	E	Volume	V_a	V_r	V_a°
H_3PO_4						
P	10.946	-338.82566	18.02	-911.4939	233.7951	-783.3983
O_1	9.641	-75.56756	141.81	-294.5223	143.3350	-186.2910
O_2	9.480	75.57466	122.06	-291.6144	140.4139	-186.1202
H	0.323	-0.30767	15.60	-4.3122	3.6951	-0.5916
$\sum A(\Omega)$	49.996	-642.04021	572.80	-2093.7959	809.4572	-1529.8247
RHF	50.000	-642.04057		-2091.9490	809.0372	
Δ	-0.004	0.2 kcal/mol		-1.8469	0.4199	
V/T = -2.0018247						
$H_2PO_4^-$						
P	10.961	-338.78165	18.21	-908.3374	230.7328	-783.4627
O_1	9.679	-75.52243	142.23	-292.2820	141.1909	-186.4046
O_2	9.466	-75.49015	122.15	-287.3838	136.3589	-185.9086
H	0.372	-0.34052	18.12	-4.9832	4.3004	-0.6555
$\sum A(\Omega)$	49.997	-641.48786	583.21	-2077.6354	794.4332	-1529.4001
RHF	50.000	-641.48730		-2075.9384	794.0406	
Δ	-0.003	-0.3 kcal/mol		-1.6970	0.3926	
V/T = -2.0016814						
HPO_4^{2-}						
P	10.964	-338.65234	18.40	-904.7166	227.3784	-783.8178
O_1	9.720	-75.43900	144.79	-288.8449	137.9290	-186.4182
O_2	9.726	-75.43641	143.50	-289.5013	138.5903	-186.4481
O_3	9.455	-75.37973	123.97	-282.3203	131.5249	-185.6531
H	0.412	-0.36374	19.46	-5.5131	4.7839	-0.7019
$\sum A(\Omega)$	49.995	-640.71022	594.91	-2059.7410	778.1354	-1529.4573
RHF	50.000	-640.71048		-2058.3281	777.8361	
Δ	-0.005	0.2 kcal/mol		-1.4130	0.2993	
V/T = -2.0014520						
H_2O						
O	9.239	-75.33476	137.51	-195.0710	44.3931	-184.9241
H	0.380	-0.34442	18.65	-2.1695	1.4799	-0.6656
$\sum A(\Omega)$	10.000	-76.02361	174.81	-199.4100	47.3529	-186.2553
RHF	10.000	-76.02361		-199.2006	47.3131	
Δ	0.000	0.0 kcal/mol		-0.2094	0.0399	
V/T = -2.0021055						

Table D7 (Cont'd).

	N	E	Volume	V_a	V_r	V_a^*
H_3O^+						
O	9.300	-75.58883	125.64	-200.9103	49.7137	-185.7502
H	0.233	-0.24048	11.79	-1.4484	0.9667	-0.4623
$\Sigma A(\Omega)$	10.000	-76.31028	161.03	-205.2556	52.6138	-187.1370
RHF	10.000	-76.31032		-204.9484	52.5562	
Δ	0.000	0.0 kcal/mol		-0.3072	0.0575	
V/T = -2.0030030						
OH^-						
O	9.383	-74.87221	152.90	-189.4215	39.6787	-184.4669
H	0.617	-0.46043	32.23	-3.0790	2.1586	-0.9113
$\Sigma A(\Omega)$	10.000	-75.33264	185.14	-192.5005	41.8373	-185.3782
RHF	10.000	-75.33266		-192.5920	41.8550	
Δ	0.000	0.0 kcal/mol		0.0915	-0.0178	
V/T = -1.9990501						

Table E1. Reaction 1: $H_4P_2O_7 + H_2O \rightarrow 2H_3PO_4$

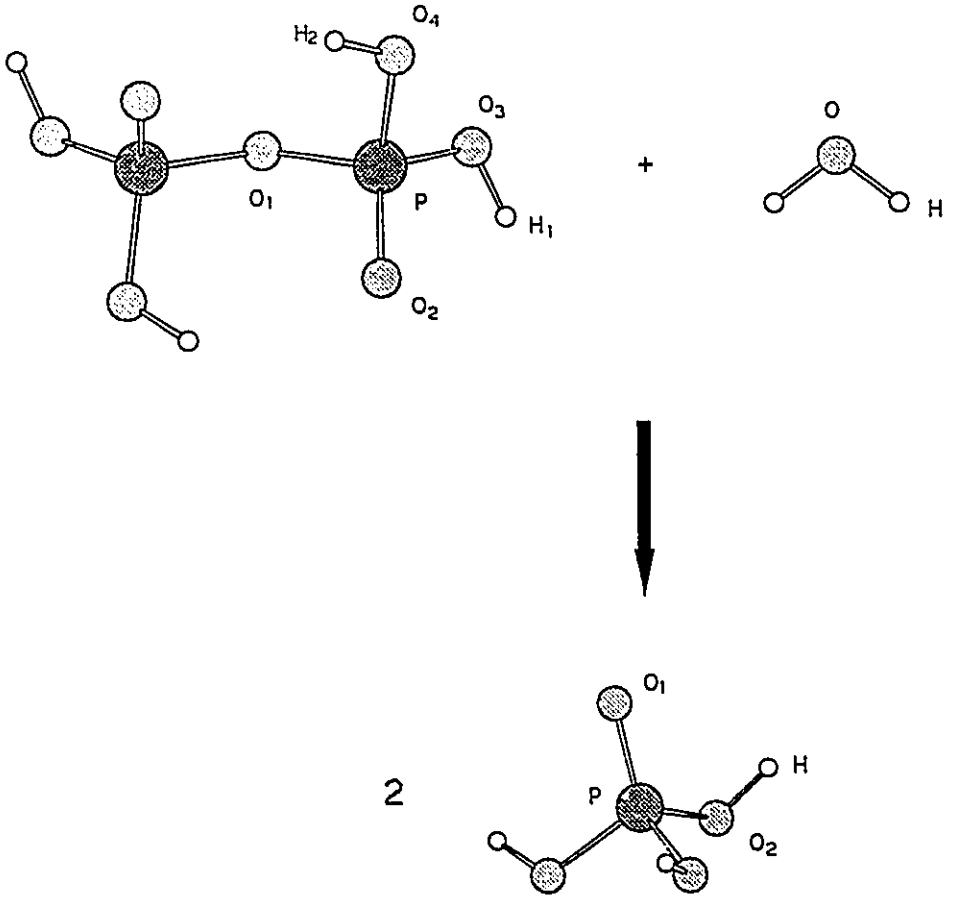

	ΔN	ΔE	ΔVol	ΔV_a	ΔV_r	ΔV_a^*
		kcal/mol				
$O_1(H_4P_2O_7) > O_2(H_3PO_4)$	-0.181	126.0	20.72	97.4417	-97.0382	0.9488
$P(H_4P_2O_7) > P(H_3PO_4)$	0.008	-12.5	1.03	71.8842	-71.9224	-0.0833
$O_2(H_4P_2O_7) > O_1(H_3PO_4)$	0.001	5.4	5.05	59.2480	-59.2296	0.0391
$O_3(H_4P_2O_7) > O_2(H_3PO_4)$	0.001	10.5	0.50	45.3630	-45.3284	0.0346
$H_1(H_4P_2O_7) > H(H_3PO_4)$	0.012	-5.0	0.84	1.1789	-1.1948	-0.0160
$O_4(H_4P_2O_7) > O_2(H_3PO_4)$	-0.020	19.1	1.87	55.2496	-55.1874	0.1238
$H_2(H_4P_2O_7) > H(H_3PO_4)$	0.032	-14.2	2.63	1.5765	-1.6217	-0.0439
$O(H_2O) > O_2(H_3PO_4)$	0.227	-178.7	-20.07	-96.4044	95.8338	-1.3077
$H(H_2O) > H(H_3PO_4)$	-0.057	23.5	-3.04	-2.1815	2.2564	0.0740
Reaction	0.000	0.9	18.40	465.5417	-465.5596	-0.1022

Table E2. Reaction 2: $H_4P_2O_7 + OH^- \text{---> } H_3PO_4 + H_2PO_4^-$

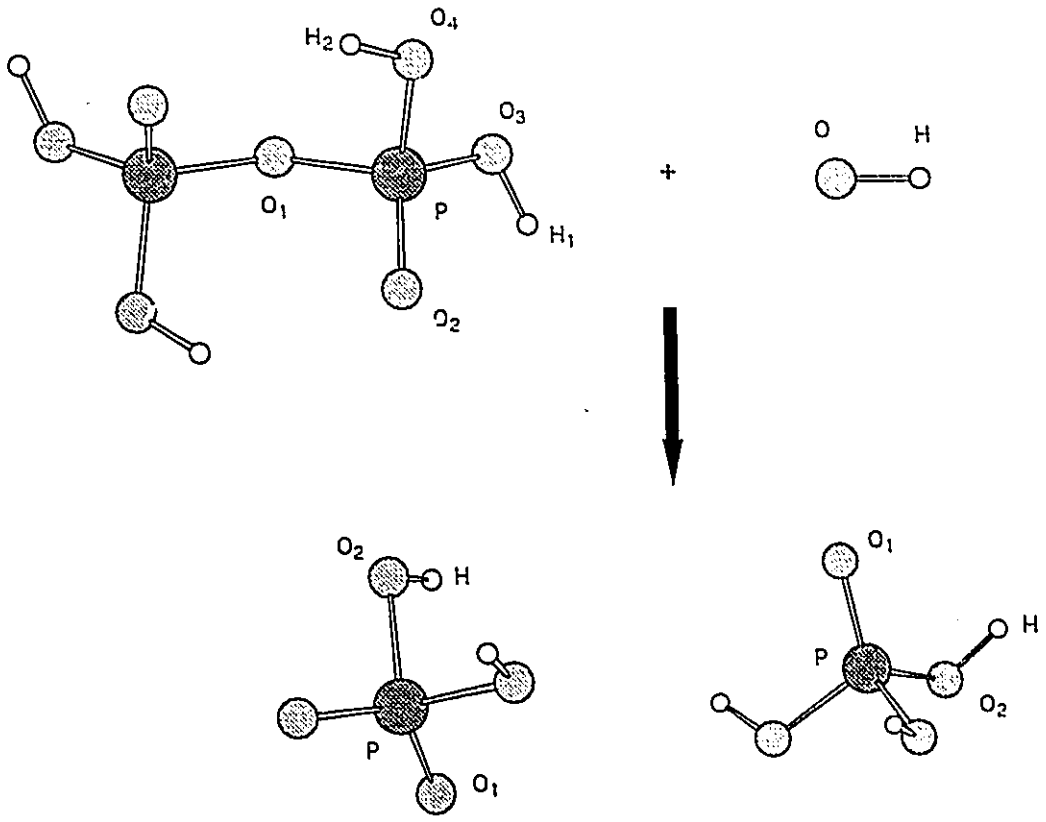

	ΔN	ΔE kcal/mol	ΔVol	ΔV_a	ΔV_r	ΔV_a^*
$O_1(H_4P_2O_7) > O_1(H_2PO_4^-)$	0.005	170.6	49.13	97.4230	-96.8781	0.8202
$P(H_4P_2O_7) > P(H_2PO_4^-)$	0.025	-12.4	1.33	75.0588	-75.0976	-0.2194
$P(H_4P_2O_7) > P(H_3PO_4)$	0.008	-12.5	1.03	71.8842	-71.9224	-0.0833
$O_2(H_4P_2O_7) > O_1(H_2PO_4^-)$	0.038	39.7	11.06	61.7238	-61.5966	0.0023
$O_2(H_4P_2O_7) > O_1(H_3PO_4)$	0.001	5.4	5.05	59.2480	-59.2296	0.0391
$O_2(H_4P_2O_7) > O_2(H_2PO_4^-)$	-0.006	63.1	5.19	49.5709	-49.3692	0.2728
$H_1(H_4P_2O_7) > H(H_2PO_4^-)$	0.064	-26.7	3.55	0.4891	-0.5743	-0.0835
$O_3(H_4P_2O_7) > O_2(H_3PO_4)$	0.001	10.5	0.50	45.3630	-45.3284	0.0346
$H_1(H_4P_2O_7) > H(H_3PO_4)$	0.012	-5.0	0.84	1.1789	-1.1948	-0.0160
$O_4(H_4P_2O_7) > O_2(H_2PO_4^-)$	-0.028	71.8	6.56	59.4574	-59.2282	0.3620
$H_2(H_4P_2O_7) > H(H_2PO_4^-)$	0.083	-35.9	5.34	0.8867	-1.0012	-0.1113
$O_4(H_4P_2O_7) > O_2(H_3PO_4)$	-0.020	19.1	1.87	55.2496	-55.1874	0.1238
$H_2(H_4P_2O_7) > H(H_3PO_4)$	0.032	-14.2	2.63	1.5765	-1.6217	-0.0439
$O(OH^-) > O_2(H_3PO_4)$	0.018	-419.3	-85.64	-102.1182	100.7801	-1.9112
$H(OH^-) > H(H_3PO_4)$	-0.235	79.2	-14.43	-1.5236	1.7760	0.2596
Reaction	0.000	-66.8	-6.01	475.3704	-475.5715	-0.5543

Table E3. Reaction 3: $H_2P_2O_7^{2-} + H_2O \rightarrow 2H_2PO_4^-$

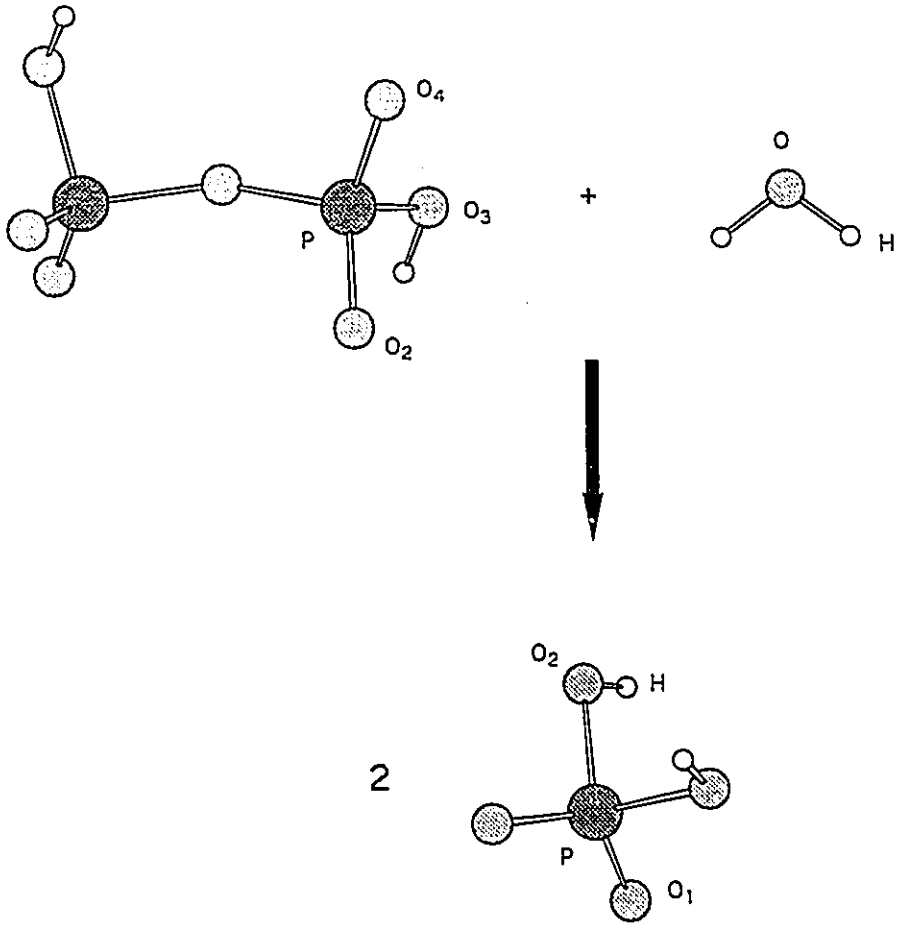

	ΔN	ΔE kcal/mol	ΔVol	ΔV_a	ΔV_r	ΔV_a°
$O_1(H_2P_2O_7^{2-}) > O_2(H_2PO_4^-)$	-0.220	160.0	22.97	97.6929	-97.1814	1.3160
$P(H_2P_2O_7^{2-}) > P(H_2PO_4^-)$	0.001	-24.4	-0.66	63.4561	-63.5328	-0.0985
$O_2(H_2P_2O_7^{2-}) > O_1(H_2PO_4^-)$	-0.005	-7.5	-0.71	48.6890	-48.7124	-0.0069
$O_3(H_2P_2O_7^{2-}) > O_2(H_2PO_4^-)$	0.014	-14.2	0.74	44.2415	-44.2861	-0.0885
$H(H_2P_2O_7^{2-}) > H(H_2PO_4^-)$	-0.012	4.1	-0.86	2.0777	-2.0647	0.0141
$O_4(H_2P_2O_7^{2-}) > O_1(H_2PO_4^-)$	0.000	-12.0	0.06	45.7402	-45.7777	-0.0305
$O(H_2O) > O_2(H_2PO_4^-)$	0.220	-126.1	-15.37	-92.1966	91.7930	-1.0696
$H(H_2O) > H(H_2PO_4^-)$	-0.006	1.8	-0.33	-2.8712	2.8770	0.0065
Reaction	0.000	-70.2	4.08	407.8701	-408.0884	-0.1609

Table E4. Reaction 4: $P_2O_7^{4-} + H_2O \rightarrow 2HPO_4^{2-}$

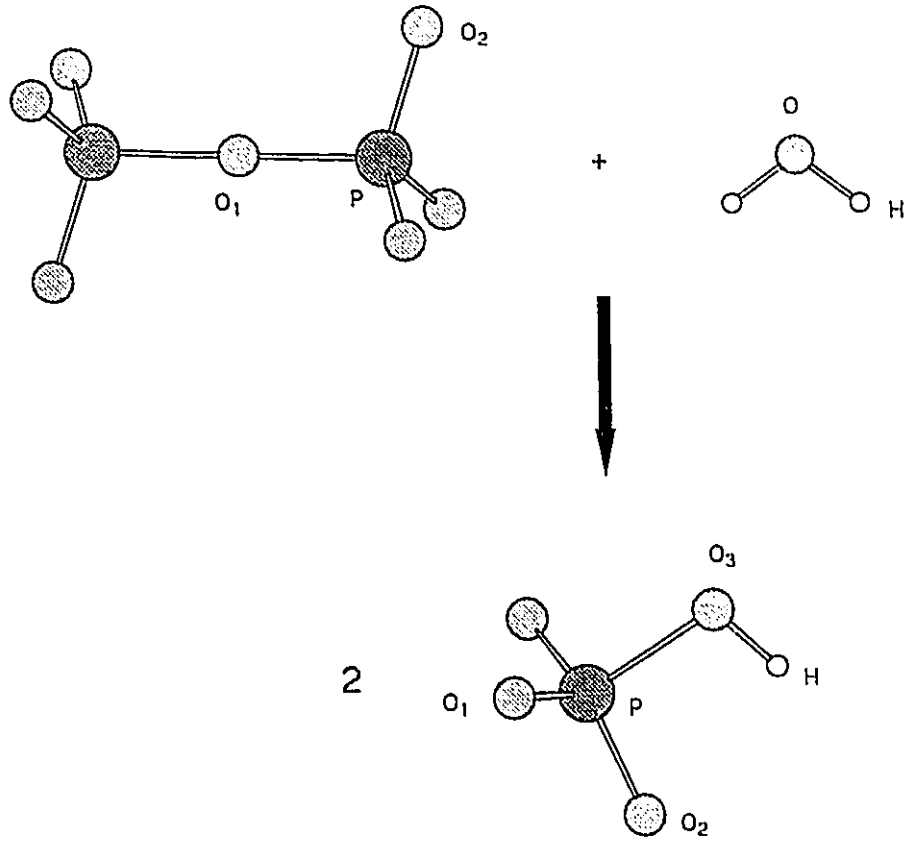

	ΔN	ΔE kcal/mol	ΔVol	ΔV_a	ΔV_r	ΔV_a^*
$O_1(P_2O_7^{4-}) > O_3(HPO_4^{2-})$	-0.229	142.7	24.02	94.4932	-94.0361	1.3262
$P(P_2O_7^{4-}) > P(HPO_4^{2-})$	0.030	-75.9	0.91	58.5384	-58.7788	-0.4282
$O_2(P_2O_7^{4-}) > O_1(HPO_4^{2-})$	-0.021	-34.6	-5.22	43.4583	-43.5671	-0.0742
$O_2(P_2O_7^{4-}) > O_2(HPO_4^{2-})$	-0.013	-29.6	-5.76	42.9729	-43.0658	-0.0876
$O(H_2O) > O_3(HPO_4^{2-})$	0.205	-49.7	-7.68	-86.9275	86.7687	-0.7403
$H(H_2O) > H(HPO_4^{2-})$	0.031	-12.3	1.25	-3.3294	3.2903	-0.0372
Reaction	0.000	-280.5	-11.73	377.5525	-378.4864	-0.8169

Table E5. Reaction 5: $P_2O_7^{4-} + Mg^{2+} \rightarrow P_2O_7Mg^{2-}$

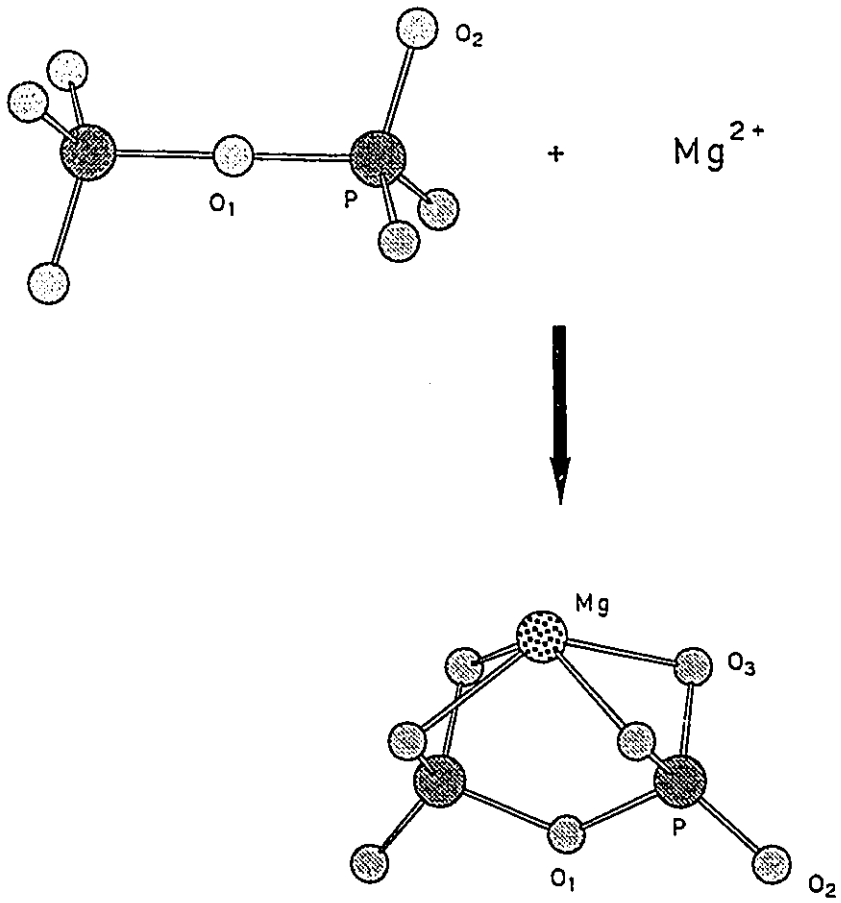

	ΔN	ΔE kcal/mol	ΔVol	ΔV_a	ΔV_r	ΔV_a°
$O_1(P_2O_7) > O_1(P_2O_7Mg^{2-})$	-0.027	1.7	-3.66	-23.7377	23.7374	0.2181
$P(P_2O_7) > P(P_2O_7Mg^{2-})$	0.013	-100.4	-0.45	-36.1516	36.1948	-0.3585
$O_2(P_2O_7) > O_2(P_2O_7Mg^{2-})$	-0.064	-84.6	-12.59	-15.4686	15.1945	-0.1035
$O_2(P_2O_7) > O_3(P_2O_7Mg^{2-})$	-0.023	-84.7	-25.32	-42.1319	41.8563	-0.3052
$Mg^{2+} > Mg(P_2O_7Mg^{2-})$	0.212	-248.8	-7.07	-192.9004	192.0998	-1.9989
Reaction	0.000	-954.7	-138.09	-489.1666	486.1563	-3.9256

Table E6. Reaction 6: $HPO_4^{2-} + Mg^{2+}$ ---> HPO_4Mg

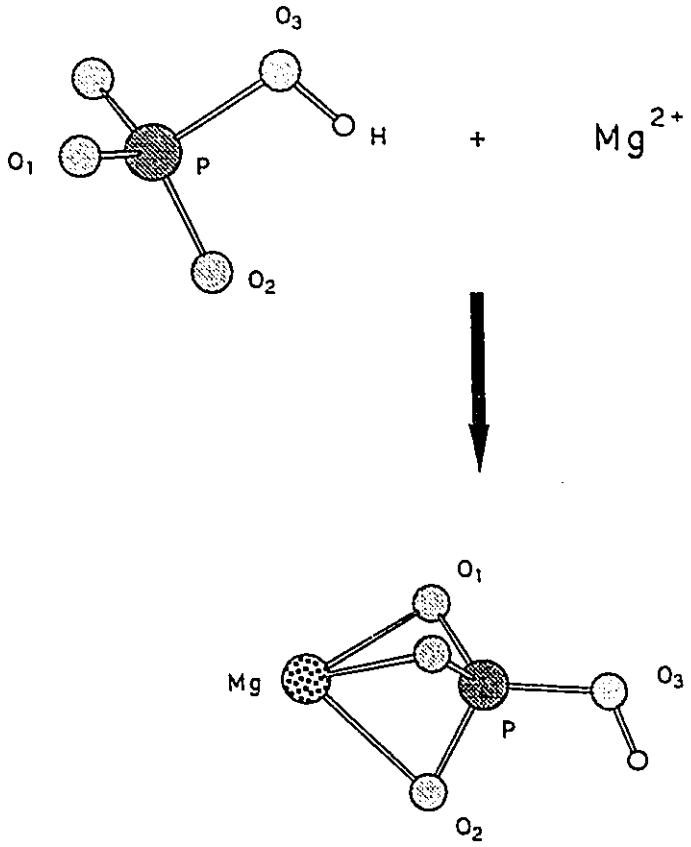

	ΔN	ΔE kcal/mol	ΔVol	ΔV_a	ΔV_r	ΔV_a°
$O_1(HPO_4^{2-}) > O_1(HPO_4Mg)$	-0.031	-62.2	-18.01	-30.7270	30.5219	-0.1369
$P(HPO_4^{2-}) > P(HPO_4Mg)$	-0.032	-80.2	-1.85	-33.2096	32.9475	0.0146
$O_2(HPO_4^{2-}) > O_2(HPO_4Mg)$	-0.029	-63.0	-16.44	-30.3391	30.1315	-0.1389
$O_3(HPO_4^{2-}) > O_3(HPO_4Mg)$	0.023	-125.7	-10.00	-20.1438	19.7373	-0.5396
$H(HPO_4^{2-}) > H(HPO_4Mg)$	-0.093	37.1	-4.61	0.8271	-0.7089	0.1163
$Mg^{2+} > Mg(HPO_4Mg)$	0.189	-209.5	46.17	-114.4753	113.6801	-1.7156
Reaction	0.000	-565.3	-22.75	-258.5789	256.8200	-2.5369

Table E7. Reaction 7: $P_2O_7Mg^{2-} + H_2O$ ---> $HPO_4Mg + HPO_4^{2-}$

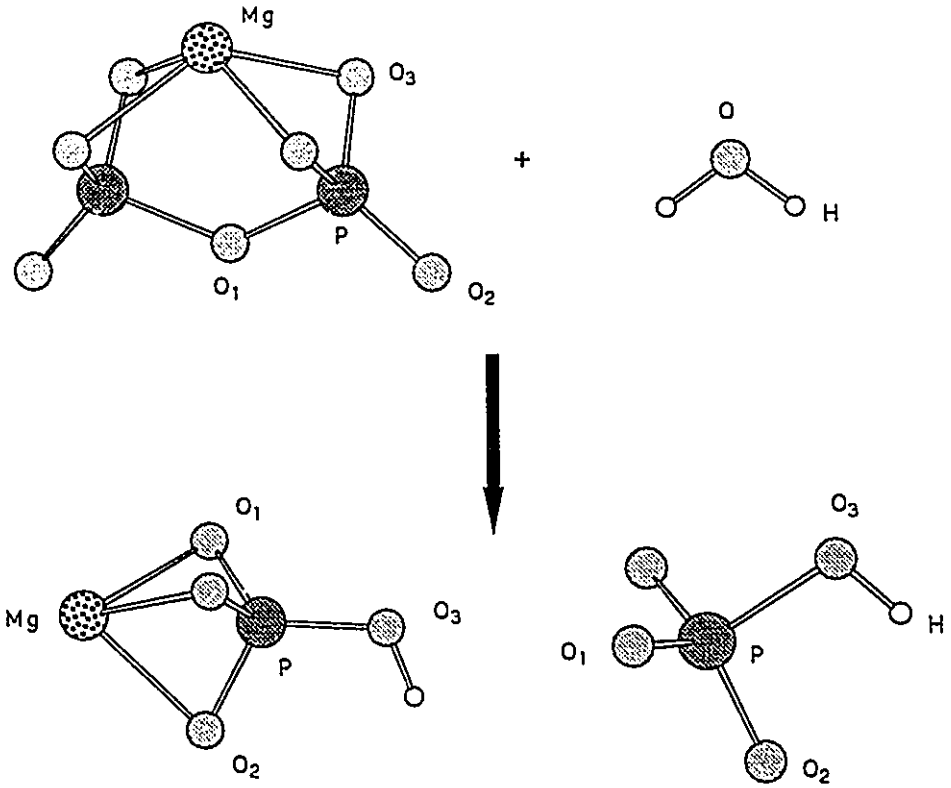

	ΔN	ΔE kcal/mol	ΔVol	ΔV_a	ΔV_r	ΔV_a^*
$O_1(P_2O_7Mg^{2-}) > O_3(HPO_4Mg)$	-0.180	15.3	17.68	98.0872	-98.0362	0.5685
$P(P_2O_7Mg^{2-}) > P(HPO_4^{2-})$	0.017	24.5	1.36	94.6900	-94.9736	-0.0697
$P(P_2O_7Mg^{2-}) > P(HPO_4Mg)$	-0.014	-55.7	-0.49	61.4805	-62.0261	-0.0552
$O_2(P_2O_7Mg^{2-}) > O_2(HPO_4^{2-})$	0.051	55.0	6.83	58.4415	-58.2604	0.0160
$O_2(P_2O_7Mg^{2-}) > O_2(HPO_4Mg)$	0.022	-8.0	-9.61	28.1024	-28.1288	-0.1229
$O_3(P_2O_7Mg^{2-}) > O_1(HPO_4^{2-})$	0.002	50.2	20.10	85.5901	-85.4234	0.2310
$O_3(P_2O_7Mg^{2-}) > O_1(HPO_4Mg)$	-0.028	-12.1	2.09	54.8631	-54.9015	0.0941
$Mg(P_2O_7Mg^{2-}) > Mg(HPO_4Mg)$	-0.023	39.4	5.62	78.5674	-78.4405	0.2833
$O(H_2O) > O_3(HPO_4^{2-})$	0.205	-49.7	-7.68	-86.9275	86.7687	-0.7403
$H(H_2O) > H(HPO_4^{2-})$	0.031	-12.3	1.25	-3.3294	3.2903	-0.0372
$H(H_2O) > H(HPO_4Mg)$	-0.061	24.9	-3.36	-2.5023	2.5814	0.0791
...or						
$O_1(P_2O_7Mg^{2-}) > O_3(HPO_4)$	-0.202	141.0	27.68	118.2310	-117.7735	1.1081
$O(H_2O) > O_3(HPO_4Mg)$	0.228	-175.4	-17.67	-107.0713	106.5060	-1.2799
Reaction	0.000	108.9	55.99	608.1403	-607.8227	0.5718

Table E8. Reaction 8: $MDP^{3-} + H_2O \rightarrow MP^{-} + HPO_4^{2-}$

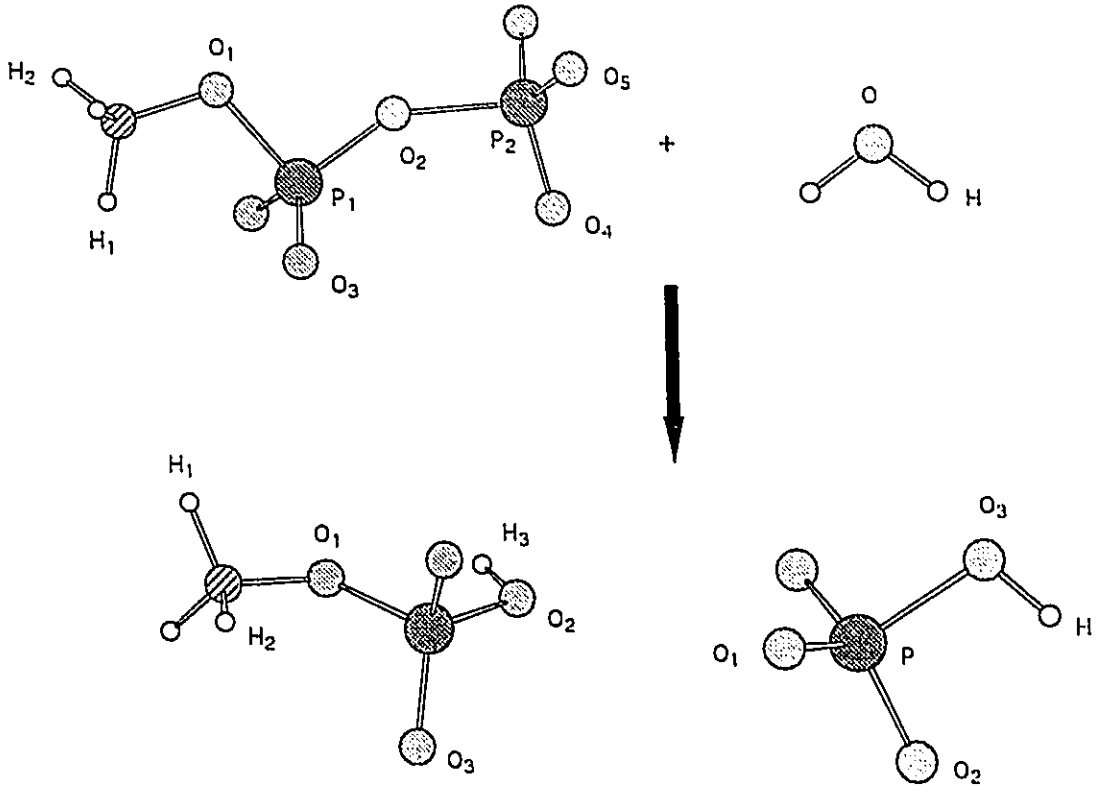

	ΔN	ΔE kcal/mol	ΔVol	ΔV_a	ΔV_r	ΔV_a^*
$P_2(MDP^{3-}) > P(HPO_4^{2-})$	-0.010	1.5	-0.54	67.9503	-67.9185	-0.4536
$O_4(MDP^{3-}) > O_2(HPO_4^{2-})$	0.013	12.9	-1.88	56.1574	-56.0934	-0.0296
$O_5(MDP^{3-}) > O_1(HPO_4^{2-})$	0.004	7.7	0.16	52.1001	-52.0541	0.0043
$O_2(MDP^{3-}) > O_2(MP^{-})$	-0.181	46.4	13.33	89.2881	-89.1109	0.7270
$P_1(MDP^{3-}) > P(MP^{-})$	-0.006	-75.1	-1.99	60.7413	-60.9617	-0.1693
$O_3(MDP^{3-}) > O_3(MP^{-})$	-0.024	-24.5	-0.48	46.0117	-46.0767	0.0505
$O_1(MDP^{3-}) > O_1(MP^{-})$	0.043	-36.9	-0.95	38.4886	-38.5960	-0.2695
$C(MDP^{3-}) > C(MP^{-})$	0.107	-49.2	4.10	16.1023	-16.2550	-0.4450
$H_1(MDP^{3-}) > H_1(MP^{-})$	-0.019	4.8	0.69	3.9340	-3.9176	0.0141
$H_2(MDP^{3-}) > H_2(MP^{-})$	-0.075	14.9	-5.47	4.4465	-4.3976	0.0522
$O(H_2O) > O_3(HPO_4^{2-})$	0.216	-28.2	-13.54	-87.2493	87.1317	-0.7290
$H(H_2O) > H(HPO_4^{2-})$	0.031	-12.1	0.81	-3.3436	3.3040	-0.0363
$H(H_2O) > H_3(MP^{-})$	-0.016	4.9	-1.49	-3.1856	3.2002	0.0187
Reaction	0.000	-134.0	-13.05	443.4148	-443.8546	-1.1586

Table E9. Reaction 9: $MDP^{3-} + H_2O$ ---> $MP^{2-} + H_2PO_4^-$

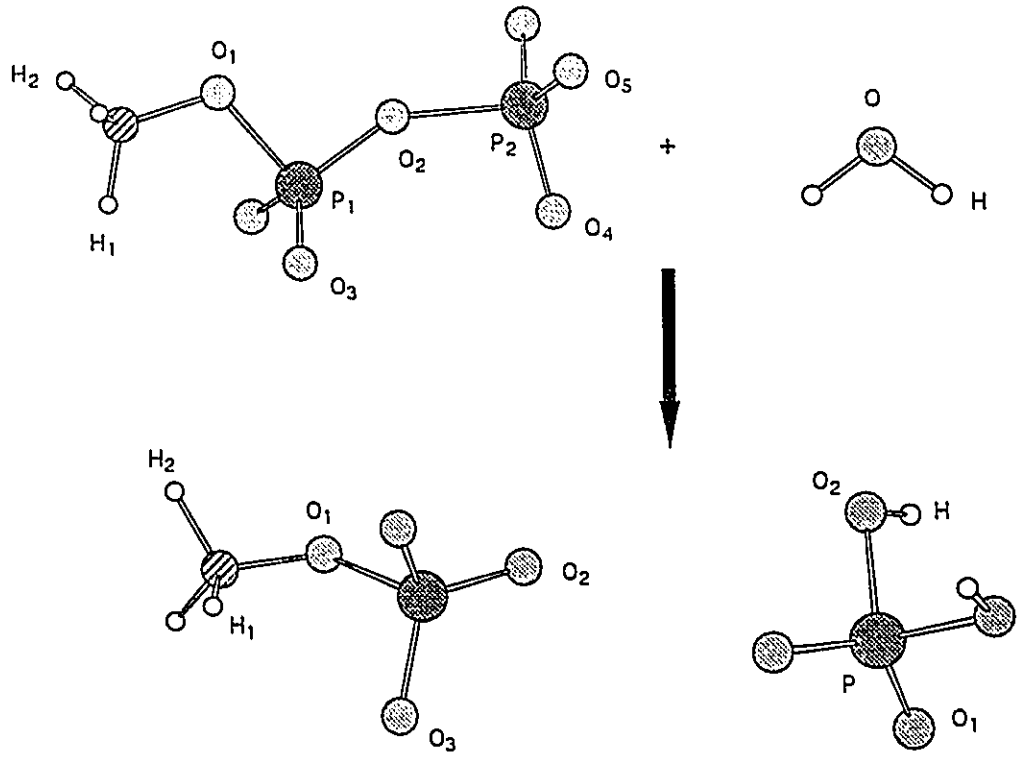

	ΔN	ΔE	ΔVol	ΔV_a	ΔV_r	ΔV_a°
		kcal/mol				
$P_2(MDP^{3-}) > P(H_2PO_4^-)$	-0.013	-79.7	-0.73	64.3296	-64.5641	-0.0985
$O_4(MDP^{3-}) > O_2(H_2PO_4^-)$	-0.246	-20.8	-23.24	58.2749	-58.3247	0.5099
$O_5(MDP^{3-}) > O_1(H_2PO_4^-)$	-0.036	-44.6	-2.40	48.6630	-48.7921	0.0179
$O_2(MDP^{3-}) > O_2(MP^{2-})$	0.064	78.3	34.26	87.7293	-87.4439	0.2563
$P_1(MDP^{3-}) > P(MP^{2-})$	-0.004	-4.8	-1.77	64.4923	-64.4806	-0.0256
$O_3(MDP^{3-}) > O_3(MP^{2-})$	0.020	19.8	0.42	48.0193	-47.9352	-0.0224
$O_1(MDP^{3-}) > O_1(MP^{2-})$	0.002	21.2	1.53	44.5778	-44.4907	0.0509
$C_1(MDP^{3-}) > C_1(MP^{2-})$	-0.008	6.5	-0.21	18.0530	-18.0244	0.0403
$H_1(MDP^{3-}) > H_1(MP^{2-})$	-0.003	0.9	-0.12	3.6869	-3.6824	0.0027
$H_2(MDP^{3-}) > H_2(MP^{2-})$	0.009	-1.5	1.21	3.7209	-3.7239	-0.0056
$O(H_2O) > O_2(H_2PO_4^-)$	0.227	-97.5	-15.36	-92.3129	91.9658	-0.9845
$H(H_2O) > H(H_2PO_4^-)$	-0.008	2.4	-0.53	-2.8137	2.8205	0.0100
Reaction	0.000	-142.4	-8.24	443.4518	-443.9106	-0.2484

Table E10. Reaction 10: $MDP^{3-} + OH^- \rightarrow MP^{2-} + HPO_4^{2-}$

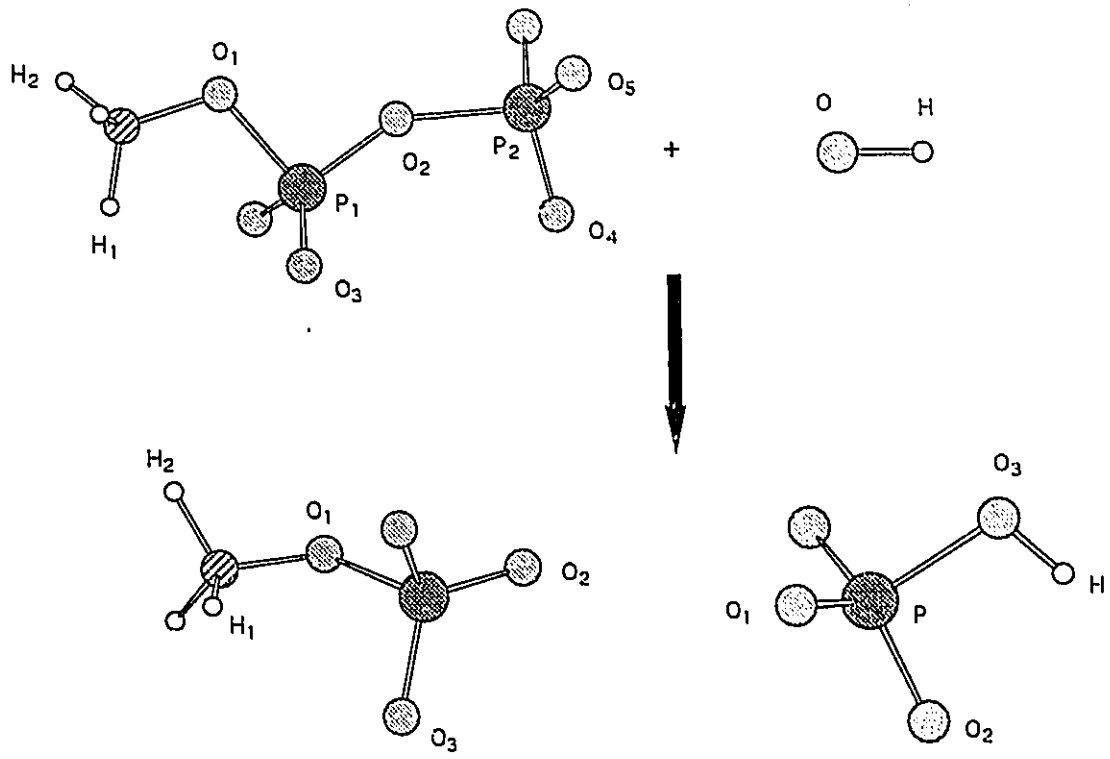

	ΔN	ΔE kcal/mol	ΔVol	ΔV_a	ΔV_r	ΔV_a°
$P_2(MDP^{3-}) > P(HPO_4^{2-})$	-0.010	1.5	-0.54	67.9503	-67.9185	-0.4536
$O_4(MDP^{3-}) > O_2(HPO_4^{2-})$	0.013	12.9	-1.88	56.1574	-56.0934	-0.0296
$O_5(MDP^{3-}) > O_1(HPO_4^{2-})$	0.004	7.7	0.16	52.1001	-52.0541	0.0043
$O_2(MDP^{3-}) > O_2(MP^{2-})$	0.064	78.3	34.26	87.7293	-87.4439	0.2563
$P_1(MDP^{3-}) > P(MP^{2-})$	-0.004	-4.8	-1.77	64.4923	-64.4806	-0.0256
$O_3(MDP^{3-}) > O_3(MP^{2-})$	0.020	19.8	0.42	48.0193	-47.9352	-0.0224
$O_1(MDP^{3-}) > O_1(MP^{2-})$	0.002	21.2	1.53	44.5778	-44.4907	0.0509
$C(MDP^{3-}) > C(MP^{2-})$	-0.008	6.5	-0.21	18.0530	-18.0244	0.0403
$H_1(MDP^{3-}) > H_1(MP^{2-})$	-0.003	0.9	-0.12	3.6869	-3.6824	0.0027
$H_2(MDP^{3-}) > H_2(MP^{2-})$	0.009	-1.5	1.21	3.7209	-3.7239	-0.0056
$O(OH^-) > O_3(HPO_4^{2-})$	0.072	-318.5	-28.93	-92.8988	91.8462	-1.1862
$H(OH^-) > H(HPO_4^{2-})$	-0.205	60.7	-12.77	-2.4341	2.6254	0.2094
Reaction	0.000	-88.5	-6.86	454.4536	-454.6571	-1.1826

Table E11. Reaction 11: PEP + H_2O ---> PA(keto form) + H_3PO_4

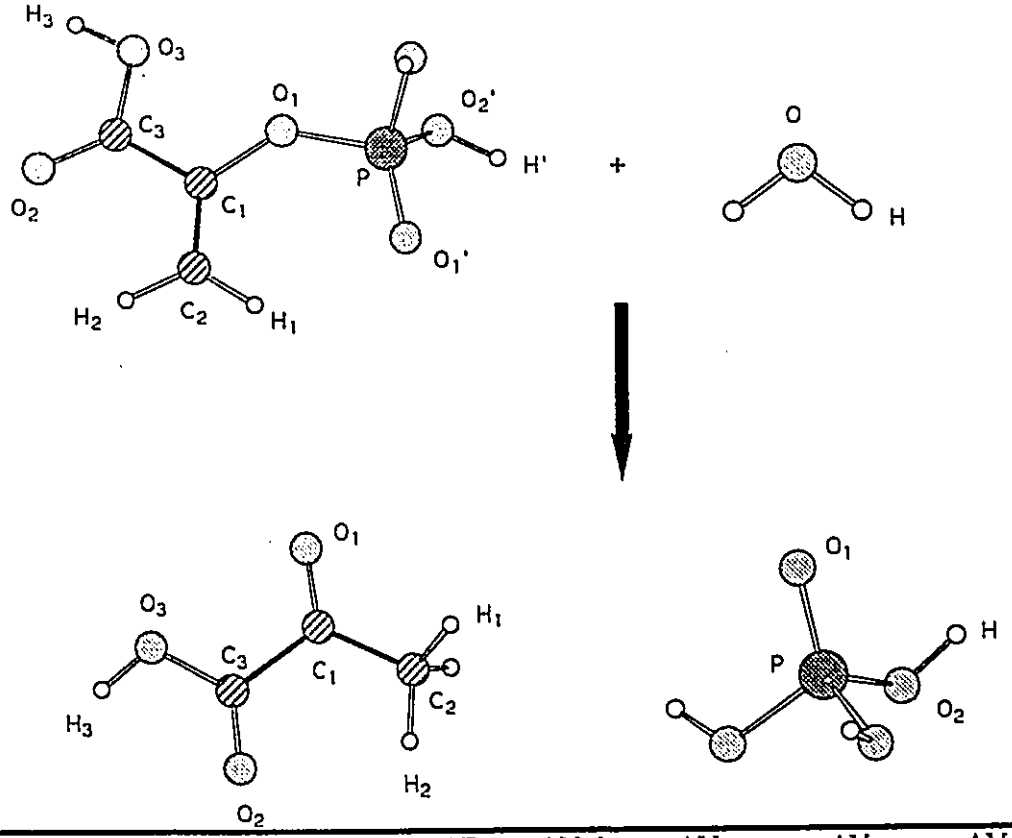

	ΔN	ΔE	ΔVol	ΔV_a	ΔV_r	ΔV_a°
		kcal/mol				
P(PEP) > P(H_3PO_4)	0.011	-5.6	0.85	55.3402	-55.3547	-0.1046
O_1'(PEP) > O_1(H_3PO_4)	0.001	11.6	4.73	44.2237	-44.1834	0.0474
O_2'(PEP) > O_2(H_3PO_4)	0.002	3.2	0.29	39.1761	-39.1629	0.0023
H'(PEP) > H(H_3PO_4)	0.005	-2.0	0.20	1.0511	-1.0573	-0.0063
O_1(PEP) > O_1(keto)	-0.243	77.3	33.36	97.3822	-97.1347	1.4678
C_1(PEP) > C_1(keto)	-0.813	304.1	-24.46	48.5751	-47.6058	3.1838
C_2(PEP) > C_2(keto)	0.086	-28.9	-20.68	32.6297	-32.7221	-0.5226
H_1(PEP) > H_1(keto)	0.089	-19.2	8.56	4.7494	-4.8107	-0.0696
H_2(PEP) > H_2(keto)	0.048	-14.2	1.80	3.4793	-3.5248	-0.0446
C_3(PEP) > C_3(keto)	0.055	-20.6	2.42	19.8574	-20.0784	-0.2215
O_2(PEP) > O_2(keto)	-0.016	-2.4	-0.09	36.5904	-36.5991	0.0809
O_3(PEP) > O_3(keto)	-0.001	-3.2	1.27	45.0282	-45.0390	0.0025
H_3(PEP) : H_3(keto)	0.000	0.4	0.26	1.3353	-1.3342	0.0010
O(H_2O) > O_2(H_3PO_4)	0.227	-178.7	-20.07	-96.4044	95.8338	-1.3077
H(H_2O) > H(H_3PO_4)	-0.057	23.5	-3.04	-2.1815	2.2564	0.0740
H(H_2O) > H_1(keto)	0.598	-162.4	28.26	-8.3331	7.8150	-0.5969
Reaction	0.000	-15.7	14.15	362.8957	-362.9606	1.9818

Table E12. Reaction 12: PEP + OH^- ---> PA^- + H_3PO_4

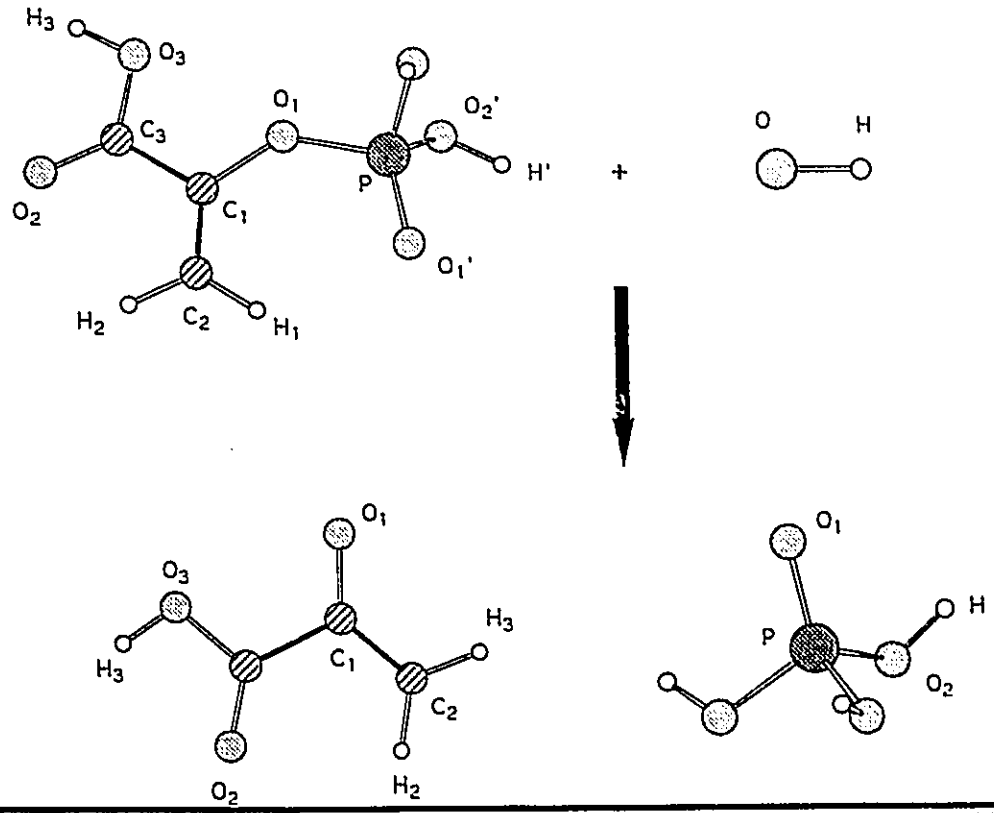

	ΔN	ΔE kcal/mol	ΔVol	ΔV_a	ΔV_r	ΔV_a^*
P(PEP) > P(H_3PO_4)	0.011	-5.6	0.85	55.3402	-55.3547	-0.1046
O_1'(PEP) > O_1(H_3PO_4)	0.001	11.6	4.73	44.2237	-44.1834	0.0474
O_2'(PEP) > O_2(H_3PO_4)	0.002	3.2	0.29	39.1761	-39.1629	0.0023
H'(PEP) > H(H_3PO_4)	0.005	-2.0	0.20	1.0511	-1.0573	-0.0063
O_1(PEP) > O_1(PA^-)	-0.075	168.8	48.66	99.5444	-99.0048	1.0652
C_1(PEP) > C_1(PA^-)	-0.651	250.9	-17.13	47.6725	-46.8724	2.5265
C_2(PEP) > C_2(PA^-)	0.307	-15.6	26.57	31.7952	-31.8450	-0.7255
H_1(PEP) > H_1(PA^-)	0.182	-37.5	15.63	4.3581	-4.4778	-0.1374
H_2(PEP) > H_2(PA^-)	0.126	-28.9	7.73	2.9948	-3.0870	-0.0983
C_3(PEP) > C_3(PA^-)	0.212	-70.2	6.04	18.1413	-18.5202	-0.7433
O_2(PEP) > O_2(PA^-)	0.053	8.5	4.90	37.7827	-37.7558	-0.1374
O_3(PEP) > O_3(PA^-)	-0.009	20.9	2.27	46.4462	-46.3796	0.1327
H_3(PEP) > H_3(PA^-)	0.042	-16.8	2.33	0.8437	-0.8971	-0.0527
O(OH^-) > O_2(H_3PO_4)	0.018	-419.3	-85.64	-102.1182	100.7801	-1.9112
H(OH^-) > H(H_3PO_4)	-0.235	79.2	-14.43	-1.5236	1.7760	0.2596
Reaction	0.000	-51.4	3.51	366.0819	-366.2549	0.1131

Table E13. Reaction 13: $PA^- + H_3O^+ \rightarrow PA(\text{enol form}) + H_2O$

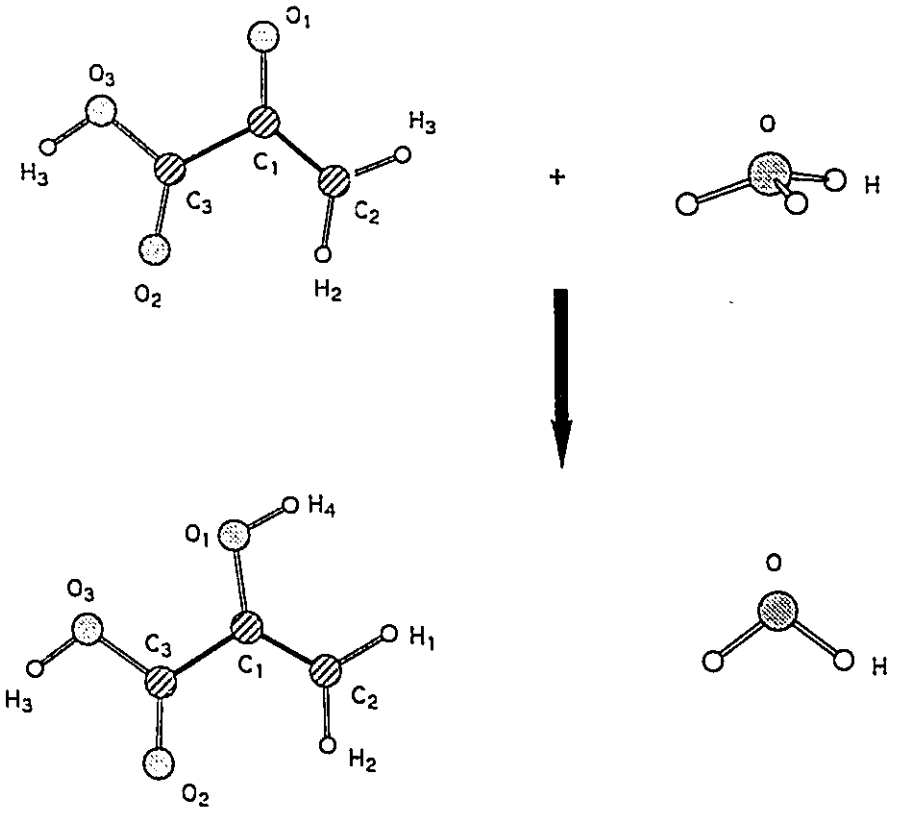

	ΔN	ΔE kcal/mol	ΔVol	ΔV_a	ΔV_r	ΔV_a°
$O_1(PA^-) > O_1(enol)$	-0.146	-29.3	-29.80	-2.0610	1.9669	0.1353
$C_1(PA^-) > C_1(enol)$	0.536	-225.9	13.22	-10.0071	9.2860	-2.1565
$C_2(PA^-) > C_2(enol)$	-0.266	15.4	-23.09	1.1887	-1.1399	0.6233
$H_1(PA^-) > H_1(enol)$	-0.075	14.0	-5.45	0.4069	-0.3623	0.0516
$H_2(PA^-) > H_2(enol)$	-0.119	27.8	-7.19	1.0824	-0.9938	0.0936
$C_3(PA^-) > C_3(enol)$	-0.203	72.6	-5.40	2.0155	-1.7843	0.6757
$O_2(PA^-) > O_2(enol)$	-0.053	-12.5	-4.63	-1.2947	1.2543	0.1335
$O_3(PA^-) > O_3(enol)$	0.008	-23.5	-1.85	-2.5849	2.5091	-0.1331
$H_3(PA^-) > H_3(enol)$	-0.040	16.0	-2.07	0.4323	-0.3815	0.0501
$O(H_3O^+) > O(H_2O)$	-0.050	145.1	19.15	5.8507	-5.3865	0.8545
$H(H_3O^+) > H(H_2O)$	0.146	-63.8	7.45	-0.7072	0.5040	-0.1981
$H(H_3O^+) > H_4(enol)$	0.125	-56.8	6.85	-2.8057	2.6244	-0.1741
Reaction	0.000	-185.4	-25.37	-9.0793	8.4820	-0.2422

Table E14. Reaction 14: PA(enol form) ---> PA(keto form)

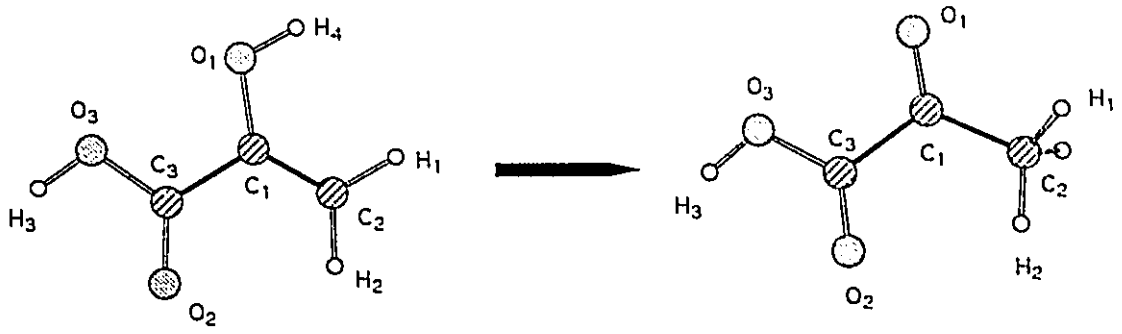

	ΔN	ΔE kcal/mol	ΔVol	ΔV_a	ΔV_r	ΔV_a^*
O_1(enol) > O_1(keto)	-0.021	-62.2	14.50	-0.1012	-0.0969	0.2673
C_1(enol) > C_1(keto)	-0.698	279.1	-20.55	10.9097	-10.0194	2.8138
C_2(enol) > C_2(keto)	0.045	-28.7	-24.16	-0.3542	0.2628	-0.4205
H_1(enol) > H_1(keto)	-0.017	4.3	-1.63	-0.0156	0.0293	0.0161
H_2(enol) > H_2(keto)	0.041	-13.2	1.25	-0.5980	0.5559	-0.0398
C_3(enol) > C_3(keto)	0.046	-23.0	1.77	-0.2994	0.2261	-0.1538
O_2(enol) > O_2(keto)	-0.016	1.5	-0.36	0.1025	-0.0975	0.0848
O_3(enol) > O_3(keto)	-0.001	-0.6	0.85	1.1669	-1.1685	0.0029
H_3(enol) > H_3(keto)	-0.002	1.2	0.00	0.0593	-0.0556	0.0035
H_4(enol) > H_1(keto)	0.618	-169.4	28.86	-6.2347	5.6945	-0.6209
Reaction	0.000	-10.1	0.53	4.5614	-4.5956	1.9532

Table E15. Reaction 15: $PEP^{3-} + H_2O$ ---> PA^-(keto form) + HPO_4^{2-}

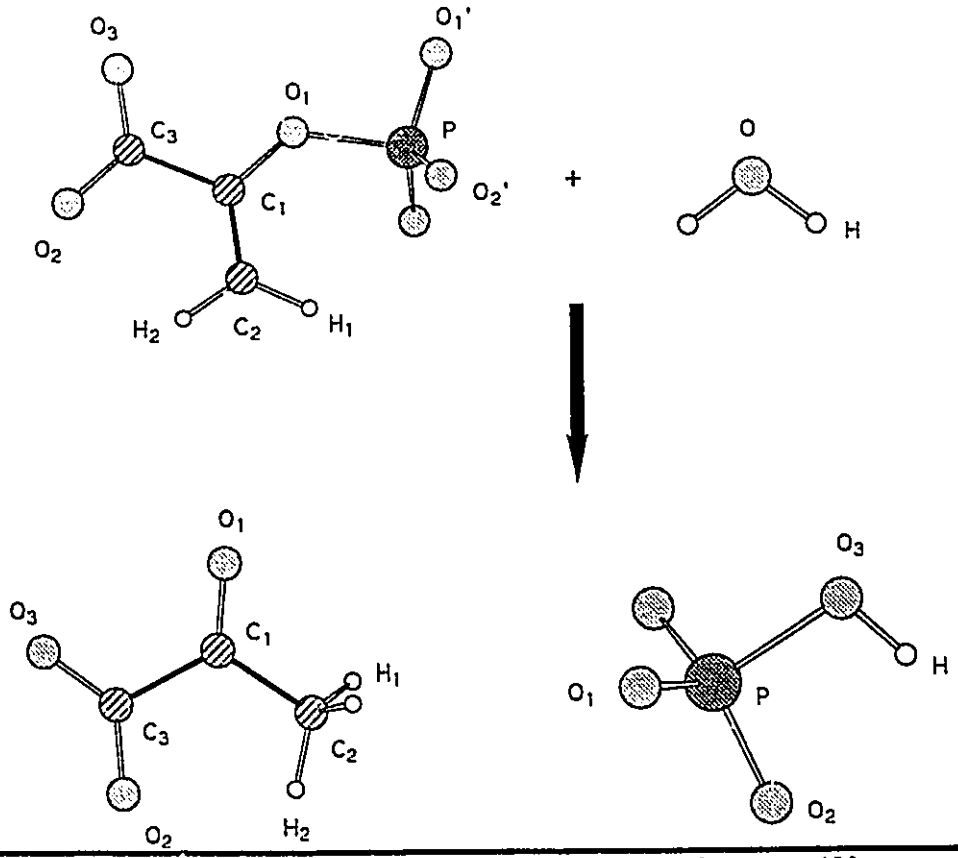

	ΔN	ΔE	ΔVol	ΔV_a	ΔV_r	ΔV_a°
		kcal/mol				
$P(PEP^{3-}) > P(HPO_4^{2-})$	0.007	1.9	0.81	51.9930	-51.9839	-0.0558
$O_1'(PEP^{3-}) > O_2(HPO_4^{2-})$	0.012	10.2	1.13	36.8454	-36.8103	-0.0084
$O_2'(PEP^{3-}) > O_1(HPO_4^{2-})$	0.000	6.3	1.48	41.9917	-41.9688	0.0221
$O_1(PEP^{3-}) > O_1$(keto)	-0.131	-11.2	32.66	86.3279	-86.3632	0.7245
$C_1(PEP^{3-}) > C_1$(keto)	-0.435	143.7	-13.44	39.0390	-38.5813	1.7390
$C_2(PEP^{3-}) > C_2$(keto)	-0.128	-13.1	-39.62	35.2925	-35.3345	0.0368
$H_1(PEP^{3-}) > H_1$(keto)	0.046	-11.3	4.19	5.8301	-5.8663	-0.0374
$H_2(PEP^{3-}) > H_2$(keto)	-0.087	17.6	-6.04	5.3620	-5.3061	0.0632
$C_3(PEP^{3-}) > C_3$(keto)	-0.117	15.6	-2.61	20.0139	-19.9644	0.3918
$O_2(PEP^{3-}) > O_2$(keto)	-0.049	-34.9	-8.51	33.8865	-33.9986	0.0442
$O_3(PEP^{3-}) > O_3$(keto)	-0.031	-24.3	26.71	40.0011	-40.0794	0.0143
$O(H_2O) > O_3(HPO_4^{2-})$	0.205	-49.7	-7.68	-86.9275	86.7687	-0.7403
$H(H_2O) > H(HPO_4^{2-})$	0.031	-12.3	1.25	-3.3294	3.2903	-0.0372
$H(H_2O) > H_1$(keto)	0.664	-178.4	31.90	-8.9060	8.3369	-0.6505
Reaction	0.000	-134.0	23.71	339.2147	-339.6607	1.5283

Table E16. Reaction 16: $PEP^{3-} + OH^- \rightarrow PA^{2-} + HPO_4^{2-}$

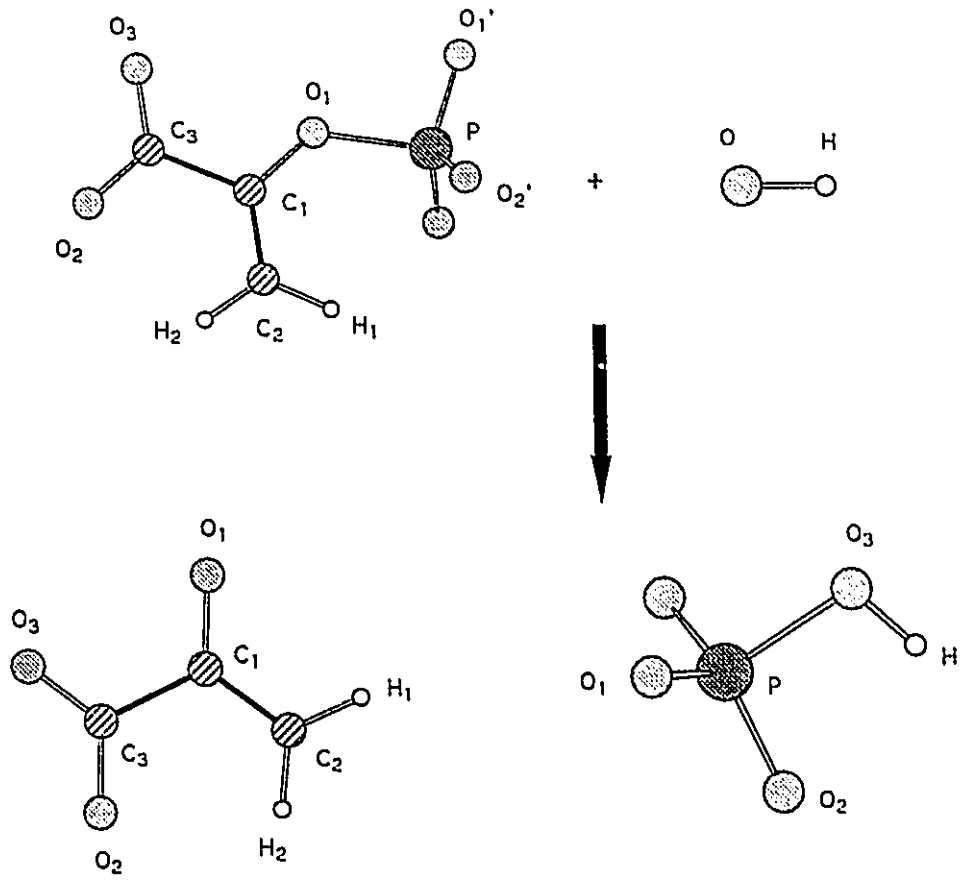

	ΔN	ΔE kcal/mol	ΔVol	ΔV_a	ΔV_r	ΔV_a^*
$P(PEP^{3-}) > P(HPO_4^{2-})$	0.007	1.9	0.81	51.9930	-51.9839	-0.0558
$O_1'(PEP^{3-}) > O_2(HPO_4^{2-})$	0.012	10.2	1.13	36.8454	-36.8103	-0.0084
$O_2'(PEP^{3-}) > O_1(HPO_4^{2-})$	0.000	6.3	1.48	41.9917	-41.9688	0.0221
$O_1(PEP^{3-}) > O_1(PA^{2-})$	-0.004	84.1	46.39	88.9461	-88.6776	0.5297
$C_1(PEP^{3-}) > C_1(PA^{2-})$	-0.297	119.2	-7.48	38.7165	-38.3369	1.1860
$C_2(PEP^{3-}) > C_2(PA^{2-})$	0.219	5.8	25.54	33.9994	-33.9811	-0.3838
$H_1(PEP^{3-}) > H_1(PA^{2-})$	0.154	-26.6	14.81	5.4362	-5.5210	-0.1016
$H_2(PEP^{3-}) > H_2(PA^{2-})$	0.013	1.7	2.93	4.8091	-4.8039	-0.0006
$C_3(PEP^{3-}) > C_3(PA^{2-})$	0.048	-20.5	1.07	18.1800	-18.2482	-0.1976
$O_2(PEP^{3-}) > O_2(PA^{2-})$	-0.003	-9.8	-0.70	35.9776	-36.0096	-0.0040
$O_3(PEP^{3-}) > O_3(PA^{2-})$	0.013	5.2	32.34	41.1721	-41.1561	-0.0130
$O(OH^-) > O_3(HPO_4^{2-})$	-0.004	-290.3	-73.25	-92.6413	91.7150	-1.3438
$H(OH^-) > H(HPO_4^{2-})$	-0.146	43.5	-10.14	-2.6715	2.8099	0.1484
Reaction	0.000	-63.9	36.39	345.0174	-345.2255	-0.2002

Table E17. Reaction 17: $PA^{2-} + H_3O^+ \text{---> } PA^-(\text{enol form}) + H_2O$

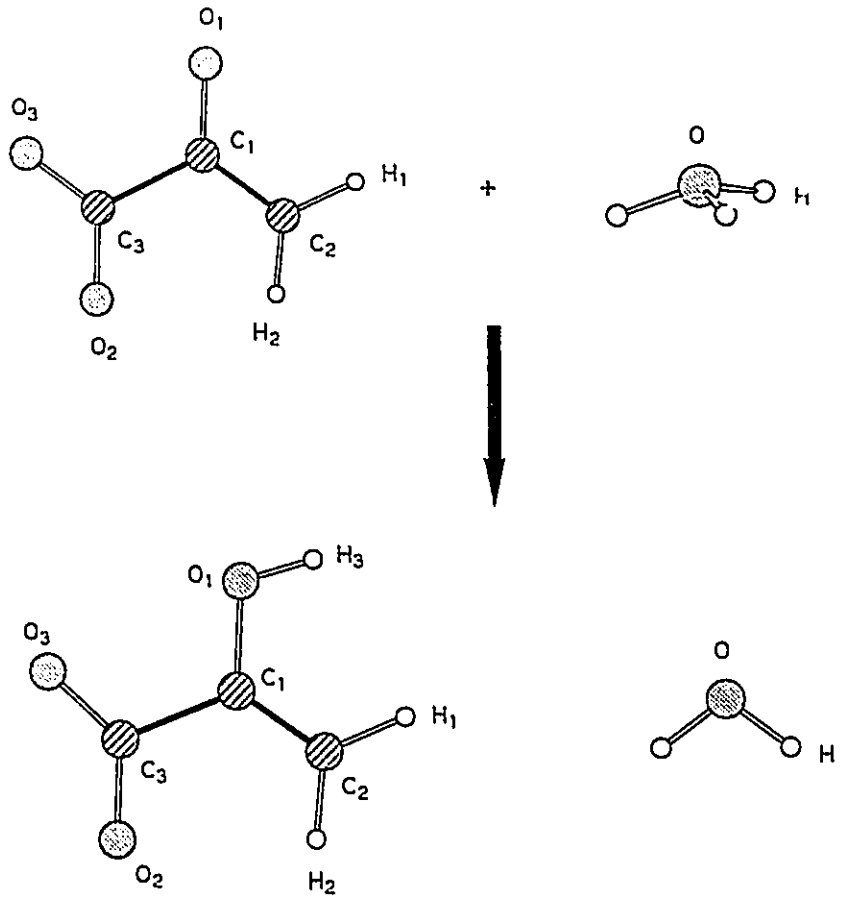

	ΔN	ΔE kcal/mol	ΔVol	ΔV_a	ΔV_r	ΔV_a°
$O_1(PA^{2-}) > O_1(\text{enol})$	-0.187	-27.2	-32.89	-1.7821	1.6952	0.2650
$C_1(PA^{2-}) > C_1(\text{enol})$	0.521	-236.5	12.10	-9.7368	8.9825	-2.0901
$C_2(PA^{2-}) > C_2(\text{enol})$	-0.293	-0.8	-31.98	0.9311	-0.9339	0.5627
$H_1(PA^{2-}) > H_1(\text{enol})$	-0.059	5.3	-7.24	0.1367	-0.1197	0.0283
$H_2(PA^{2-}) > H_2(\text{enol})$	-0.107	21.9	-7.45	0.8515	-0.7818	0.0770
$C_3(PA^{2-}) > C_3(\text{enol})$	-0.216	65.4	-5.08	2.4097	-2.1988	0.7981
$O_2(PA^{2-}) > O_2(\text{enol})$	-0.039	-28.2	-6.85	-1.6873	1.5973	0.0040
$O_3(PA^{2-}) > O_3(\text{enol})$	-0.038	-28.2	-7.76	-2.3446	2.2544	0.0073
$O(H_3O^+) > O(H_2O)$	-0.050	145.1	19.15	5.8507	-5.3865	0.8545
$H(H_3O^+) > H(H_2O)$	0.146	-63.8	7.45	-0.7072	0.5040	-0.1981
$H(H_3O^+) > H_3(\text{enol})$	0.168	-73.8	8.52	-3.2522	3.0170	-0.2273
Reaction	0.000	-283.9	-44.58	-10.3088	9.3898	-0.1167

Table E18. Reaction 18: PA^-(enol form) ---> PA^-(keto form)

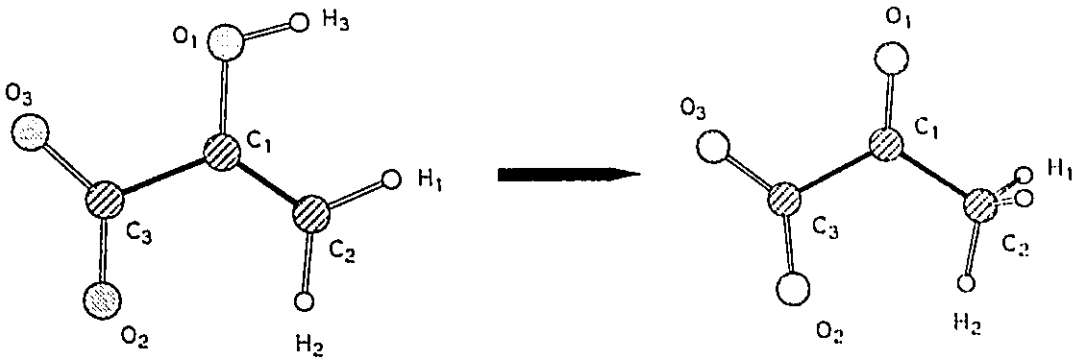

	ΔN	ΔE kcal/mol	ΔVol	ΔV_a	ΔV_r	ΔV_a^*
O_1(enol) > O_1(keto)	0.059	-68.1	19.15	-0.8361	0.6192	-0.0702
C_1(enol) > C_1(keto)	-0.659	261.0	-18.06	10.0592	-9.2268	2.6431
C_2(enol) > C_2(keto)	-0.054	-18.1	-33.18	0.3620	-0.4195	-0.1422
H_1(enol) > H_1(keto)	-0.048	9.9	-3.38	0.2572	-0.2255	0.0359
H_2(enol) > H_2(keto)	0.007	-6.0	-1.52	-0.2986	0.2796	-0.0132
C_3(enol) > C_3(keto)	0.051	-29.3	1.41	-0.5759	0.4826	-0.2088
O_2(enol) > O_2(keto)	-0.007	3.1	-0.96	-0.4037	0.4137	0.0442
O_3(enol) > O_3(keto)	-0.006	-1.4	2.14	1.1736	-1.1777	0.0200
H_3(enol) > H_1(keto)	0.642	-168.5	30.83	-6.3611	5.8239	-0.6213
Reaction	0.000	-17.5	-3.58	3.1745	-3.2329	1.6876

Table E19. Reaction 19: $HPO_4^{2-} + H_3O^+ \dashrightarrow H_2PO_4^- + H_2O$

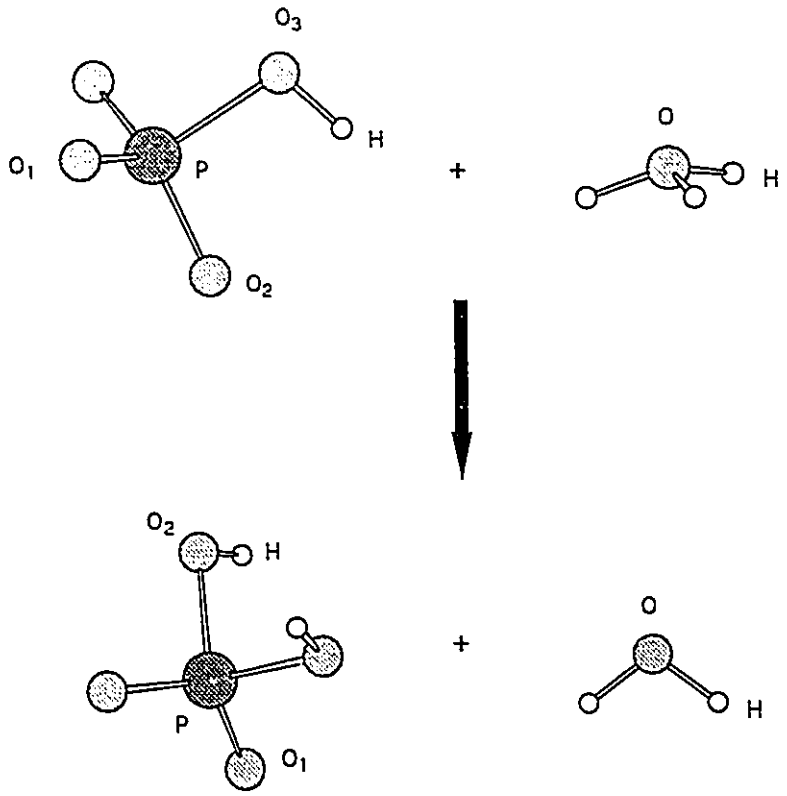

	ΔN	ΔE kcal/mol	ΔVol	ΔV_a	ΔV_r	ΔV_a°
$P(HPO_4^{2-}) > P(H_2PO_4^-)$	-0.040	1.4	-1.06	-2.8938	2.8969	0.3101
$O_1(HPO_4^{2-}) > O1(H_2PO_4^-)$	-0.039	-64.9	-8.42	-3.7361	3.5279	-0.1012
$O_2(HPO_4^{2-}) > O2(H_2PO_4^-)$	-0.241	-61.9	-31.59	0.9757	-1.1742	0.2789
$O_3(HPO_4^{2-}) > O2(H_2PO_4^-)$	0.014	-76.4	-7.69	-5.2691	5.0244	-0.3293
$H(HPO_4^{2-}) > H(H_2PO_4^-)$	-0.037	14.1	-1.58	0.4582	-0.4134	0.0438
$O(H_3O^+) > O(H_2O)$	-0.050	145.1	19.15	5.8507	-5.3865	0.8545
$H(H_3O^+) > H(H_2O)$	0.146	-63.8	7.45	-0.7072	0.5040	-0.1981
$H(H_3O^+) > H(H_2PO_4^-)$	0.140	-62.0	7.12	-3.5785	3.3809	-0.1916
Reaction	0.000	-297.3	-17.61	-13.3074	12.3746	0.3678

Table E20. Reaction 20: $H_2PO_4^- + H_3O^+ \rightarrow H_3PO_4 + H_2O$

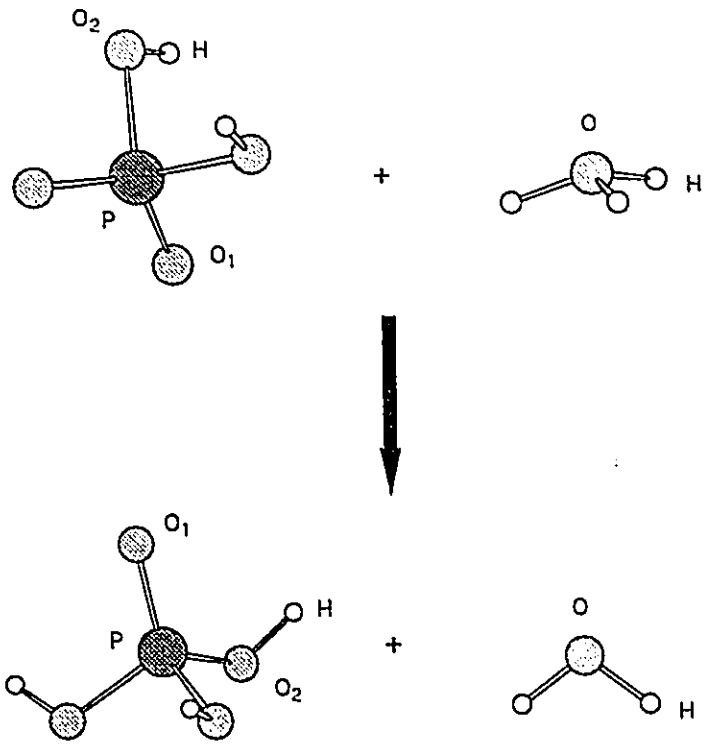

	ΔN	ΔE kcal/mol	ΔVol	ΔV_a	ΔV_r	ΔV_a^*
$P(H_2PO_4^-) > P(H_3PO_4)$	-0.017	0.0	-0.30	-3.1747	3.1752	0.1361
$O_1(H_2PO_4^-) > O_2(H_3PO_4)$	-0.187	-44.6	-28.40	0.0187	-0.1600	0.1286
$O_1(H_2PO_4^-) > O_1(H_3PO_4)$	-0.037	-34.3	-6.01	-2.4757	2.3670	0.0369
$O_2(H_2PO_4^-) > O_2(H_3PO_4)$	0.008	-52.6	-4.70	-4.2078	4.0408	-0.2381
$H(H_2PO_4^-) > H(H_3PO_4)$	-0.052	21.7	-2.71	0.6897	-0.6205	0.0674
$O(H_3O^+) > O(H_2O)$	-0.050	145.1	19.15	5.8507	-5.3865	0.8545
$H(H_3O^+) > H(H_2O)$	0.146	-63.8	7.45	-0.7072	0.5040	-0.1981
$H(H_3O^+) > H(H_3PO_4)$	0.088	-40.3	4.41	-2.8888	2.7604	-0.1241
Reaction	0.000	-163.6	-11.07	-11.1604	10.6039	0.2944